The role of Fbw7 and its substrates Notch and c-Jun in neural stem cells, the brain and development

Jörg Dominik Hoeck

University College London

and

Cancer Research UK London Research Institute

PhD Supervisor: Dr Axel Behrens

A thesis submitted for the degree of

Doctor of Philosophy

University College London

December 2011

Declaration

I Jörg Dominik Hoeck confirm that the work presented in this thesis is my own. Where information has been derived from other sources, I confirm that this has been indicated in the thesis.

Abstract

Activation of the oncogenic transcription factor c-Jun by the Jun N-terminal kinase (JNK) has been implicated in diverse biological effects, for example promoting intestinal proliferation or inducing neural apoptosis. Apart from differentiation, apoptosis plays an important role in the specification of neuronal networks in the developing brain. However, the molecular mechanisms governing differentiation and apoptosis during brain development are incompletely understood. In my PhD studies, I have shown for the first time that the E3 ubiquitin ligase substrate recognition component Fbw7 (F-box and WD repeat domain containing-7), a negative regulator of phosphorylated c-Jun and other oncoproteins such as Notch, is a key factor of differentiation and survival in the developing brain. Fbw7-deficiency caused Notch-dependent accumulation of radial glia stem cells and c-Jun-dependent loss of progenitors and differentiated cells. Thus, Fbw7 acts as a key molecular switch to allow neural stem cells to differentiate and neural progenitor cells to survive by antagonising Notch and JNK/c-Jun signalling respectively.

Whilst sustained JNK/c-Jun signalling contributes to abnormal brain development in conditional Fbw7-knockout mice, c-Jun activation by JNK has been suggested to be dispensable for mouse development but necessary for c-Jun oncogenic function. By mutating the four main JNK-phosphorylation sites in the *Jun* gene (*Jun*4A), I could show that $Jun^{4A/4A}$ mice are viable, do not exhibit histological abnormalities and are able to recover from intestinal or neural pathology. Furthermore, moderate activation of JNK/c-Jun signalling in the nervous system of ROSA26-LSL-JNKK2-$JNK1^{\Delta N/+}$ mice did not impair brain histology but led to slightly improved nerve regeneration. *In vitro*, $Jun^{4A/4A}$ mouse embryonic fibroblasts underwent premature senescence independent of

oxidative stress and p53 levels. These findings may prove important for targeting JNK/c-Jun signalling in order to promote nerve regeneration and to inhibit tumour growth in a p53-independent manner with the potential of limited side effects.

Acknowledgement

First of all, I would like to thank my supervisor Dr Axel Behrens for giving me the opportunity to do my PhD in his laboratory, for his kind supervision and stimulating discussion. I would also like to thank my thesis committee Dr Giampietro Schiavo and Dr Richard Treisman for valuable advice and discussion.

I am greatly indebted to Dr Anna Wade and Dr Clive Da Costa for their kind support and valuable advice and for critically reading the thesis.

I am grateful to Dr Nnennaya Kanu for her friendly support and advice. I would like to thank Dr Anett Jandke for providing the *Fbxw7*$^{f/f}$ mice and for her help with the radioactive *in situ* hybridisation, Emma Nye for her help with immunohistochemistry, Dr Bradley Spencer-Dene for his help with the non-radioactive *in situ* hybridisation, Dr Rocio Sancho for her help with the analysis of *Fbxw7* isoform expression and her advice on intestinal histology, Dr Sophia Blake for her help with adherent NSC cultures, Dr Xavier Fontana, Dr Milan Makwana, Smriti Patodia, Dr Mariya Hristova and Prof Gennadij Raivich for their help with the facial axotomy and the whisker test, the LRI Transgenic Services for their help with generating the *Jun*4A and the ROSA26-LSL-JNKK2-JNK1 mice, Lieven Haenebalcke and Dr Jody Haigh for their help with generating the ROSA26-LSL-JNKK2-JNK1 mice and Dr Freddy Radtke for providing the *Notch*$^{f/f}$ mice. Furthermore I would like to thank the animal technicians in the LRI Bio Resources Unit for taking care of my mice, the members of the LRI FACS Lab for their help with FACS measurements and analysis and all the members of the Mammalian Genetics Laboratory for making it a great place to do science. I would like

to thank the LRI Academic Director Dr Sally Leevers and her team for their support and Cancer Research UK for funding.

Finally, I cannot say thank you enough to my family and friends for their invaluable support during my studies and for always being there for me.

My work on Fbw7 and its substrates Notch and c-Jun in neural stem cells and the developing brain was published by the Nature Publishing Group in the November 2010 issue of Nature Neuroscience (Hoeck et al., 2010).

http://www.nature.com/neuro/journal/v13/n11/full/nn.2644.html

Table of Contents

Table of figures

List of tables

Abbreviations

°C	Degrees Celsius
A	Alanine
AB	Alcian blue
ADAM	A disintegrin and metalloprotease
AGO	Archipelago
Ala	Alanine
ALS	Amyotrophic lateral sclerosis
AMP	Ampicillin
ampR	Ampicillin-resistance
AP-1	Activator protein 1
APC/C	Anaphase promoting complex/cyclosome
APS	Ammonium persulfate
Arg	Arginine
ASA	Ascorbic acid
ASK	Apoptosis signal regulating kinase
ATF	Activating transcription factor
ATM	Ataxia telangiectesia mutated
ATP	Adenosine triphosphate
BAC	Bacterial artificial chromosome

Bad	BCL2-associated agonist of cell death
BCIP	5-bromo-4-chloro-3-indolyl phosphate
Bcl2l11	Bcl2-like 11 (apoptosis facilitator)
BDNF	Brain derived neurotrophic factor
Bim	Bcl-2 interacting mediator of cell death
BLBP	Brain-lipid binding protein
BMP	Bone morphogenetic protein
bp	Base pair
BR	Basic region
BrdU	5-bromo-2'-deoxyuridine
Brn2	Brain-2
BSA	Bovine serum albumin
bZIP	Basic-zipper
CAM	Chloramphenicol
cAMP	cAMP-responsive element
Casp3	Active caspase-3
CD133	Prominin 1
Cdc2	Cell division control protein 2
CDK	Cyclin-dependent kinase

cDNA	Complementary DNA
Cdx2	Caudal type homeobox 2
c-Fos	Cellular Fos
CFSE	Carboxyfluorescein diacetate succinimidyl ester
ChIP	Chromatin immunoprecipitation
CIP	Calf Intestinal Alkaline Phosphatase
c-Jun	Cellular Jun
CNS	Central nervous system
COUP-TF1	Chicken-ovalbumin upstream promoter-transcription factor 1
CP	Cortical plate
CPD	Cdc4 phospho-degron
CR-UK	Cancer Research UK
Ctip2	COUP-TF interacting protein 2
CUL1	Cullin 1
Cx43	Connexin 43
Cys	Cysteine
d	Day
DAB	3,3′-Diaminobenzidine
DAPI	4-6-diamidino-2-phenylindole

DAPT	*N*-[*N*-(3,5-difluorophenacetyl-l-alanyl)]-*S*-phenylglycine *t*-butyl ester
Dcx	Doublecortin
DD	Delta docking
ddH_2O	Double-distilled water
D domain	Dimerisation domain
DEPC	Diethyl pyrocarbonate
DIG	Digoxigenin
Dkk1	Dickkopf homolog 1
DMEM	Dulbecco's modified eagle's medium
DMSO	Dimethyl sulfoxide
DNA	Deoxyribonucleic acid
dNTPs	Deoxynucleotide triphosphates
dp5	Death protein 5
DRG	Dorsal root ganglia
DSL	Delta, Serrate and Lag-2
DSS	Dextran sodium sulfate
DTA	Diphteria Toxin A
E	Embryonic day
EDTA	Ethylenediaminetetraacetic acid

EGF	Epidermal growth factor
Emx2	Empty spiracles homeobox 2
ER	Endoplasmic reticulum
ERK	Extracellular signal-regulated kinase (ERK)
ES cell	Embryonic stem cell
Ezh2	Enhancer of zeste homolog 2
f	Floxed
FACS	Fluorescence-activated cell sorter
FasL	Fas ligand
fb	Forebrain
Fbw7	F-box and WD repeat domain containing-7
Fbxw7	F-box and WD repeat domain containing-7
$Fbxw7^{\Delta N}$	$Fbxw7^{f/f}$: Nestin-Cre^{+}
FCS	Foetal calf serum
Flk-1	Fetal liver kinase 1
FGF	Fibroblast growth factor
Foxa2	Forkhead box A2
g	Gram
Gapdh	Glyceraldehyde-3-phosphate dehydrogenase

GATA6	GATA binding protein 6
Gcn4	General control nonderepressible 4
GF	Growth factors
GFAP	Glial fibrillary acidic protein
GFP	Green fluorescent protein
GLAST	Astrocyte-specific glutamate transporter
GLI3	GLI family zinc finger 3
Gly	Glycine
GSK3	Glycogen synthase kinase-3
h	Hour
HA	Haemagglutinin
H&E	Haematoxylin and eosin
HECT	Homologous to E6-associated protein C-terminus
Hes	Hairy and Enhancer of Split
Hey	Hairy/enhancer-of-split related with YRPW motif
HRP	Horseradish peroxidase
HSC	Haematopoietic stem cell
IC	Inner cell
ICC	Immunocytochemistry

ICM	Inner cell mass
IF	Immunofluorescence
IgG	Immunoglobulin G
IgM	Immunoglobulin M
IHC	Immunohistochemistry
IMS	Industrial methylated spirit
iPS cell	Induced pluripotent stem cell
ISH	*In situ* hybridisation
IZ	Intermediate zone
JAK2	Janus kinase 2
JIP1	JNK interacting protein 1
JNK	Jun N-terminal kinase
JNKK	JNK kinase
Jun^{4A}	$Jun^{Ser63Ala,\ Ser73Ala,\ Thr91Ala,\ Thr93Ala}$
Jun^{AA}	$Jun^{Ser63Ala,\ Ser73Ala}$
$Jun^{\Delta N/+}$	$Jun^{f/+}$: Nestin-Cre^{+}
kb	Kilo base pairs
kDa	Kilodalton
l	Litre

LB	Lysogeny broth
LIN	Lin-Notch
LRI	London Research Institute
LSL	Lox-STOP-Lox
Lys	Lysine
LZ	Leucine zipper
mA	Milliampere
Mam	Mastermind
MAP	Mitogen-activated protein
Map2	Microtubule-associated protein 2
MAP2K	MAPK kinase
MAP3K	MAPKK kinase
MAPK	MAP kinase
MAPKK	MAPK kinase
MAPKKK	MAPKK kinase
mb	Midbrain
Mbd3	Methyl-CpG binding domain protein 3
MEF	Mouse embryonic fibroblast
MEK	MAP/ERK kinase

MEKK	MEK kinase
mg	Milligram
Mib	Mindbomb
min	Minute
MKK	MAPK kinase
ML	Mantle layer
MLK	Mixed lineage kinase
ml	Millilitre
mM	Millimolar
MPTP	1-methyl-4-phenyl-1,2,4,6 tetrahydropyridine
Msi1	Musashi 1
mTOR	Mammalian target of rapamycin
Nanog	Nanog homeobox
NB	Neurobasal medium
NBF	Neutral buffered formalin
NBT	Nitro blue tetrazolium
neoR	Neomycin-resistance
NeuN	Neuronal nuclei
Neur	Neuralized

ng	Nanogram
NG2	Chondroitin sulfate proteoglycan NG2
NGF	Nerve growth factor
NICD	Notch intracellular domain
NLS	Nuclear localisation signal
nm	Nanometre
NPC	Neural progenitor cell
n.s.	not significant
NSC	Neural stem cell
NuRD	Nucleosome remodelling and histone deacetylation complex
O4	Oligodendrocyte marker O4
OC	Outer cell
Oct4	POU domain transcription factor Oct4
OD	Optical density
O-Fut	O-fucosyl transferase
ORF	Open reading frame
ORI	Origin of replication
p	Phosphorylated
PAS	Periodic acid-Schiff

Pax6	Paired box 6
PBS	Phosphate buffered saline
PcG	Polycomb Group
p-c-Jun	N-terminally phosphorylated c-Jun
p-c-Myc	Thr58- and Ser62-phosphorylated c-Myc
p-cyclin E	Thr395-phosphorylated cyclin E
PCR	Polymerase chain reaction
PD	Parkinson's Disease
PDGFR	Platelet-derived growth factor receptor
PDX1	Pancreatic and duodenal homeobox 1
PFA	Paraformaldehyde
pH3	phospho-histone H3
PI	Propidium Iodide
PI3K	Phosphoinositide-3-kinase
PMSF	Phenylmethylsulfonyl fluoride
PPi	Pyrophosphate
PS	Primitive streak
qRT-PCR	Quantitative real-time PCR
R	Arginine

RA	Retinoic acid
Rb	Retinoblastoma protein
RBPJ	Recombination signal binding protein for immunoglobulin kappa J region
RBX1	RING box 1
RC2	Intermediate filament-associated protein RC2
RGC	Radial glia cell
RMS	Rostral migratory stream
RNA	Ribonucleic acid
rpm	Rounds per minute
rRNA	Ribosomal RNA
Runx1	Runt-related transcription factor 1
s	Second
S	Serine
S100	S100 calcium binding protein
SA	Splice acceptor
SAPK	Stress activated protein kinase
SCF	SKP1/CUL1/F-box protein
Scl	Stem cell leukaemia protein
s.d.	Standard deviation

SDS	Sodium dodecyl sulfate
SDS-PAGE	Sodium dodecyl sulfate-polyacrylamide gel electrophoresis
s.e.m.	Standard error of the mean
Ser	Serine
Shh	Sonic hedgehog
SKIP	Ski-interacting protein
SKP1	S-phase kinase-associated protein 1
Sox2	SRY-box 2
Sp8	Transcription factor Sp8
SREBP	Sterol regulatory element binding protein
SRY	Sex determining region Y
STAT3	Signal transducer and activator of transcription 3
SV40	Simian virus 40
SVZ	Subventricular zone
T	Threonine
TACE	Tumour necrosis factor-α converting enzyme
TAE	Tris Acetate EDTA buffer
T-ALL	T cell acute lymphocytic leukaemia
Tbr1	T-box brain protein 1

Tbr2	T-box brain protein 2
TBS-T	Tris buffered saline Tween-20
TCR	T cell receptor
TEMED	Tetramethylethylenediamine
TET	Tetracycline
TGF-β	Transforming growth factor beta
Th	T helper
Thr	Threonine
TPA	12-O-tetradecanoyl phorbol 13-acetate
Tris	Tris(hydroxymethyl)aminomethane
trxG	Trithorax Group
TUNEL	TdT-mediated dUTP-biotin nick end labeling
u	Ubiquitin
U	Unit
USP28	Ubiquitin-specific peptidase 28
V	Volt
VEGFR	Vascular endothelial growth factor receptor
v-Jun	Viral Jun
v/v	volume per volume

VZ	Ventricular zone
WB	Western blot
Wnt	Wingless type MMTV integration site
wt	Wild type
w/v	weight per volume
x g	gravitational force
YFP	Yellow fluorescent protein
β-gal	β-galactosidase
Δ	Deleted
μg	Microgram
μl	Microlitre
μm	Micrometre
μM	Micromolar

Chapter 1. Introduction

1.1 Stem cells, signalling and differentiation

A big part of human life is about differentiation. It starts with the totipotent zygote which develops into a new organism, a new individual. Intrinsic factors inherited from the parents and extrinsic signals from the environment determine one's fate. However, on a molecular and cellular level, we are strikingly similar, not only amongst human beings but amongst all mammals and other vertebrates and invertebrates. Evolutionary conserved genetic and epigenetic programmes specify the destiny of a cell in the body in the process of differentiation. Differentiation is a series of cell fate decisions which render a hierarchically more potent cell into a more specialised cell which fulfils a certain function in the body. Understanding which molecules govern cell fate decisions is a prerequisite to understanding life and being able to develop cell replacement therapies for regenerative medicine.

1.1.1 Early embryonic development

During embryonic development, differentiation starts after the 8-cell morula stage when totipotent blastomeres develop into either apolar inner cells (ICs) or polar outer cells (OCs) (**Figure 1a**) (Johnson and Ziomek, 1981, Yamanaka et al., 2006). It has been suggested that signalling through different cell-cell contact patterns of blastomeres are responsible for the differentiation into ICs or OCs. ICs are the precursors of pluripotent primitive ectoderm cells in the inner cell mass (ICM) of the blastocyst whereas OCs develop into trophectoderm cells of the trophoblast (**Figure 1a**,**b**). At the late morula

stage, OCs express high levels of the transcription factor Cdx2 (caudal type homeobox 2) which mediates OC development into trophectoderm cells (Niwa et al., 2005). ICs show high expression of the transcription factor Oct4 (POU domain transcription factor Oct4) which is accompanied by the upregulation of the transcription factor Nanog (Nanog homeobox) (Chambers et al., 2003, Mitsui et al., 2003). At the blastocyst stage, Nanog and GATA6 (GATA binding protein 6) show a mutually exclusive expression pattern in the ICM where Nanog-expressing ICs differentiate into pluripotent primitive ectoderm cells whilst GATA6-expressing OCs develop into primitive endoderm cells (**Figure 1b**) (Chazaud et al., 2006). Primitive ectoderm cells in the ICM of the blastocyst are the source of pluripotent embryonic stem (ES) cells in culture whereas the primitive endoderm develops into extra-embryonic tissue (Evans and Kaufman, 1981, Thomson et al., 1998). Apart from genetic regulatory networks determined by the transcription factors Oct4, Sox2 [SRY (sex determining region Y)-box 2] and Nanog, pluripotency is also defined by a unique epigenetic state. Polycomb Group (PcG) proteins such as Ezh2 (enhancer of zeste homolog 2) induce repressive histone modifications (H3K27me3) and at the same genetic locus, trithorax Group (trxG) proteins provide gene expression activating marks (H3K4me3). On the one hand, these bivalent domains are necessary for the repression of genes involved in differentiation. On the other hand, they provide a mechanism to rapidly induce expression of these developmental genes once the repressive marks are removed during differentiation (Bernstein et al., 2006, Boyer et al., 2006).

1.1.2 Post-implantation embryonic development

After implantation of the blastocyst into the uterus, the three germ layers, i.e. the ectoderm, endoderm and mesoderm are formed in the process of gastrulation. In the mouse, gastrulation starts after the generation of the primitive streak (PS) in the epiblast which gives rise to the embryonic tissue. Upon expression of the TGF-β (transforming growth factor beta) family members BMP4 (bone morphogenetic protein 4) and Nodal and activation of the Wnt (wingless type MMTV integration site) signalling pathway, epiblast cells migrate through the PS and develop into endoderm and mesoderm (**Figure 1c**). In the absence of BMP-, Wnt- and activin/Nodal signalling, epiblast cells undergo a default differentiation programme into ectoderm cells. A marker of cells throughout the PS is Brachyury (T) whereas the expression of other transcription factors such as Foxa2 (forkhead box A2) is regionally restricted. High Foxa2 expression accompanied by sustained activin/Nodal signalling in the anterior PS triggers endoderm formation, while low Foxa2 levels and sustained BMP- and Wnt-signalling are detected in the posterior PS where the mesoderm is generated (**Figure 1c**). Thus, spatial and temporal expression of agonists and inhibitors of these signalling pathways regulate the differentiation into the three germ layers (reviewed in Gadue et al., 2005).

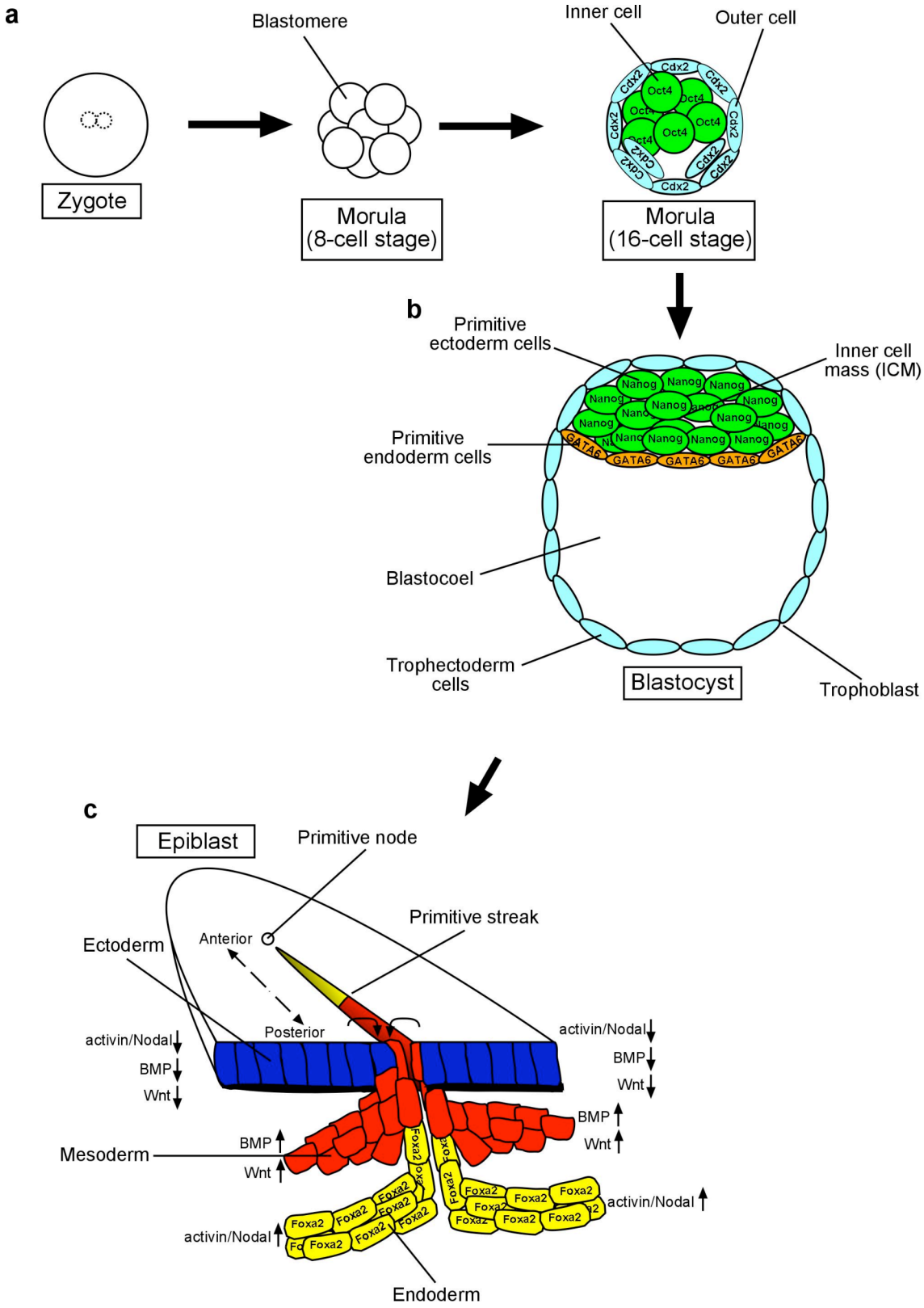

Figure 1 Early embryonic development: From zygote to epiblast
(**a**) Schematic representation of the transition from the zygote harbouring the two pronuclei via the 8 blastomeres morula stage to the 16-cell morula stage. Outer cells,

blue. Inner cells, green. (**b**) Drawing depicts the blastocyst including inner cell mass (ICM), trophoblast and blastocoel. Trophectoderm cells, blue. Primitive ectoderm cells, green. Primitive endoderm cells, orange. (**c**) Schematic representation of the epiblast including primitive node and primitive streak. Up- and downregulation of pathways or factors involved in ectoderm (blue), mesoderm (red) and endoderm (yellow) formation, cell migration through the primitive streak and the anteroposterior axis are indicated in the drawing.

1.1.3 The three germ layers - endoderm, mesoderm and ectoderm

Endoderm-derived tissues include the liver and the pancreas which are target organs for potential cell replacement therapies. Activin-induced endoderm cells were reported to adopt the hepatic fate upon addition of FGF (fibroblast growth factor) and BMP4 to ES cell cultures (Gouon-Evans et al., 2006), while retinoic acid (RA) together with sonic hedgehog (Shh) inhibition induces the pancreatic fate (**Figure 2**) (D'Amour et al., 2006). BMP- and Wnt-signalling mediate the generation of mesoderm cells which are characterised by the expression of the tyrosine kinase receptors Flk-1 (fetal liver kinase 1; also known as vascular endothelial growth factor receptor, VEGFR) and PDGFR (platelet-derived growth factor receptor). Mesoderm-derived tissues include the haematopoietic and cardiac system, vasculature and skeletal muscle. Hematopoietic mesoderm can be induced by concerted activation of Wnt, activin/Nodal and BMP signalling (**Figure 2**) (Nostro et al., 2008). While Wnt/β-catenin signalling is required for the initial induction of the mesoderm, transient inhibition of this pathway has been shown to be essential for the subsequent specification into cardiac mesoderm (Naito et al., 2006, Ueno et al., 2007). As mentioned above, ectoderm development is the default pathway, since the absence of serum and primitive streak inducers leads to the development of ectoderm cells in ES cell cultures. Furthermore, the default differentiation of ectoderm cells is the neuroectoderm pathway. Sox2 is a key pluripotency transcription factor in ES cells, but is also required for specification of the

neural lineage. Being already expressed in ES cells, Sox2 seems to mediate the default differentiation of ES cells into the neural lineage (Kishi et al., 2000). Despite being the default pathway, the development into neuroectoderm cells is still an event dependent on signalling molecules. It has been shown that neuroectoderm lineage differentiation is dependent on endogenously produced FGF signals (Ying et al., 2003). Apart from the nervous system, ectoderm cells also generate the skin. Inhibition of BMP-signalling in ectoderm cells has been shown to block neural development and to induce epidermal differentiation (**Figure 2**) (Kawasaki et al., 2000).

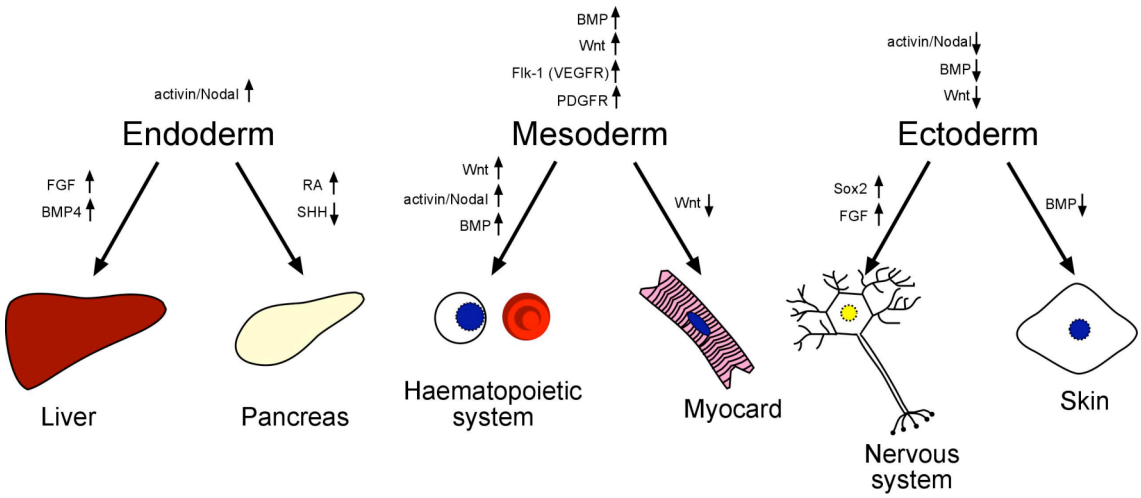

Figure 2 Differentiation of endoderm-, mesoderm- and ectoderm-derived cells
Schematic representation of the differentiation of endoderm, mesoderm and ectoderm cells into tissue-specific cells upon up- and downregulation of different factors and signalling pathways.

1.1.4 *In vitro*-differentiation of ES cells

As seen with mouse ES cells, human ES cells differentiate by default into neuroectoderm while activin/Nodal signalling induces endoderm and BMP-signalling promotes mesoderm formation (Davis et al., 2008, Kennedy et al., 2007, Ng et al., 2005, Pick et al., 2007, Tropepe et al., 2001). Whereas studies in various species have

revealed conserved signalling events which determine the specification of the primary germ layers, we have limited knowledge of the plethora of molecules involved in the differentiation of tissue-specific stem cells and functional differentiated cells. One of the best studied organ systems so far is the haematopoietic system. Cultured with serum, mouse ES cells differentiate by default into the haematopoietic lineage (reviewed in Keller, 2005). Gene targeting studies identified factors such as Scl (stem cell leukaemia protein) and Runx1 (runt-related transcription factor 1) to be involved in the embryonic development of the haematopoietic system (Begley et al., 1989, Wang and Speck, 1992). The same factors were also found to be upregulated during haematopoietic differentiation in ES cell cultures and thus indicating that *in vitro*-differentiation faithfully recapitulates the embryonic development of the haematopoietic system (**Figure 3**) (Dzierzak and Speck, 2008). Further down the differentiation route, haematopoietic stem cells (HSCs) have been shown to develop into the myeloid lineage upon the expression of the transcription factor PU.1 or into the erythroid lineage upon the expression of the PU.1-antagonist GATA1 (**Figure 3**) (Visvader et al., 1992, Wang and Speck, 1992, Zhang et al., 1999, Zhang et al., 2000). Upon co-culture with bone-marrow derived OP9 stromal cells, mouse and human ES cells have been reported to differentiate into haematopoietic progenitors with lymphoid potential (**Figure 3**) (Galic et al., 2006, Schmitt et al., 2004). Concerted Notch activation leads to further differentiation into T cells rather than the default differentiation into B cells (Schmitt et al., 2004, Schmitt and Zuniga-Pflucker, 2002, Watarai et al., 2010).

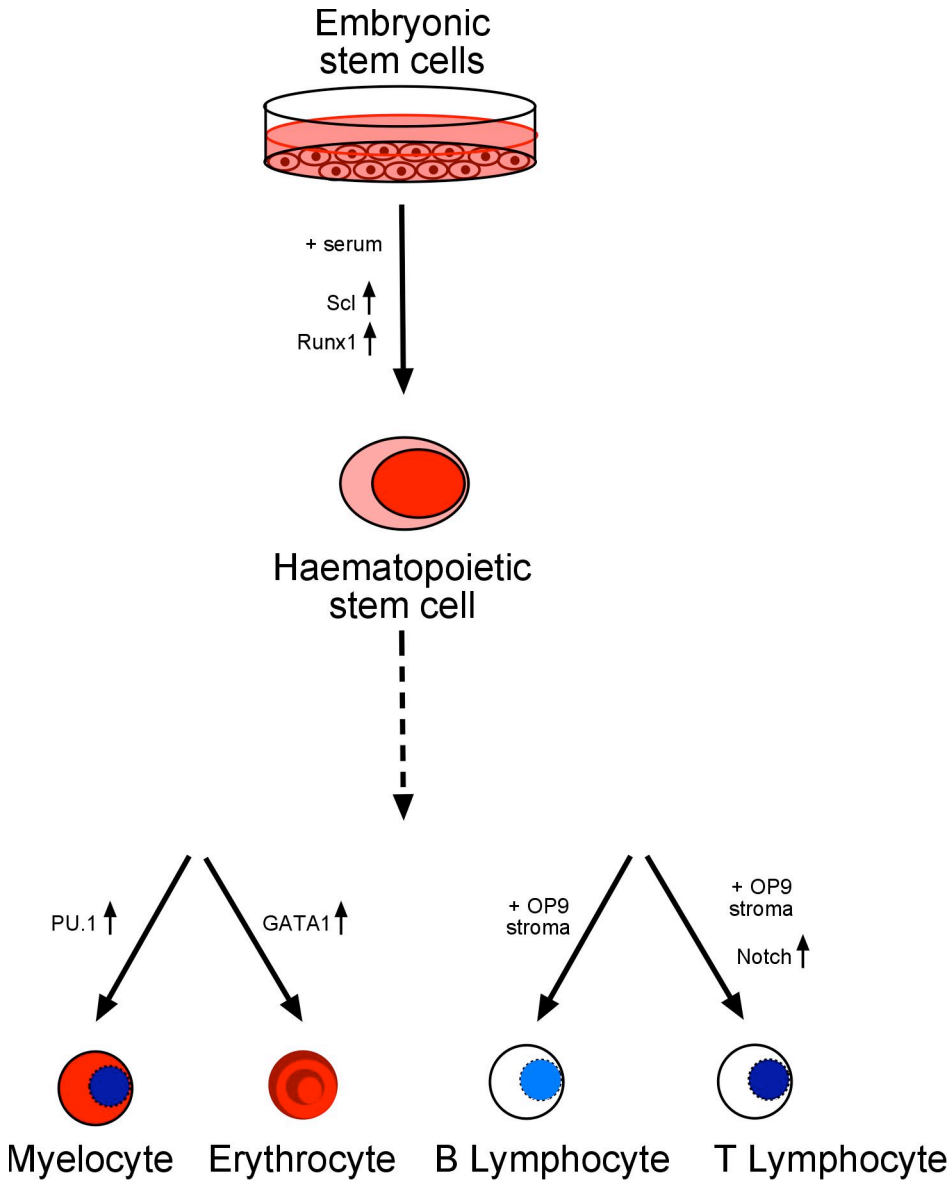

Figure 3 *In vitro*-differentiation of ES cells into haematopoietic cells
Schematic representation of ES cell differentiation into haematopoietic stem cells and differentiated blood cells and the factors involved. The various haematopoietic precursor cells are not included in this depiction for clarity.

1.1.5 *In vitro*-differentiated ES cells in cell replacement therapies

Along these lines, progress has been made in making use of factors discovered during embryogenesis for *in vitro* differentiation of cell types from various tissues. Activation of activin/Nodal- and BMP-signalling in combination with inhibition of p38 MAP

(mitogen-activated protein) kinase has been described to significantly enhance cardiomyocyte differentiation in human ES cell cultures (**Figure 4**) (Graichen et al., 2008). Efficient generation of cardiomyocytes in human ES cell cultures together with the development of prosurvival cocktails led to the successful transplantation of human cardiomyocytes into the infarcted rat heart which resulted in the prevention of the progression from myocardial infarction to heart failure (Laflamme et al., 2007, Laflamme et al., 2005). With regard to pancreas development and the cell-based treatments of Type I Diabetes, various protocols have been described to promote differentiation of ES cells into insulin-producing β cells. Shim *et al*. differentiated human ES cells to a PDX1 (pancreatic and duodenal homeobox 1)-positive pancreatic progenitor stage in culture by adding activin and retinoic acid (**Figure 4**) (Shim et al., 2007). After transplantation of these cells into the kidney capsule of hyperglycaemic mice, blood glucose levels were significantly reduced. However, other studies using similar stratagies reported less efficient rescues of hyperglycaemic mice and that transplanted $PDX1^+$ progenitors derived from human ES cells can only show efficient maturation into insulin-producing β cells when fetal pancreatic tissue is co-transplanted into the kidney capsule (Brolen et al., 2005, Jiang et al., 2007).

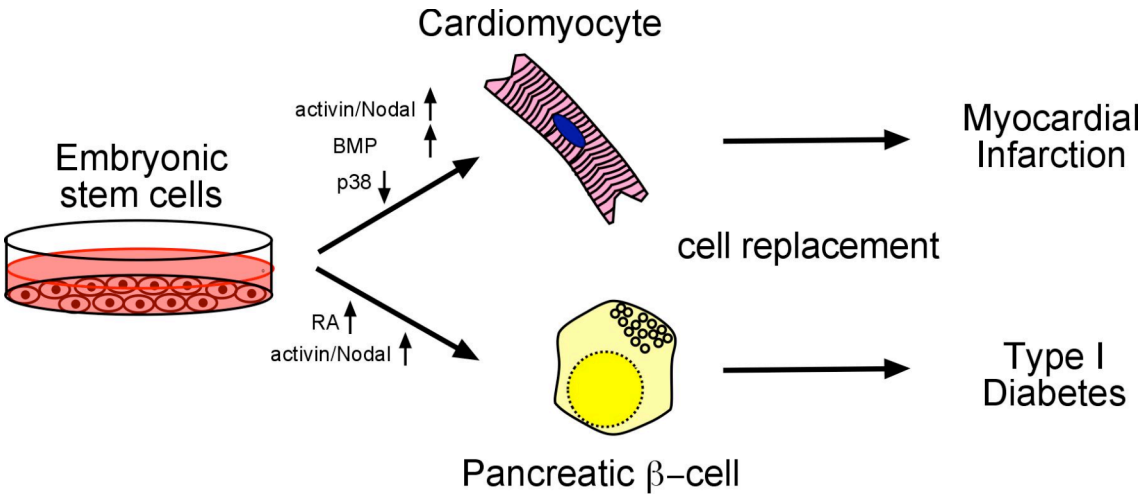

Figure 4 *In vitro*-differentiation of ES cells into cardiomyocytes and pancreatic β-cells
The drawing depicts the *in vitro*-differentiation of ES cells into cardiomyocytes and pancreatic β-cells and the factors involved. *In vitro*-generated cardiomyoctes and pancreatic β-cells are a promising tool for cell replacement therapies after Myocardial Infarction or in Type I Diabetes respectively.

1.1.6 Induced pluripotent stem cells

Apart from the promising results from the transplantation of *in vitro*-generated cardiomyocytes and β cells into animal models of heart failure and diabetes, there are many hurdles to overcome before these cell-based therapies are safe to use in the clinic. Two problems of using ES cell-derived cells are on the one hand the ethical issue of destroying an embryo to isolate ES cells, and on the other hand, grafted donor ES cell-derived cells might be rejected by the host immune system. Both issues can be overcome by using induced pluripotent stem (iPS) cells. iPS cells can be generated from patient fibroblasts by introducing the key pluripotency factors Oct4 and Sox2 and the ES cell self-renewal factors c-Myc and Klf4 (**Figure 5**) (Takahashi et al., 2007, Takahashi and Yamanaka, 2006). The generation of iPS cells has revolutionised stem cell research. Currently, protocols are being developed to improve iPS cell generation,

for example by only transient factor expression or the discovery of small molecule inducers of pluripotency (Li et al., 2011). Having in hand patient-derived pluripotent cells gives stem cell researchers the promise of being able to study, modify and inhibit pathogenesis by using these cells for patient-specific cell-based therapies. However, iPS cells have been reported to show significant discrepancies to pluripotent ES cells, particularly in their epigenetic state (Kim et al., 2010, Lister et al., 2011, Polo et al., 2010). This makes iPS cells a hybrid of pluripotent embryonic cells and aged adult cells and thus an even more artificial cell system than *in vitro*-cultured ES cells. Both cell types have been reported to harbour genomic abnormalities which can predispose ES and iPS cells to increased self-renewal and elevated expression of oncogenes (Laurent et al., 2011). Thus, implantation of these cells can induce tumour development *in vivo*, as was shown after stem cell transplantation of ES cell-derived immature Nestin^{+} neuroepithelial cells into the striatum of Parkinsonian rats (Roy et al., 2006). *In vitro*-differentiation and subsequent transplantation might limit tumour growth in engrafted hosts. Furthermore, it has been described that in certain pathologies and tissues, differentiation signals are absent, for example in the chemically lesioned brains of rats (Ben-Hur et al., 2004). Thus, differentiation signals have to be provided in advance *in vitro* before transplantation.

However, the transplantation of differentiated cells carries other risks. On the one hand, transplanted differentiated cells seem to be more unlikely to be integrated into the host tissue and thus do not survive as was shown for example in the brain (Park et al., 2005). On the other hand, *in vivo*-differentiation of many cell types is incompletely understood. Conditions for the *in vitro*-differentiation of many cell types, for example many subtypes of neurons, have not been established yet and the functionality of many *in*

vitro-differentiated cells still has to be proved (Wu et al., 2007). Therefore, understanding stem cell differentiation during embryonic development is a prerequisite for the efficient *in vitro*-differentiation of functional cells for cell-replacement therapies.

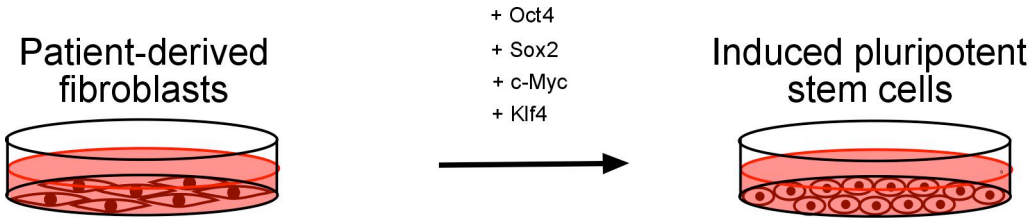

Figure 5 Induced pluripotent stem cells
Schematic representation of the *in vitro*-generation of induced pluripotent stem cells by the introduction of the genes *Oct4*, *Sox2*, *c-Myc* and *Klf4* into fibroblasts isolated from patients.

1.2 Neural stem cells and cortical brain development

As mentioned above, during gastrulation of mammalian development, the three primary germ layers are formed. The specification of epiblast cells into ectoderm, endoderm and mesoderm cells follows defined spatial and temporal signals which form gradients alongside different axes of the embryo.

1.2.1 Neurulation

For the induction of ectoderm cells, it is necessary to inhibit BMP-, Wnt- and Nodal-signalling which induce endoderm and mesoderm formation (**Figure 1**). Antagonists of these pathways such as Noggin and Chordin for BMP-signalling, Dkk1 (dickkopf homolog 1) for Wnt-signalling and Cerberus for Wnt- and Nodal-signalling are secreted by cells in the primitive node or cells adjacent to the ectoderm (del Barco Barrantes et al., 2003). Additionally, FGF-signalling supports efficient induction of the neuroectoderm fate and is required for the expansion of neural stem cells (NSCs) in the neural plate (Streit et al., 2000). Recent data in non-vertebrates has shown that neural induction requires FGF signals leading to the activation of the MEK (MAPK/ERK kinase)/ERK (extracellular signal-regulated kinase)-signalling pathway (Hudson et al., 2007, Pera et al., 2003). Furthermore, it is believed that early signals from primitive node cells already specify a regional identity for neural stem cells in the neural plate and thus determine which parts of the nervous system will be formed by which NSCs (reviewed in Stiles and Jernigan, 2010). During neurulation, invagination of the neural plate creates the neural tube which will develop into the central nervous system (CNS) (**Figure 6**). A Wnt-gradient determines anterior and posterior cells. Posterior cells show highly activated Wnt-signalling whereas Cerberus and Dkk1 inhibit Wnt-signalling at

the anterior end (Ciani and Salinas, 2005). Furthermore, retinoic acid (RA) signalling has been shown to be highly expressed in the posterior neural tube (reviewed in Maden, 2007). The dorsoventral axis of the neural tube is determined by opposite gradients of BMP and sonic hedgehog (Shh) where BMP is secreted dorsally by the cells of the overlying ectoderm and Shh ventrally by the notochord (**Figure 6**) (reviewed in Dhara and Stice, 2008). The anterior part of the neural tube is the embryonic precursor of the brain, the posterior part develops into the spinal cord. The hollow cavity of the anterior neural tube eventually forms the ventricular system of the brain. The most undifferentiated cells line up in an area adjacent to the ventricles which is called the ventricular zone (VZ).

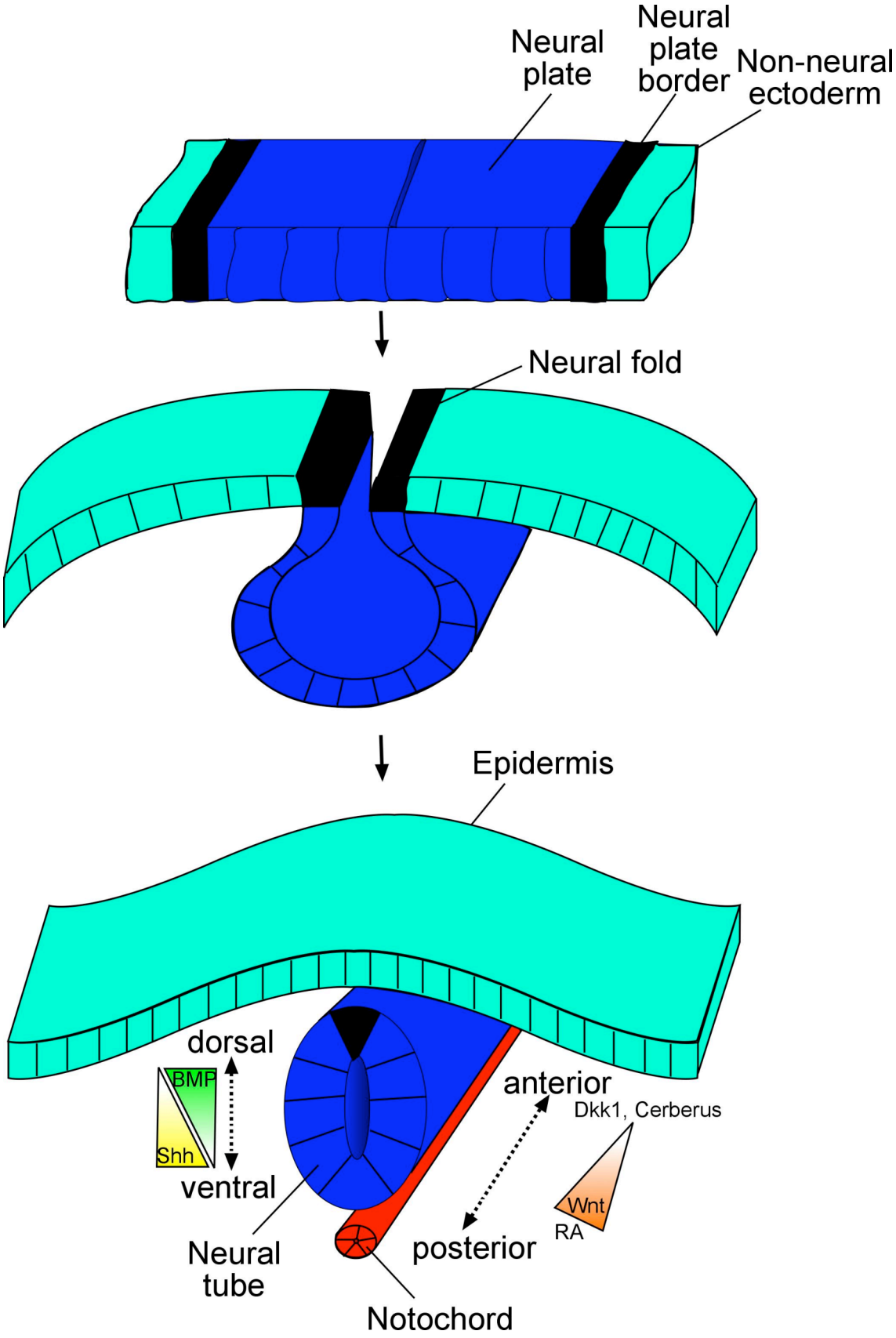
Neural plate
Neural plate border
Non-neural ectoderm
Neural fold
Epidermis
dorsal
BMP
Shh
ventral
anterior
Dkk1, Cerberus
Wnt
RA
posterior
Neural tube
Notochord

Figure 6 Neurulation
Schematic representation of neural plate invagination and neural tube formation during neurulation. Patterning of the ectoderm-derived neural tube along the anteroposterior and dorsoventral axes occurs by gradients of different factors secreted by adjacent cells from the ectoderm-derived epidermis and the mesoderm-derived notochord.

1.2.2 Brain development

After neurulation, the anterior part of the neural tube expands to develop into the three primary brain vesicles. The most anterior vesicle, the prosencephalon is the precursor of the forebrain, followed by the mesencephalon which is the precursor of the midbrain and most posterior the rhombencephalon which gives rise to the hindbrain (**Figure 7a**). The prosencephalon and the rhombencephalon further divide into the telencephalon and the diencephalon or the metencephalon and the myelencephalon respectively (**Figure 7b**). The mesencephalon does not further divide. FGF-signalling, particularly induced by FGF8, has been shown to be important for the formation of the mesencephalon-derived midbrain (Crossley et al., 1996, Lee et al., 1997). The dorsal part of the mesencephalon develops into the midbrain tectum which is involved in the processing of auditory and visual reflexes. The telencephalon, the forebrain precursor, is divided into the ventral telencephalon (subpallium) and the dorsal telencephalon (pallium). The subpallium gives rise to the three ganglionic eminences (medial, lateral and caudal) which develop into the basal ganglia deep in the forebrain underneath the cortex (Anderson et al., 2001, Corbin et al., 2001, Nery et al., 2002). The ganglionic eminences produce various inhibitory interneurons which migrate throughout the forebrain for example tangentially into the cortex. The main components of the basal ganglia are the striatum, the pallidum, the substantia nigra and the subthalamic nucleus. The brain structure generated by the pallium is the forebrain cortex. The dorsoventral axis of the telencephalon is determined by opposite GLI3 (GLI family zinc finger 3) and

Shh-gradients (**Figure 7b**) (Motoyama et al., 2003, Aboitiz and Montiel, 2007). GLI3 is the dorsalising factor activating BMP- and Wnt-signalling whereas Shh-signalling is essential for the formation of the ventral telencephalon.

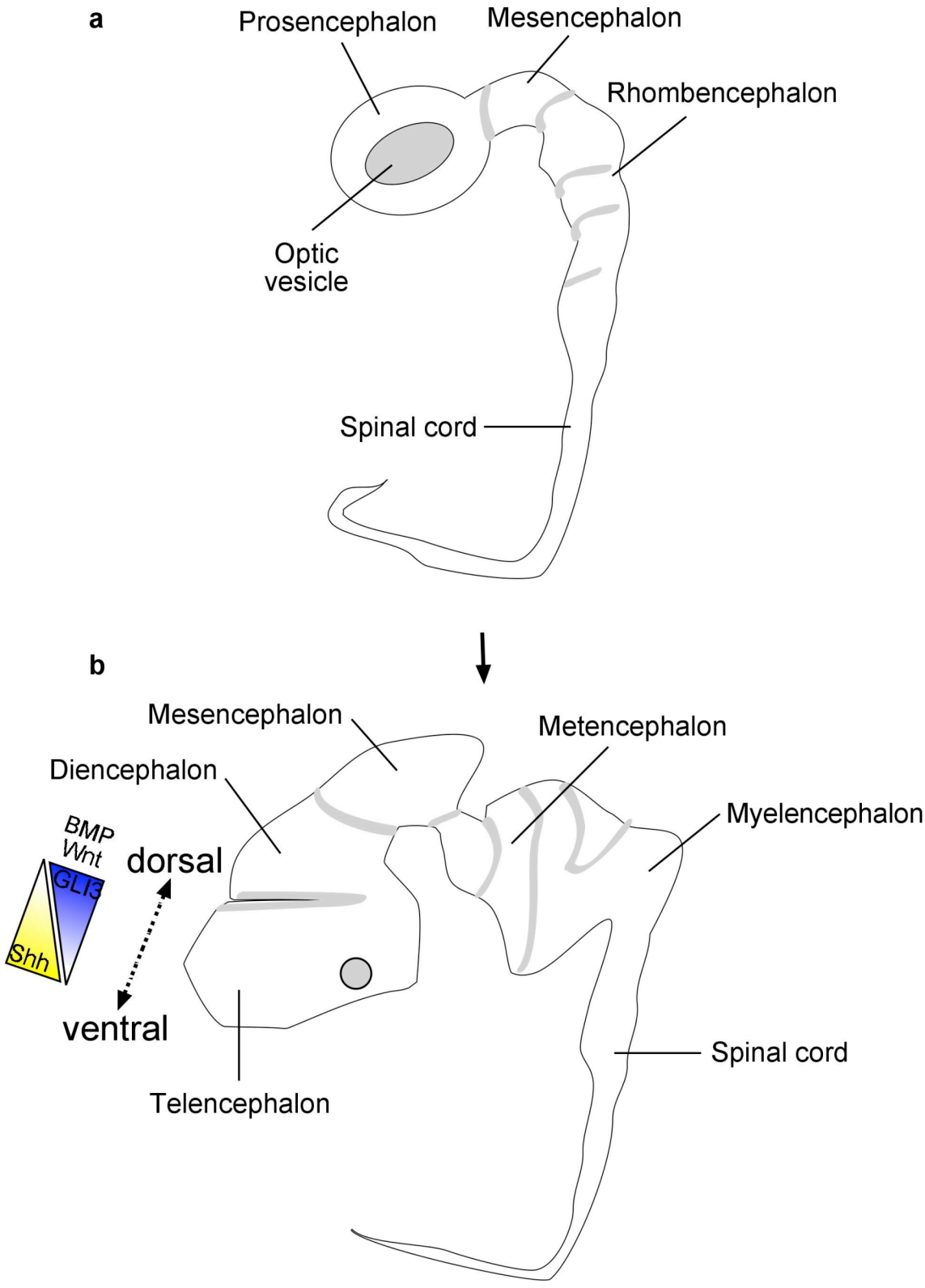

Figure 7 Early brain development
(**a**) Drawing of the human embryo around embryonic day (E) 28 when the primary brain vesicles, i.e. the prosencephalon, the mesencephalon and the rhombencephalon are

formed. (**b**) Drawing of the E49 human embryo showing the secondary brain vesicles, i.e. the telencephalon, the diencephalon, the mesencephalon, the metencephalon and the myelencephalon. The dorsoventral axis of the telencephalon is determined by opposite GLI3-Shh gradients.

1.2.3 Cortex development

The cortex is the most complex and most evolved structure of the mammalian brain. It is the largest part of the human brain and is involved in higher brain function such as thought, speech, memory and the processing of various stimuli. Neural stem cells in the ventricular zone of the developing cortex are refined alongside the anteroposterior axis by expression of opposite gradients of the anterior factors Pax6 (paired box 6) and Sp8 (transcription factor Sp8) and the posterior factors Emx2 (empty spiracles homeobox 2) and COUP-TF1 (chicken-ovalbumin upstream promoter-transcription factor 1) (**Figure 8**) (reviewed in O'Leary and Nakagawa, 2002, O'Leary and Sahara, 2008, O'Leary et al., 2007). High levels of Pax6 and Sp8 in combination with low Emx2 and COUP-TF1 levels specify neural progenitors for the formation of the motor cortex whereas the reverse combination is responsible for the specification of NSCs in the visual cortex (**Figure 8**). Intermediate levels of the anteroposterior factors induces NSCs forming the somatosensory cortex. Apart from the tangentially migrating inhibitory neurons generated in the subpallium, most of the excitatory neurons in the cortex are formed in the cortical ventricular zone from where they migrate radially into the upper layers of the cortex (**Figure 9**) (Rakic, 1972). At the onset of cortex development, the pool of early neuroepithelial stem cells expressing markers such as CD133 (Prominin 1), Musashi 1 (Msi1) and Nestin expands rapidly in the cortical VZ by symmetrical cell division in which one stem cell gives rise to two identical daughter stem cells. At the beginning of neurogenesis, neuroepithelial stem cells give rise to

radial glia stem cells (RGCs) which represent the major population of NSCs at later stages of embryonic cortex development (**Figure 9**). Radial glia cells (RGCs) were initially identified as “radial glia guides” (Rakic, 1972) whose processes formed a scaffold for radially migrating neurons in the cortex. Only decades later, it has been shown that apart from supporting neuron migration, radial glia cells are in fact neural stem cells (Noctor et al., 2001, Malatesta et al., 2000, Tamamaki et al., 2001, Miyata et al., 2001). RGC somata are found in the cortical VZ from which a short apical process connects it to the ventricular surface through RGC endfeet whereas the long basal process extends to the pial surface where it also forms endfeet (reviewed in Gotz and Huttner, 2005). At the onset of neurogenesis, RGCs divide asymmetrically to generate one RGC and one neuron, the former staying in the VZ, the latter migrating alongside the basal process into the intermediate zone (IZ) and the cortical plate (CP), areas of more differentiated cells (**Figure 9**). Cajal-Retzius cells at the pial surface control the correct neuronal migration and cortical lamination by expression of the signalling molecule Reelin. Furthermore, RGCs can give rise to intermediate progenitor cells which populate the subventricular zone (SVZ) adjacent to the VZ (**Figure 9**). Intermediate progenitors in the cortical SVZ express the specific marker Tbr2 (T-box brain protein 2) (Englund et al., 2005) and can divide symmetrically either to produce two progenitors or to generate two neurons (Haubensak et al., 2004, Miyata et al., 2004, Noctor et al., 2004).

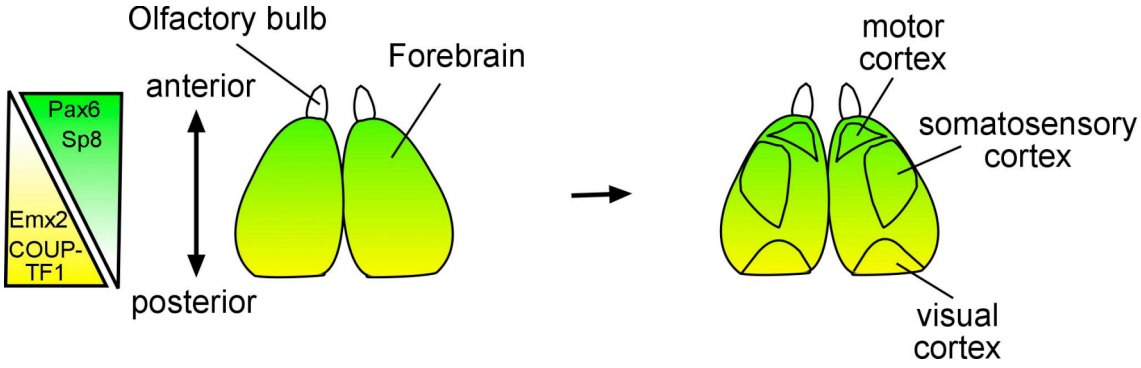

Figure 8 Patterning of the cortex
Schematic representation of the mouse forebrain and areas forming the motor, somatosensory and visual cortex. The anteroposterior axis of the cortex is determined by opposite Pax6/Sp8 and Emx2/COUP-TF1 gradients.

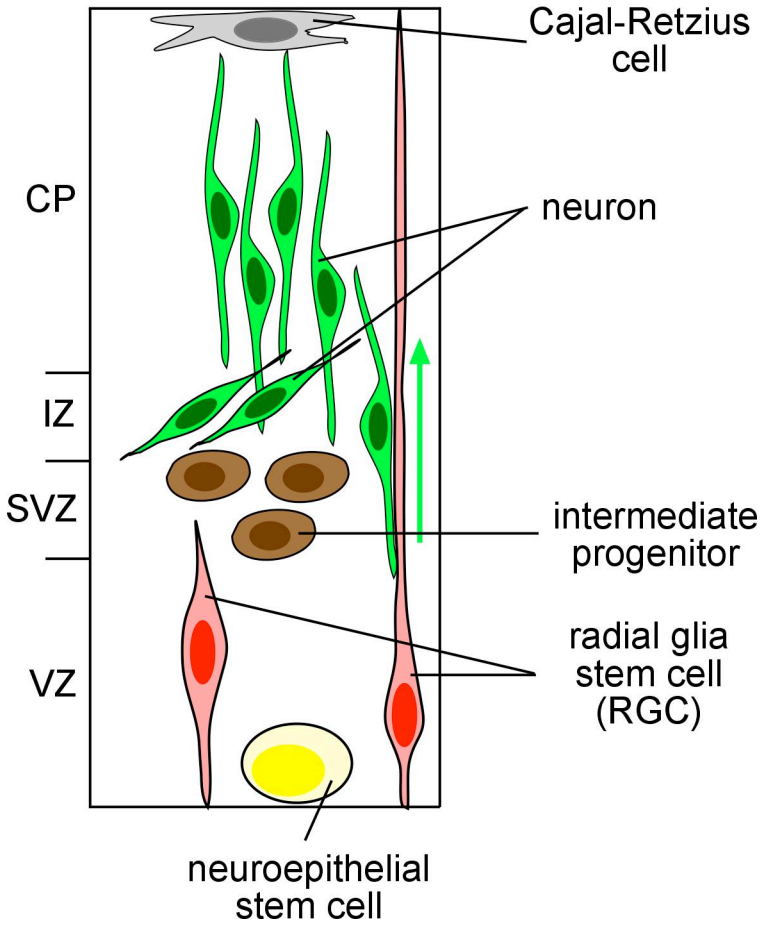

Figure 9 Neurogenesis in the cortex
The ventricular zone (VZ) harbours early neuroepithelial stem cells as well as radial glia stem cells (RGCs). RGCs act as radial guides for new-born neurons which migrate into the intermediate zone (IZ) and the cortical plate (CP) of the cortex. RGCs also act as neural stem cells and can give rise to intermediate progenitors in the subventricular zone (SVZ) and differentiated neurons and glia. Cajal-Retzius cells at the pial surface are important for correct cortical layering.

1.2.4 Radial glia stem cells

Since the identification of radial glia cells as a subpopulation of neural stem cells a decade ago, radial glia stem cells (RGCs) have been of major interest in the field of neuroscience (Noctor et al., 2001, Malatesta et al., 2000, Tamamaki et al., 2001, Miyata et al., 2001). Following the discovery of RGCs as glia cells (Rakic, 1972), several groups identified and defined marker expression for radial glia cells (reviewed in Hartfuss et al., 2001). RGCs express the stem cell marker Nestin [also known as

intermediate filament protein (Misson et al., 1988, Edwards et al., 1990)] and RC2 [(intermediate filament-associated protein RC2 (Misson et al., 1988)] as well as the glial markers GLAST [astrocyte-specific glutamate transporter; (Shibata et al., 1997)], Vimentin (Dahl et al., 1981, Schnitzer et al., 1981), and BLBP [brain-lipid binding protein; (Feng et al., 1994)] (**Figure 10**) (reviewed in Chanas-Sacre et al., 2000, Hartfuss et al., 2001). Interestingly, BLBP is a downstream target of the Notch signalling pathway which has been shown to be crucial for radial glia maintenance via its Hairy and Enhancer of Split (*Hes*) target genes (Hatakeyama et al., 2004). It has been described that during neurogenesis, subpopulations of RGCs exist which express distinct levels of the radial glia markers RC2, BLBP and GLAST. Subpopulations of RGCs show distinct lineage potentiality, for example early BLBP-positive RGCs have been shown to be mainly bi-potential developing into neurons and glia whereas RGCs expressing GLAST have been shown to mainly produce neurons (reviewed in Pinto and Gotz, 2007). It is believed that lineage specification already occurs early during RGC development defining neurogenic and gliogenic radial glia cells, although neurons and differentiated glia are formed at different time points with neurogenesis preceding gliogenesis (reviewed in Miller and Gauthier, 2007). Furthermore, regional and temporal specification has been shown to be important also within the RGC population (reviewed in Pinto and Gotz, 2007). *In vitro*-differentiation and transplantation experiments have shown that, when isolated at various stages of embryonic cortex development, region-specific neural stem cells are determined to develop into specific cortical layer neurons (McConnell and Kaznowski, 1991, Frantz and McConnell, 1996). This was corroborated by the discovery that precursors committed towards a layer-specific neuron already show marker expression of these neurons (Kriegstein and Gotz,

2003). Furthermore, it has been shown that whereas ectopic transplantation of early NSCs into a mouse embryo at later stages of development has the potential to generate the correct neurons formed during the host stage of development, the reverse experiment showed that late NSCs are restricted in their fate and cannot generate stage- and region-specific neurons in the younger embryo (Desai and McConnell, 2000). The crucial transcription factor restricting late NSCs in their differentiation potential is FoxG1 (Hanashima et al., 2004, Shen et al., 2006). Up to E15 in mouse development, FoxG1 inactivation can reprogramme late NSCs into early NSCs which have the potential to differentiate into early born cortical neurons such as Cajal-Retzius cells (Shen et al., 2006). It has been suggested that NSC fate restrictions are dependent on extrinsic cues contained within the NSC population as well as on intrinsic signalling events (Shen et al., 2006, Leone et al., 2008), but the critical signalling pathways involved in cell fate decisions into neuronal subtypes of the cortex remain poorly defined (reviewed in Molyneaux et al., 2007).

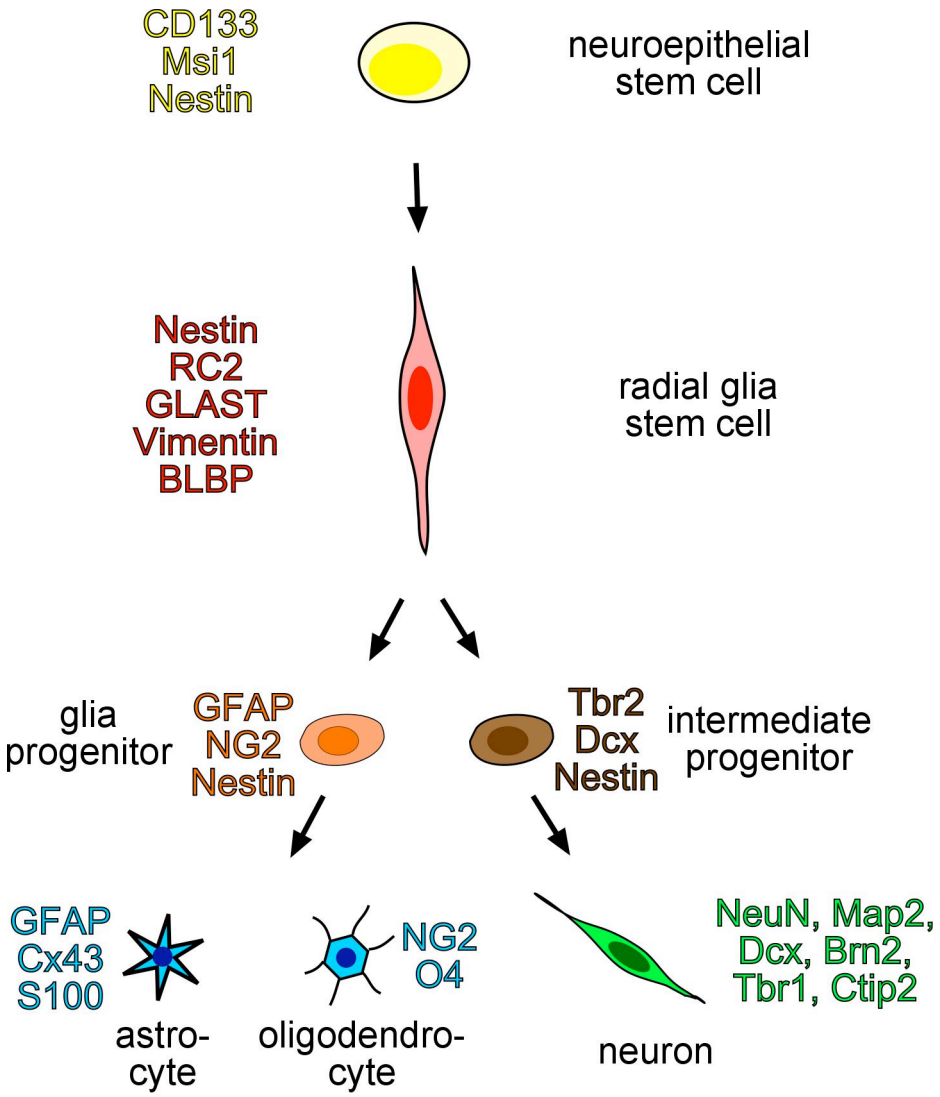

Figure 10 Neural stem cell differentiation
Early neuroepithelial stem cells marked by CD133 (Prominin 1), Musashi1 (Msi1) and Nestin develop into radial glia stem cells which express Nestin, RC2, GLAST, Vimentin and BLBP. Radial glia stem cells give rise to glial [marker: GFAP (glial fibrillary acidic protein), NG2 (chondroitin sulfate proteoglycan NG2) and Nestin] and neuronal [marker: Tbr2, Doublecortin (Dcx) and Nestin] progenitors which differentiate into GFAP/Connexin 43 (Cx43)/S100-positive astrocytes and NG2/O4 (oligodendrocyte marker O4)-positive oligodendrocytes or neurons respectively. Typical neuronal markers are NeuN (neuronal nuclei), Map2 (microtubule-associated protein 2), Dcx, Brn2 (brain-2), Tbr1 (T-box brain protein 1) and Ctip2 (COUP-TF interacting protein 2).

1.2.5 Apoptosis in the developing brain

Apart from NSC proliferation and differentiation, programmed cell death, i.e. apoptosis, of NSCs and neurons, plays a crucial role in the specification of the developing brain (Rakic and Zecevic, 2000). Dependent on the brain region, up to 70% of neural cells, as seen in some cortical layers (Rabinowicz et al., 1996), undergo apoptosis during brain development. Interestingly, levels of apoptotic cells are particularly high among NSC and progenitor populations during early neural development (Rakic and Zecevic, 2000, de la Rosa and de Pablo, 2000, Yeo and Gautier, 2004). The physiological disposal of neural cells occurs due to competition of cells for neurotrophic survival factors and thus guarantees the formation of correct neuronal networks in the developing brain (Levi-Montalcini, 1964, Huang and Reichardt, 2001). Furthermore, it is believed that apoptosis is also responsible for correcting errors in wrongly produced or migrated neurons (Buss and Oppenheim, 2004). However, the intrinsic signalling events governing apoptosis of neural cells during brain development are incompletely understood.

1.2.6 *In vitro*-differentiation of NSCs

Embryonic brain development is a series of refinements and specifications of neural stem cells through the expression of various signalling molecules. Based on discoveries from studies of embryonic brain development, signalling molecule combinations are now widely used to propagate and differentiate specific NSC and neuron subtype populations. Inhibitors of BMP-signalling such as Noggin and the activation of retinoic acid (RA) signalling have been widely used to potentiate neural induction in human and mouse ES cell cultures (**Figure 11**) (Bain et al., 1996, Schuldiner et al., 2001). FGF

signalling activation is commonly used to expand NSC cultures *in vitro* (Carpenter et al., 2001, Okabe et al., 1996) whereas activation of Shh and Notch signalling keeps NSCs in an undifferentiated and plastic state (Elkabetz et al., 2008). Several groups have been able to direct differentiation into various neuronal subtypes (**Figure 11**). FGF2 treatment followed by FGF8 and Shh generate forebrain dopaminergic neurons whereas FGF8 and Shh followed by ascorbic acid (ASA) and BDNF (brain derived neurotrophic factor) generates midbrain dopaminergic neurons (Yan et al., 2005, Perrier et al., 2004, Kim et al., 2002). In a similar protocol, using FGF4 instead of FGF8 induces hindbrain serotonin neuron formation (Barberi et al., 2003). Furthermore, retinoic acid followed by Shh led to efficient production of motoneurons (Li et al., 2005, Shin et al., 2005). Also cortical neurons were derived from ES cells *in vitro* treated with Shh signalling inhibitor (Gaspard et al., 2008). Interestingly, Gaspard *et al*. were able to show that the temporally specified generation of distinct layer-specific neuronal subtypes is recapitualed *in vitro* suggesting that after inhibition of Shh signalling, intrinsic mechanisms govern corticogenesis (Gaspard et al., 2008).

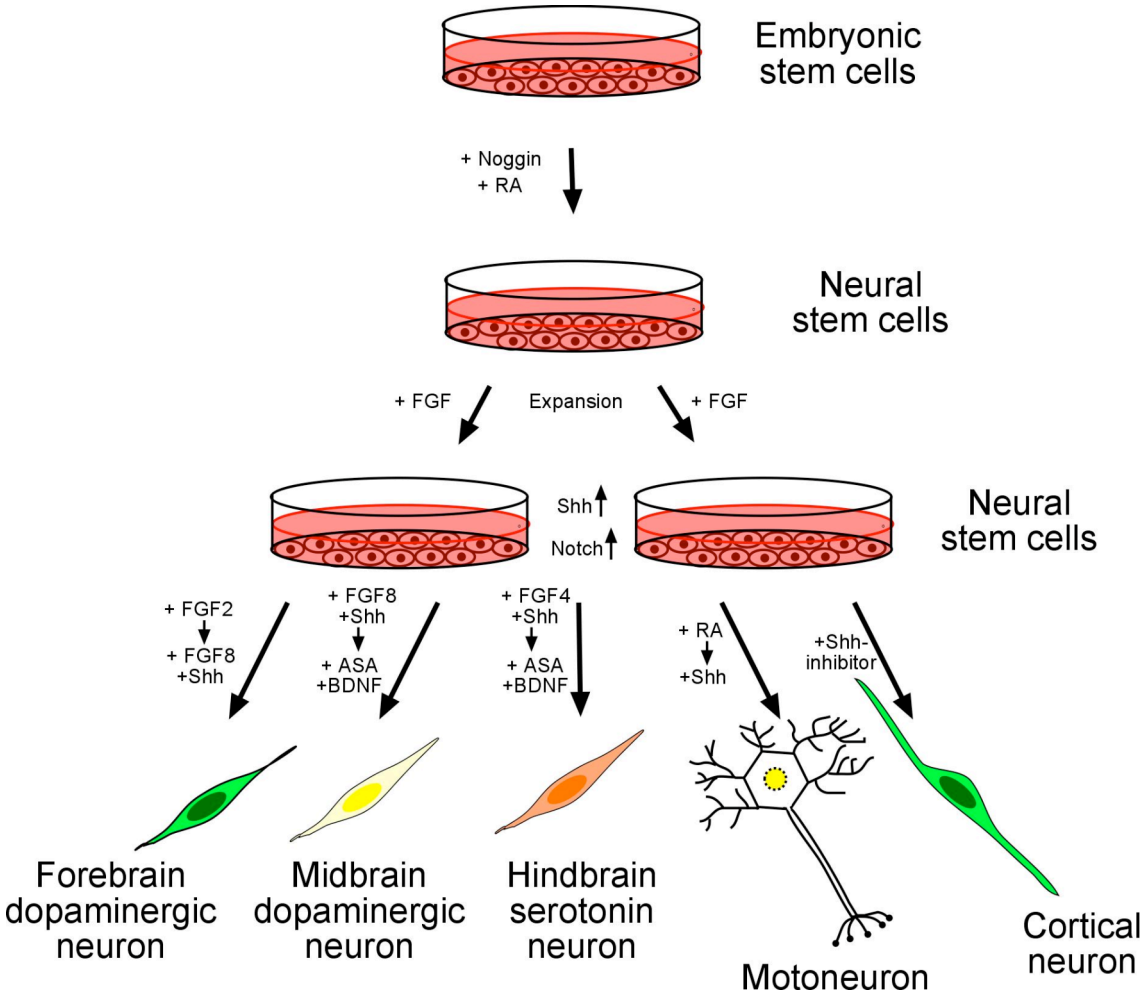

Figure 11 *In vitro*-differentiation into neurons
Schematic representation of *in vitro*-differentiation from ES cells via NSCs into various types of differentiated neurons including factors involved in the differentiation into specific neurons.

1.2.7 Cell replacement therapies and their risks and promises for the treatment of neurological disorders

Some of the *in vitro*-generated neurons either from ES cells or iPS cells have been shown to functionally integrate into physiological neuronal networks in mice (Gaspard et al., 2008) or even in pathological conditions for example in an animal model for Parkinson's Disease (PD) or spinal cord injury (Kim et al., 2002, Keirstead et al., 2005, Wernig et al., 2008).

However in humans, cell-based transplantations are only in their infancy. Transplantation of fetal midbrain tissue into the brains of PD patients only showed modest improvements of the condition and some patients developed dyskinesias most likely from overdosing with graft cells (Lindvall and Hagell, 2001, Hagell et al., 2002, Freed et al., 2001). Currently, human umbilical cord blood cells as well as adult stem cells are used in clinical trials for a wide range of diseases including neurological disorders. Up to date, many studies involving autologous transplantation of haematopoietic, mesenchymal and neural stem cells have shown that these cells are safe to use in patients (Trounson et al., 2011). However, the efficacy of treatments has often been limited, mainly due to insufficient survival and functional integration of engrafted cells for example in haematopoietic and mesenchymal stem cell transplantation for myocardial regeneration in heart attack patients (Kearns-Jonker et al., 2010, Rangappa et al., 2010, Sun et al., 2010). Consequently, in many cases, there is need for optimisation of treatment timing, cell type, dose and delivery method. Recently, it has been reported that cardiac stem cells can efficiently improve myocardial contractility in heart attack patients (Bolli et al., 2011). Moreover, the use of haematopoietic stem cells in autoimmune disorders such as multiple sclerosis and Wiskott-Aldrich disease has shown to markedly improve the patients' condition (Boztug et al., 2010, Capello et al., 2009). Nevertheless, in many cell-based therapies, it is still unclear whether there is long-term remission and whether the therapeutic benefits can outweigh the risks for example regarding the immunosuppression required for allogenic transplantation (Pasquini et al., 2010).

Studies using neural stem cells isolated from adult CNS biopsies and the fetal and neonatal brain are less advanced - although until now, no adverse effects have been

detected after transplantation of these cells in Phase I clinical trials for example in patients of the myelination disorder Pelizaeus-Merzbacher disease (PMD), patients with spinal cord injury and patients of amyotrophic lateral sclerosis (ALS) (Trounson et al., 2011). The efficacy of treatments using neural stem cells in various neurological disorders is unclear to date. However, there is evidence of persistent clinical benefits with regard to motor recovery and dopamine uptake in Phase II clinical trials with patients of Parkinson's disease after autologous NSC transplantation (Lévesque et al., 2009). Interestingly, the manipulation of NSCs might be an option for anti-cancer therapy. Modified NSCs producing a pro-drug activating enzyme (cytosine deaminase) have been transplanted into inoperable glioblastoma patients, where the NSCs target the tumour (Ostertag et al., 2011, Trounson et al., 2011). After the application of the non-toxic pro-drug 5-Fluorocytosine, the enzyme converts it into the cytotoxic anti-cancer drug 5-Fluorouracil which is expected to destroy the tumour. Glioblastoma patients are currently treated in Phase I/II clinical trials, but the efficacy of this treatment is still to be evaluated.

Preclinical studies for the first clinical application of human ES cell-derived cells is underway for the transplantation of ES-cell-derived oligodendrocytes into patients with spinal cord injury (comment in Alper, 2009). Furthermore, human ES cells have been successfully differentiated into pigmented epithelial progenitor cells and injected into patients of juvenile and age-related macular degeneration (Mason et al., 2011, Trounson et al., 2011). Similar to many studies using adult stem cells, the efficacy of treatments involving ES cells still needs to be proven. Unlike for adult neural stem cells, it remains elusive whether ES cells can be differentiated and purified sufficiently to prevent tumour formation in humans after transplantation. We are still at the very beginning of

characterising iPS cells and identifying the potential and risks of artificially induced pluripotency in cell-based therapy (Hayden, 2011, Dolgin, 2011).

Understanding *in vivo*-differentiation and survival of stem cells and their progeny is a prerequisite to governing *in vitro*-differentiation and functional integration of cells into tissues in general and of neurons into the diseased brain in particular.

1.3 Notch: Stem cell guard and fate determinator

One of the crucial factors in stem cell maintenance and cell fate decision from mid-gestation onwards is Notch. Notch signalling is one of a small number of pathways which is used iteratively in development to control stem cell function and regulate the generation of differentiated cells.

1.3.1 The discovery of Notch

Much from what is known to date about the Notch signalling pathway has been discovered in studies in *Drosophila*. The *Notch* locus was described almost a century ago when John S. Dexter found a X-linked dominant mutation in *Drosophila* which led to a notch in the wings of the mutant fruit fly (Dexter, 1914, Mohr, 1919, Morgan and Bridges, 1916). In 1983, the *Drosphila* Notch gene was cloned and since then, many studies have contributed to defining Notch signalling as one of the best-conserved pathways involved in development and stem cell biology (Artavanis-Tsakonas et al., 1983, Artavanis-Tsakonas et al., 1999). However, apart from elucidating more and more aspects of Notch signalling, recent work on Notch has also added a considerable complexity to what seemed to be a straightforward ligand-receptor interaction with no downstream secondary messengers (reviewed in Bray, 2006).

1.3.2 Notch receptors and Notch ligands

In contrast to the one Notch receptor in fruit flies, humans and mice carry four genes encoding for Notch receptors: *NOTCH1*, *NOTCH2*, *NOTCH3* and *NOTCH4*. Deficiency of Notch1 or Notch2 function leads to embryonic lethality in mice around embryonic

day (E) 11.5 with normal development observed until E9, indicating that Notch signalling does not play an essential role in early embryogenesis (Swiatek et al., 1994, Conlon et al., 1995, Hamada et al., 1999, Shi et al., 2005). Consistently, Notch activation in ES cells *in vitro* does not block differentiation of these cells (Schmitt et al., 2004). Lack of Notch3 and Notch4 does not result in abnormal development suggesting that Notch1 and Notch2 can compensate for their loss during embryogenesis (Krebs et al., 2000, Krebs et al., 2003). However, it has been reported that Notch3 and Notch4 are involved in vascular morphogenesis (Krebs et al., 2000, Domenga et al., 2004). Apart from the four Notch receptors, there are six Notch ligands known in mammals which are Delta1, Delta2, Delta3, Delta4, Jagged1 and Jagged2. Inactivation of Delta1, Delta4 or Jagged1 has been shown to lead to embryonic lethality in mice around mid-gestation similar to that seen in Notch1- or Notch2-deficient mice, whereas Jagged2-knockout mice die perinatally (Hrabe de Angelis et al., 1997, Duarte et al., 2004, Gale et al., 2004, Xue et al., 1999, Jiang et al., 1998). Prominent phenotypes in the above mentioned Notch receptor and Notch ligand mutants are excessive neuronal differentiation, abnormal vasculature and impaired somitogenesis.

1.3.3 The Notch protein

Notch receptors are single-pass transmembrane proteins containing large extracellular domains which consist mainly of epidermal growth factor (EGF)-like repeats which are sites for glycosylation and cysteine rich LIN (Lin-Notch) repeats (**Figure 12a**) (reviewed in Haines and Irvine, 2003). The Notch receptor generated in the endoplasmic reticulum (ER) interacts with the O-fucosyl transferase (O-Fut) which adds the first fucose which is essential for the generation of a functional Notch receptor

(**Figure 12b**) (Shi and Stanley, 2003, Sasamura et al., 2003, Okajima and Irvine, 2002). Furthermore, O-Fut has been shown to act as a chaperone for correct Notch folding and to mediate Notch transport from the ER to the plasma membrane (Okajima et al., 2005). Cell-type dependent O-Fut expression patterns have been suggested to contribute to spatial regulation of Notch activity (Okajima and Irvine, 2002). Intramolecular cleavage (S1) by Furin-like convertase in the Golgi apparatus generates the mature Notch receptor which is further glycosylated by other glycosyl transferases, such as the Fringe family of glycosyl transferases, on its way to the plasma membrane (**Figure 12c**) (reviewed in Haines and Irvine, 2003). Variations in glycosylation have been shown to alter Notch receptor ligand-affinity and -specificity (Haines and Irvine, 2003, Bruckner et al., 2000, Moloney et al., 2000, Sato et al., 2002).

1.3.4 Delta and Jagged

The physiological activation of Notch occurs by binding of a Notch ligand expressed in a neighbouring signal-sending cell to the Notch receptor in the signal-receiving cell. The Notch ligands Delta and Jagged are transmembrane proteins whose extracellular domain contains a N-terminal DSL (Delta, Serrate and Lag-2) domain essential for binding to the Notch receptor, several EGF-like repeats and in the case of Jagged Notch ligands, they also carry a cysteine rich domain (**Figure 12a**). Posttranslational modifications of these ligands have been shown to regulate Notch ligand activity. The E3 ubiquitin ligases Neuralized 1 and 2 (Neur1/2) and Mindbomb 1 and 2 (Mib1/2) have been shown to ubiquitinate Notch ligands enabling the interaction between Notch ligands and the ubiquitin-binding protein Epsin and Auxilin which is required for Notch ligand endocytic activation (**Figure 12d**) (Pavlopoulos et al., 2001, Le Borgne et al.,

2005, Wang and Struhl, 2004, Wang and Struhl, 2005, Hagedorn et al., 2006). Furthermore, in *Drosophila*, the immunoglobulin C2-type cell adhesion molecule Echinoid has been suggested to contribute to endocytic activation of Delta and Echinoid-mediated cell-cell contact can promote Notch-Delta interactions (Escudero et al., 2003, De Joussineau et al., 2003). Thus ligand localisation in the plasma membrane seems to also play a role in Notch ligand activity. This is corroborated by studies characterising protein-protein interaction domains such as PDZ-binding motifs in the intracellular domains of some Notch ligands. It has been shown that via these domains, Notch ligands bind to cytoplasmic scaffolding proteins which determine their localisation (Wright et al., 2004, Ascano et al., 2003, Pfister et al., 2003). Another factor to influence Notch signalling activity are soluble Notch ligands. Proteolytic cleavage at the plasma membrane results in soluble Delta and Jagged ligands which have been shown to inhibit Notch signalling in most circumstances (Klueg et al., 1998, Qi et al., 1999, Hicks et al., 2002, Mishra-Gorur et al., 2002, Sun and Artavanis-Tsakonas, 1997), although there are also reports about soluble Notch ligands activating the Notch pathway in certain cellular contexts (Hicks et al., 2002, Sapir et al., 2005, Chen and Greenwald, 2004).

1.3.5 Notch receptor endocytosis and trafficking

Another way of regulating the Notch pathway is via endocytosis and trafficking of the Notch receptor which controls the amount of Notch receptor available for signalling in the plasma membrane. The cytoplasmic Notch inhibitor Numb has been shown to be involved in Notch receptor ubiquitination, endocytosis and subsequent proteasome-dependent degradation (**Figure 12e**) (McGill and McGlade, 2003, Berdnik et al., 2002).

Furthermore, disruptions in certain parts of the endocytic pathway such as the sorting of ubiquitinated membrane proteins by the ESCRT complex results in dramatic hyperplasia due to Notch overactivation (Thompson et al., 2005, Vaccari and Bilder, 2005). Another protein involved in Notch internalisation is the E3 ubiquitin ligase Deltex which has been shown to either promote or inhibit Notch signalling by ubiquitination of the Notch intracellular domain dependent on Deltex binding partners and the cellular context (Mukherjee et al., 2005, Matsuno et al., 1995, Hori et al., 2004, Wilkin et al., 2008). Furthermore, the Itch/NEDD4/Su(dx) family of HECT domain E3 ubiquitin ligases have been reported to act as negative regulators of Notch signalling by adding ubiquitin to the Notch intracellular domain as a degradation signal. However, mutations in these HECT E3 ligases only lead to mild phenotypes suggesting that they are not critically involved in Notch regulation (Lai, 2002, Qiu et al., 2000, Sakata et al., 2004, Bray, 2006).

1.3.6 Notch activation

As a consequence of successful ligand binding to the Notch receptor, the metalloproteases ADAM10 (A disintegrin and metalloprotease 10; also known as Kuzbanian) and ADAM 17 (also known as TACE, tumour necrosis factor-α converting enzyme) mediates cleavage (S2) within the extracellular domain (**Figure 12f**) (Mumm et al., 2000, Fortini, 2001, Brou et al., 2000, Jarriault and Greenwald, 2005). This triggers intracellular cleavages (S3/4) of the Notch receptor by the Presenilin proteases of the γ-secretase complex which releases the transcriptionally active Notch intracellular domain (NICD) from the plasma membrane (Fortini, 2002, Selkoe and Kopan, 2003, Mumm and Kopan, 2000, Struhl and Adachi, 2000).

1.3.7 The Notch Intracellular Domain

The NICD consists of a RAM domain, six ankyrin repeats, nuclear localisation signals (NLS), a PEST domain and dependent on the type of Notch receptor additional protein-protein interaction motifs (**Figure 12a**). After S3/4 cleavages, the NICD translocates to the nucleus where it binds to the highly conserved DNA-binding protein RBPJ (recombination signal binding protein for immunoglobulin kappa J region; also known as CBF1, CSL) (**Figure 12g**). RBPJ is constitutively bound to the DNA and forms a trimeric complex with NICD and the co-activator Mastermind (Mam) (Nam et al., 2006, Wilson and Kovall, 2006, Wu et al., 2000, Petcherski and Kimble, 2000). This complex can then recruit further co-activators such as SKIP (Ski-interacting protein) and epigenetic modifiers such as histone acetylase p300 (Zhou et al., 2000, Wallberg et al., 2002). Another factor recruited to the complex is cyclin-dependent kinase-8 (CDK8). Precise regulation of the Notch pathway is a prerequisite for Notch function in the spatial and temporal regulation of cell fate decisions during development requiring that the nuclear effectors do not have a long half-life. CDK-8 phosphorylates NICD and thus NICD becomes a target for the F-box domain E3 ubiquitin ligase Fbw7 (F-box and WD repeat domain containing-7; also known as SEL-10) which ubiquitinates NICD for proteasome-dependent degradation (**Figure 12g**) (Fryer et al., 2004, Fryer et al., 2002, Gupta-Rossi et al., 2001, Wu et al., 2001, Oberg et al., 2001). In the absence of NICD, RBPJ remains bound to the DNA and forms a repressor complex recruiting the co-repressors Groucho, CtBP, SMRT, SHARP, SKIP, CIR and histone deacetylases (Zhou et al., 2000, Fryer et al., 2004, Nagel et al., 2005, Morel et al., 2001, Kao et al., 1998, Oswald et al., 2005, Hsieh et al., 1999). However, RBPJ-mutants only show modest derepression in a small number of cells such as sensory organ precursors in *Drosphila* (Barolo et al., 2000, Koelzer and Klein, 2003, Castro et al., 2005) indicating that RBPJ-

repressor complexes are only responsible for a small part of transcriptional repression of target genes while RBPJ function seems to be primarily to mediate NICD driven transcription (Morel and Schweisguth, 2000). Apart from the canonical RBPJ-dependent Notch pathway, Notch has been shown to act in some circumstances in a RBPJ-independent manner. For example, Notch inhibits muscle cell differentiation and can associate with components of the Wnt-signalling pathway such as β-catenin to regulate its transcriptional activity, both autonomously of RBPJ (Shawber et al., 1996, Nofziger et al., 1999, Brennan et al., 1997, Axelrod et al., 1996, Hayward et al., 2005). Rapid attenuation of Notch signalling has been shown to occur in some cells through an autoinhibitory feedback loop in which the Notch target genes of the Hes family of transcription factors can suppress Notch transcription (Pourquie, 2003, Giudicelli and Lewis, 2004). Furthermore, transient Notch pathway activation has been suggested to be controlled by destruction of the NICD (Fryer et al., 2004, Fryer et al., 2002).

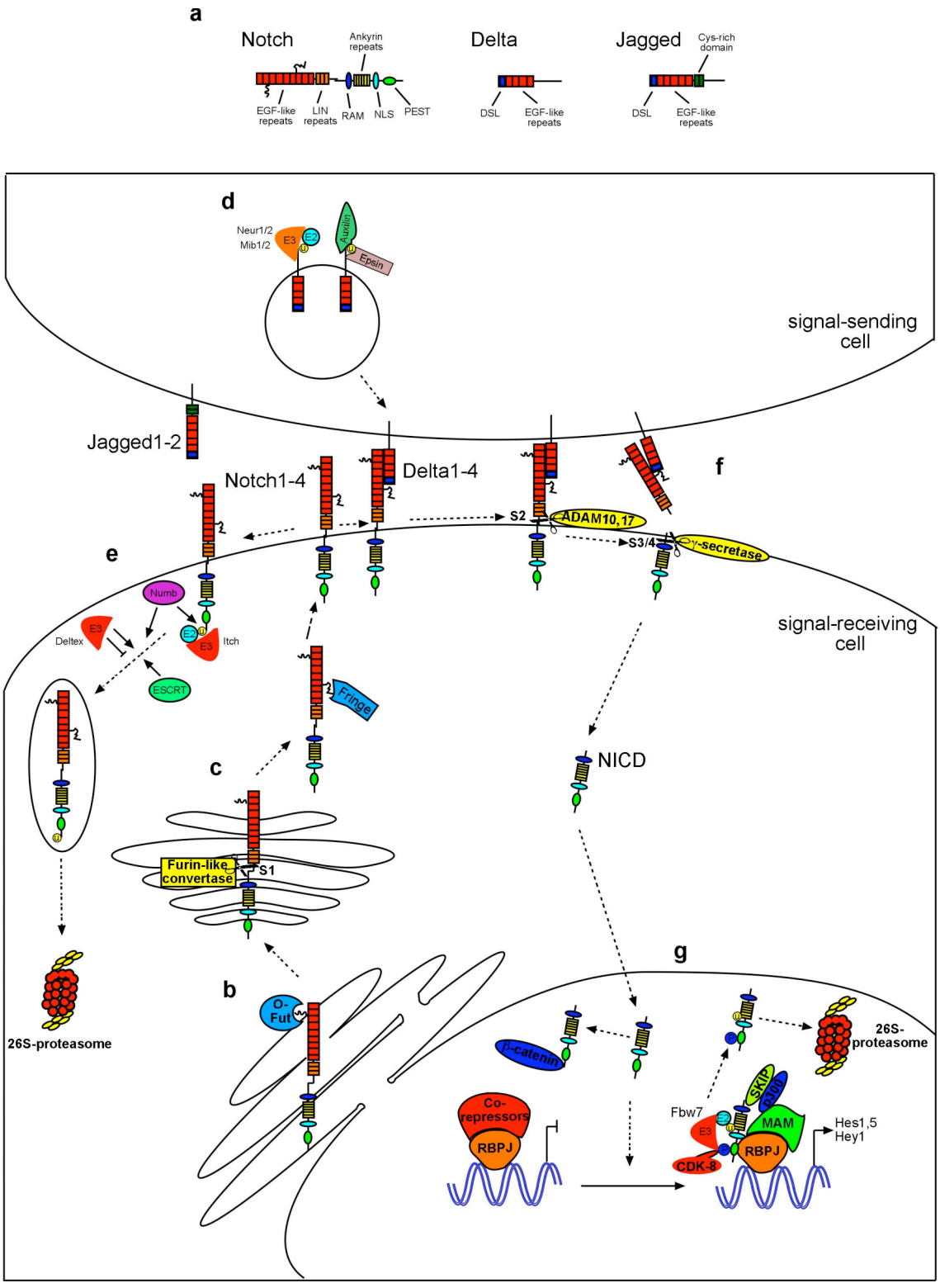

Figure 12 The Notch-signalling pathway
(**a**) Structural motifs of the Notch receptor and the Notch ligands Delta and Jagged. (**b**) Posttranslational fucosylation of the Notch receptor by the O-fucosyl transferase (O-Fut) in the endoplasmic reticulum (ER). (**c**) Intramolecular cleavage (S1) of the

Notch receptor by the Furin-like convertase in the Golgi apparatus and subsequent glycosylation of the Notch receptor by the Fringe family of glycosyl transferases. (**d**) Ubiquitination of Notch ligands by Neuralized 1 and 2 (Neur1/2) and Mindbomb 1 and 2 (Mib1/2) and subsequent binding of Epsin and Auxilin which is required for endocytic activation of Notch ligands. (**e**) Notch trafficking, endocytosis and potential proteasomal degradation is mediated by Numb, ESCRT and the E3 ubiquitin ligases Deltex and Itch. (**f**) Activation of the Notch receptor by ligand binding leads to S2 cleavage by ADAM10/17 and S3/4 cleavages by the γ-secretase complex, Notch intracellular domain (NICD) release from the plasma membrane and NICD translocation to the nucleus. (**g**) In the nucleus, NICD binds to RBPJ and Mastermind (Mam) and together with other co-activators such as SKIP and p300 activates transcription of typical target genes such as *Hes1/5* and *Hey1* (Hairy/enhancer-of-split related with YRPW motif 1). In the absence of NICD, RBPJ is bound by co-repressors. Fbw7 ubiquitinates the NICD after NICD-phosphorylation by CDK8 which leads to proteasomal degradation. The NICD can also interact with other proteins in the nucleus for example β-catenin.

1.3.8 Notch in lateral inhibition

The Notch ligand-receptor interaction proves to be ideal for cell fate decisions which follow the lateral inhibition model. Cells undergoing differentiation upregulate Notch ligands which inhibit differentiation in the Notch receptor expressing neighbouring cell (Doe and Goodman, 1985, Seydoux and Greenwald, 1989, Nye et al., 1994, Kopan et al., 1994, Henrique et al., 1995, Chitnis et al., 1995, Henrique et al., 1997, Kawaguchi et al., 2008b). Recent work from Sprinzak *et al.* showed that apart from activating *trans*-interactions of Notch receptor and ligand expressed on neighbouring cells, *cis*-interactions of Notch receptor and ligand which inhibit each other can occur on the same cell (Sprinzak et al., 2010). By this mechanism, the difference in Notch receptor and ligand between neighbouring cells is amplified and generates mutually exclusive Notch signalling states in these cells. Furthermore, it has been reported that in *Drosophila* neural development, filopodia containing Delta can also activate Notch signalling in non-neighbouring cells allowing one cell to influence a cohort of cells in tissue development (De Joussineau et al., 2003, Milan and Cohen, 2010). The required

cell-cell contact makes Notch signalling dispensable for early embryogenesis where gradients of soluble factors activate for example BMP-, Wnt- and Shh-signalling for patterning and germ layer specification (Shi et al., 2005). However, Notch has been implicated in boundary formation between different developmental structures (reviewed in Irvine, 1999).

1.3.9 Notch in cell fate decisions

Within various tissues, Notch-signalling has been shown to be involved in somatic stem cell maintenance and lineage decisions. In the haematopoietic system, Notch is essential for the formation of haematopoietic stem cells (HSCs) from early haematogenic endothelial cells (**Figure 13a**) (Kumano et al., 2003, Hadland et al., 2004). Also in the adult, Notch activation in HSCs by neighbouring cells in the osteoblastic niche is crucial for HSC maintenance and inhibits differentiation (Calvi et al., 2003, Duncan et al., 2005). Furthermore, Notch signalling has been reported to inhibit myeloid differentiation from precursors (reviewed in Suzuki and Chiba, 2005), to favour T cell development over B cell development at the progenitor stage (Radtke et al., 1999, Pui et al., 1999), to promote thymocyte differentiation and proliferation (Ciofani et al., 2004, Hadland et al., 2001) and to be crucial for marginal B cell development in the spleen (Kuroda et al., 2003, Saito et al., 2003, Tanigaki et al., 2002). During vasculature formation, Notch is involved in endothelial cell migration and proliferation (Iso et al., 2003, Krebs et al., 2000), smooth muscle cell maturation (Domenga et al., 2004), vascular remodelling processes (Iso et al., 2003) and arterial-venous specification promoting the arterial fate (Domenga et al., 2004, Duarte et al., 2004, Gale et al., 2004, Krebs et al., 2004, You et al., 2005). Furthermore, it has been shown that Notch

function in the vascular system is highly dependent on its target genes of the Hey (Hairy/enhancer-of-split related with YRPW motif) family of transcription factors (Fischer et al., 2004, Iso et al., 2003). To date, Notch has been found to control lineage specification in many tissues. In the pancreas, Notch inhibits endocrine-lineage differentiation (Apelqvist et al., 1999, Jensen et al., 2000). In the intestine, Notch is required for stem cell/progenitor maintenance and promotes absorptive progenitor differentiation while inhibiting the secretory lineages (**Figure 13b**) (Fre et al., 2005, Milano et al., 2004, Sancho et al., 2010, van Es et al., 2005).

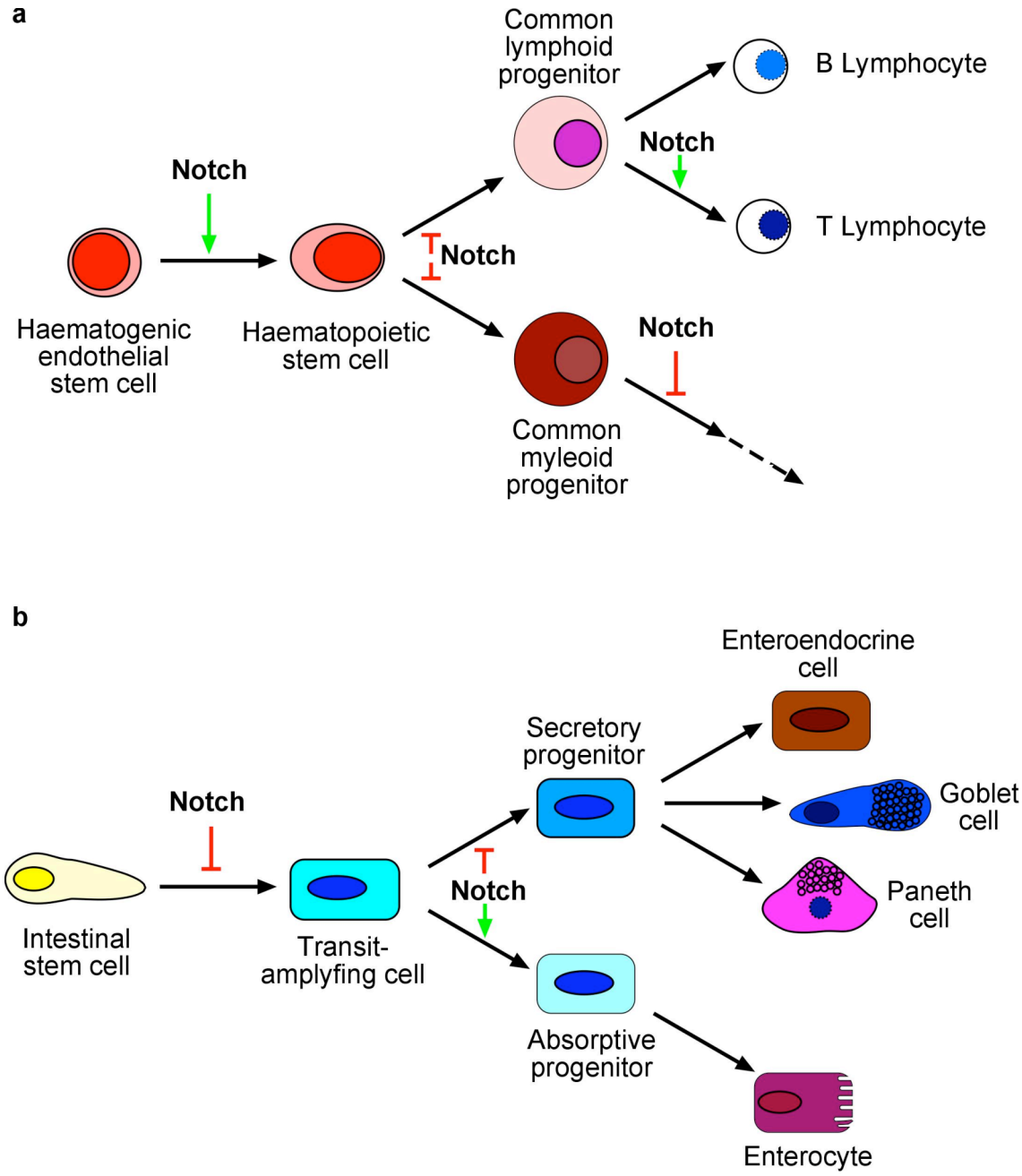

Figure 13 Notch signalling in haematopoietic and intestinal differentiation
(**a**,**b**) Schematic representation of (**a**) haematopoietic and (**b**) intestinal differentiation and the role of Notch in inhibiting or promoting cell fates. In (**a**), further differentiation of the common myeloid progenitor is not depicted for clarity.

1.3.10 Notch in neural development

The paradigm of Notch function in cell fate decisions has been established in *Drosophila* neural development (Artavanis-Tsakonas et al., 1995, Poulson, 1940). Attenuation of Notch signalling has been shown to result in precocious neuronal differentiation of neuroectodermal cells (Poulson, 1940, Gaiano and Fishell, 2002, de la Pompa et al., 1997, Lutolf et al., 2002). Furthermore, Notch is essential for neural stem cell maintenance (**Figure 14**) (Hitoshi et al., 2002). In the nervous system, Notch function is predominantly mediated by its target genes of the Hes (particularly *Hes1* and *Hes5*) and Hey family of transcription factors which repress pro-neural transcription factors such as Ascl1 in the ventral forebrain and Neurogenin1 and 2 in the cortex (Ishibashi et al., 1995, Kageyama and Ohtsuka, 1999, Ohtsuka et al., 1999, Hatakeyama et al., 2004, Kageyama et al., 2008, Nieto et al., 2001, Powell and Jarman, 2008). Furthermore, Notch downregulation has been shown to be crucial for correct neuronal maturation, for example with regard to dendritic arborisation and axonal guidance (Berezovska et al., 1999, Redmond et al., 2000, Sestan et al., 1999, Giniger, 1998, Le Gall et al., 2008, Song and Giniger, 2011). Apart from inhibiting neurogenesis, Notch can promote gliogenesis in some contexts (Morrison et al., 2000, Furukawa et al., 2000). It has been proposed that Notch acts in a stepwise manner, in which it firstly promotes glia precursor development and then favours astrocyte over oligodendrocyte differentiation (**Figure 14**) (Grandbarbe et al., 2003). However, recent work has suggested that the role of Notch in glia differentiation is rather permissive than instructive (reviewed in Cau and Blader, 2009). Interestingly, recent findings propose that Notch might also play a role in binary fate choices in neuronal differentiation. It has been reported that Notch is involved in the formation of excitatory and inhibitory interneurons in the spinal cord where Notch acts in a context-dependent manner.

Whereas Notch activation promotes excitatory interneuron generation dorsally, it favours inhibitory interneuron generation ventrally (Mizuguchi et al., 2006, Peng et al., 2007).

Direct transcriptional targets of Notch in neural development are BLBP and GFAP which are markers of subsets of radial glia and astroglia cells (Anthony et al., 2005, Ge et al., 2002). Notably, as discussed above, radial glia cells and reactive astroglia are subpopulations of neural stem cells in the developing and adult central nervous system (CNS) linking Notch's function in stem cell maintenance to its function in gliogenesis (reviewed in Gaiano and Fishell, 2002). With regard to radial glia cells in the developing cortex, it has been suggested that differentiating neurons which express Notch ligands migrate alongside the radial glia process into the upper layers of the cortex, thereby activating the Notch pathway in the radial glia cell to maintain its stem cell character (**Figure 9**) (Campos et al., 2001). Furthermore, recent work from Yoon *et al*. reported that Mib1 which is essential for Notch ligand activation is primarily expressed in intermediate progenitors in the cortical subventricular zone and that Mib1 deletion resulted in depletion of radial glia cells and precocious differentiation (Yoon et al., 2008). This study showed that apart from differentiating neurons, also intermediate progenitors are an important source for Notch ligands to stimulate radial glia stem cell maintenance. Furthermore, the notion that Notch signalling is attenuated in intermediate progenitors was corroborated by identifying Tbr2, a *bona fide* marker for intermediate progenitors, as a target of the pro-neural transcription factor Neurogenin 2 which is repressed by Notch in radial glia cells (Ochiai et al., 2009). Apart from differences in Notch activation between intermediate progenitors in the cortical SVZ and radial glia in the VZ, two distinct cell populations differing in Notch/Hes5 levels have been identified

within the VZ (Kawaguchi et al., 2008a, Basak and Taylor, 2007, Mizutani et al., 2007). This suggests that Notch is also involved in generating stem cell heterogeneity in the VZ, however the mechanism of how distinct subsets of stem cells utilise Notch is unclear (Pierfelice et al., 2011). It is likely that cell type-dependent Notch function is due to signalling integration into the network of other pathways. For example, the Notch-targets Hes1 and Hes5 form complexes with JAK2 (Janus kinase 2) and STAT3 (signal transducer and activator of transcription 3) for mutual positive regulation in radial glia which has been shown to be important for stem cell maintenance (Kamakura et al., 2004). Also in the adult brain, Notch has been shown to be required for stem cell maintenance (Ables et al., 2010, Breunig et al., 2007, Ehm et al., 2010, Imayoshi et al., 2010).

Taken together, Notch signalling is of crucial importance during later stages of embryonic development where it regulates somatic stem cell maintenance and makes binary cell fate decisions within various tissues. However, the mechanisms controlling Notch activation or attenuation required at specific developmental steps is incompletely understood.

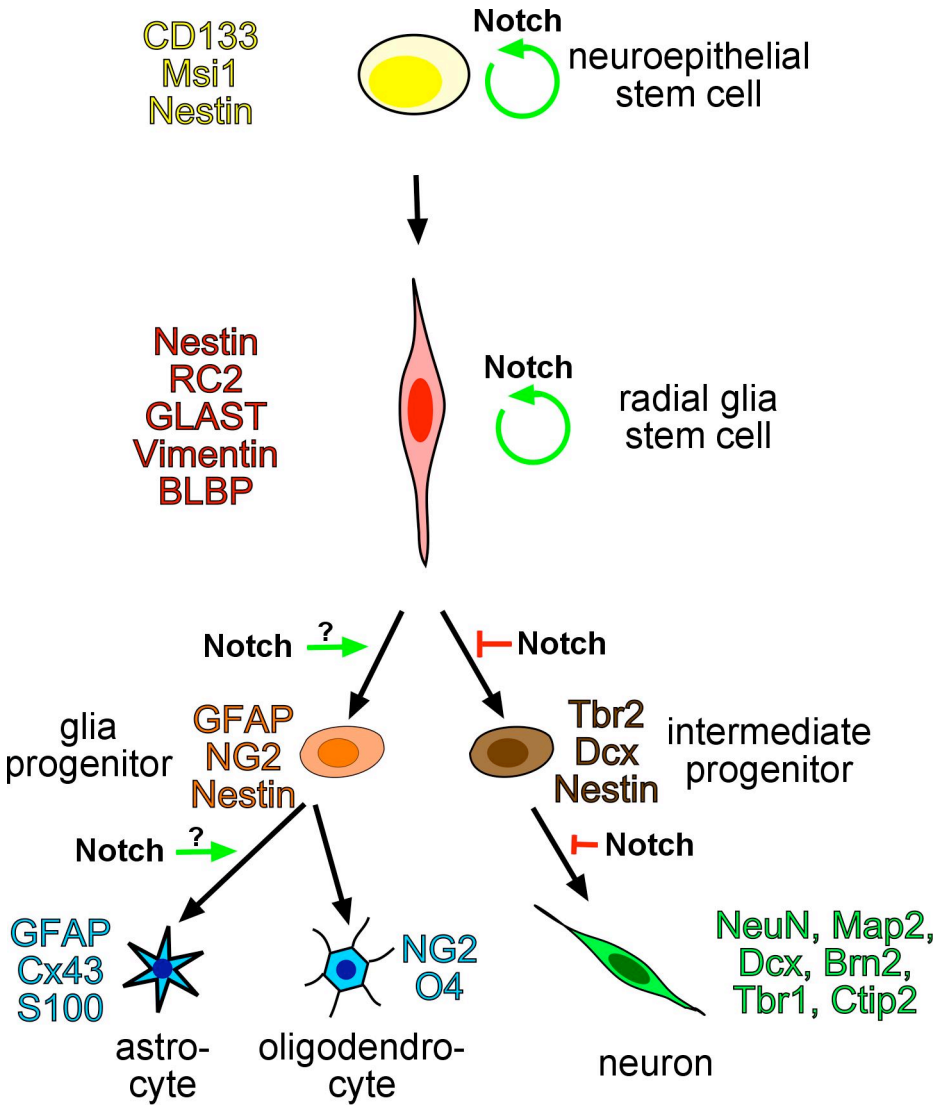

Figure 14 Notch signalling in neural differentiation
Schematic representation of neural differentiation and Notch signalling inhibiting or promoting cell maintenance (round arrow) and cell fate decisions.

1.4 JNK/c-Jun signalling: Proliferate, die or regenerate

1.4.1 The discovery of the *Jun* oncogene

In contrast to Notch, Jun was not discovered due to its role in development. In 1987, Lee *et al*. found a DNA-binding protein which was able to induce gene transcription and therefore was named activator protein 1 (AP-1), but the encoding gene was not identified at the time (Lee et al., 1987). AP-1 dependent transcription of the model genes used [metallothionein, collagenase and the oncogenic Simian virus 40 (SV40)] was strongly induced by treatment with the tumour promoter 12-O-tetradecanoyl phorbol 13-acetate (TPA). Thus the AP-1 binding site is also known as the TPA response element (Lee et al., 1987, Angel et al., 1987). Strikingly, the AP-1 binding site sequence TGA(C/G)TCA was the same as the DNA binding site of the yeast protein Gcn4 (general control nonderepressible 4) which had been shown to activate transcription (Lucchini et al., 1984, Thireos et al., 1984, Hope and Struhl, 1985). At the same time as the discovery of AP-1, Maki *et al*. cloned the *Jun* oncogene from avian sarcoma virus 17 which showed sequence homology to Gcn4 and was proven to also share functional homology (Maki et al., 1987, Vogt et al., 1987, Struhl, 1987). Shortly after that, Bohmann *et al*. and Angel *et al*. reported that indeed, Jun was AP-1 (Bohmann et al., 1987, Angel et al., 1988a). Thus, Jun was the first oncogenic transcription factor.

1.4.2 c-Jun homo- and heterodimerisation

Apart from Gcn4 and Jun, the oncoprotein Fos shared the same DNA binding site sequence (Curran et al., 1982, Curran and Teich, 1982a, Franza et al., 1988, Rauscher et al., 1988b). Interestingly, Fos was found to be tightly associated with a protein called

p39 (Curran and Teich, 1982b). The fact that Gcn4 can dimerise led to the discovery that indeed, Jun is p39 and can dimerise with Fos (Rauscher et al., 1988a, Sassone-Corsi et al., 1988). The structural explanation followed promptly by Landschulz *et al*. who discovered that several DNA-binding proteins including Jun and Fos contain a protein dimerisation domain called the leucine zipper domain (Landschulz et al., 1988). Apart from Jun [identified as viral Jun (v-Jun) and homologous to cellular Jun (c-Jun)] and Fos (c-Fos), other members of these basic-zipper (bZIP) families of transcription factors have also been discovered, namely JunB and JunD of the Jun-family (Nakabeppu et al., 1988, Ryder et al., 1988) and FosB, Fra1 and Fra2 of the Fos-family (Franza et al., 1988, Cohen and Curran, 1988, Foletta et al., 1994, Zerial et al., 1989). Dimerisation of c-Jun is essential for DNA-binding (Halazonetis et al., 1988, Smeal et al., 1989). While c-Jun can either homo- or heterodimerise, Fos cannot form homodimers (Halazonetis et al., 1988). Other bZIP-transcription factor families have been identified to heterodimerise with c-Jun, such as the activating transcription factor (ATF) family (Benbrook and Jones, 1990). Furthermore, it has been shown that the heterodimerisation partners can alter DNA-binding specificity, for example the c-Jun/ATF2 dimer binds to the cAMP-responsive element (CRE) sequence TGACGTCA rather than the TPA response element TGA(C/G)TCA (Hai and Curran, 1991, Ivashkiv et al., 1990).

1.4.3 Mitogen-activated protein (MAP) kinase signalling

Another milestone was the discovery of the Jun N-terminal kinase (JNK), also known as stress activated protein kinase (SAPK) (reviewed in Kyriakis et al., 1994), which phosphorylates and activates c-Jun linking it to the mitogen-activated protein (MAP) kinases signalling pathway (Pulverer et al., 1993, Hibi et al., 1993, Derijard et al.,

1994). For its growth-promoting and oncogenic activity, c-Jun requires the upstream signal from JNK (reviewed in Vogt, 2001). Together with extracellular signal-regulated kinase (ERK) and p38, JNK constitutes the MAP kinases (MAPKs) (**Figure 15a**). JNKs are expressed from three different genetic loci. *JNK1*, *JNK2* and *JNK3* give rise to multiple isoforms due to alternative splicing (reviewed in Davis, 2000). Whereas JNK1 and JNK2 are widely expressed throughout the body, JNK3 expression is restricted to neural and cardiac cells (Gupta et al., 1996). JNK1, 2 and 3 can be activated by MAPK kinases (MAPKKs, MAP2Ks, MKKs, JNKKs). JNKK1 and JNKK2 (also known as MKK4 and MKK7) phosphorylate the activation (or T) loop of JNK, which is a common structural feature of all protein kinases (Hagemann and Blank, 2001, Goldsmith and Cobb, 1994). Upstream to JNKK1 and JNKK2, there is a large number of MAPKKK (MAP3Ks) which can act in a stimulus- and cell type-specific manner (Davis, 1995). The most potent activators of JNK signalling are the MEK (MAP/ERK kinase) kinases (MEKK). MEKK1, 2, 3 and 4 phosphorylate and activate JNKK1 and MEKK1, 2 and 3 can also activate JNKK2 (Minden et al., 1994, Blank et al., 1996, Gerwins et al., 1997). Other MAP3Ks discovered to activate JNK signalling are for example the apoptosis signal regulating kinases 1 and 2 (ASK1, 2) (Ichijo et al., 1997, Wang et al., 1998) and the mixed lineage kinases 2 and 3 (MLK2, 3) (Tibbles et al., 1996, Hirai et al., 1996).

Signalling specificity within the MAPK pathways with their large number of possible protein-protein interactions is mediated via scaffolding proteins which form JNK signalling modules (**Figure 15b**). The JNK interacting protein 1 (JIP1) for example provides a scaffold for MLK3/JNKK2/JNK1 interaction after excitotoxic stress in neurons which leads to c-Jun activation (Yasuda et al., 1999, Morrison and Davis,

2003). However, some MAP3Ks can serve as scaffolds on their own, for example MEKK2 mediates the formation of the MEKK2/JNKK2/JNK1 module which activates c-Jun (Cheng et al., 2000). Notably, other stimuli in other cell types trigger distinct JNK signalling module formation and target activation. For instance, T cell receptor (TCR) or TGF-β receptor signalling results in MEKK1/JNKK1/JNK1 module assembly and subsequent activation of the JNK target Itch (Xia et al., 1998).

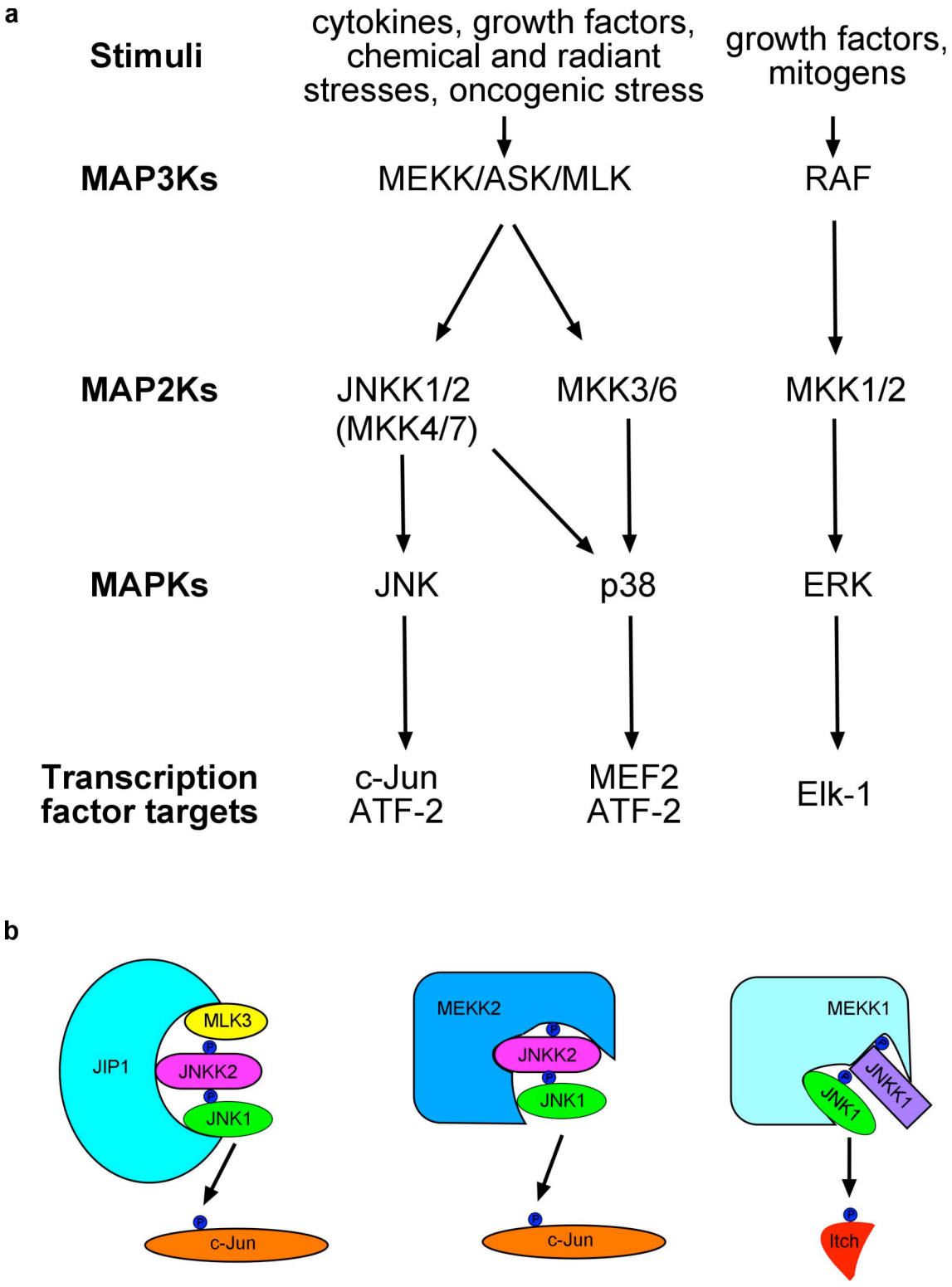

Figure 15 MAPK signalling and JNK signalling modules
(**a**) Schematic representation of MAPK signalling cascades which are activated by various stimuli. MAP3Ks phosphorylate and activate MAP2Ks. MAP2Ks, in turn, phosphorylate and activate MAPKs which phosphorylate and activate specific transcription factor targets. (**b**) Drawing of JNK signalling modules which provide

signalling specificity. Scaffolding proteins such as JIP1 together with MAP3Ks bind JNK signalling proteins to induce specific JNK signalling cascades which results in distinct target gene activation and biological outcome. P, phosphate.

1.4.4 Regulation of JNK/c-Jun signalling

JNK/c-Jun signalling can be activated by various extracellular stimuli, such as growth factors, inflammatory cytokines, oncogenic stress, for instance through Ras, chemical stress, e.g. phorbol-esters, and radiant stress, for example UV-irradiation (**Figure 15a**) (Lamph et al., 1988, Dunn et al., 2002). JNK binds to the delta docking (DD) region at the c-Jun N-terminus and phosphorylates c-Jun N-terminally at serine 63 and serine 73 within the c-Jun transactivation domain which has been shown to enhance c-Jun transactivation funtion (**Figure 16**) (Smeal et al., 1991). Furthermore, recent publications showed that JNK also phosphorylates threonine 91 and threonine 93 within the N-terminal transactivation domain, which was implicated in promoting apoptosis as a consequence of DNA-damage through continous genotoxic stress (Morton et al., 2003, Vinciguerra et al., 2008). Threonine 91 and threonine 93 phosphorylation by JNK is facilitated by phosphorylation of threonine 95 by kinases of the ataxia telangiectesia mutated (ATM)-signalling pathway (Vinciguerra et al., 2008). However, which c-Jun functions depend on phosphorylation at serine 63 and 73 or threonine 91 and 93 or at all of these four sites is incompletely understood. Apart from the function in transactivation, phosphorylation at serine 63 and 73 and threonine 91 and 93 has also been shown to be important for c-Jun recognition by the E3 ubiquitin ligase Fbw7 for subsequent degradation of N-terminally phosphorylated c-Jun (**Figure 16**) (Nateri et al., 2004). Notably, these four JNK-phosphorylation sites can be moderately phosphorylated by ERK, however the *in vivo* effects of this phosphorylation might be sub-threshold (Morton et al., 2003, Raivich, 2008).

An indirect way of ERK- and phosphoinositide-3-kinase (PI3K)-signalling to influence c-Jun action is via phosphorylation and thus inactivation of glycogen synthase kinase-3 (GSK3). After a priming phosphorylation by an unidentified kinase at threonine 243, GSK3 phosphorylates c-Jun at threonine 239, which is an alternative way to render c-Jun into a Fbw7-target independent of JNK-phosphorylation (**Figure 16**) (Wei et al., 2005). Furthermore, activation of MAPK signalling by various stimuli has been shown to induce dephosphorylation at threonine 243 by an unidentified phosphatase which results in stabilisation of c-Jun (Morton et al., 2003, Wei et al., 2005). Another way of degrading c-Jun has been shown in T cells where c-Jun is targeted by the E3 ubiquitin ligase Itch independently of c-Jun phosphorylation status (Gao et al., 2004). Itch can be phosphorylated and activated by JNK and subsequently degrades c-Jun in a negative feedback mechanism (Gao et al., 2004). However, the *Jun* gene is a target of the c-Jun transcription factor so that c-Jun can autoregulate its levels in a positive feedback loop (Angel et al., 1988b).

Furthermore, ERK plays a role in regulating c-Jun transactivation by phosphorylating and activating p300 (**Figure 16**). The co-activator p300 acetylates lysines 268, 271 and 273 in the c-Jun C-terminal basic region (BR) which together with the leucine zipper (LZ) domain is responsible for DNA binding. Consequently, p300 and acetylated c-Jun form a DNA binding complex which can enhance c-Jun transactivation function (Wang et al., 2006).

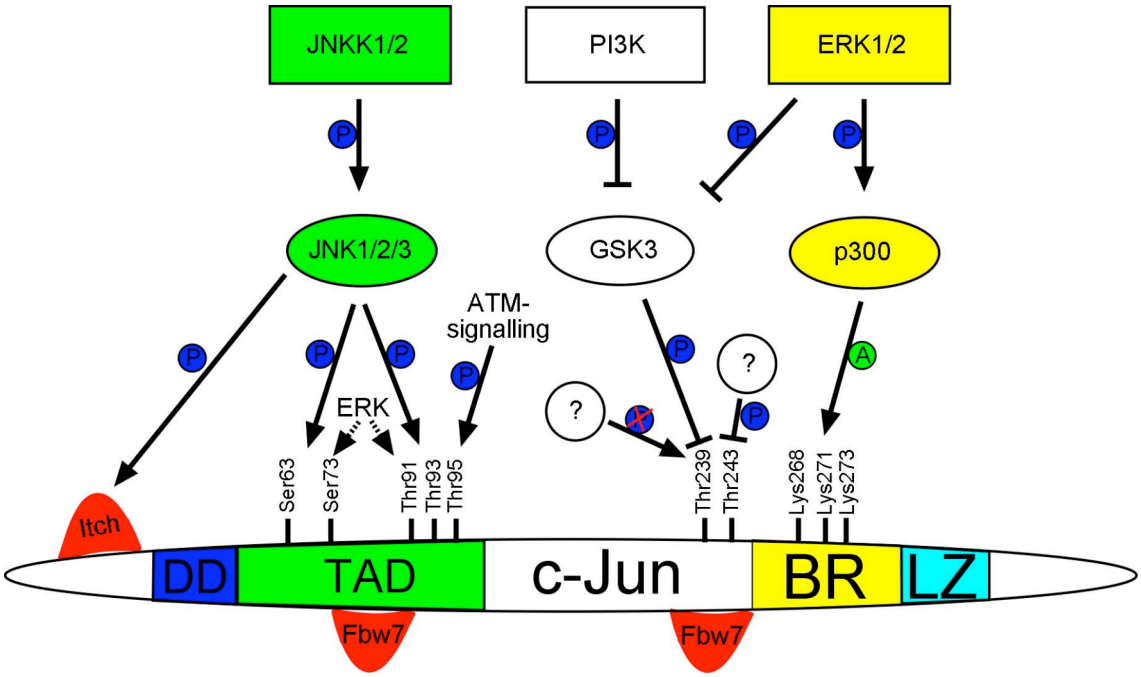

Figure 16 c-Jun regulation
Schematic representation of the c-Jun transcription factor and its regulation by JNKK/JNK-, PI3K- and ERK-signalling. DD, delta docking region. TAD, transactivation domain. BR, basic region. LZ, leucine zipper domain. P, phosphorylation. A, acetylation.

1.4.5 JNK/c-Jun signalling function

During embryonic development, JNKs seem to have at least in part redundant functions. Neither *JNK1*$^{-/-}$ nor *JNK2*$^{-/-}$ nor *JNK3*$^{-/-}$ mice show lethality or obvious developmental defects (Yang et al., 1997, Yang et al., 1998, Dong et al., 1998, Chang and Karin, 2001). Also *JNK1*$^{-/-}$; *JNK3*$^{-/-}$ and *JNK2*$^{-/-}$; *JNK3*$^{-/-}$ double mutant mice survive and exhibit no apparent phenotypes (Kuan et al., 1999). However, *JNK1*$^{-/-}$; *JNK2*$^{-/-}$ double mutant mice die around E11.5 due to defects in neural tube closure resulting in hindbrain exencephaly which might be in part due to dysregulated apoptosis (Kuan et al., 1999). c-Jun-deficient mice are embryonic lethal around mid- and late-gestation with the latest time point to derive mutant embryos around E15.5 (Hilberg et al., 1993). *Jun*$^{-/-}$ embryos exhibit a severe defect in hepatogenesis.

In order to study JNK-dependency of c-Jun actions, Behrens *et al*. generated $Jun^{AA/AA}$ mice which carry *Jun* alleles with inactivating mutations of the two major N-terminal JNK-phosphorylation sites (Ser63Ala, Ser73Ala) (Behrens et al., 1999). Interestingly, $Jun^{AA/AA}$ mice are viable and show no apparent developmental defects indicating that c-Jun function during embryogenesis does not require serine 63 and 73 phosphorylation (**Figure 17**). On the contrary, $Jun^{AA/AA}$ mice are protected from neuronal apoptosis induced by excitotoxic stress (kainate) suggesting that c-Jun action in neuronal apoptosis is dependent on JNK-mediated phosphorylation at serine 63 and 73 (Behrens et al., 1999). Moreover, mouse embryonic fibroblasts (MEFs) isolated from c-Jun-deficient embryos exhibit a severe proliferation defect and undergo premature senescence (Johnson et al., 1993). In contrast, Behrens *et al*. have reported a moderate defect in MEF proliferation and no premature senescence in $Jun^{AA/AA}$ cultures indicating that serine 63 and 73 phosphorylation by JNK is partially involved in c-Jun action in proliferation and not in senescence (**Figure 17**) (Behrens et al., 1999). However, the function of these phosphorylations in preventing premature senescence is unclear, since data from two studies point towards JNK-independent and JNK-dependent c-Jun action (Behrens et al., 1999, Wada et al., 2004).

Furthermore, JNK/c-Jun signalling is involved in epithelial sheet migration during development. In *Drosophila*, the JNK/c-Jun pathway plays an essential role for epithelial cell elongation and migration in dorsal closure during mid-embryogenesis (Glise et al., 1995, Riesgo-Escovar and Hafen, 1997a, Riesgo-Escovar and Hafen, 1997b, Hou et al., 1997, Kockel et al., 1997). Reminiscent to dorsal closure in *Drosophila*, fusion of the developing eyelids during mammalian embryogenesis is JNK/c-Jun-dependent (Xia and Karin, 2004).

At later stages of embryonic development and in the adult, JNK1 and JNK2 play similar roles in activating c-Jun to induce programmed cell death of inactive thymocytes (Behrens et al., 2001, Sabapathy et al., 2001, Rincon et al., 1998). However, in other cellular contexts, JNK1 and JNK2 have been suggested to have opposite effects. After exiting the thymus, T helper (Th) cells differentiate into two classes of effector T cells, i.e. Th1 and Th2 cells, which differ in their profiles of secreted cytokines. Whereas *JNK1*$^{-/-}$ mice preferentially express a Th2 profile of secreted cytokines (Dong et al., 1998), *JNK2*$^{-/-}$ mice show the inverse phenotype, i.e. an increased Th1 response (Yang et al., 1998). Similarly, whereas JNK1 phosphorylates c-Jun to increase fibroblast proliferation upon serum stimulation, JNK2 phosphorylates c-Jun in unstimulated fibroblasts and thus contributes to its degradation (Sabapathy et al., 2004). In the intestine, it has recently been reported that activation of JNK/c-Jun signalling leads to increased progenitor proliferation and accelerated tumour development (Sancho et al., 2009).

Furthermore, JNK/c-Jun signalling has been shown to be involved in metabolic control (reviewed in Hotamisligil, 2003). It has been suggested that obesity-induced expression of pro-inflammatory cytokines leads to JNK activation which contributes to the development of insulin resistance and subsequent Type II Diabetes (Aguirre et al., 2000, Hirosumi et al., 2002). Strikingly, *JNK1*$^{-/-}$ mice as well as *JIP1*$^{-/-}$ mice show decreased fat build up and are resistant to developing insulin-resistance, whereas *JNK2*$^{-/-}$ mice are indistinguishable from wild type (wt) mice (Hirosumi et al., 2002, Jaeschke et al., 2004). In the light of these findings, JNK inhibitors have been tested and found to induce improved insulin sensitivity in animal models of diabetes (reviewed in Bogoyevitch et al., 2004).

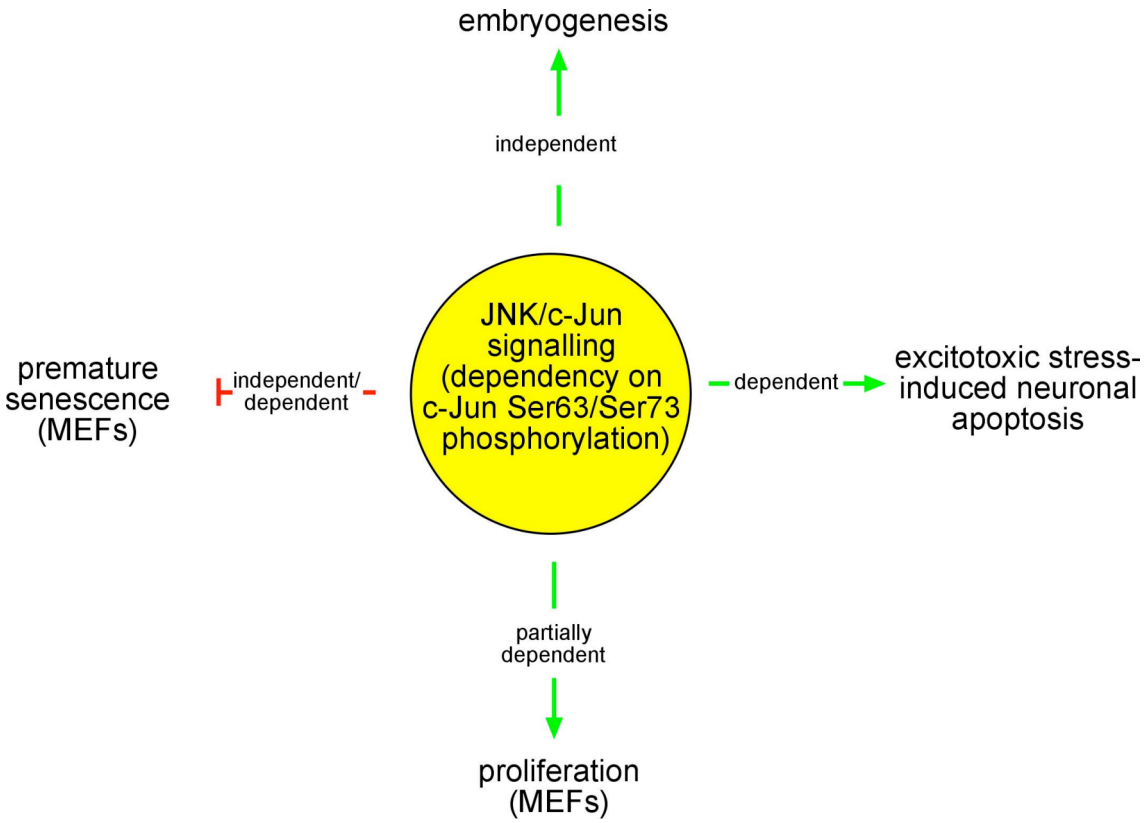

Figure 17 Dependency of c-Jun functions on Ser63/Ser73 phosphorylation by JNK
Schematic representation of c-Jun functions and their dependency on N-terminal phosphorylation of c-Jun at serine 63 and serine 73 by JNK. Green lines point towards actions promoted by JNK/c-Jun, red lines point towards actions inhibited by JNK/c-Jun.

1.4.6 JNK/c-Jun signalling in the nervous system

Many of the JNK signalling components show particularly high expression in the nervous system underscoring the importance of JNK signalling in this tissue (Nateri et al., 2004, English et al., 1995, Casanova et al., 1996, Gupta et al., 1996, Lee et al., 1999, Kim et al., 1999, Zhang et al., 2003a, Zhang et al., 2003b). JNK/c-Jun signalling has mainly been associated with regulating apoptosis in the nervous system. c-Jun mediated apoptosis has been shown to involve expression of target genes Fas ligand (*FasL*) and pro-apoptotic members of the *Bcl2*-family of genes such as *Bim* (Bcl-2 interacting mediator of cell death) and *dp5* (death protein 5) (Le-Niculescu et al., 1999, Bossy-

Wetzel et al., 1997, Whitfield et al., 2001, Ma et al., 2007). During embryonic neural development, c-Jun is widely expressed after neurulation (Bennett et al., 1997). Strong c-Jun expression has been detected before and during periods of intense programmed cell death (Sun et al., 2005). Motoneurons that lack survival-promoting signals and thus undergo apoptosis exhibit high levels of phosphorylated c-Jun (in the following, 'phosphorylated c-Jun' stands for 'N-terminally phosphorylated c-Jun'). Also *in vitro*, withdrawal of nerve growth factor (NGF) trophic support from PC12 neuronal cell cultures results in upregulation of phosphorylated c-Jun and increased cell death which can also be induced by c-Jun over-expression and can be prevented by dominant-negative c-Jun expression (Ham et al., 1995). In the early developing brain, JNK/c-Jun signalling acts in a more complex way. Around E9.5, *JNK1*$^{-/-}$; *JNK2*$^{-/-}$ mice show reduced apoptosis in the hindbrain followed by increased apoptosis in the forebrain and hindbrain at E10.5 (Kuan et al., 1999, Sabapathy et al., 1999). This indicates that JNK/c-Jun signalling has anti- and pro-apoptotic function during brain development dependent on the spatial and temporal context. However, c-Jun is not essential for apoptosis during CNS development as deletion of c-Jun does not alter physiological cell death (Roffler-Tarlov et al., 1996, Herzog et al., 1999). In the postnatal brain, c-Jun has been implicated with apoptosis following a plethora of excitotoxic stresses. c-Jun activation has been reported after brain ischaemia (Kindy et al., 1991, Wessel et al., 1991), trauma (Herdegen et al., 1991, Jenkins and Hunt, 1991, Raivich et al., 2004) and seizures (Morgan and Curran, 1988, Gall et al., 1990, Gass et al., 1993). Furthermore, upregulation of phosphorylated c-Jun has also been linked to loss of neurons in neurodegenerative diseases such as amyotrophic lateral sclerosis (ALS) (Migheli et al., 1997), Alzheimer's dementia (Pearson et al., 2006, Thakur et al., 2007) and Parkinson's

disease (Oo et al., 1999, Saporito et al., 2000) making JNK/c-Jun signalling a promising therapeutical target in these diseases (Silva et al., 2005, Borsello and Forloni, 2007).

As mentioned, *Jun*$^{AA/AA}$ mice show resistance to neuronal apoptosis induced by kainate which causes seizures and apoptosis of hippocampal neurons (Behrens et al., 1999). Similarly, *JNK3*$^{-/-}$, but not *JNK1*$^{-/-}$ and *JNK2*$^{-/-}$ mice are resistant to kainate-induced apoptosis (Yang et al., 1997, Kuan et al., 1999). Furthermore, *JNK3*$^{-/-}$ mice have been shown to be resistant to ischaemic apoptosis and to cell death of dopaminergic neurons in an animal model of Parkinson's disease [1-methyl-4-phenyl-1,2,4,6 tetrahydropyridine (MPTP) treatment] (Kuan et al., 2003, Hunot et al., 2004). Thus, it has been suggested that JNK1 is required for basal JNK activity in the brain whereas JNK3 mediates stress-induced apoptosis but is not required in brain development (Yang et al., 1997, Le-Niculescu et al., 1999, Kuan et al., 2003).

Apart from its role in neuronal apoptosis, JNK/c-Jun signalling plays an important role in promoting neurite outgrowth (Dragunow et al., 2000, Leppa et al., 1998, Levkovitz and Baraban, 2002). After injury, c-Jun deficient axotomised motoneurons fail to undergo apoptosis and gradually become atrophic (Raivich et al., 2004). Furthermore, they show decreased perineuronal sprouting and reduced target re-innervation leading to a significant delay in regeneration.

All in all, the role of JNK/c-Jun signalling during embryonic development as well as postnatally is only insufficiently defined, in particular in the brain where many JNK signalling components are highly expressed. Furthermore, the JNK-dependency of physiological and pathological c-Jun functions are incompletely understood. For the

establishment of JNK/c-Jun signalling as a therapeutical target, it will be important to dissect JNK-dependent from JNK-independent c-Jun actions.

1.5 Fbw7: The significance of degradation

One protein that brings both of the signalling pathways Notch and JNK/c-Jun together and leads them into ubiquitin-proteasome-dependent proteolysis is the F-box protein Fbw7 (F-box and WD repeat domain containing-7; also known as Fbxw7, SEL-10, Ago, hCdc4).

1.5.1 The ubiquitin-proteasome pathway

Fbw7 is part of the ubiquitin-proteasome pathway of degradation which is the major regulated destruction system for proteins in eukaryotic cells. Apart from cellular homeostasis, the ubiquitin-proteasome pathway has been shown to be involved in many cellular processes such as stem cell regulation, proliferation, DNA damage repair and apoptosis and dysregulation of the pathway has been linked to many diseases such as cancer, inflammatory diseases and neurodegenerative diseases (reviewed in Schwartz and Ciechanover, 2009). The degradation system is initiated by a three-stepped enzymatic cascade (**Figure 18**) (reviewed in Hershko, 1983, Schwartz and Ciechanover, 2009). Firstly, the E1 ubiquitin-activating enzyme forms a thiol ester bond with the small regulatory protein ubiquitin in an adenosine triphosphate (ATP)-dependent manner and thus activates it. Secondly, activated ubiquitin is transferred to the E2 ubiquitin-conjugating enzyme and binds via a thiol ester bond to the E2. Thirdly, the E3 ubiquitin ligase binds on the one hand to the E2 and on the other hand to a substrate and thus brings ubiquitin and the target protein in close spatial proximity. Consequently, ubiquitin is transferred and covalently bound to lysine residues of the substrate. Ubiquitin itself has multiple acceptor lysine sites which determine the length of the ubiquitin chain and the effect of ubiquitination on the substrate (reviewed in Pickart and

Eddins, 2004). Ubiquitin chains extending from ubiquitin lysines 11 and 48 have been shown to target substrates to the 26S-proteasome where they are subsequently degraded (Xu et al., 2009). Other ubiquitin chains extending from lysines 29 and 63 for example or mono-ubiquitination do not function as degradation signals but are important for substrate localisation or activity (Mukhopadhyay and Riezman, 2007).

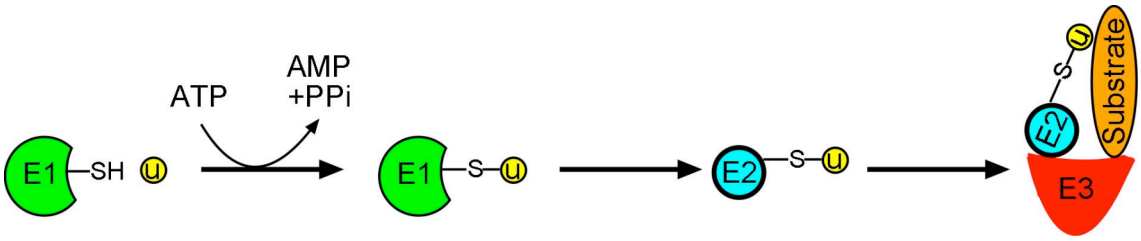

Figure 18 Ubiquitination
Drawing of the three steps of ubiquitination. Firstly, the E1 ubiquitin-activating enzyme forms a thiol-ester bond with ubiquitin (u) in an adenosine triphosphate (ATP) dependent manner. Secondly, ubiquitin is transferred to the E2 ubiquitin-conjugating enzyme. Thirdly, the E3 ubiquitin ligase brings E2 and substrate in close spatial proximity and ubiquitin is covalently bound to the substrate. AMP, adenosine monophosphate. PPi, pyrophosphate.

1.5.2 E3 ubiquitin ligases

Whereas E2 ubiquitin-conjugating enzymes have been reported to be crucial for the assembly of the various types of ubiquitin chains, E3 ubiquitin ligases are responsible for substrate specificity (reviewed in Pickart and Eddins, 2004, Ye and Rape, 2009). Classes of E3 ubiquitin ligases share common structural motifs. The two biggest classes are the HECT (homologous to E6-associated protein C-terminus) domain and the RING-finger domain containing E3 ligases (reviewed in Weissman, 2001). RING-finger E3 ligases can be either single proteins or multi-subunit complexes. The main subclasses of multi-subunit RING-finger E3 ligases are the anaphase promoting complex/cyclosome (APC/C) and the complex of SKP1/CUL1/F-box protein (SCF)

ligases (reviewed in Skaar and Pagano, 2009). The SCF complex contains an invariable part consisting of S-phase kinase-associated protein 1 (SKP1) and cullin 1 (CUL1). The RING box 1 (RBX1) protein, another constant component of the SCF complex, was identified later. CUL1 serves as a scaffold protein and binds RBX1 and SKP1 on opposite ends (**Figure 19**). RBX1 recruits the E2 ubiquitin-conjugating enzyme through its RING-finger domain whereas SKP1 binds to the F-box protein (Schulman et al., 2000, Zheng et al., 2002). The F-box protein is the variable part of the SCF E3 ubiquitin ligase complex and is responsible for substrate specificity. Over 70 F-box proteins have been identified so far in humans (reviewed in Winston et al., 1999, Onoyama and Nakayama, 2008). The common structural motif of these proteins is the F-box domain which is essential for the binding of the F-box protein to SKP1 (Bai et al., 1996).

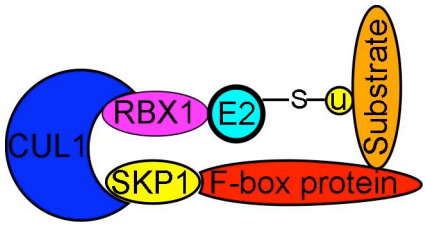

Figure 19 The SCF complex
Schematic representation of the SCF complex. The constant part consists of CUL1, RBX1 which recruits the E2 ubiquitin-conjugating enzyme and SKP1 which binds the F-box protein. The F-box protein is the variable part of the SCF complex and is responsible for substrate specificity. u, ubiquitin.

1.5.3 The F-box protein Fbw7

One of the F-box proteins is the tumour suppressor Fbw7. Fbw7 is responsible for the recognition of phosphorylated forms of important oncoproteins such as c-Myc (Yada et al., 2004, Welcker et al., 2004a), cyclin E (Moberg et al., 2001, Strohmaier et al., 2001, Koepp et al., 2001), Notch (Hubbard et al., 1997, Gupta-Rossi et al., 2001, Oberg et al.,

2001, Wu et al., 2001, Sundaram and Greenwald, 1993) and c-Jun (Nateri et al., 2004, Wei et al., 2005) (**Figure 20**). Apart from the F-box domain, Fbw7 contains eight WD40 tandem repeats which provide substrate specificity. The WD40 repeats form a barrel-shaped eight-bladed β-propeller structure which carries binding pockets for the interaction with specific substrates (Orlicky et al., 2003, Hao et al., 2007). Most critical for Fbw7-substrate interaction are three highly conserved arginine residues (R465, R479 and R505) within WD40 repeats 3 and 4 which recognise the Cdc4 phospho-degron (CPD), a specific consensus phospho-motif found in most of Fbw7-target proteins (Hao et al., 2007, Nash et al., 2001). The main characteristics of the CPD are a serine or threonine phosphorylation site together with a negative charge at the +4 position which is provided either through glutamate or phosphorylation. Phosphorylation of serines and threonines within the CPDs of some Fbw7 targets such as c-Myc and c-Jun has been shown to be mediated by glycogen synthase kinase-3 (GSK3) (Wei et al., 2005, Cohen and Frame, 2001, Welcker et al., 2004b). However, it has been reported that other arginine residues within the WD40 propeller also contribute to substrate binding and that Fbw7 can target substrates in a CPD-independent manner (Orlicky et al., 2003, Hao et al., 2007, Kitagawa et al., 2010).

Furthermore, Fbw7 contains a N-terminal dimerisation domain (D domain). Fbw7 forms homodimers which has been shown to play a role in substrate-affinity and -specificity (Hao et al., 2007, Welcker and Clurman, 2007, Tang et al., 2007, Zhang and Koepp, 2006, Kominami et al., 1998). For example, the prototype Fbw7-target in yeast, Sic1 does not contain an optimal consensus CPD but carries several low-affinity degrons (Orlicky et al., 2003, Verma et al., 1997a). Thus, Fbw7-Sic1 interaction requires Fbw7 dimerisation (Tang et al., 2007). On the contrary, monomeric Fbw7 is

sufficient to target substrates containing high-affinity degrons such as cyclin E and c-Myc (Hao et al., 2007, Welcker and Clurman, 2007).

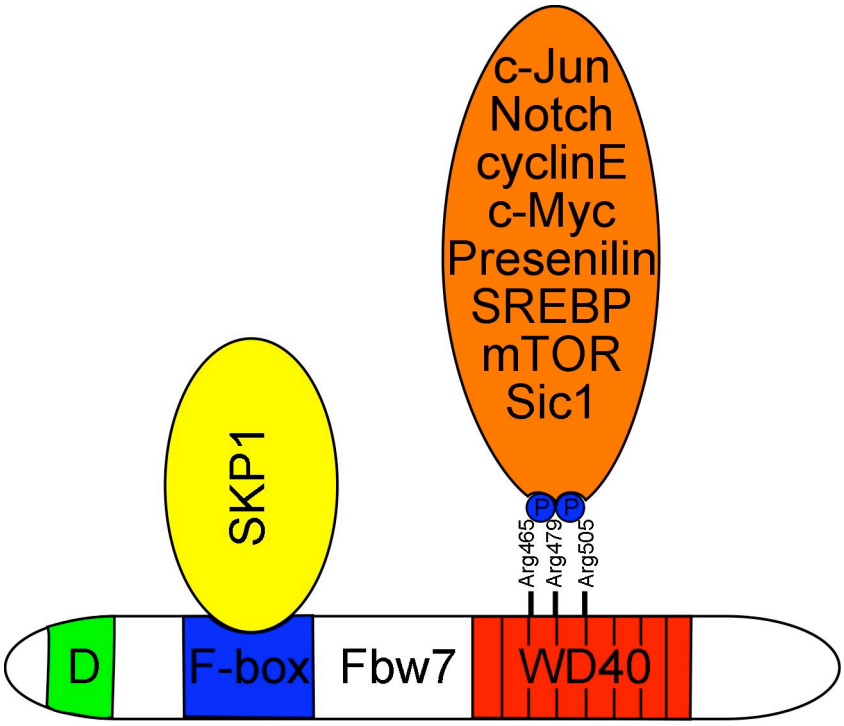

Figure 20 Fbw7 and its substrates
Schematic representation of Fbw7 including the dimerisation (D) domain, the F-box domain which binds to SKP1 and the WD40 repeats which are responsible for substrate recognition.

1.5.4 Fbw7 isoforms

The D domain, F-box domain and the WD40 repeats are structural motifs shared by all three Fbw7 isoforms, Fbw7α, β and γ. Human FBW7 is encoded by 11 exons spreading over the more than 200 kb *FBXW7* locus on chromosome 4 (4q32), a region which is frequently lost in tumours (Spruck et al., 2002). All Fbw7 isoforms share the last 10 exons and only differ in exon 1. *Fbxw7*α, *Fbxw7*β and *Fbxw7*γ transcripts are produced by alternative splicing of the first exon. Furthermore, each *Fbxw7* isoform has its own promoter allowing differential transcriptional control in diverse tissues (Spruck

et al., 2002). Whereas Fbw7α is ubiquitously expressed in the mouse, Fbw7β levels are high in the brain and Fbw7γ has been detected in muscle tissue and the haematopoietic system (Matsumoto et al., 2006). Little is known about *Fbxw7* isoform-specific regulation apart from *Fbxw7*β being a p53 target (Kimura et al., 2003, Mao et al., 2004). Although all three Fbw7 isoforms are in general functionally identical, the difference in the N-terminus has been shown to determine distinct subcellular localisation. Fbw7α localises to the nucleoplasm, Fbw7β to the cytoplasm and Fbw7γ to the nucleolus (Spruck et al., 2002, Welcker and Clurman, 2008, Kimura et al., 2003).

1.5.5 Fbw7 and its substrates

The ever growing list of Fbw7 target proteins started with the cyclin-dependent kinase (CDK) inhibitor Sic1 in yeast where the Fbw7 orthologue Cdc4 was first identified (**Figure 20**) (Verma et al., 1997a, Hartwell et al., 1973, Schwob et al., 1994, Verma et al., 1997b, Skowyra et al., 1997, Feldman et al., 1997). In *C. elegans*, it was reported that SEL-10, the nematode Fbw7 orthologue, regulates Notch1 (Hubbard et al., 1997, Sundaram and Greenwald, 1993). Homology to SEL-10 led to the identification of Fbw7 in mice and humans where its function in Notch1 degradation is conserved (Gupta-Rossi et al., 2001, Oberg et al., 2001, Wu et al., 2001, Maruyama et al., 2001). Fbw7 seems to play a prominent role in Notch regulation. Apart from targeting Notch, Fbw7 ubiquitinates two other proteins involved in Notch signalling, Presenilin and c-Myc (Yada et al., 2004, Wu et al., 1998, Li et al., 2002). Presenilin is part of the γ-secretase complex which is required for Notch activation. c-Myc is a direct transcriptional target of Notch and has been shown to play a critical role in Notch-

associated leukaemia (Klinakis et al., 2006, Palomero et al., 2006, Weng et al., 2006). Furthermore, considering that Notch signalling plays a critical role in vascular development, it is noteworthy that Fbw7-knockout mice, which die around E10.5 due to vascular and placental defects, exhibit increased abundance of Notch (**Figure 21**) (Tetzlaff et al., 2004, Tsunematsu et al., 2004).

Moreover, archipelago (AGO), the *Drosophila* Fbw7 orthologue, was described as a negative regulator of the cell cycle progression protein cyclin E (Moberg et al., 2001). Also Fbw7 function in cyclin E degradation was shown to be conserved in mammals (Strohmaier et al., 2001, Koepp et al., 2001). The cyclin E CPD can be phosphorylated by GSK3 or is autophosphorylated by the cyclin E-cyclin dependent kinase 2 (CDK2) complex (Clurman et al., 1996, Won and Reed, 1996). Disruption of Fbw7-dependent degradation of cyclin E has been reported to result in a large expansion of progenitors and impaired erythropoiesis in the haematopoietic system and increased proliferation and apoptosis in mammary epithelia (**Figure 21**) (Strohmaier et al., 2001, Minella et al., 2008). Also, Fbw7-knockout mice, which die around E10.5 due to vascular and placental defects, exhibit increased levels of cyclin E in placental tissues (Tetzlaff et al., 2004).

Furthermore, the transcription factor and oncoprotein c-Myc which positively regulates proliferation for example in ES cells [notably Fbw7 expression is low in ES cells (Reavie et al., 2010)] has been identified as a Fbw7-substrate (Yada et al., 2004). Fbw7-mediated degradation of c-Myc depends on the phosphorylation of its CPD by GSK3 and ERK (Welcker et al., 2004a). c-Myc regulation by Fbw7 has been shown to be of major importance in the haematopoietic system (**Figure 21**) (Reavie et al., 2010,

Matsuoka et al., 2008, Thompson et al., 2008). Absence of Fbw7 causes loss of quiescent HSCs and haematopoietic precursor expansion. Although other Fbw7-substrates such as Notch1 and cyclin E were upregulated in the haematopoietic system in the Fbw7-knockout background, only attenuation of c-Myc was able to correct the proliferative abnormalities (Onoyama et al., 2007), suggesting that c-Myc is the key substrate of Fbw7 in the haematopoietic system (Welcker and Clurman, 2008). Recently, one study showed that overexpression of Fbw7α, which is localised to the nucleoplasm, leads to decreased c-Myc levels and sustained HSC quiescence (Iriuchishima et al., 2011). Furthermore, it has been reported that the de-ubiquitinating enzyme ubiquitin-specific peptidase 28 (USP28) antagonises Fbw7α activity and stabilises c-Myc levels in the nucleoplasm and its function in proliferation (Popov et al., 2007). Interestingly, growth-promoting c-Myc function has been at least partially attributed to c-Myc action at ribosomal DNA transcription sites in the nucleolus (Gomez-Roman et al., 2006, Grandori et al., 2005). Consistently, Fbw7γ which is localised to the nucleolus has been shown to target c-Myc in the nucleolus and to regulate its growth-promoting activity (Welcker et al., 2004a).

Another oncoprotein identified to be ubiquitinated by Fbw7 is the transcription factor c-Jun (Nateri et al., 2004). Targeting of c-Jun by Fbw7 has been reported to occur either in a JNK-dependent or in a GSK3-dependent manner (Nateri et al., 2004, Wei et al., 2005). Recent work on Fbw7 function in the intestine suggests that following loss of Fbw7 in the gut, Notch and c-Jun levels are upregulated in this tissue leading to increased progenitor proliferation and impaired goblet and paneth cell differentiation (**Figure 21**) (Sancho et al., 2010).

Other prominent Fbw7-substrates recently identified are for example the sterol regulatory element binding protein (SREBP) which controls membrane synthesis and lipid metabolism (Sundqvist et al., 2005) and the oncoprotein mTOR (mammalian target of rapamycin) which is involved in cell growth, proliferation and survival (Mao et al., 2008, Crusio et al., 2010).

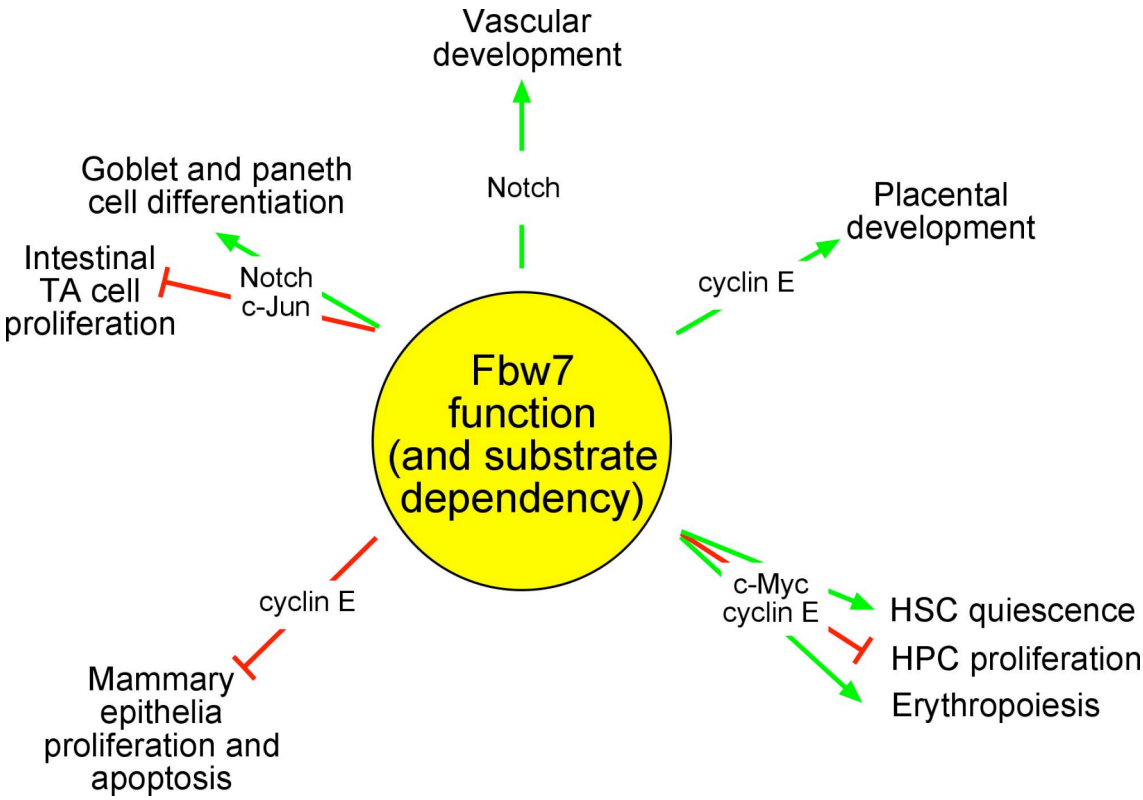

Figure 21 Substrate-dependent Fbw7 function
Schematic representation of Fbw7 functions in various tissues and their dependency on the degradation of specific Fbw7 target proteins. Green lines point towards actions promoted by Fbw7, red lines point towards actions inhibited by Fbw7. TA cell, transit amplifying cell.

1.5.6 The tumour suppressor Fbw7

The tumour suppressor Fbw7 has been reported to be mutated or inactivated in a variety of human cancers. Overall, 6% of all tumours carry Fbw7 mutations (Akhoondi et al.,

2007). Fbw7 mutations were found in 35% of cholangio-carcinomas, 31% of T cell acute lymphocytic leukaemia (T-ALL) and 9% of colon and endometrial tumours (Akhoondi et al., 2007). Interestingly, other tumour types such as leukaemias other than T-ALL and cancers of the liver, lung, breast, bladder, ovary and bone have not or rarely been associated with Fbw7 mutations pointing towards a tissue-specific tumour suppressor function of Fbw7 (Nowak et al., 2006, Woo Lee et al., 2006, Kwak et al., 2005, Sgambato et al., 2007, Yan et al., 2006). Remarkably, 43% of Fbw7 mutations were identified to be missense mutations that lead to amino acid substitutions at the key substrate binding arginines within the WD40 domain (Calhoun et al., 2003). Consistently, mutations within the CPDs of Fbw7-substrates have been detected in various cancers, for example mutations of the c-Myc CPD in Burkitt lymphoma and mutations in the Notch CPD in T-ALL (Gregory and Hann, 2000, Bahram et al., 2000, Maser et al., 2007). Strikingly, ~50% of T-ALL tumours carry Notch-activating mutations (Weng et al., 2004) and the second most commonly mutated gene in T-ALL is *Fbxw7* (~30%) (Maser et al., 2007). The role of Fbw7 inactivation in lymphomatogenesis however has been linked to c-Myc upregulation (Onoyama et al., 2007). In the brain, ~80% of glioblastoma, the most aggressive brain tumour type, exhibit reduced Fbw7 levels and consequently increased Notch levels rendering Fbw7 a prognostic marker for survival for brain cancer patients (Hagedorn et al., 2007). Furthermore, in endometrial tumours, Fbw7 mutations have been shown to result in cyclin E accumulation and genomic instability (Hubalek et al., 2004). Recently, Fbw7 inactivation has been reported to promote intestinal tumourigenesis in a Notch- and c-Jun dependent manner (Sancho et al., 2010). Furthermore, it has been suggested that

loss of Fbw7 and loss of p53 can cooperatively promote tumourigenesis (Welcker and Clurman, 2008, Minella et al., 2007).

1.6 The aim of this thesis

The ubiquitin ligase Fbw7 has been shown to mediate degradation of important oncoproteins involved in cell cycle regulation, apoptosis and differentiation. Tissue-specific Fbw7 isoform and Fbw7 substrate expression patterns point towards distinct functions of Fbw7 in different contexts. Apart from the well-established role of Fbw7 in the haematopoietic and vascular system, Fbw7 function in various other tissues remains enigmatic. Due to the fact that Fbw7-knockout embryos die around E10.5 because of vascular and placental defects (Tetzlaff et al., 2004, Tsunematsu et al., 2004), it had not been possible to investigate Fbw7 function in the brain. Thus, I analysed CNS-specific conditional Fbw7-knockout mice (*Fbxw7*$^{f/f}$; Nestin-Cre) which die perinatally suggesting that Fbw7 is also essential during brain development. The aim of my thesis is to investigate Fbw7 function in the developing brain.

Furthermore, JNK/c-Jun signalling has been shown to mediate different biological effects dependent on the organ system, e.g. it promotes proliferation in the intestine while inducing apoptosis in the brain (Sancho et al., 2009, Behrens et al., 1999). Previous studies suggested that c-Jun action is essential for mouse development whereas JNK-dependent c-Jun function is dispensable for development but is required for tumourigenesis (Behrens et al., 1999, Hilberg et al., 1993, Behrens et al., 2000). To establish JNK/c-Jun signalling as a target for tumour therapy, it is necessary to dissect JNK-independent from JNK-dependent c-Jun functions. Thus, I generated two transgenic mouse lines which either lack JNK-dependent c-Jun phosphorylation at the four main sites (*Jun*4A; Ser63Ala, Ser73Ala, Thr91Ala, Thr93Ala) or which carry constitutively active JNK (ROSA26-LSL-JNKK2-JNK1). The aim of my thesis is to

examine JNK-dependency of various c-Jun functions under physiological and pathological conditions.

Chapter 2. Materials and Methods

2.1 Materials

2.1.1 Reagents and consumables

The following reagents and consumables used in this study were obtained from the given companies or the London Research Institute (LRI)/Cancer Research UK (CR-UK) Central Services:

0.5 ml, 1.5 ml, 2 ml tubes	Eppendorf (Cambridge, UK)
1 kb DNA ladder	Invitrogen (Paisley, UK)
15 ml, 50 ml tubes	Corning (Corning, USA)
2-propanol	Fisher Scientific (Loughborough, UK)
5 ml, 10 ml, 25 ml serological pipettes	Corning (Corning, USA)
1 ml, 5 ml, 10 ml syringes	BD Plastipak (Oxford, UK)
18-gauge needles	BD Microlance (Oxford, UK)
25cm^2-flasks (adherent cells)	Corning (Corning, USA)
75cm^2-flasks (adherent cells)	Corning (Corning, USA)
150cm^2-flasks (adherent cells)	Corning (Corning, USA)
25cm^2-flasks (suspension culture)	Sarstedt (Leicester, UK)
75cm^2-flasks (suspension culture)	Greiner bio-one (Stonehouse, UK)
6-well plate (flat bottom)	BD Falcon (Oxford, UK)
24-well plate (flat bottom)	BD Falcon (Oxford, UK)
96-well plate (flat bottom)	BD Falcon (Oxford, UK)
ABC Kit	Vector Laboratories (Peterborough, UK)

AccuMax™	PAA (Yeovil, UK)
Acetic acid	Fisher Scientific (Loughborough, UK)
Acrylamide mix (30%)	National Diagnostics (Hessle, UK)
Agarose	Bioline (London, UK)
Albumin	Sigma-Aldrich (Poole, UK)
Alcian blue	Sigma-Aldrich (Poole, UK)
Ammonium persulfate	Sigma-Aldrich (Poole, UK)
Ampicillin	Sigma-Aldrich (Poole, UK)
Anisomycin	Sigma-Aldrich (Poole, UK)
B27 Supplement	Invitrogen (Paisley, UK)
BCIP	Roche Applied Science (Burgess Hill, UK)
Blocking Reagent	Roche Applied Science (Burgess Hill, UK)
Bovine serum albumin	Sigma-Aldrich (Poole, UK)
BrdU	Sigma-Aldrich (Poole, UK)
Bromophenol blue	Sigma-Aldrich (Poole, UK)
Cell strainer (70 μm Nylon)	BD Falcon (Oxford, UK)
CellTrace™ CFSE Cell Proliferation Kit	Molecular Probes/Invitrogen (Paisley, UK)
Chloramphenicol	Sigma-Aldrich (Poole, UK)
Chromatography paper (3 mm)	Whatman (Brentford, UK)
CIP	New England Biolabs (NEB, Hitchin, UK)
Coverslips	Menzel-Glaeser (Braunschweig, Germany)
Cuvettes	Fisher Scientific (Loughborough, UK)
DAB solution	BioGenex (Burlingame, UK)

DAPI	Sigma-Aldrich (Poole, UK)
ddH_2O	LRI/CR-UK (London, UK)
DirectPCR Lysis Reagent	Viagen Biotech (Los Angeles, USA)
DeadEnd™ Colorimetric TUNEL System	Promega (Southampton, UK)
Disodium tetraborate	AppliChem (Darmstadt, Germany)
DMEM	Invitrogen (Paisley, UK)
DMSO	Sigma-Aldrich (Poole, UK)
DPX mounting medium	Raymond A. Lamb (London, UK)
DSS	MP Biomedicals (Illkirch, France)
DyeEx® 2.0 Spin Kit	QIAGEN (Crawley, UK)
ECL Western Blotting Detection Reagents	GE Healthcare (Little Chalfont, UK)
EDTA	Sigma-Aldrich (Poole, UK)
EGF (human)	PeproTech (London, UK)
EGTA	Sigma-Aldrich (Poole, UK)
Embedding cassettes	Tissue Tek (Basingstoke, UK)
Eosin Y	Sigma-Aldrich (Poole, UK)
Ethanol	Fisher Scientific (Loughborough, UK)
Ethidium bromide	Sigma-Aldrich (Poole, UK)
FACS tubes	Becton Dickinson (Oxford, UK)
FGF-basic (human)	PeproTech (London, UK)
Fluorescent Mounting Medium	DAKO (Ely, UK)
Foetal calf serum (FCS)	PAA (Yeovil, UK)
Gelatin	Sigma-Aldrich (Poole, UK)

Glycerol	Sigma-Aldrich (Poole, UK)
Glycine	Sigma-Aldrich (Poole, UK)
Goat serum	Sigma-Aldrich (Poole, UK)
Harris`s haematoxylin	LRI/CR-UK (London, UK)
HBSS + Ca^{2+}/Mg^{2+}	Invitrogen (Paisley, UK)
Hydrochloride acid	Sigma-Aldrich (Poole, UK)
Hydrogen peroxide	Sigma-Aldrich (Poole, UK)
illustra™ GFX™ DNA Purification Kit	GE Healthcare (Little Chalfont, UK)
Industrial methylated spirit (IMS)	LRI/CR-UK (London, UK)
Kanamycin	Sigma-Aldrich (Poole, UK)
Laminin	Sigma-Aldrich (Poole, UK)
L-arabinose	Sigma-Aldrich (Poole, UK)
L-glutamine	Invitrogen (Paisley, UK)
L-glycine	Sigma-Aldrich (Poole, UK)
LB medium	LRI/CR-UK (London, UK)
Marvel skimmed milk powder	A1 Laboratory Supplies Ltd (Enfield, UK)
Mayer`s haematoxylin	LRI/CR-UK (London, UK)
Magnesium chloride	LRI/CR-UK (London, UK)
β-mercaptoethanol	Sigma-Aldrich (Poole, UK)
Methanol	Fisher Scientific (Loughborough, UK)
Microscope slides	Menzel-Glaeser (Braunschweig, Germany)
N-2 supplement	Invitrogen (Paisley, UK)
NBT	Roche Applied Science (Burgess Hill, UK)

Neurobasal Medium	Gibco/Invitrogen (Paisley, UK)
NeuroCult® Differentiation Supplement	StemCell Technologies (London, UK)
Neutral buffered formalin (NBF)	LRI/CR-UK (London, UK)
Nuclear fast red	Vector Laboratories (Peterborough, UK)
NucleoBond® Plasmid Purification Kit	Clontech (Saint-Germain-en-Laye, France)
Ponceau S	Sigma-Aldrich (Poole, UK)
Paraffin wax	Tissue Tek (Basingstoke, UK)
Paraformaldehyde	Sigma-Aldrich (Poole, UK)
PBS	LRI/CR-UK (London, UK)
Penicillin/Streptomycin	Invitrogen (Paisley, UK)
Periodic Acid-Schiff	Sigma-Aldrich (Poole, UK)
PIPES	Sigma-Aldrich (Poole, UK)
Phenylmethylsulfonyl fluoride (PMSF)	Sigma-Aldrich (Poole, UK)
Poly-L-ornithine	Sigma-Aldrich (Poole, UK)
Protease Inhibitor	Sigma-Aldrich (Poole, UK)
Proteinase K	Melford Laboratories (Ipswich, UK)
Protein Assay Dye Reagent	Bio-Rad (Hemel Hempstead, UK)
QIAGEN Plasmid Maxi Kit	QIAGEN (Crawley, UK)
QIAprep Spin Miniprep Kit	QIAGEN (Crawley, UK)
Rainbow markers	GE Healthcare (Little Chalfont, UK)
Restriction endonucleases	New England Biolabs (NEB, Hitchin, UK)
RIPA buffer	New England Biolabs (NEB, Hitchin, UK)
RNase-Free DNase Set	QIAGEN (Crawley, UK)

RNeasy Midi-kit	QIAGEN (Crawley, UK)
RNeasy Mini-kit	QIAGEN (Crawley, UK)
Senescence Histochemical Staining Kit	Sigma-Aldrich (Poole, UK)
Shandon Cytoblock® Cell Preparation	Thermo Scientific (Basingstoke, UK)
Sodium acetate	Sigma-Aldrich (Poole, UK)
Sodium azide	Sigma-Aldrich (Poole, UK)
Sodium chloride	LRI/CR-UK (London, UK)
Sodium dodecyl sulfate	Sigma-Aldrich (Poole, UK)
Sodium fluoride	Sigma-Aldrich (Poole, UK)
Sodium orthovanadate	New England Biolabs (NEB, Hitchin, UK)
Superfrost Ultra Plus charged slides	Menzel-Glaeser (Braunschweig, Germany)
Superscript III cDNA synthesis kit	Invitrogen (Paisley, UK)
SYBR Green	Invitrogen (Paisley, UK)
T4 DNA ligase	New England Biolabs (NEB, Hitchin, UK)
Taq PCR Core Kit	Qiagen (Crawley, UK)
TEMED	Sigma-Aldrich (Poole, UK)
Tetracycline	Sigma-Aldrich (Poole, UK)
Tris	Sigma-Aldrich (Poole, UK)
Trisodium citrate	Sigma-Aldrich (Poole, UK)
Triton X-100	Sigma-Aldrich (Poole, UK)
Trypan Blue	Sigma-Aldrich (Poole, UK)
Trypsin	Invitrogen (Paisley, UK)
Vi-Cell™ sample vial	Beckman Coulter (High Wycombe, UK)

X-ray film, Fuji	Fisher Scientific (Loughborough, UK)
Xylene	LRI/CR-UK (London, UK)

2.1.2 Buffers and media

Blocking buffer (*in situ* hybridisation)

10 % Blocking Reagent (Roche)

dissolved in 1X Maleic Acid Buffer

Citrate buffer

Trisodium citrate	2.94 g
HCl (0.2 M)	22 ml
ddH_2O	up to 1 l

Detection buffer (*in situ* hybridisation)

5 M NaCl	1 ml
1 M MgCl	2 ml
0.5M Tris-HCl (pH 9.5)	10 ml
Levamisol (2 mM final conc.)	24mg

make up to 50 ml with ddH_2O

Disodium tetraborate buffer	**final conc.:**
Disodium tetraborate in ddH_2O	150 mM
pH 8.5	

DMEM + 10% FCS (MEFs)

DMEM	445 ml
(+ 4.5 g/l glucose, + l-glutamine, + pyruvate)	
FCS	50 ml
1% (v/v) Penicillin/Streptomycin (10000 U/ml)	5 ml

Harris`s haematoxylin

Haematoxylin	2.5 g
Absolute alcohol	25 ml
Potassium alum	50 g
ddH_2O	500 ml
Sodium iodate	0.5 g
Glacial acetic acid	20 ml

Hybridisation solution	**final conc.:**
Deionized formamide	50%
Dextran sulfate	10%
Denhardt's Solution	1x
Tris-HCl pH7.5	10 mM
NaCl	600 mM
EDTA	1 mM
SDS	0.25%
tRNA	1 mg/ml
diluted in DEPC water	

Loading buffer (for agarose gels)	
Xylenecyanol	0.025 g
EDTA (0.5M)	1.4 ml
Glycerol	3.6 ml
ddH_2O	7.0 ml

10x Maleic acid buffer	
Maleic acid	116g
NaCl	88g
ddH_2O	800 ml

Mayer`s haematoxylin

Haematoxylin	1 g
ddH_2O	1000 ml
Potassium alum	50 g
Sodium iodate	0.2 g
Citric acid	1 g
Chloral hydrate SLR	50 g

NB + Differentiation Supplement (for 50 ml)

Neurobasal Medium	43 ml
2% (v/v) B27 Supplement	1 ml
1% (v/v) L-Glutamine (200 mM)	0.5 ml
1% (v/v) Penicillin/Streptomycin (10000 U/ml)	0.5 ml
10% NeuroCult® Differentiation Supplement	5 ml

NB + GF (embryonic neurospheres; for 500 ml)

Neurobasal Medium	479.8 ml
2% (v/v) B27 Supplement	10 ml
1% (v/v) L-Glutamine (200 mM)	5 ml
1% (v/v) Penicillin/Streptomycin (10000 U/ml)	5 ml
20 ng/ml EGF (100 µM)	100 µl
20 ng/ml FGF-basic (100 µM)	100 µl

NB + GF (adult neurospheres; for 500 ml)

Neurobasal Medium	474.8 ml
2% (v/v) B27 Supplement	10 ml
1% (v/v) L-Glutamine (200 mM)	5 ml
1% (v/v) Penicillin/Streptomycin (10000 U/ml)	5 ml
1% (v/v) N-2 supplement	5 ml
20 ng/ml EGF (100 µM)	100 µl
20 ng/ml FGF-basic (100 µM)	100 µl

NB + GF + laminin (adherent NSCs; for 500 ml)

Neurobasal Medium	474.8 ml
2% (v/v) B27 Supplement	10 ml
1% (v/v) L-Glutamine (200 mM)	5 ml
1% (v/v) Penicillin/Streptomycin (10000 U/ml)	5 ml
1% (v/v) N-2 supplement	5 ml
20 ng/ml EGF (100 µM)	100 µl
20 ng/ml FGF-basic (100 µM)	100 µl
Laminin	0.5 mg

Phosphate buffered saline (PBS)	**final conc.:**
NaCl	136 mM
KCl	3 mM
$Na_2HPO_4 \cdot 2\ H_2O$	8 mM
KH_2PO_4	15 mM

PIPES buffer (in ddH_2O)	**final conc.:**
PIPES	80 mM
$MgCl_2$	1 mM
EGTA	5 mM
Triton X-100	0.5%
pH 6.8	

Protein loading buffer (Laemmli buffer)	**final conc.:**
Tris-HCl (pH 6.8)	63 mM
SDS (w/v)	2%
Glycerol (v/v)	10%
bromophenol blue (w/v)	0.0025%
+ β-mercaptoethanol (v/v)	2.5%

10% Resolving gel

ddH_2O	19.8 ml
30% acrylamide mix (v/v)	16.7 ml
1.5 M Tris (pH 8.8) (v/v)	12.5 ml
10% SDS (v/v)	500 µl
10% ammonium persulfate (APS)	500 µl
TEMED	20 µl

RIPA cell and tissue lysis buffer (for 5 ml)

RIPA buffer (10 x)	500 µl
Protease inhibitor (100 x)	50 µl
PMSF	50 µl
NaF	50 µl
$NaVO_4$	25 µl
ddH_2O	4.325 ml

10x SDS-PAGE Running buffer

Tris	300 g
Glycine	1400 g
20% SDS (v/v)	250 ml
ddH_2O	up to 10 l

1x Semi-dry transfer buffer	**final conc.:**
Tris	24 mM
Glycine	192 mM
Methanol (v/v)	20%
SDS (v/v)	0.01%

Sodium acetate buffer	
1 M sodium acetate	99 ml
1 M acetic acid	960 µl
ddH_2O up to 1 l	

20x SSC	
NaCl	17.53g
sodium citrate	8.82g
DEPC water, pH 5.0	80 ml

5% Stacking gel	
ddH_2O	6.8 ml
30% acrylamide mix	1.7 ml
1.0 M Tris (pH 6.8)	1.25 ml
10% SDS	100 µl
10% ammonium persulfate (APS)	100 µl
TEMED	10 µl

50x TAE buffer

Tris (0.2 M)	242 g
Acetic acid	57.1 ml
Na_2EDTA x 2 H_2O	37.2 g
ddH_2O	up to 1 l

Tail buffer

DirectPCR Lysis Reagent (mouse tail)	100 µl
Proteinase K (10 mg/ml)	3 µl

20x Tris buffered saline Tween-20 (TBS-T)

NaCl (5 M)	3 l
Tris (1 M; pH 7.5)	2 l
Tween-20	200 ml
ddH_2O	up to 10 l

2.1.3 Bacteria

For the expression of plasmid DNA, XL10-Gold® Ultracompetent Cells (Stratagene) were transformed. For the expression of the pENTR1A-vector containing a *ccd*B gene, transformation was performed using *ccd*B-tolerant Library Efficiency DB3.1™ Competent Cells (Invitrogen).

2.1.4 Vectors and expression plasmids

pBabe-JNKK2-JNK1

The plasmid consists of a 5.1 kb pBabe backbone vector containing an ampicillin-resistance gene and a 2.7 kb JNKK2-JNK1 construct which was inserted into the SnaBI restriction site of the pBabe vector. The insert consists of a 3 x HA-tag followed by the human JNKK2 cDNA, a 5 x Gly-Gly repeat sequence and the human JNK1 cDNA. Apart from the BamHI restriction site in the multiple cloning site of the pBabe-vector, another BamHI restriction site located at the 3` end of the insert behind the human JNK1 cDNA was identified by restriction digest and DNA sequencing.

pENTR1A

The pENTR1A-vector was obtained from Invitrogen (Paisley, UK). It contains a kanamycin resistance gene for selection in *E. coli* and a multiple cloning site flanked by *att*L1 and *att*L2 sites for site-specific recombination between the entry clone and a Gateway® destination vector (Invitrogen). Furthermore, it contains a toxin encoding *ccd*B gene between the two *att*L1 and *att*L2 sites for negative selection.

pSc101-BAD-gbaA^{tet}

The pSc101-BAD-gbaA^{tet} expression plasmid was obtained from Gene Bridges (Heidelberg, Germany). It contains genes for Red/ET recombination protein expression

and a tetracycline resistance gene. Transformation of *E. coli* hosts with this plasmid leads to acquisition of tetracycline resistance at 30°C, expression of the Red/ET recombination proteins is induced by L-arabinose activation of the BAD promoter at 37°C.

Minimal vector

The minimal vector (Gene Bridges) served as a PCR-template for the generation of a linear vector carrying a ColE1 origin and an ampicillin resistance gene.

loxP-PGK-gb2-neo-loxP

The plasmid was obtained from Gene Bridges. It contains a PGK-gb2-neo cassette with a kanamycin/neomycin resistance gene. This cassette is flanked by loxP-sites.

pMSCV-*Jun*4A

This plasmid contains a pMSCV backbone vector with an ampicillin resistance gene and an insert of the mouse *Jun* cDNA carrying mutations in four JNK-phosphorylation sites: Ser63Ala, Ser73Ala, Thr91Ala, Thr93Ala.

2.1.5 Oligonucleotides

The following primers were used in this study. Oligonucleotides were synthesised by Sigma-Aldrich (Poole, UK).

Table 1 Primers for genotyping

PCR-product	Primer sequences	Band size
Fbxw7 wild type(wt)/ floxed(f)/ deleted	forward: 5`-CAG TGG AGT GAA GTA CAA CTC TGG-3` reverse: 5`-GCA TAT TCT AGA GGA GGG TAT CGG-3` deletion reverse: 5`-G GCC AGC CTG GTC TGT ATA GAG-3`	wt: 288 bp floxed: 388 bp deleted: 744 bp
Jun wt/floxed (f)/ deleted/AA	forward: 5`-CTC ATA CCA GTT CGC ACA GGC GGC-3` reverse: 5`-CCG CTA GCA CTC ACG TTG GTA GGC-3` deletion reverse: 5`-CAG GGC GTT GTG TCA CTG AGC T-3`	wt: 300 bp floxed: 350 bp deleted: 700 bp AA: 380 bp
Jun wt/4A	forward: 5`-AGA ACT TGA CTG GTT GCG ACA-3` reverse: 5`-AGT CCA TCG TTC TGG TCG CGC-3`	wt: 198 bp 4A: 248 bp

PCR-product	Primer sequences	Band size
Notch1 wt/floxed (f)/ deleted	forward: 5`-CTG ACT TAG TAG GGG GAA AAC-3` reverse: 5`-AGT GGT CCA GGG TGT GAG TGT-3` deletion reverse: 5`- TAA AAA GCG ACA GCT GCG GAG-3`	wt 300 bp floxed: 350 bp deleted: 470 bp
Cre	forward 5`-CGG TCG ATG CAA CGA GTG ATG AGG-3` reverse 5`-CCA GAG ACG GAA ATC CAT CGC TCG-3`	*Cre*: 600 bp
eGFP	forward: 5`-CCT ACG GCG TGC AGT GCT TCA GC-3` reverse: 5`-CGG CGA GCT GCA CGC TGC GTC CTC-3`	*eGFP*: 300 bp

Table 2 Sequencing primers

Sequencing DNA	Primer sequences
pBabe-JNKK2-JNK1	forward (T3): 5`-GCA ATT AAC CCT CAC TAA AGG-3` reverse (T7): 5`-TAA TAC GAC TCA CTA TAG GG-3`
pENTR1A-JNKK2-JNK1	forward: 5`-GTT CGT TGC AAC AAA TTG ATA AGC-3` reverse: 5`-GTA ACA TCA GAG ATT TTG AGA CAC-3`
*Jun*4A	forward: 5`-TGA ACC TGG CCG ACC CGG TGG-3` reverse: 5`- TCA GCC AGG GCG CGC ACG AAG-3`

Table 3 Primers used to generate the *Jun*4A targeting construct

forward: 5`-AGT TCC TAG TAC AGT ACC TGA CAC ATA GTG AAT GTT CAT AAA ATA ATA TTT TGG TAC CCG AGT AAA CAC AGT TTA AAC TCA CAG CTT GTC TGT AAG CGG ATG-3`
reverse: 5`- TGT AGA AAT GTA CTT CTT GCT CAG GGT CAG AAG GGT TTT GCT TAA TGT GTT TAA CTA GTC TGA AGA TGG TAC GCG TGC TCT CCT GAG TAG GAC AAA TC-3`

Table 4 qRT-PCR primers

Gene	Primer sequences	Amplicon
Bad	forward: 5`-CAG GGA GAA GAG CTG ACG TAC A-3` reverse: 5`-CCA CCC CTC CGT GGC TAT-3`	65 bp
Bcl2 (beta)	forward: 5`-GCT CCC CTG ACC TCT CAC TCT-3` reverse: 5`-CTG GAT TCT TGC TCC CTC ACA-3`	97 bp
Bcl2l11 (*Bim*)	forward: 5`-CCC CTA CCT CCC TAC AGA CAG A-3` reverse: 5`-GCG CAG ATC TTC AGG TTC CT-3`	329 bp
Jun	forward: 5`-TGA AAG CTG TGT CCC CTG TC-3` reverse: 5`-ATC ACA GCA CAT GCC ACT TC-3`	220 bp
*Fbxw7*α	forward: 5`-CTG ACC AGC TCT CCT CTC CAT T-3` reverse: 5`-GCT GAA CAT GGT ACA AGG CCA-3`	147 bp
*Fbxw7*β	forward: 5`-TTG TCA GAG ACT GCC AAG CAG-3` reverse: 5`-GAC TTT GCA TGG TTT CTT TCC C-3`	177 bp
*Fbxw7*γ	forward: 5`-AAC CAT GGC TTG GTT CCT GTT G-3` reverse: 5`-CAG AAC CAT GGT CCA ACT TTC-3`	148 bp

Gene	Primer sequences	Amplicon
Fbxw7 (exon5)	forward: 5`-TTC ATT CCT GGA ACC CAA AGA-3` reverse: 5`-TCC TCA GCC AAA ATT CTC CAG TA-3`	70 bp
Gapdh	forward: 5`-TGA AGC AGG CAT CTG AGG G-3` reverse: 5`-CGA AGG TGG AAG AGT GGG AG-3`	102 bp
Hes1	forward: 5`-TCA GCG AGT GCA TGA ACG A-3` reverse: 5`-TGC GCA CCT CGG TGT TAA C-3`	68 bp
Hes5	forward: 5`-TGC AGG AGG CGG TAC AGT TC-3` reverse: 5`-GCT GGA AGT GGT AAA GCA GCT T-3`	74 bp
Hey1	forward: 5`-GGC AGC CCT AAG CAC TCT CA-3` reverse: 5`-TTC AGA CTC CGA TCG CTT ACG-3`	76 bp

2.1.6 Antibodies

Table 5 Primary antibodies

Primary antibody	Species	Application, dilution	Supplier
Actin (β)	rabbit, polyclonal	WB: 1:2000	Sigma (Poole, UK)
activated Notch1	rabbit, polyclonal	IHC: 1:200 WB: 1:500	Abcam (Cambridge, UK)
active Caspase-3	rabbit, polyclonal	IHC: 1:300	R&D Systems (Abingdon, UK)
BLBP	rabbit, polyclonal	IF, IHC: 1:100	Abcam (Cambridge, UK)
Brn2	goat, polyclonal	IHC: 1:50	Santa Cruz (Calne, UK)
Chromogranin	rabbit, polyclonal	IHC: 1:200	Abcam (Cambridge, UK)
CD133 (Prominin1)	rat, monoclonal	IF: 1:50	eBioscience (Hatfield, UK)
c-Jun (H-79)	rabbit, polyclonal	WB: 1:500	Santa Cruz (Calne, UK)
Connexin-43	rabbit, polyclonal	IF: 1:50	Zymed/Invitrogen (Paisley, UK)
Ctip2	rat, monoclonal	IHC: 1:100	Abcam (Cambridge, UK)
Doublecortin	goat, polyclonal	IHC: 1:50	Santa Cruz (Calne, UK)
Fbw7	rabbit, polyclonal	WB: 1:500	Abcam (Cambridge, UK)
GFP	rabbit, polyclonal	IHC: 1:200	Invitrogen (Paisley, UK)
GFAP	rabbit, polyclonal	IF, IHC: 1:500	DAKO (Ely, UK)
GLAST	guinea pig, polyclonal	IHC: 1:200	LifeSpan Biosciences (Nottingham, UK)
HA	rabbit, polyclonal	WB: 1:500	Sigma (Poole, UK)
Ki67	rat, monoclonal	IHC: 1:125	DAKO (Ely, UK)
Lysozyme	rabbit, polyclonal	IHC: 1:500	DAKO (Ely, UK)

Primary antibody	Species	Application, dilution	Supplier
Map2	mouse, monoclonal	IF: 1:100	Sigma (Poole, UK)
Musashi-1	rabbit, polyclonal	IHC: 1:200	Chemicon/Millipore (Watford, UK)
Nestin	mouse, monoclonal	IF: 1:300	BD (Oxford, UK)
Nestin	mouse, monoclonal	IHC: 1:75	Chemicon/Millipore (Watford, UK)
Nestin	rabbit, polyclonal	IF: 1:100	Abcam (Cambridge, UK)
NeuN	mouse, monoclonal	IHC: 1:1000	Chemicon/Millipore (Watford, UK)
NG2	rabbit, polyclonal	IHC: 1:200	Chemicon/Millipore (Watford, UK)
O4	mouse, monoclonal	IF: 1:200	Chemicon/Millipore (Watford, UK)
p53	mouse, monoclonal	WB: 1:500	Santa Cruz (Calne, UK)
p-c-Jun (Ser63)	rabbit, polyclonal	IF, IHC: 1:50; WB: 1:500	Cell Signaling (Hitchin, UK)
p-c-Jun (Ser73)	rabbit, polyclonal	IHC: 1:50; WB: 1:500	Cell Signaling (Hitchin, UK)
p-c-Myc (Thr 58/ Ser 62)	rabbit, polyclonal	WB: 1:500	Santa Cruz (Calne, UK)
p-cyclin E (Thr 395)	rabbit, polyclonal	WB: 1:500	Santa Cruz (Calne, UK)
pH3	rabbit, polyclonal	IHC: 1:250	Millipore (Watford, UK)
RC2	mouse, monoclonal	IF: 1:50	DSHB (Iowa City, USA)
S100	rabbit, polyclonal	IHC: 1:10	Abcam (Cambridge, UK)
Tbr1	rabbit, polyclonal	IHC: 1:500	Abcam (Cambridge, UK)
Tbr2	rabbit, polyclonal	IHC: 1:500	Abcam (Cambridge, UK)
Vimentin	mouse, monoclonal	IF: 1:50	Abcam (Cambridge, UK)

Table 6 Secondary antibodies

Secondary antibody	Application, dilution	Supplier
Alexa Fluor® 488 or 546 goat anti-mouse IgG	IF: 1:500; IHC: 1:350	Invitrogen (Paisley, UK)
Alexa Fluor® 488 goat anti-mouse IgM (μ chain)	IF: 1:500	Invitrogen (Paisley, UK)
Alexa Fluor® 488 or 546 goat anti-rabbit IgG	IF: 1:500; IHC: 1:350	Invitrogen (Paisley, UK)
Alexa Fluor® 488 goat anti-guinea pig IgG	IHC: 1:350	Invitrogen (Paisley, UK)
Biotinylated goat anti-mouse IgG	IHC: 1:250	Vector Laboratories (Peterborough, UK)
Biotinylated goat anti-rabbit IgG	IHC: 1:250	Vector Laboratories (Peterborough, UK)
Biotinylated goat anti-rat IgG	IHC: 1:250	Vector Laboratories (Peterborough, UK)
Biotinylated rabbit anti-goat IgG	IHC: 1:250	Vector Laboratories (Peterborough, UK)
Cy3-conjugated AffiniPure goat anti-mouse IgG (subclasses 1 + 2a + 2b + 3), Fc_γ fragment specific	IF: 1:500	Jackson Immuno Research Laboratories (Newmarket, UK)
Horseradish peroxidase-conjugated goat anti-mouse IgG	WB: 1:15000	Jackson Immuno Research Laboratories (Newmarket, UK)
Horseradish peroxidase-conjugated goat anti-rabbit IgG	WB: 1:15000	Jackson Immuno Research Laboratories (Newmarket, UK)
Sheep anti-DIG alkaline phosphatase-conjugated polyclonal antibody	ISH: 1:1000	Roche Applied Science (Burgess Hill, UK)

2.2 Methods

2.2.1 Animal work

2.2.1.1 Animal handling

Mice were housed in the London Research Institute animal facilities at Lincoln's Inn Fields Laboratories and Clare Hall Laboratories. In agreement with Schedule 1 of the Animal Scientific Procedures Act 1986, culling of adult mice was performed by cervical dislocation, culling of mouse embryos was performed by decapitation. All experiments involving mice were approved by the London Research Institute Animal Ethics Committee following UK Home Office guidelines.

2.2.1.2 Mouse lines

The floxed exon 5 *Fbxw7* mice were generated by Dr Anett Jandke in the Mammalian Genetics Lab (Jandke et al., 2011). The *Jun*4A and the ROSA26-Lox-STOP-Lox(LSL)-JNKK2-JNK1 transgenic constructs were electroporated into ES cells, stable transfectants were selected and mice generated according to standard protocols (Behrens et al., 1999). $Jun^{f/f}$, $Jun^{AA/AA}$, $Notch1^{f/f}$, ROSA26-LSL-YFP and Nestin-Cre mice have been described (Srinivas et al., 2001, Behrens et al., 1999, Radtke et al., 1999, Raivich et al., 2004).

2.2.1.3 BrdU injection

To study proliferation of cells in the gut, mice were injected intraperitoneally with 100 µg (per g bodyweight) 5-bromo-2'-deoxyuridine (BrdU; Sigma; stock: 20 µg/µl in endotoxin-free PBS). Mice were culled and analysed 1.5 h after injection.

To examine proliferation of cells in the SVZ and the RMS of the adult brain, mice were given 1 mg/ml BrdU in drinking water. BrdU drinking water was changed daily. Mice were culled and analysed after 14 days.

2.2.1.4 DSS treatment

To induce colitis and study gut regeneration, 2- to 3-month old mice were treated with dextran sodium sulfate (DSS). The mice received 2% DSS in drinking water for 7 days followed by three days of normal drinking water for recovery, after which mice were culled and analysed.

2.2.1.5 Facial axotomy and whisker movement test

Facial axotomy and whisker movement test were performed as previously described (Raivich et al., 2004). The right facial nerve fibers (including the retroauricular branch) of 2- to 3-month-old mice were crushed at the stylomastoid foramen under tri-brom-ethanol (Avertin) anaesthesia. 7-26 days after facial axotomy, whisker pad reinnervation was assessed by scoring whisker movement on the axotomised side in comparison to whisker movement on the control side. Scores were given in steps of 0.5 between 0 = no whisker movement and 3 = normal whisker movement. The whisker movement test was performed blindly and independently by two observers.

2.2.2 Cell Culture

2.2.2.1 Embryonic neurosphere cultures

Fore- and midbrains were dissected from E14.5 mouse embryos, transferred to PBS and crushed by trituration with a pipet. Cells were cultured under self-renewal (growth) conditions in neurobasal medium (NB; Invitrogen) supplemented with 1% (v/v) penicillin and streptomycin (10,000 U/ml; Invitrogen), 1% (v/v) l-glutamine (200 mM; Invitrogen), 2% (v/v) B27 supplement (Invitrogen) and human epidermal growth factor (EGF; 20 ng/ml; PeproTech) and fibroblast growth factor (FGF-basic; 20 ng/ml; PeproTech). Cells were cultured in tissue culture flasks for suspension cultures (Sarstedt; Greiner bio-one) in a humidified incubator at 37°C, 5% CO_2. Medium was changed every three days. All experiments were performed using secondary and tertiary neurospheres.

2.2.2.2 Adherent neural stem cell cultures

Adherent NSC cultures were derived as previously described (Pollard et al., 2006). Cells were cultured in neurobasal medium (Invitrogen) supplemented with 1% (v/v) penicillin and streptomycin (10,000 U/ml; Invitrogen), 1% (v/v) l-glutamine (200 mM; Invitrogen), 2% (v/v) B27 supplement (Invitrogen), 1% (v/v) N-2 supplement (Invitrogen), 20 ng/ml EGF (PeproTech), 20 ng/ml FGF-basic (PeproTech) and 1 μg/ml laminin (Sigma). Cells were cultured in tissue culture flasks for adherent cells (Corning) in a humidified incubator at 37°C, 5% CO_2. Medium was changed every three days.

2.2.2.3 Adult neurosphere cultures

Adult brains were dissected from 2- to 3-month-old mice. The midbrain was removed and the forebrain was embedded in low melting point agarose [dissolved in phosphate buffered saline (PBS); Invitrogen]. Brains were sectioned at 230 µm thickness using a vibratome (Leica VT1000). Sections containing the SVZ were carefully collected with a pasteur pipet and transferred into PBS. The SVZ was dissected from every section under a dissecting microscope and transferred into a 1.5 ml tube containing 200 µl PBS. The tissue was crushed by trituration with a pipet and the cell suspension was added to a well of a 6-well plate containing 4 ml neurobasal medium (Invitrogen) supplemented with 1% (v/v) penicillin and streptomycin (10,000 U/ml; Invitrogen), 1% (v/v) l-glutamine (200 mM; Invitrogen), 2% (v/v) B27 supplement (Invitrogen), 1% (v/v) N-2 supplement (Invitrogen), 20 ng/ml EGF (PeproTech), 20 ng/ml FGF-basic (PeproTech). Adult neurospheres were cultured in plates/flasks for suspension cultures [Becton Dickinson (BD) Falcon; Sarstedt] in a humidified incubator at 37°C, 3% O_2, 5% CO_2 and medium was changed every three days.

2.2.2.4 Generation of single cell suspensions from neurospheres

For the generation of single cell suspensions, neurospheres were treated with AccuMax™ (PAA Laboratories). Neurospheres were harvested and resuspended in 1 ml PBS and the same amount of AccuMax™ was added. Cells were incubated at 37°C for 7 min applying gentle agitation every other minute. After that, 10 ml PBS were added and the cell suspension was pipetted through a cell strainer (70 µm Nylon; BD Falcon) to remove remaining neurospheres. The cell strainer was rinsed twice with 10 ml PBS. The single cell supension was spun down and cells were resuspended in fresh medium.

2.2.2.5 Mouse embryonic fibroblast cultures

For the preparation of mouse embryonic fibroblast (MEFs) cultures, the head and the internal organs of E13.5 mice were removed. The remaining body was transferred into PBS and crushed by passing it through a 1 ml syringe (BD) and a 18-gauge needle (BD). Cell suspension was added to a well of a 6-well plate (BD) containing 4 ml Dulbecco's Modified Eagle Medium (DMEM, + 4.5 g/l glucose, + l-glutamine, +pyruvate; Invitrogen) medium supplemented with 10% foetal calf serum (FCS; Sigma) and 1% (v/v) penicillin and streptomycin (10,000 U/ml; Invitrogen). Confluent MEFs were trypsinised for 10 min and passaged to three times bigger plates/flasks for adherent cultures (BD Falcon; Corning) or one third of MEFs was plated to a same size plate/flask. MEFs were cultured in a humidified incubator at 37°C, 5% CO_2 either at standard atmospheric O_2 or 3% O_2.

2.2.2.6 Determination of cell numbers in vitro

Cells were counted using an Improved Neubauer counting chamber (Weber). To exclude dead cells, 40 µl of Trypan Blue solution (Sigma) was added to 40 µl of cell suspension and applied to the counting chamber. Viable cells in the 4 big quadrants (containing 16 small quadrants) were counted under the microscope. The number of counted cells was divided by two and multiplied with 10^4 to determine the cell number per ml.

For the growth curve analysis, MEFs were harvested by trypsinisation, resuspended in 1 ml medium and transferred to a Vi-Cell™ sample vial (Beckman Coulter). To

determine the number of cells, the cell suspension was passed through a Vi-Cell™ XR Cell Viability Analyzer (Beckman Coulter).

2.2.3 Cell Biology

2.2.3.1 Differentiation of neurospheres

For the differentiation of neurospheres, single cell suspensions were generated as described above. 5 x 10^5 cells were cultured under self-renewal conditions for two days. After that, neurospheres were transferred to neurobasal medium containing 1% (v/v) penicillin and streptomycin (10,000 U/ml; Invitrogen), 1% (v/v) l-glutamine (200 mM; Invitrogen), 2% (v/v) B27 supplement (Invitrogen) without growth factors, but supplemented with 10% (v/v) NeuroCult® Differentiation Supplement (StemCell Technologies). Neurospheres were added to a well of a 24-well plate (BD) containing a 12 mm diameter glass cover slip which was coated with poly-L-ornithine (0.01% solution; Sigma; diluted 1:10 in 150 mM disodium tetraborate buffer; Sigma). Cells were cultured in a humidified incubator at 37°C, 5% CO_2. Differentiation medium was changed every other day.

2.2.3.2 Neurosphere formation assay

Single cell suspensions were generated from neurospheres using AccuMax™ (PAA Laboratories) as described above. Neurosphere derived cells were counted and plated in a limiting dilution from 500 to 4 cells per well of a 96-well plate (BD). Cells were cultured under self-renewal conditions in a humidified incubator at 37°C, 5% CO_2 and every 5 days, 100 µl of fresh medium was added to each well. To assess neurosphere

formation, newly formed neurospheres were counted under the microscope after two weeks in culture.

2.2.3.3 Neurosphere sections

In order to obtain neurosphere sections, the Shandon Cytoblock® Cell Preparation System (Thermo Fisher Scientific) was used according to the manufacturer's instructions. For fixation, neurospheres were sedimented in a tube for 5 min. All but 0.5 ml medium was removed and double the amount of 10% neutral buffered formalin (NBF) was added. Neurospheres were incubated at 37°C overnight. Cytoblock cassettes were assembled into the horizontal Cytoclip and three drops of Cytoblock solution #1 was applied into the center of the well in the board insert. Next, a Cytofunnel disposable chamber was placed over the prepared Cytoblock and the metal clip holder was secured. Afterwards, the assembled Cytoclip was clamped into the Cytospin-Rotor. After removal of the 10% NBF, four drops of Cytoblock solution #2 was added to the neurospheres. The mixed cell suspension was subsequently applied into the Cytofunnel. After placing the Cytospin rotor in the Shandon Centrifuge Cytospin2 (Thermo Fisher Scientific), centrifugation took place at 1500 rpm, low acceleration for 5 min. After that, Cytofunnel assemblies were removed, Cytoclip was placed horizontally, the clip was released and the funnel was discarded. One drop of Cytoblock solution #1 was applied onto the cell button in the well. Next, the board insert was carefully removed and placed into a Tissue Tek® embedding cassette with two filter papers on the bottom and two filter papers on top. The cassette was placed in 10%

NBF to await processing. Processing was performed as described for tissues below. For embedding, the filter paper was folded back, the cell button was dislodged from the insert and embedded in paraffin wax (Tissue Tek) in the base mould.

Alternatively, fixed neurospheres were washed with PBS and sedimented in agarose (Bioline). After that, the agarose block containing the neurospheres was embedded in paraffin. Neurosphere sections at a thickness of 4 µm were cut with a manual microtome (RM2235, Leica, U.K.) and were allowed to uncrease in a water bath at 37°C. Afterwards, sections were mounted on Superfrost Ultra Plus charged slides (Menzel-Glaeser).

2.2.3.4 CFSE cell proliferation assay

Single cell suspensions were generated from neurosphere cultures using AccuMax™ (PAA Laboratories) as described above. For the assessment of CFSE (carboxyfluorescein diacetate succinimidyl ester; CellTrace CFSE Cell Proliferation Kit, Invitrogen) intensity over a period of 7 days, 1 x 10^6 cells were necessary for the following flow cytometry measurements with a fluorescence-activated cell sorter (FACS; BD). CFSE staining was performed according to the manufacturer's instructions with minor modifications. One fifth of the cell suspension remained unstained and served as unstained control (u). The rest of the cells were spun down at 450 x g, 4°C for 5 min and resuspended in 1 ml PBS + 7 µl 5 mM CFSE (Invitrogen). Cells were incubated for 5 min at room temperature for CFSE staining of cellular proteins. In order to stop the reaction, 13 ml of neurobasal medium + 20% FCS (Sigma)

was added. After centrifugation at 450 x g, 4°C for 5 min, stained and unstained cells were resuspended in fresh medium. Cells were cultured under self-renewal conditions in 25cm^2-culture tissue flasks for suspension cultures (Sarstedt), one culture for each measurement: unstained control (u), day 1 (d1), day 3 (d3), day 5 (d5) and day 7 (d7). Each day before the FACS measurements, single cell suspensions were prepared using AccuMax™. Cells were spun down at 450 x g, 4°C for 5 min, resuspended in 1 ml PBS and transferred to FACS tubes (BD). After washing the cells once again in PBS, 2 µl of 4-6-diamidino-2-phenylindole (DAPI, 200 µg/ml) was added to the samples to be able to exclude dead cells. 3 x 10^4 viable cells were counted for each sample with a LSR II Flow Cytometer from BD. Analysis was carried out using CellQuestPro (BD) and FlowJo (Tree Star) software.

2.2.3.5 TUNEL apoptosis assay

For the identification of apoptotic cells, TdT-mediated dUTP-biotin nick end labeling (TUNEL) was performed using the DeadEnd™ Colorimetric TUNEL System (Promega) according to the manufacturer's instructions. Neurosphere and tissue sections were incubated twice for 5 min in xylene to remove paraffin. After that, slides were washed in 100% ethanol for 5 min before rehydration in decreasing concentrations of ethanol. Next, neurosphere sections were washed in 0.85% NaCl and in PBS for 5 min each. Slides were immersed in 4% paraformaldehyde (PFA) solution for 15 min. Sections were washed twice in PBS and subsequently incubated with 100 µl of 20 µg/ml Proteinase K solution (Melford Laboratories) at room temperature for 10 min for permeabilisation. After that, slides were washed with PBS and fixation was repeated

with 4% PFA for 5 min. Sections were washed with PBS and equilibrated in equilibration buffer at room temperature for 5 min. For labeling of apoptotic cells, 100 µl of TdT reaction mix was added to each slide, the slide was covered with a plastic cover slip and incubated at 37°C in a dark, humidified chamber for 1 h. To stop the reaction, cover slips were removed and slides were immersed twice in 2x SSC buffer for 15 min. Sections were washed three times with PBS and then incubated in 0.3% hydrogen peroxide (H_2O_2; Sigma) for 3 min. Slides were washed three times with PBS before adding 100 µl streptavidin horseradish peroxidase (HRP; diluted 1:500 in PBS) to the slides. After incubation at room temperature for 30 min, slides were washed three times with PBS and 100 µl diaminobenzidine (DAB) was added to the sections. Staining reaction was stopped by washing the slides several times in deionized water. Nuclei were counterstained with Mayer's haematoxylin and sections were mounted using DPX mounting medium (Raymond A. Lamb). Sections were analysed by light microscopy (AX10 Imager.A1, Carl Zeiss).

2.2.3.6 β-galactosidase senescence assay

Cellular senescence was detected in MEFs using the Senescence Cells Histochemical Staining Kit (Sigma) according to the manufacturer's instructions. Cells were incubated in the staining mixture at 37°C in a non CO_2 enriched environment overnight. The next day, cells were washed with PBS and cells were analysed by light microscopy (AX10 Imager.A1, Carl Zeiss). The number of blue-stained β-galactosidase-positive cells represents the number of senescent cells.

2.2.3.7 Immunocytochemistry with cell permeabilisation

After removal of the medium, cells plated on 12 mm diameter cover slips were washed once with PBS. Next, cells were incubated for 30 s in 500 µl PIPES buffer [80 mM PIPES (Sigma), 1 mM $MgCl_2$ (LRI/CRUK), 5 mM EGTA (Sigma), 0.5% Triton X-100 (Sigma); pH 6.8]. After that, cells were fixed with 1 ml methanol (Fisher Scientific) for 3 min at –20°C and washed three times with 500 µl PBS + 0.1% Triton X-100 for 5 min. For blocking of unspecific binding, cells were incubated in PBS + 0.1% Triton X-100 + 5% goat serum (Sigma) + 0.1% sodium azide (Sigma) for 15 min. Next, 250 µl of primary antibodies (for a list of primary antibodies and dilutions, see page 124) diluted in PBS + 0.1% Triton X-100 (Sigma) + 5% goat serum (Sigma) + 0.1% sodium azide (Sigma) were added to the cells. After 45 min of incubation at room temperature, primary antibodies were removed and cells were washed three times with 500 µl PBS + 0.1% Triton X-100 for 5 min. Next, corresponding fluorochrome labeled secondary antibodies (for a list of secondary antibodies and dilutions, see page 126) diluted in PBS + 0.1% Triton X-100 + 5% goat serum were added and cells were incubated for 45 min in the dark at room temperature. As a control for antibody specificity, some cells were only incubated with 250 µl of secondary antibodies but not with primary antibodies. Cells were washed three times with 500 µl PBS + 0.1% Triton X-100 and DNA was counterstained with 500 µl Hoechst 33342 solution (10 mg/ml, Sigma) diluted 1:2000 in PBS + 0.1% Triton X-100 for 5 min. Cells were washed once with 500 µl PBS. Cover slips were washed once in ddH_2O and mounted upside down on a drop of Fluorescent Mounting Medium (DAKO) on microscope slides (Menzel-Glaeser). The next day, the cover slips were sealed on the microscope slides with nail polish. Slides were stored in

the dark at 4°C. Cells were analysed by confocal microscopy (LSM 510 Inverted Microscope, Carl Zeiss; software: LSM 510 version 2.8 SP1, Carl Zeiss).

2.2.3.8 Immunocytochemistry without cell permeabilisation

For staining of the surface sulfatide O4, immunocytochemistry was performed without cell permeabilisation. After removal of the medium, cells plated on 12 mm diameter cover slips were washed once with PBS. Next, 250 µl of primary O4-antibody (Chemicon; diluted 1:200 in PBS + 5% goat serum) was added to each well and cells were incubated for 20 min at 37°C, 5% CO_2. Cells were washed twice with 500 µl warm HBSS + Ca^{2+}/Mg^{2+} (Invitrogen). For fixation, cells were incubated in 4% PFA solution (Sigma; dissolved in PBS; pH 7.4) for 20 min. After three washes with PBS, 250 µl of Alexa Fluor® 488 goat anti-mouse IgM (µ chain, Invitrogen; diluted 1:500 in PBS + 5% goat serum) was added to each well and cells were incubated for 90 min in the dark at room temperature. Cells were washed three times with PBS and DNA was counterstained with 500 µl Hoechst 33342 solution (10 mg/ml, Sigma) diluted 1:2000 in PBS for 5 min. Cells were washed once with 500 µl PBS. Cover slips were washed once in ddH_2O and mounted upside down on a drop of Fluorescent Mounting Medium (DAKO) on microscope slides (Menzel-Glaeser). The next day, the cover slips were sealed on the microscope slides with nail polish. Slides were stored in the dark at 4°C. Cells were analysed by confocal microscopy (LSM 510 Inverted Microscope, Carl Zeiss; software: LSM 510 version 2.8 SP1, Carl Zeiss).

For the O4/Map2/Cx43 (for primary antibody details, see page 124) triple staining, the primary antibody incubation step with O4 was performed before fixing the cells using 4% PFA and antibody staining for Map2 and Cx43. Secondary antibodies used for the triple staining were Alexa Fluor® 633 goat anti-rabbit (Invitrogen; diluted 1:500 in PBS + 5% goat serum), Alexa Fluor® 488 goat anti-mouse IgM (μ chain, Invitrogen; diluted 1:500 in PBS + 5% goat serum) and Cy3-conjugated AffiniPure goat anti-mouse IgG (subclasses 1 + 2a + 2b + 3), Fc_γ fragment specific (Jackson ImmunoResearch Laboratories, diluted 1:500 in PBS + 5% goat serum) (for secondary antibody details, see page 126).

2.2.4 Histology

2.2.4.1 Tissue processing

Tissues were fixed in 10% neutral buffered formalin (NBF) overnight. The next day, the tissue was incubated at 40°C in 70% (v/v) ethanol for 30 min, in 85% (v/v) ethanol for 1 h, in 95% (v/v) ethanol for 1 h and three times in 100% (v/v) ethanol for 1 h for dehydration. Afterwards, the tissue was cleared three times in xylene for 1 h at 40°C and infiltrated three times with paraffin wax for 1 h at 60°C. Tissue processing after fixation was performed with a Tissue-Tek VIP® 5 Vacuum Infiltration Processor. Heads were cut sagittally. Tissue was embedded in paraffin wax (Tissue Tek) in Tissue-Tek® embedding cassettes and cooled for 30 min at 4°C. Tissue sections were cut at a thickness of 4 μm using a manual microtome (RM2235, Leica) and were allowed to unfurl in a water bath at 37°C. Afterwards, sections were mounted on Superfrost Ultra

Plus charged slides (Menzel-Glaeser).

2.2.4.2 Haematoxylin and eosin (H&E) staining

Haematoxylin stains basophilic structures such as nucleic acids blue whereas eosin stains eosinophilic structures such as proteins pink. Consequently, in H&E stained tissue sections, nuclei appear blue while the cytoplasm is stained pink.

Paraffin sections were dewaxed in xylene three times for 3 min. After that, sections were hydrated through graded alcohols to water: 2 x in 100% industrial methylated spirit (IMS) for 3 min, 2 x in 70% (v/v) IMS for 3 min and 2 x in water for 3 min. The sections were stained for 5 min in Harris`s haematoxylin and subsequently washed in running tap water for 5 min. Next, sections were differentiated in 1% (v/v) acid alcohol (1% HCl in 70% alcohol) for 5 s and washed in running tap water for 5 min. The sections were stained in 1% (w/v) eosin Y and washed in running tap water for 5 min. After that, sections were dehydrated through graded alcohols: 2 x in 70% (v/v) IMS for 3 min and 2 x in 100% IMS for 3 min. Finally, sections were cleared twice in xylene for 3 min and mounted with DPX mounting medium (Raymond A. Lamb).

2.2.4.3 Immunohistochemistry

Paraffin sections were dewaxed in xylene three times for 3 min. After that, sections were hydrated through graded alcohols to water: 2 x in 100% industrial methylated spirit (IMS) for 3 min, 2 x in 70% (v/v) IMS for 3 min and 2 x in water for 3 min. Next, citrate

buffer (2.94 g trisodium citrate plus 22 ml 0.2 M HCl filled up to 1 l with ddH_2O) was heated for 5 min at full power in a microwave, sections were added and for antigen retrieval microwaved for 10 min at full power. Sections were then allowed to cool for 30 min at room temperature. Sections were incubated in 1.6% H_2O_2 (v/v) in PBS for 10 min and subsequently washed three times with PBS for 3 min. To block unspecific binding, 10% (v/v) goat serum diluted in 1% (w/v) bovine serum albumin (BSA)/PBS was added and sections were incubated for 30 min at room temperature. After removal of the goat serum, primary antibodies (for a list of primary antibodies and dilutions, see page 124) diluted in 1% (w/v) BSA/PBS were applied to the sections for 1 h at room temperature. Sections were washed three times with PBS for 5 min and subsequently incubated with corresponding fluorochrome-conjugated secondary antibodies (for a list of secondary antibodies and dilutions, see page 126) for 1 h at room temperature. Alternatively, sections were incubated with corresponding biotinylated secondary antibodies (diluted in 1% BSA/PBS) for 1 h at room temperature. Sections were washed three times in PBS for 5 min and incubated in ABC reagent (horseradish peroxidase avidin-biotin complex; Vector Laboratories, Vectastain Elite, ABC Kit) for 30 min. After washing the sections three times for 5 min in PBS, sections were incubated in diaminobenzidine/H_2O_2 (DAB solution; Biogenex) for 2-5 min and color reaction was monitored microscopically. Staining was stopped by rinsing the sections with distilled water. Sections were counterstained with Mayer`s haematoxylin for 3 min and subsequently washed in running tap water for 5 min. Sections were dehydrated through graded alcohols: 2 x in 70% IMS for 3 min and 2 x in 100% IMS for 3 min. Finally, sections were cleared twice

in xylene for 3 min and mounted using DPX mounting medium (Raymond A. Lamb). Sections were analysed by light or fluorescence microscopy (Carl Zeiss Axioplan 2 Imaging).

For staining of alkaline phosphatase-positive enterocytes, nitro blue tetrazolium (NBT; Roche)/5-bromo-4-chloro-3-indolyl phosphate (BCIP; Roche) substrate solution was used and nuclei were counterstained with nuclear fast red (Vector Laboratories). To visualise mucous glycoconjugate-containing goblet cells, alcian blue (AB; Sigma)/periodic acid-Schiff (PAS; Sigma) staining was performed.

For the GFP-staining on E14.5 mouse embryos, samples fixed in 4% PFA were embedded in 1.5 g gelatin and 90 g albumin dissolved in 300 ml 0.1 M sodium acetate buffer (for recipe see page 115). For polymerisation, 500 µl 25% glutaraldehyde was added to 10 ml of the gelatin/albumin solution. After solidifying, the samples were cut at 200 µm using a vibratome (Leica VT1000). Permeabilisation was performed using PBS + 0.5% Triton X-100 (Sigma). Unspecific binding was blocked by incubation with PBS + 0.5% Triton X-100 (Sigma) + 10% goat serum. The sections were incubated with polyclonal rabbit anti-GFP primary antibody (Invitrogen) at 4°C overnight. After washing with PBS + 0.5% Triton X-100 (Sigma), samples were incubated with Alexa Fluor® 488 goat anti-rabbit IgG secondary antibody (Invitrogen) at room temperature for 2 h. After washing with PBS + 0.5% Triton X-100 (Sigma) and PBS, sections were mounted and images were acquired by confocal microscopy (LSM 510 Inverted Microscope, Carl Zeiss; software: LSM 510 version 2.8 SP1, Carl Zeiss).

2.2.4.4 Determination of cell numbers

In order to be able to obtain comparable sections of the developing brain from different mice, serial sections were cut and every 5th section was stained with H&E. By analysing the H&E stainings, comparable sections were selected according to prominent brain structures such as the lateral ventricle. Cell numbers were counted throughout the cortex and the tectum on one representative section per brain in comparable areas of the same width which are represented by the low magnification pictures in the results chapters. Layer boundaries were determined by cell morphology and layer-specific marker expression.

In the adult brain, comparable sections were obtained as described for the developing brain. Cellularity was determined by counting cells throughout the rostral migratory stream on low magnification pictures.

In the intestine, comparable areas of the ileum and the colon were selected at the distal part of the small or the large bowel respectively. Cellularity was determined by counting cells in 10 villi or 10 crypts per mouse.

2.2.4.5 In situ hybridisation

For non-radioactive *in situ* hybridisation (ISH), all steps were performed under RNase-free conditions using Digoxigenin (DIG)-labelled RNA-probes which were designed and generated by Dr Rocio Sancho. Tissues were dissected in ice-cold PBS and fixed in 10% NBF overnight. Tissues were then processed, embedded in paraffin and sectioned at 8 µm. Paraffin sections were dewaxed in xylene twice for 5 min. Next, sections were hydrated through graded alcohols to water: 2 x in 100% ethanol for 5 min, 1 x in 95%

(v/v) ethanol for 5 min, 1 x in 70% (v/v) ethanol for 5 min and 1 x in DEPC water. Slides were washed once in PBS for 5 min and incubated in 10 µg/ml Proteinase K diluted in pre-warmed (37°C) 100 mM Tris-HCl pH7.5/50 mM EDTA for 15 min. Sections were washed once in 0.2% glycine in PBS and incubated in 4% PFA for 10 min. After washing three times in PBS, sections were incubated once in 4x SSC buffer for 2 min. Next, sections were pre-hybridised in hybridisation solution (for recipe, see page 110) without the probe for 1 h at 57°C in a humidified chamber. Then, 1 ng/ml from the *in vitro* transcription probe was added to the hybridisation solution and denatured at 75°C for 15 min. After cooling on ice for 5 min, the hybridisation solution including the probe is pipetted onto the sections and hybridisation takes place at 57°C overnight in a humidified chamber. The next day, sections were processed as follows: 1 x in 5x SSC at 60°C for 10 min, 1 x in 50 % formamide/2x SSC at 60°C for 30 min, 1 x in 2x SSC at 60°C for 30 min, 2 x in 0.2x SSC at 60°C for 30 min, 1 x in maleic acid buffer at room temperature for 5 min and 1 x in blocking buffer (for recipes see pages 108, 110, 115) at room temperature for 30 min. After that, sections were incubated in sheep anti-DIG alkaline phosphatase-conjugated antibody (Roche; diluted 1:1000 in blocking buffer) at 37°C for 2 h. Next, sections were washed twice in maleic acid buffer at room temperature for 15 min before incubation in detection buffer (for recipe see page 108) at room temperature for 5 min. To develop, sections were incubated in the dark with 1 ml detection buffer plus 4.5 µl nitro blue tetrazolium (NBT; Roche) and 3.5 µl 5-bromo-4-chloro-3-indolyl phosphate (BCIP; Roche) and the chromogenic reaction was monitored under the microscope. The reaction was stopped by incubation of the sections in

detection buffer for 15 min and then water for 15 min. After that, sections were mounted in VectaMount AQ (Vector Laboratories).

For the radioactive *in situ* hybridisation, probes were designed and generated by Dr Anett Jandke and the labelling and sample processing was performed by the LRI *In Situ* Hybridisation Service. Images were acquired using a darkfield microscope (Olympus).

2.2.5 Biochemistry

2.2.5.1 Protein extraction

Cells or tissues were washed in PBS and spun down at 1500 rpm, 4°C for 5 min. Afterwards, cells or tissues were treated with 400 µl of 1x RIPA buffer (NEB, 10x RIPA buffer (for recipe see page 114; diluted 1:10 in ddH_2O) supplemented with 1:100 protease inhibitor (PI; 100 x; Sigma), 1:100 phenylmethylsulfonyl fluoride (PMSF) and 1:100 sodium fluoride and incubated on ice for 15 min. Cells were sonicated three times for 15 s at an amplitude of 10 microns (MSE Soniprep 150, SANYO) and immediately put on ice afterwards. Tissues were disrupted three times for 15 s using the Ultra Turrax® disperser (IKA). After that, suspensions were spun down at 16000 x g, 4°C (Eppendorf Centrifuge 5415 R) for 10 min and supernatants containing the protein extracts were removed for use or storage at -20°C.

2.2.5.2 Determination of protein amounts (Bradford assay)

By means of a Bradford assay, protein amounts of protein extracts were determined. The Protein Assay Dye Reagent (Bradford Reagent (BR), Bio-Rad) contains Coomassie Brilliant Blue G-250 which binds to proteins and consequently changes the absorption maximum from 465 nm to 595 nm. This increase can be measured with a spectrophotometer and used to determine protein amounts in protein extracts. To obtain a standard curve, 0, 1, 2, 4, 8, 16 and 32 µl of a 1.5 mg/ml BSA solution were added to cuvettes containing 1 ml BR (diluted 1:5 in ddH_2O) and absorption was measured with a spectrophotometer (Ultrospec 3100 pro, GE Healthcare). Afterwards, 1 µl of protein extracts was added to cuvettes containing 1 ml BR and absorption was measured with a spectrophotometer. In reference to the standard curve, protein amounts could be determined. Protein amounts of comparative samples were standardised to the lowest protein concentration by diluting the samples containing higher protein levels with the corresponding amount of RIPA buffer plus supplements. Protein extracts were stored at -20°C.

2.2.5.3 Sodium Dodecyl Sulfate-Polyacrylamide Gel Electrophoresis (SDS-PAGE)

After determination of protein amounts and standardisation of protein concentrations of comparative samples, protein loading buffer (Laemmli buffer; for recipe, see page 113) was added 1:5 to protein extracts and samples were boiled for 5 min on a heat block (Techne Dri-Block DB-2D). Furthermore, 5% stacking gel solution and 10% resolving gel solution were prepared (for recipes see pages 114, 115). For polymerisation,

tetramethylethylenediamine (TEMED) and ammonium persulfate (APS) were added directly before pouring gels into assembled glass plates for vertical electrophoresis (C.B.S Scientific). After filling ~3/4 of the gel chamber between assembled glass plates with 10% resolving gel, 1 ml 2-propanol (Fisher Scientific) were pipetted on top of the resolving gel solution in order to obtain an even edge at the top of the gel. After polymerisation of the resolving gel and removal of the 2-propanol, the rest of the gel chamber was filled with 5% stacking gel and a gel comb (C.B.S Scientific) was inserted. After polymerisation of the stacking gel, the gel chamber was clamped into an Adjustable Slab Gel Kit (C.B.S Scientific), the tank was filled with 1x SDS-PAGE Running Buffer (for recipe see page 114), the gel comb was removed and samples and rainbow markers (GE Healthcare) were loaded. Protein separation took place at 45 mA for 2.5 h.

2.2.5.4 Western Blot

Western blotting was performed in a semi-dry blot chamber (Hoefer Scientific Instruments). Proteins separated in SDS gels were transferred on nitrocellulose membranes (Whatman) with three layers of blotting paper (Whatman) underneath the membrane and three layers of blotting paper on top of the gel. Before, the blotting paper was soaked with 1x semi-dry transfer buffer (recipe see page 115) and the nitrocellulose membrane was equilibrated with ddH_2O and then transfer buffer. Proteins were transferred for 2 h at 144 mA. To visualise transferred proteins, nitrocellulose membranes were incubated briefly in Ponceau S solution (Sigma) and afterwards washed with distilled H_2O. Unspecific binding was blocked by incubating the membrane for at

least 1 h in 10% (w/v) skimmed milk [A1 Laboratory Supplies Ltd; dissolved in Tris-Buffered Saline Tween-20 (TBS-T)] supplemented with 1% (v/v) sodium fluoride (Sigma), 0.5% (v/v) sodium orthovanadate (NEB) and 0.02% (v/v) sodium azide (Sigma). After that, membranes were incubated with primary antibodies diluted in 5% (w/v) skimmed milk or 5% BSA at 4°C overnight on a shaker. The next day, membranes were washed three times with TBS-T at room temperature for 10 min on a shaker. Membranes were incubated with horseradish peroxidase(HRP)-conjugated secondary antibodies (Jackson Laboratories) diluted in 5% skimmed milk or 5% BSA at room temperature for 1 h on a shaker. Afterwards, membranes were washed again three times with TBS-T at room temperature for 10 min on a shaker and subsequently, membranes were incubated for 3 min in ECL Detection Solution 1 and 2 (1:1 dilution; GE Healthcare). According to signal intensities, Fuji X-ray films (Fisher Scientific) were exposed to the membranes in developing chambers for various periods of time.

2.2.6 Molecular Biology

2.2.6.1 DNA isolation

For genotyping, murine material was incubated in 100 µl DirectPCR Lysis Reagent (Viagen) + 3 µl Proteinase K (10 mg/ml, Melford) overnight at 56°C. The next day, samples were incubated at 85°C for 45 min to inactivate Proteinase K. Samples were then vortexed and centrifuged at full speed for 15 min (Eppendorf Centrifuge 5415 D). Afterwards, 2 µl of the lysates were used for genotyping and lysates were stored at -20°C.

For cloning, cell suspensions were incubated in 500 µl DNA Lysis buffer (50 mM Tris, pH 8; 100 mM EDTA; 100 mM NaCl; 1% SDS) + 30 µl Proteinase K (10 mg/ml, Melford) overnight at 56°C. The next day, samples were shaken for 5 mins at 37°C on a heat block (Eppendorf Thermomixer compact) and subsequently 200 µl of 5 M NaCl was added. After shaking the samples again at 37°C for 5 min, they were centrifuged at full speed for 15 min (Eppendorf Centrifuge 5415 D). Supernatants were transferred to new tubes and 500 µl of 2-propanol (Fisher Scientific) was pipetted to each sample. After shaking the samples at 37°C for 10 min, samples were spun down at full speed for 10 min. Supernatants were discarded and DNA-pellets were air dried for 20 min. Afterwards, 40 µl ddH_2O was added and samples were shaken for 1 h at 37°C to dissolve the DNA.

2.2.6.2 Genotyping PCR

After DNA isolation, genotyping polymerase chain reaction (PCR) mix was prepared using 2 µl DNA per reaction:

1 x PCR-Mix (Qiagen):

1 x CoralLoad PCR Buffer:	2 µl (10 x stock)
1 x Solution Q:	4 µl (5 x stock)
dNTPs (0.25 mM):	0.2 µl (25 mM stock)
Primer forward (1 µM):	0.2 µl (100 µM stock)
Primer reverse (1 µM):	0.2 µl (100 µM stock)
Taq-Polymerase (0.2 U):	0.2 µl (5 U/µl stock)
ddH_2O:	11.2 µl
+ DNA	2 µl
	20 µl

For a list of genotyping primer combinations and sizes of expected bands, see page 119.

Table 7 PCR programme
For *Fbxw7*, *Jun*, *Notch1*, *Cre* and *eGFP* PCR:

Step	Temperature	Time	Number of cycles
initial denaturation	94°C	3 min	1
denaturation	94°C	30 s	35
annealing	60°C	45 s	
extension	72°C	45 s	
final extension	72°C	10 min	1

2.2.6.3 Agarose gel electrophoresis

PCR products were separated on a 1.5% agarose (Bioline) gel (diluted in 1x TAE; + 1:10 ethidium bromide (10 mg/ml; Sigma-Aldrich) for 1 h at 120 V. To determine band size, 10 µl of a 1 kb DNA ladder (Invitrogen) was loaded.

2.2.6.4 Transformation of bacteria

For the amplification of plasmid DNA, bacteria were transformed using XL10-Gold® Ultracompetent Cells (Stratagene) according to the manufacturer's instructions with minor modifications. Ultracompetent cells were thawed on ice and 150 µl of cell suspension were transferred to pre-chilled polypropylene round-bottom tubes (BD Falcon). 6 µl of β-mercaptoethanol (Stratagene) were added and after gently mixing the cells, they were incubated for 10 min on ice gently swirling them every other minute. After that, 20-50 ng of plasmid DNA or 2-4 µl of a ligation mixture were added to the cells and tubes were incubated on ice for 30 min. Next, transformation was induced by heat shock for 30 s in a 42°C water bath. After that, cells were incubated on ice for 2 min, 1 ml of SOC-medium (Invitrogen) was added and cells were incubated at 37°C for 1 h shaking at 250 rpm. Afterwards, 50 µl, 100 µl and 200 µl of the transformation mixture were plated on lysogeny broth (LB; LRI/CRUK) agar plates containing the appropriate antibiotic. The plates were incubated at 37°C overnight and the following day, colonies were picked and grown in 2 ml LB containing the appropriate antibiotic or plates were stored at 4°C. Alternatively, 1 ml of transformation mixture was used to inoculate 200 ml of LB containing the appropriate antibiotic.

For the amplification of pENTR-vectors containing a *ccd*B gene, transformation was performed as described using Library Efficiency DB3.1™ Competent Cells (Invitrogen).

2.2.6.5 Preparation of plasmid DNA

After centrifugation of the bacterial cell suspensions at 1350 x g, 4°C for 10 min, plasmid DNA was isolated from bacterial cell pellets using the QIAprep Spin Miniprep Kit (QIAGEN) or the QIAGEN Plasmid Maxi Kit (QIAGEN) for high copy plasmids and the NucleoBond® Plasmid Purification Kit (Clontech Laboratories) for low copy plasmids according to the manufacturers' instructions. DNA concentrations and quality were measured using the NanoDrop spectrophotometer (Thermo Scientific). The ratio of OD_{260}/OD_{280} should be ~1.8. Plasmid DNA was verified by restriction enzyme digest followed by gel electrophoresis or DNA sequencing.

2.2.6.6 Restriction enzyme digest and DNA purification

DNA was analysed or DNA fragments were excised by cutting DNA with restriction endonucleases (NEB; Fermentas, Thermo Scientific) for at least 2 hours or overnight according to manufacturer's instructions. DNA product from enzymatic reactions were either purified using the illustra™ GFX™ PCR DNA and Gel Band Purification Kit (GE Healthcare) according to manufacturer's instructions or DNA fragments were separated by gel electrophoresis, excised from the gel and subsequently purified.

2.2.6.7 DNA sequencing

For DNA sequencing, 200 ng of DNA was added to the sequencing PCR mix and made up to 20 µl with ddH_2O:

1 x sequencing PCR-Mix:

8 µl BigDye Terminator reaction mix (BDT)

0.32 µl Primer (from 10 µM stock)

For a list of sequencing primers, see page 121.

The sequencing PCR programme consisted of the following steps repeated over 28 cycles:

1. 95°C for 30 s

2. 55°C for 30 s

3. 60°C for 4 min

Next, sequencing PCR-products were purified using the DyeEx® 2.0 Spin Kit (QIAGEN). Samples were dried in a Savant DNA Speed Vac® Concentrator (Thermo Scientific) at high drying rate for 20 min and sent to the LRI Equipment Park for sequencing.

2.2.6.8 Ligation of DNA fragments

DNA fragments were ligated using T4 DNA ligase (NEB) according to the manufacturer's instructions with minor modifications. To reduce the self-ligation of a vector digested with restriction enzymes creating compatible sticky ends, vector DNA was pre-treated with Calf Intestinal Alkaline Phosphatase (CIP; NEB) at 37°C for 1 h. 25 ng vector DNA was pipetted to the ligation reaction mix. Insert DNA was added in a 5 (insert):1 (vector) or 3:1 molar ratio. The amount of insert DNA to use can be calculated as follows:

$$\text{insert DNA ng} = \frac{\text{ratio}\ (5:1\ \ 3:1)\ \downarrow\ \downarrow \quad \text{vector input}\ \downarrow \quad (5 \text{ or } 3 \times \text{bp insert}) \times 25\ \text{ng}}{\text{bp vector}}$$

The ligation mix was incubated at 16°C overnight and 2-4 µl of ligation mix was used in a subsequent transformation of bacteria to amplify the DNA. All ligations were performed together with a vector only control.

2.2.6.9 BAC subcloning

Bacterial artificial chromosome (BAC) subcloning by Red®/ET® Recombination was performed using the BAC Subcloning Kit (Gene Bridges) according to the

manufacturer's instructions with minor modifications. I designed oligonucleotides consisting of 50 bp BAC homology arms (flanking a 10 kb region containing the *Jun* locus), a unique restriction site and a given primer sequence for amplification of a linear vector carrying a ColE1 origin and an ampicillin (AMP) resistance gene from a minimal vector PCR-template (2.7 kb; Gene Bridges). The 2.7 kb PCR-product was purified using the illustra™ GFX™ PCR DNA and Gel Band Purification Kit (GE Healthcare) according to manufacturer's instructions. Next, the bacteria containing the BAC clone with the *Jun* locus [RP23 117A16 (BPRC), chloramphenicol (CAM) resistance] were plated on LB agar plates containing 12.5 µg/ml CAM (Sigma). The next day, 10 colonies were picked and grown in 1 ml LB medium + 12.5 µg/ml CAM shaking at 37°C overnight. The next day, 1.4 ml LB medium + 12.5 µg/ml CAM were inoculated with 30 µl of the overnight culture and incubated for 2 hours shaking at 37°C. After that, 2 µl the Red/ET recombination protein expression plasmid pSC101-BAD-gbaA^{tet} carrying a tetracycline resistance gene was electroporated into the cells using a Bio-Rad Gene Pulser® II at the following settings: Voltage: 1.8 kV, capacitance: 25 µF, resistance: 200 Ω, pulse: 5 ms. Electroporated cells were then incubated in 1 ml LB medium without antibiotics and shaking at 30°C for 70 min. Next, 200 µl of the cells were plated on LB agar plates containing 12.5 µg/ml CAM and 3 µg/ml tetracycline (TET, Sigma) and incubated at 30°C in the dark for 48 h. After that, 10 colonies were picked and incubated in 1 ml LB medium plus 12.5 µg/ml CAM and 3 µg/ml TET shaking at 30°C overnight. The next day, 1.4 ml LB medium plus 12.5 µg/ml CAM and 3 µg/ml TET were inoculated with 30 µl of the overnight culture and incubated shaking at 30°C until OD600 ~0.3. After that, 50 µl of 10% L-arabinose were added to half of the tubes to

induce the expression of the Red/ET recombination proteins while the other half was used as negative control. The cells were incubated shaking at 37°C for 1 h. Cells were then spun down at 11000 rpm, 2°C for 30 s and washed twice with 1 ml chilled ddH_2O. After a further centrifugation step, the supernatant was discarded, so that 20-30 µl were left in the tube with the pellet. Next, 3 µl (0.1-0.2 µg) of the prepared linear vector fragment PCR-product with homology arms was added and electroporation was performed using the Bio-Rad Gene Pulser® II as described above. 1 ml of LB medium with 50 µl 10% L-arabinose (Sigma; not added in the negative control) but without antibiotics was added and the cells were incubated at 37°C for 2 h to allow recombination to occur. Next, 100 µl of the cultures were plated on LB agar plates containing 100 µg/ml AMP and incubated at 37°C for 48h, at which temperature the Red/ET recombination plasmid will be lost. Whereas there were no colonies detectable on the negative control (without L-arabinose) plates, individual colonies were picked from the plates with the L-arabinose induced cultures and cultured in 3 ml LB plus 100 µg/ml AMP shaking at 37°C overnight. Plasmid DNA was prepared using the QIAprep Spin Miniprep Kit (QIAGEN) as described above. Successful homologous recombination was confirmed by restriction digest using various restriction enzyme combinations. Subsequently, parts of the genomic BAC sequence were excised by restriction digest and substituted by mutated sequences. To generate the final targeting construct, a loxP-PGK-gb2-neo-loxP fragment was excised from a plasmid DNA template (Gene Bridges) by restriction digest. This fragment contains a neomycin resistance gene and was inserted into a unique restriction site of the genomic locus after

the *Jun* open reading frame (ORF) as a selective marker to be able to identify properly targeted ES cell clones. Correct insertion of the neomycin cassette was confirmed by restriction digest. The final targeting construct was sequenced and linearised by restriction digest.

For a list of primers used to generate the *Jun*4A targeting construct, see page 121.

2.2.6.10 Southern Blot

Southern blot analysis for correct insertion of the LSL-JNKK2-JNK1 targeting construct into the ROSA26 locus was performed by Lieven Haenebalcke in Dr Jody Haigh's Lab at the University of Gent, Belgium as previously described (Nyabi et al., 2009). 5' integration was assessed by using a 550bp 5'-external probe which, after BamHI digest of genomic DNA, detects the wt allele at 5.8 kb and the targeted allele at 3.0 kb. 3' integration was analysed by using a 800bp 3'-external probe which, after KpnI digest detects the wt allele at 37 kb and the targeted allele at 8.8 kb.

2.2.6.11 RNA isolation

RNA was isolated from cells using the RNeasy Mini- or RNeasy Midi-kit (QIAGEN) according to the manufacturer's instructions. To homogenise the lysates, samples were passed through an 18-gauge needle (BD) several times. On-Column DNase digestion was performed using the RNase-Free DNase Set (QIAGEN). RNA quality was checked by gel electrophoresis where two distinct bands representing 28s-rRNA and 18s-rRNA are expected to be seen. RNA concentrations and quality were measured using the

NanoDrop spectrophotometer (Thermo Scientific). The ratio of OD_{260}/OD_{280} should be between 1.8 and 2.0. RNA was used immediately for cDNA-synthesis or stored at -80°C.

2.2.6.12 cDNA-synthesis

RNA amounts were standardised using RNase-free water and cDNA-synthesis was performed using the Superscript III First-Strand cDNA synthesis kit (Invitrogen) and random hexamer primers (Invitrogen) according to the manufacturer's instructions.

2.2.6.13 Quantitative real-time PCR analysis

For quantitative real-time PCR (qRT-PCR) analysis, cDNA was diluted 1:5 in ddH_2O. 3.5 µl of cDNA were used per qRT-PCR reaction which was conducted in triplicates. qRT-PCR was performed measuring SYBR Green incorporation (Platinum Quantitative PCR SuperMix-UDG w/ROX, Invitrogen) on an ABI7900HT (Applied Biosystems). Data were analysed using the SDS 2.3 software (Applied Biosystems). Primers were designed using Primer Express 3.0 software (Applied Biosystems).

For a list of qRT-PCR primers, see page 122.

3x qRT-PCR-Mix (triplicate):

37.5 µl Platinum SYBR Green

34.5 µl ddH_2O

1.5 µl Primer 1 (10 µM stock)

1.5 µl Primer 2 (10 µM stock)

+ 3.5 µl cDNA

To exclude primer dimer and unspecific amplification, 'no template' control was included and a dissociation curve performed. To retrieve Ct values, the threshold was set within the exponential phase of the amplification plots.

2.2.7 Statistical analysis

Statistical evaluation was performed by Student's unpaired *t*-test. Data are presented as mean ± standard error of the mean (s.e.m.); $P \leq 0.05$ was considered statistically significant. *n* represents the number of independent biological replicates, i.e. for histology the number of mice analysed per genotype and for cytology the number of mice used per genotype to isolate primary cell lines for independent experiments.

Chapter 3. Results

3.1 Fbw7 controls cell number and differentiation in the developing brain

3.1.1 Conditional deletion of Fbw7 in the nervous system

Due to the fact that Fbw7 knockout mice die around embryonic day (E) 10.5 as a consequence of placental and vascular defects (Tetzlaff et al., 2004, Tsunematsu et al., 2004), conditional Fbw7 knockout mice were generated in our laboratory (Jandke et al., 2011) to investigate the importance of Fbw7 at later stages of development. These floxed *Fbxw7* (*Fbxw7*^{f}) mice carry a *Fbxw7* allele in which exon 5 is flanked by loxP-sites (**Figure 22a**). Exon 5 encodes for the essential F-box domain of the protein which is responsible for the binding of Fbw7 to the SCF E3 ubiquitin ligase complex. Upon crossing *Fbxw7*$^{f/f}$ mice to transgenic mice expressing Cre recombinase, exon 5 is excised and the open reading frame (ORF) of the *Fbxw7* gene is disrupted. Cre expression under the control of a Nestin-promoter has previously shown to result in Cre-mediated recombination specifically in the nervous system (Kramer et al., 2006, Raivich et al., 2004). As proof of principle, crossing Nestin-Cre mice to ROSA26-LSL-YFP mice resulted in tissue-specific deletion of the loxP-STOP-loxP (LSL) cassette and consequently reporter gene expression in the nervous system with no recombination detectable in neural crest-derived cells (**Figure 22b**,**c**). By crossing Nestin-Cre mice to *Fbxw7*$^{f/f}$ mice, the resulting *Fbxw7*$^{f/f}$: Nestin-Cre^{+} (*Fbxw7*$^{\Delta N}$) mice show tissue-specific deletion of Fbw7 in the central nervous system. Neither RNA nor protein levels of Fbw7 were detectable by *in situ* hybridisation in the E18.5 brain or by western blot

analysis on protein extracts from neural cells isolated from E14.5 *Fbxw7*$^{\Delta N}$ mice (**Figures 22d** and **41**).

Apart from its crucial role in vascular development (Tetzlaff et al., 2004, Tsunematsu et al., 2004), Fbw7 also seems to be of major importance for the development of the nervous system since *Fbxw7*$^{\Delta N}$ mice exhibited perinatal lethality.

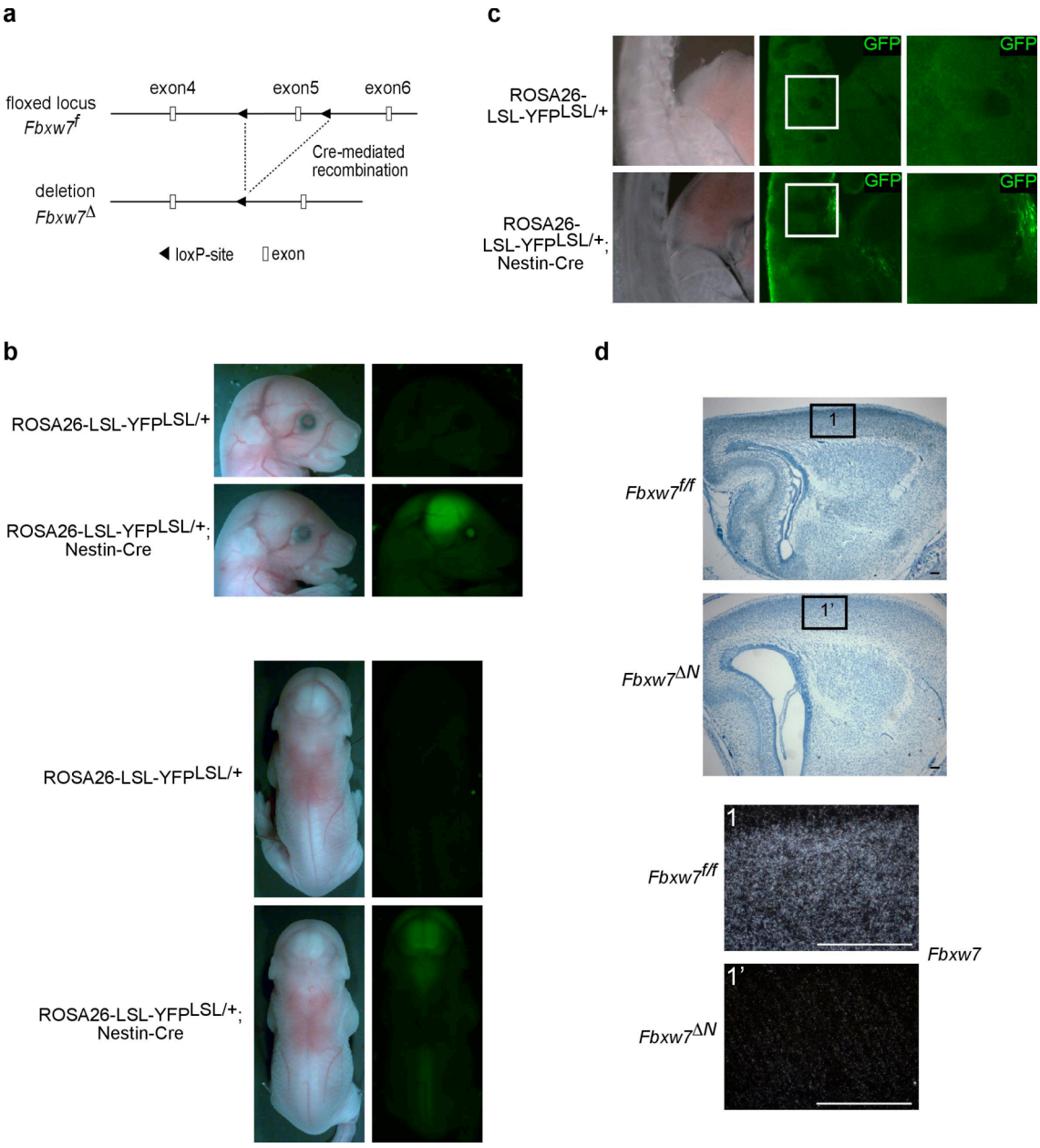

Figure 22 Efficient *Fbxw7* deletion in *Fbxw7*$^{\Delta N}$ mice.
(**a**) Schematic representation of the targeting construct before and after Cre recombination. Exon 5 of the *Fbxw7* allele is flanked by loxP-sites (*Fbxw7*^{f}) and excised upon crossing *Fbxw7*$^{f/f}$ mice to transgenic mice expressing Cre recombinase. Conditional knockout of *Fbxw7* in the brain occurs by expressing Cre under the control of a Nestin promoter (*Fbxw7*$^{\Delta N}$). (**b**) Bright field and fluorescence microscopy pictures of ROSA26-LSL-YFP$^{LSL/+}$ and ROSA26-LSL-YFP$^{LSL/+}$; Nestin-Cre E14.5 embryos lateral view (upper panels) and dorsal view (lower panels). (**c**) Bright field pictures and immunocytochemistry for GFP (green) on comparable sagittal sections from ROSA26-LSL-YFP$^{LSL/+}$ and ROSA26-LSL-YFP$^{LSL/+}$; Nestin-Cre E14.5 embryos showing dorsal root ganglia (DRG). White squares mark areas shown in high magnification in panels on the right. GFP-positive cells were only detectable in the spinal cord of ROSA26-

LSL-YFP$^{LSL/+}$; Nestin-Cre mice but not in the neural crest derived DRG. (**d**) *Fbxw7* (exon 2–5 specific probe) *in situ* hybridization (lower panels) with Giemsa counterstain (blue, upper panels). Rectangles mark comparable regions of the cortex (1, 1') shown below in high magnification for *Fbxw7*$^{f/f}$ and *Fbxw7*$^{\Delta N}$ E18.5 heads. Scale bars: 100 μm.

3.1.2 Absence of Fbw7 affects cellularity in the developing brain

Due to the perinatal lethality, the latest time point I was able to obtain *Fbxw7*$^{\Delta N}$ embryos was around E18.5. By histological analysis of the E18.5 wild type (wt) and Fbw7-deficient brain, I could not detect differences in the overall structure of the brain, e.g. the size and the thickness of the forebrain cortex was unaffected in the mutant brain (**Figure 23**). However, haematoxylin and eosin (H&E) staining revealed a widespread reduction in cell number in the midbrain tectum and the forebrain cortex (**Figure 24a-d**). Interestingly, the decreased cellularity was only detectable in areas of progenitors and differentiated cells. In the midbrain tectum, cell numbers in the mantle layer (ML) were reduced by 34%. In the forebrain cortex, the cellularity in the subventricular zone (SVZ) was decreased by 29%, in the intermediate zone (IZ) by 27% and in the cortical plate by 30%. On the contrary, cell numbers in areas which harbour stem cells, i.e. the tectal and cortical ventricular zones (VZ), were either unaltered as seen in the cortex or increased as seen in the tectum of the mutant brains (**Figure 24a-d**). Also other regions of the developing brain such as the lateral ventricle and the thalamus showed no obvious structural abnormalities in the Fbw7-deficient brain. However, the cerebellar anlage seemed to be slightly reduced in size and showed abnormal fissure formation (**Figure 24e**) in the *Fbxw7*$^{\Delta N}$ developing brain, which has recently been shown to result in a smaller cerebellum and atypical fissures in the adult brain of cerebellum-specific conditional Fbw7-knockout mice (Jandke et al., 2011). As seen in the cortex and the tecum, Fbw7 deletion also led to decreased cellularity in areas of differentiated cells in the cerebellar anlage and the thalamus (**Figure 24e,f**).

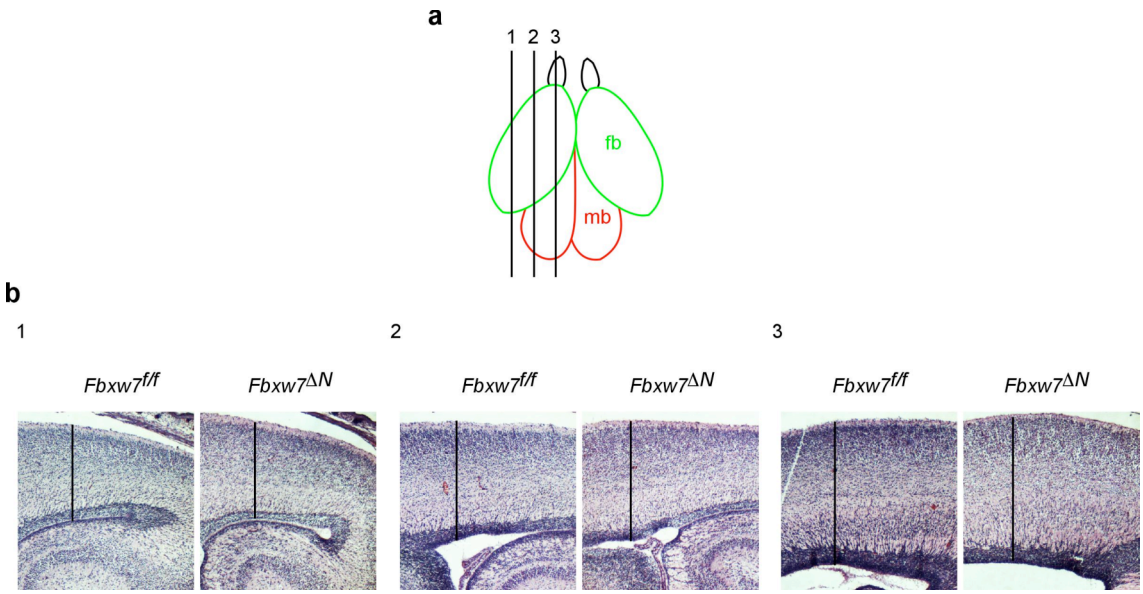

Figure 23 Cortex size in the *Fbxw7*$^{\Delta N}$ brain.
(**a**) Schematic representation of the E18.5 mouse forebrain (fb; green) and midbrain (mb; red) dorsal view. Comparable sagittal sections of *Fbxw7*$^{f/f}$ and *Fbxw7*$^{\Delta N}$ E18.5 heads were taken alongside the lateral-medial axis (1, 2, 3) and are shown in (**b**) stained with haematoxylin and eosin (H&E). Scale bars: in 1, 580 µm; in 2, 730 µm; in 3, 870 µm.

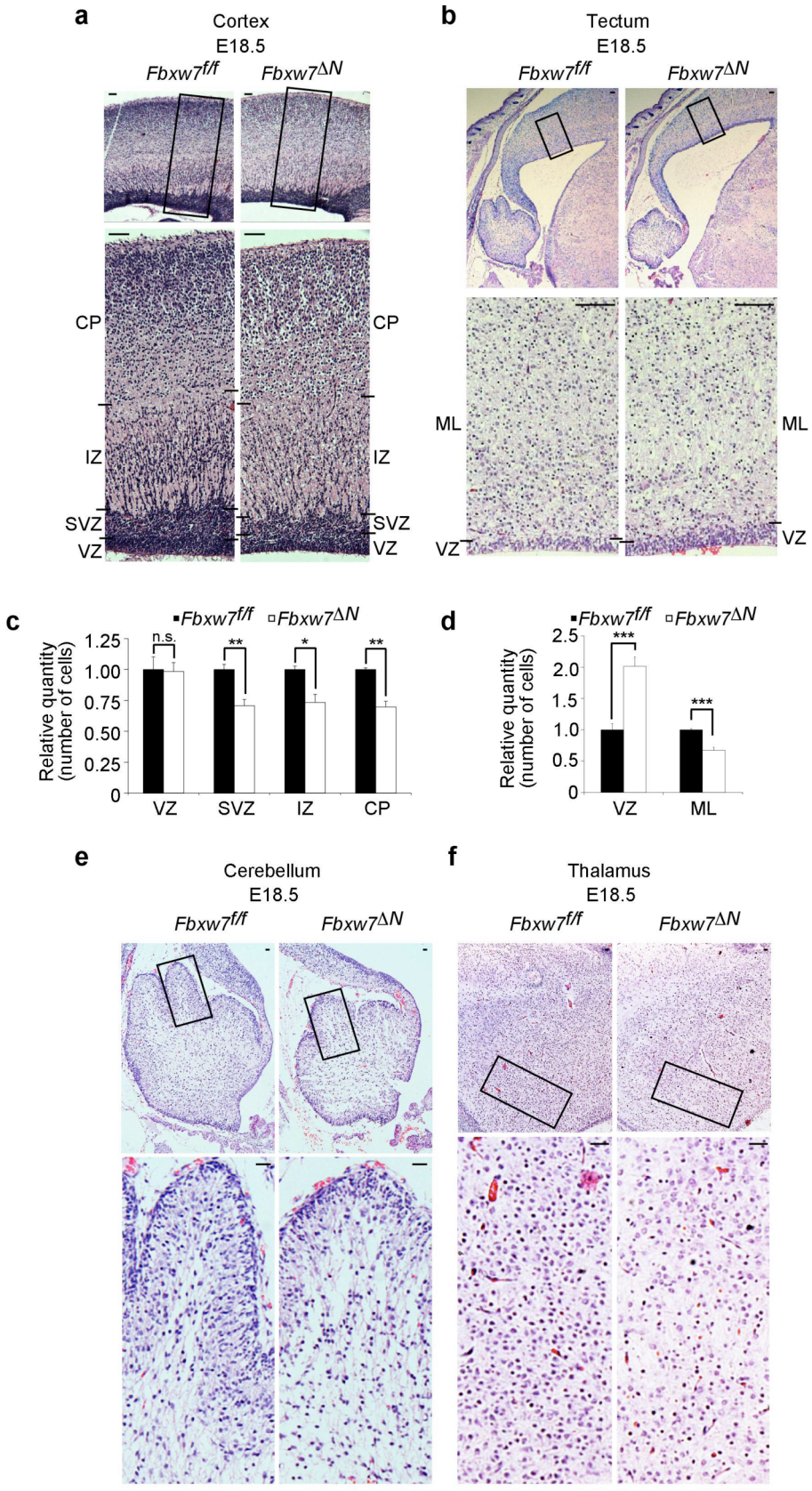
a
Cortex
E18.5
Fbxw7f/f
Fbxw7ΔN
CP
IZ
SVZ
VZ
b
Tectum
E18.5
Fbxw7f/f
Fbxw7ΔN
ML
VZ
c
Fbxw7f/f
Fbxw7ΔN
Relative quantity (number of cells)
n.s.
**
*
**
VZ
SVZ
IZ
CP
d
Fbxw7f/f
Fbxw7ΔN
Relative quantity (number of cells)
***
***
VZ
ML
e
Cerebellum
E18.5
Fbxw7f/f
Fbxw7ΔN
f
Thalamus
E18.5
Fbxw7f/f
Fbxw7ΔN

Figure 24 Fbw7 controls cell number in the brain.
(**a**) H&E staining of the E18.5 forebrain cortex from *Fbxw7*$^{f/f}$ and *Fbxw7*$^{\Delta N}$ mouse embryos. Rectangles mark comparable regions of the cortex shown below in high magnification. Scale bars, 100 μm. (**b**) H&E staining of comparable regions of the *Fbxw7*$^{f/f}$ and *Fbxw7*$^{\Delta N}$ E18.5 midbrain tectum. Rectangles mark the area of the tectum shown below in high magnification. Scale bars, 200 μm. (**c**) Histogram showing the relative quantity of cells in the ventricular zone (VZ), subventricular zone (SVZ), intermediate zone (IZ) and cortical plate (CP) of the *Fbxw7*$^{f/f}$ and *Fbxw7*$^{\Delta N}$ E18.5 cortex. Cell number in the *Fbxw7*$^{f/f}$ E18.5 cortex is normalized to 1 (100%); $n = 3$. (**d**) Histogram showing the relative quantity of cells in the VZ and the mantle layer (ML) of the *Fbxw7*$^{f/f}$ and *Fbxw7*$^{\Delta N}$ E18.5 tectum. Cell numbers in the *Fbxw7*$^{f/f}$ E18.5 tectum are normalized to 1 (100%); $n = 5$. (**e**,**f**) H&E staining of the E18.5 (**e**) cerebellum and (**f**) thalamus from *Fbxw7*$^{f/f}$ and *Fbxw7*$^{\Delta N}$ mouse embryos. Rectangles mark comparable regions shown below in high magnification. Scale bars: 50 μm.
Error bars, standard error of the mean (s.e.m.); n.s., not significant; $*P \leq 0.05$; $**P \leq 0.01$; $***P \leq 0.001$ (unpaired *t*-test).

3.1.3 Loss of Fbw7 does not alter proliferation but apoptosis in the developing brain

The question arising from the widespread reduction in cellularity in areas of progenitors and differentiated cells in the *Fbxw7*$^{\Delta N}$ brain was, which cellular mechanism is involved in this phenotype? Thus, I analysed the number of proliferative cells in the Fbw7-deficient brain at different stages of embryonic development. The number of cells expressing the mitotic marker phospho-histone H3 (pH3) in the E16.5 mutant midbrain tectum was not significantly altered in comparison to the wt midbrain tectum (**Figure 25a,b**). Similarly, the number of Ki67-positive proliferative cells was the same in the wt and Fbw7 mutant forebrain cortex at E10.5, E14.5, E16.5 and E18.5 (**Figure 25c-g**). Another cellular mechanism which could explain the decreased cellularity in areas of progenitors and differentiated cells is apoptosis. Although the number of apoptotic cells expressing active Caspase-3 was similar in the E18.5 wt and Fbw7 mutant midbrain tectum, I could detect a significant increase in the number of apoptotic cells at an earlier stage of development, at E16.5 (**Figure 26a**,**b**). Interestingly, the increase in the number of apoptotic cells was mainly detectable in the lower part of the ML where progenitors migrate out of the VZ and differentiate on their way into the upper part of the tectum. This was the first indication that there is increased progenitor apoptosis in the absence of Fbw7. In the forebrain cortex, the number of apoptotic cells was markedly increased in the Fbw7 mutants at E14.5 (**Figure 26c**,**d**). Notably, also in the cortex, elevated levels of apoptosis were detected mainly in the SVZ where Tbr2-positive intermediate progenitors reside whose numbers were markedly reduced in the *Fbxw7*$^{\Delta N}$ cortex (**Figures 26c**,**e** and **29a**,**b**). This suggested that loss of Fbw7 results in increased progenitor apoptosis and consequently decreased numbers of progenitors and differentiated cells.

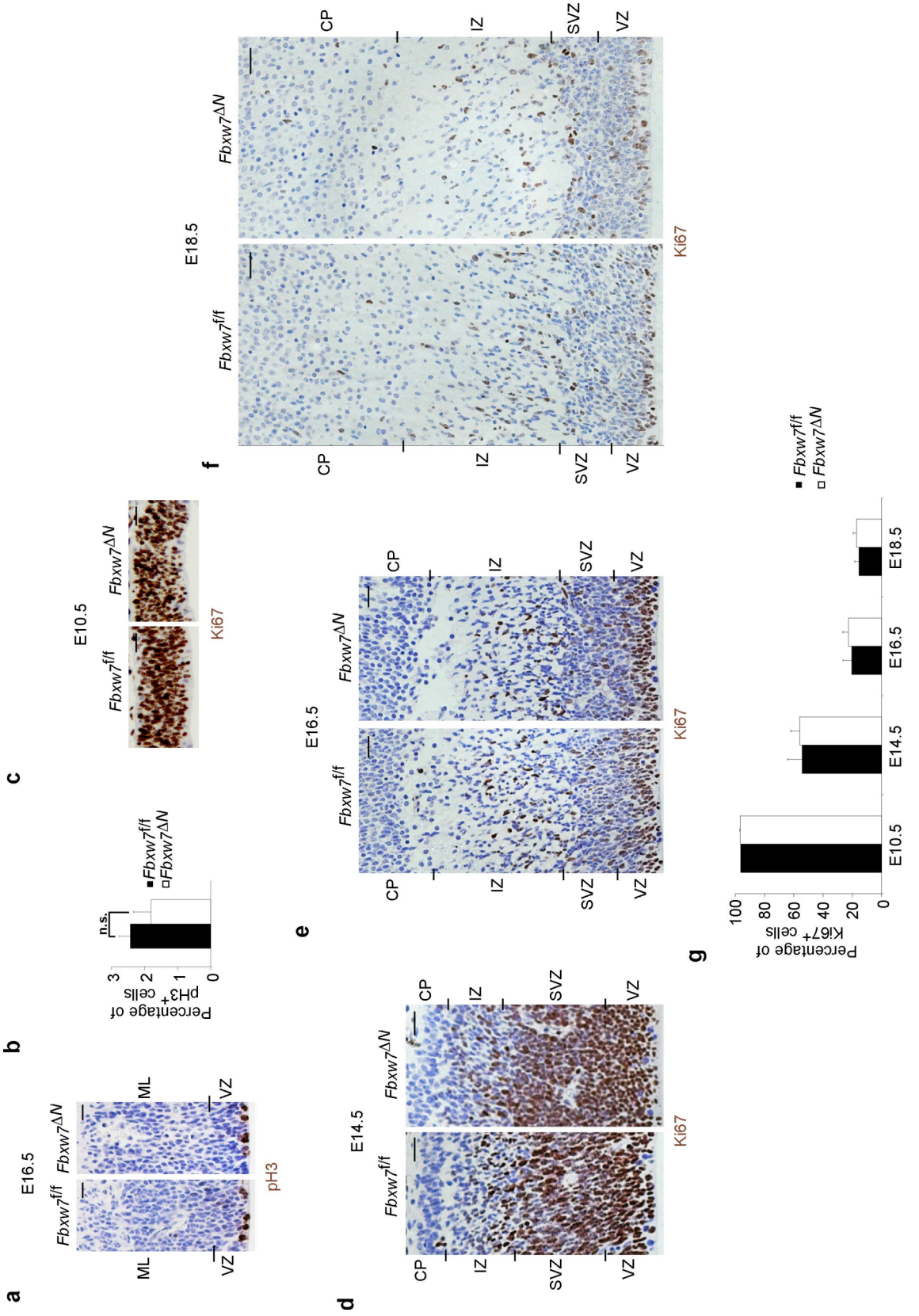
a
E16.5
Fbxw7f/f
Fbxw7ΔN
ML
VZ
pH3
b
n.s.
Percentage of pH3+ cells
Fbxw7f/f
Fbxw7ΔN
c
E10.5
Fbxw7f/f
Fbxw7ΔN
Ki67
d
E14.5
CP
IZ
SVZ
VZ
e
E16.5
f
E18.5
g
Percentage of Ki67+ cells
E10.5
E14.5
E16.5
E18.5

Figure 25 Loss of Fbw7 does not affect proliferation *in vivo*.
(**a**) 3,3′-Diaminobenzidine (DAB) staining for the mitotic marker phosphorylated histone H3 (pH3) on representative sections of the *Fbxw7*$^{f/f}$ and *Fbxw7*$^{\Delta N}$ E16.5 tectum. Cells are counterstained with haematoxylin. Scale bars, 50 μm. (**b**) Quantification of pH3-positive cells in the *Fbxw7*$^{f/f}$ and *Fbxw7*$^{\Delta N}$ E16.5 tectum; $n = 3$. (**c**-**f**) DAB staining for the S-phase marker Ki67 on representative sections of the *Fbxw7*$^{f/f}$ and *Fbxw7*$^{\Delta N}$ cortex at (**c**) E10.5, (**d**) E14.5, (**e**) E16.5 and (**f**) E18.5. Cells are counterstained with haematoxylin. Scale bars: 50 μm. (**g**) Quantification of Ki67-positive cells in the E10.5 *Fbxw7*$^{f/f}$ and *Fbxw7*$^{\Delta N}$ cortex and in the SVZ of the E14.5, E16.5 and E18.5 *Fbxw7*$^{f/f}$ and *Fbxw7*$^{\Delta N}$ cortex. $n = 3$.
Error bars, s.e.m.; n.s., not significant (unpaired *t*-test). CP: cortical plate, IZ: intermediate zone, ML: mantle layer, SVZ: subventricular zone, VZ: ventricular zone.

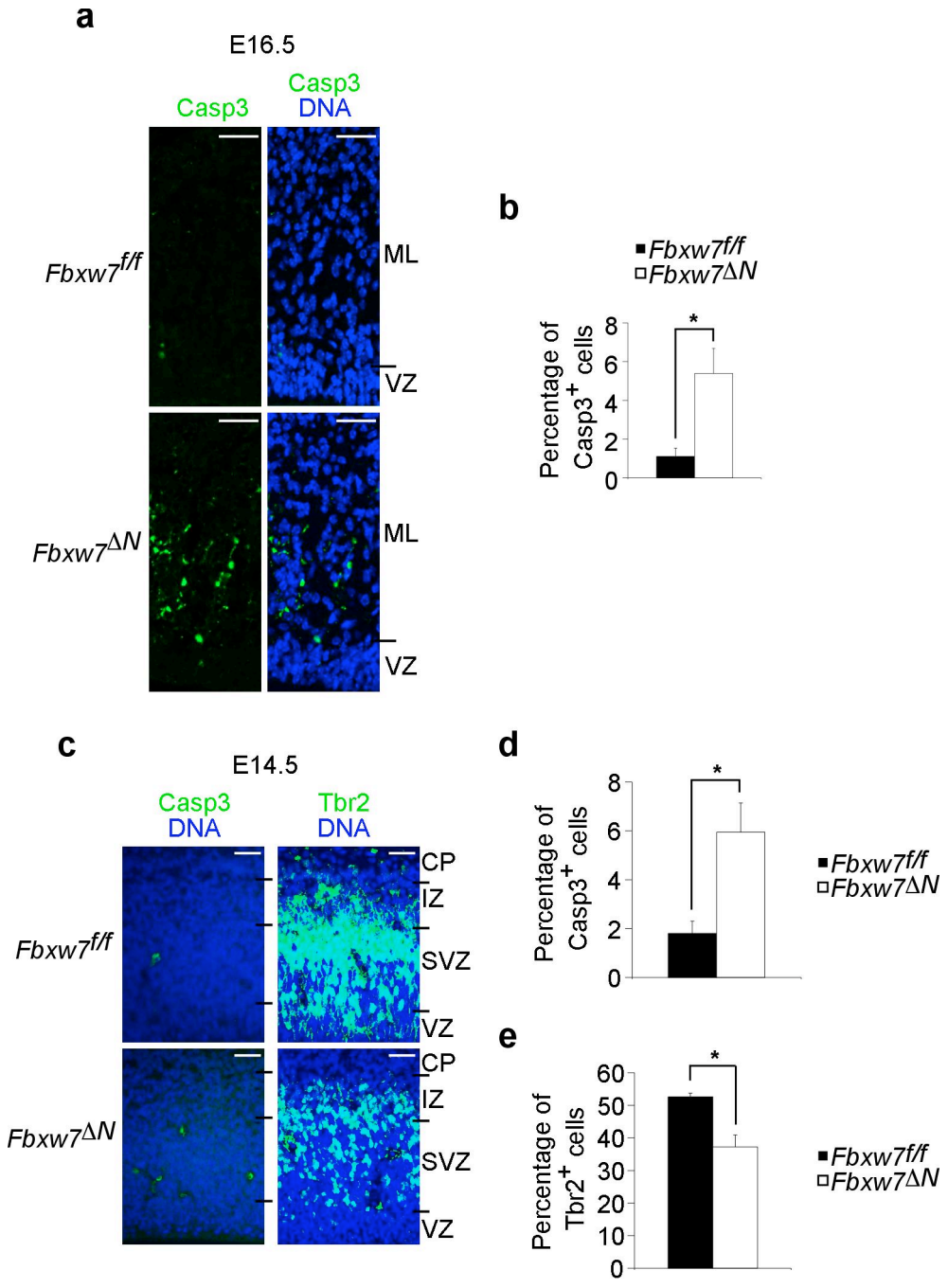

Figure 26 Loss of Fbw7 leads to increased apoptosis
(**a**) Immunohistochemistry for active caspase-3 (Casp3; green) on representative sections of the *Fbxw7*$^{f/f}$ and *Fbxw7*$^{\Delta N}$ E16.5 tectum. DNA (blue) is counterstained with DAPI. Scale bars, 50 µm. (**b**) Quantification of active Casp3^{+} cells in the *Fbxw7*$^{f/f}$ and *Fbxw7*$^{\Delta N}$ E16.5 tectum; $n = 3$. (**c**) Immunohistochemistry for active caspase-3 (Casp3; green; left panels) and Tbr2 (green; right panels) on representative sections of the *Fbxw7*$^{f/f}$ and *Fbxw7*$^{\Delta N}$ E14.5 cortex. DNA (blue) is counterstained with DAPI. Scale bars, 50 µm. (**d**,**e**) Quantification of (**d**) active Casp3^{+} and (**e**) Tbr2^{+} cells in the *Fbxw7*$^{f/f}$ and *Fbxw7*$^{\Delta N}$ E14.5 cortical SVZ; $n = 3$.

Error bars, s.e.m.; *$P \leq 0.05$ (unpaired *t*-test). CP: cortical plate, IZ: intermediate zone, ML: mantle layer, SVZ: subventricular zone, VZ: ventricular zone.

3.1.4 Fbw7-deficiency leads to stem cell accumulation in the brain

To further investigate the role of Fbw7 in the developing brain, I examined the Fbw7 expression pattern by *in situ* hybridisation. In the E14.5 wt cortex, Fbw7 was highly expressed in areas of stem cells and progenitors, i.e. the cortical SVZ and VZ, whereas there was only scattered Fbw7 expression detectable in areas of more differentiated cells, i.e. the IZ and the CP (**Figure 27a**). The increased number of cells in the tectal VZ was a first indication that Fbw7 plays a role in stem cell regulation (**Figure 24b,d**). Indeed, when I performed immunofluorescence staining for the stem cell and progenitor marker Nestin on the E14.5 wt and mutant brain, Nestin expression was substantially increased in the absence of Fbw7 throughout the cortex (**Figure 27b**). The difference in Nestin reactivity between the wt and Fbw7-deficient brain became more pronounced at later stages of development, i.e. at E16.5 and E18.5 (**Figure 27c,d**). Furthermore, the expression of BLBP and GLAST, markers for the main subset of stem cells at this stage of development, radial glia stem cells, was also significantly elevated in the E16.5 and E18.5 mutant brain (**Figure 27c,e-g**). Similar results were obtained when analysing the E18.5 tectum where the expression of the early stem cell marker Musashi 1 (Msi1), the expression of the radial glia stem cell marker BLBP and the expression of the stem cell and progenitor marker Nestin was significantly increased in the mutant embryonic brain (**Figure 28**). Considering that there is no difference in proliferation during embryonic brain development in the absence of Fbw7 (**Figure 25**), the accumulation of stem cells during embryonic brain development might be due to a differentiation defect of neural stem cells lacking Fbw7 – a hypothesis I went on to test.

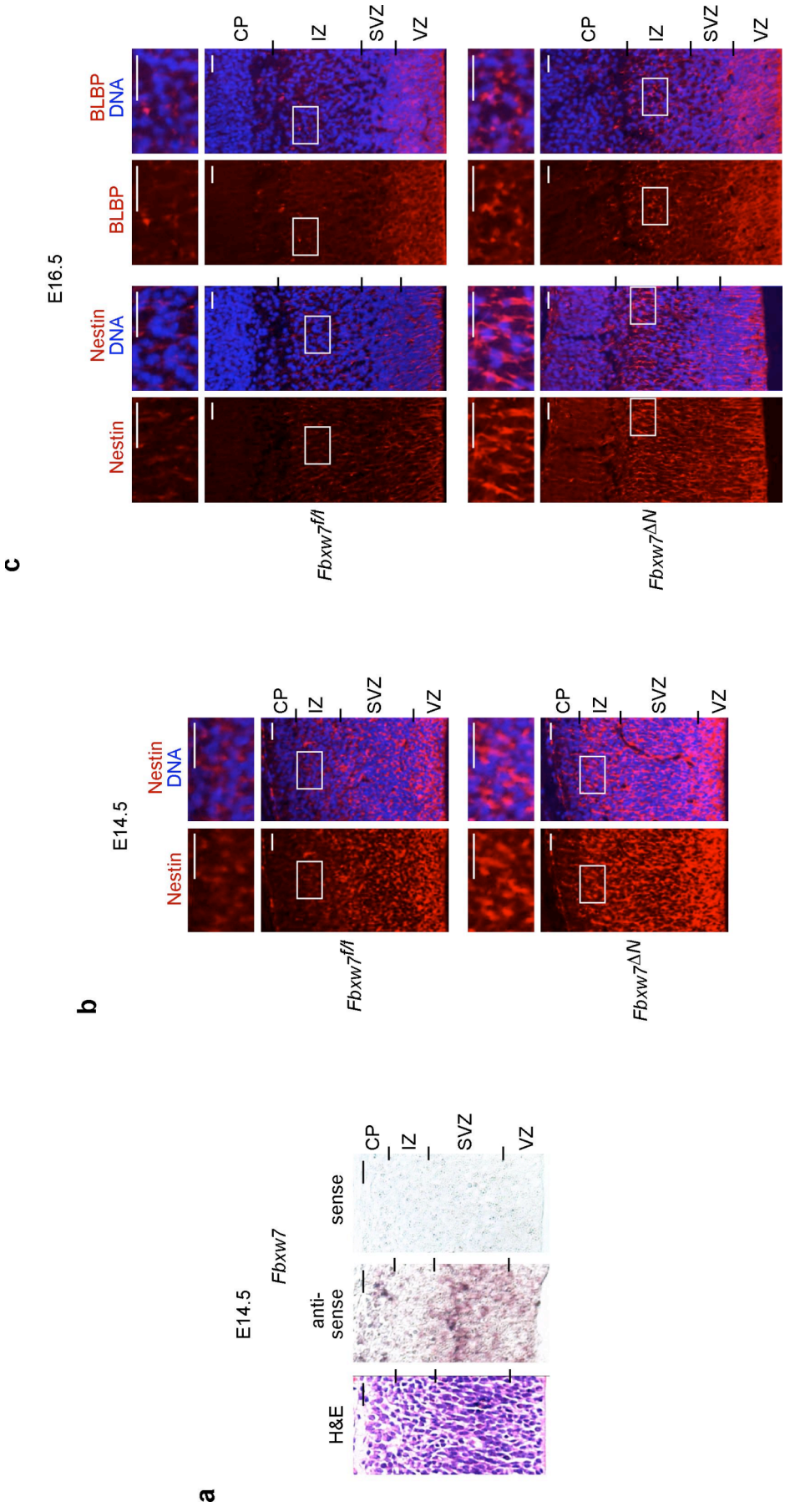
a
E14.5
Fbxw7
anti-sense
sense
H&E
CP
IZ
SVZ
VZ
b
E14.5
Nestin
Nestin DNA
Fbxw7f/f
Fbxw7ΔN
c
E16.5
Nestin
Nestin DNA
BLBP
BLBP DNA
Fbxw7f/f
Fbxw7ΔN

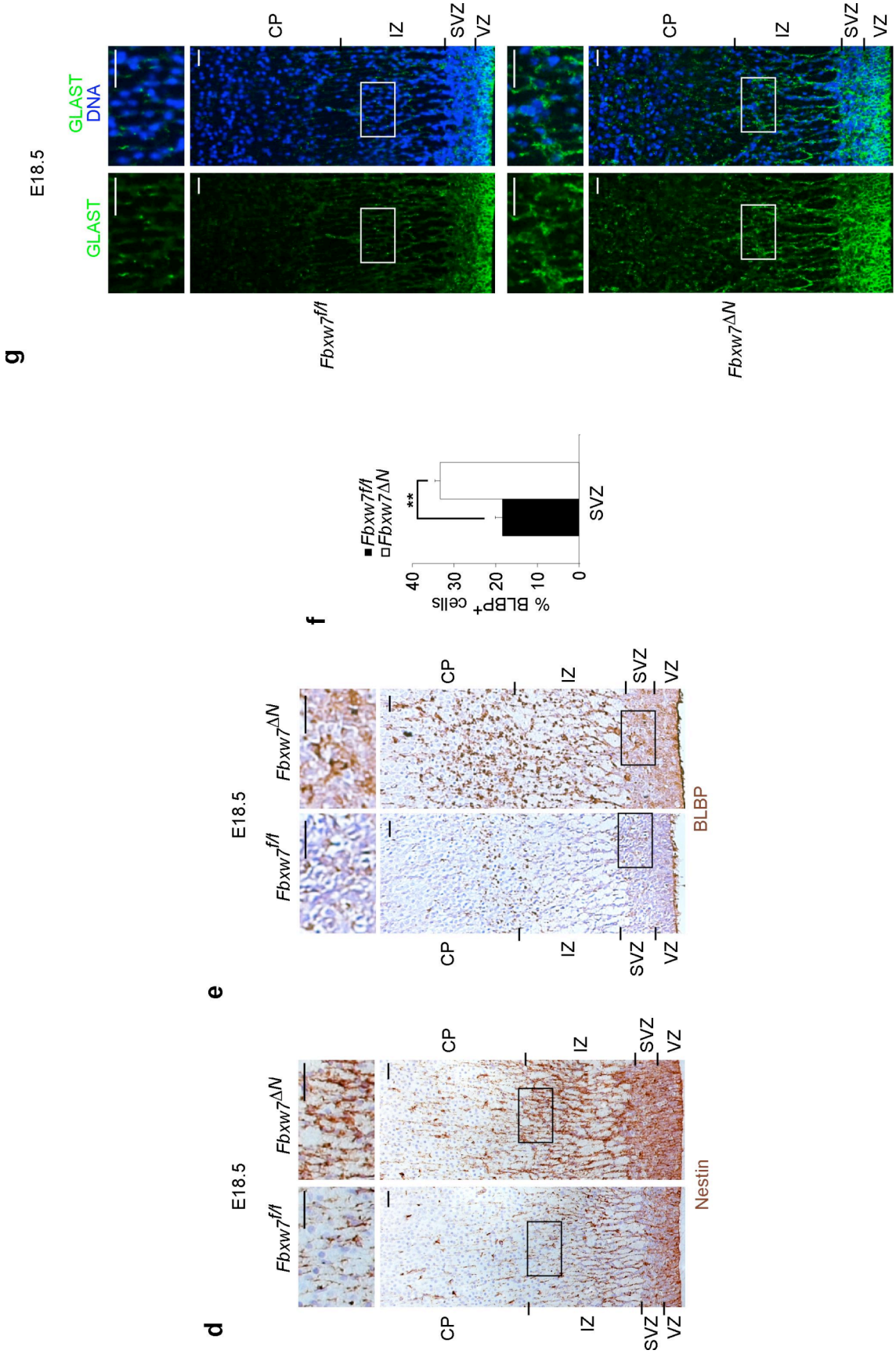
g
E18.5
GLAST
GLAST DNA
Fbxw7f/f
Fbxw7ΔN
CP
IZ
SVZ
VZ
f
Fbxw7f/f
Fbxw7ΔN
**
% BLBP+ cells
40
30
20
10
0
SVZ
e
E18.5
Fbxw7f/f
Fbxw7ΔN
BLBP
d
Nestin

Figure 27 Increased number of stem cells in the forebrain cortex in the absence of Fbw7

(**a**) *Fbxw7* (probe specific to exons 6–10) *in situ* hybridisation and sense control with haematoxylin stain (left) on the $Fbxw7^{f/f}$ E14.5 cortex. Scale bars, 50 μm. (**b**) Immunohistochemistry for Nestin (red) on the $Fbxw7^{f/f}$ and $Fbxw7^{\Delta N}$ E14.5 cortex. White rectangles mark areas shown in high magnification in panels at the top. DNA (blue) is counterstained with DAPI. Scale bars, 50 μm. (**c**) Immunohistochemistry for Nestin (red; left panels) and BLBP (red; right panels) on the $Fbxw7^{f/f}$ and $Fbxw7^{\Delta N}$ E16.5 cortex. White rectangles mark areas shown in high magnification in panels at the top. DNA (blue) is counterstained with DAPI. Scale bars, 50 μm. (**d**,**e**) DAB staining for (**d**) Nestin and for (**e**) BLBP on the $Fbxw7^{f/f}$ and $Fbxw7^{\Delta N}$ E18.5 cortex. Black rectangles mark areas shown in high magnification in panels at the top. Cells are counterstained with haematoxylin. Scale bars, 50 μm. (**f**) Quantification of BLBP-positive cells in the SVZ of the $Fbxw7^{f/f}$ and $Fbxw7^{\Delta N}$ E18.5 cortex. $n = 3$. Error bars, s.e.m.; $^{**}P \leq 0.01$. (unpaired *t*-test). (**e**) Immunohistochemistry for GLAST (green) on the $Fbxw7^{f/f}$ and $Fbxw7^{\Delta N}$ E18.5 cortex. White rectangles mark areas shown in high magnification in panels at the top. DNA (blue) is counterstained with DAPI. Scale bars, 50 μm.

CP: cortical plate, IZ: intermediate zone, SVZ: subventricular zone, VZ: ventricular zone.

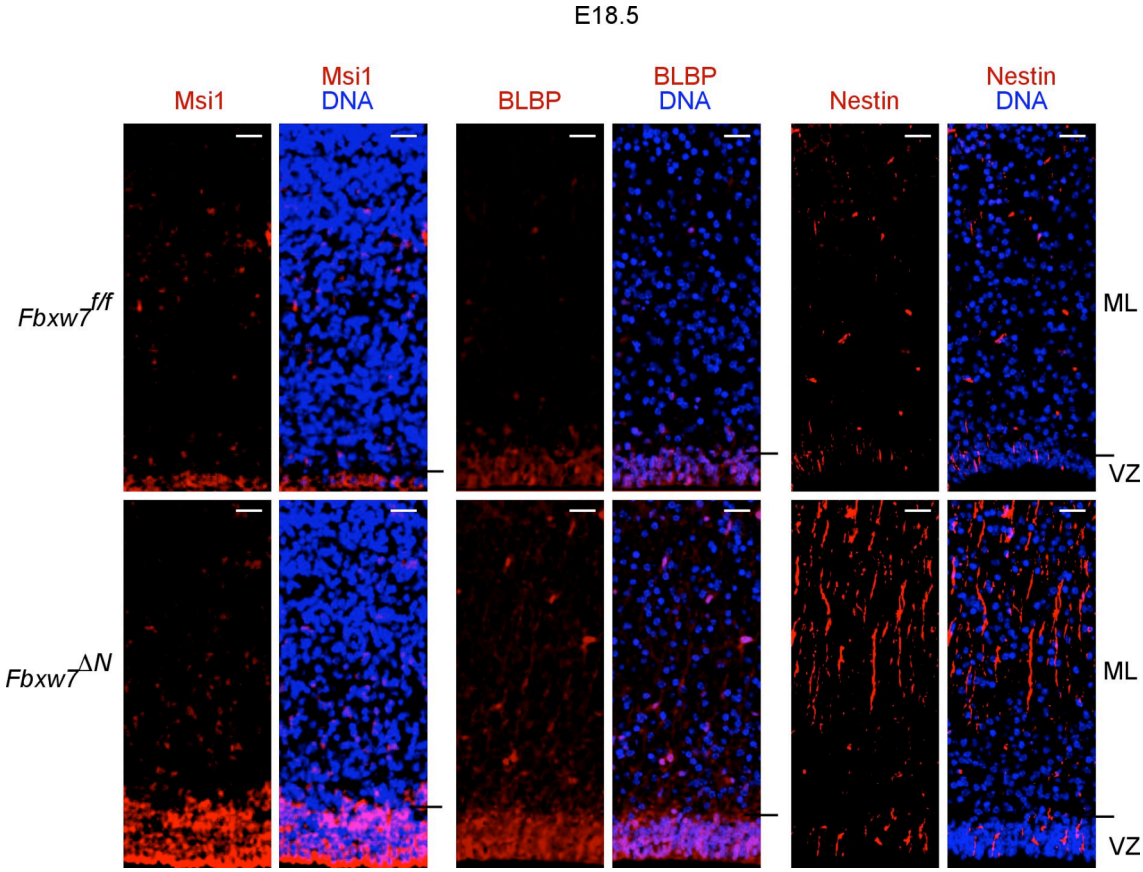

Figure 28 Increased number of stem cells in the *Fbxw7*$^{\Delta N}$ midbrain tectum
From left to right: Immunohistochemistry for Musashi 1 (Msi1; red), BLBP (red) and Nestin (red) on representative sections of the *Fbxw7*$^{f/f}$ and *Fbxw7*$^{\Delta N}$ E18.5 tectum. DNA (blue) is counterstained with DAPI. ML: mantle layer, VZ: ventricular zone. Scale bars: 50 µm.

3.1.5 Decreased numbers of progenitors and neurons in the *Fbxw7$^{\Delta N}$* brain

After examining stem cell marker expression in the developing brain, I performed immunohistochemistry (IHC) for markers of more committed progenitors and differentiated cells. The number of Tbr2-positive intermediate progenitors was significantly reduced in the absence of Fbw7 (**Figures 26c**,**e** and **29a**,**b**). Similarly, the number of Doublecortin (Dcx)-positive progenitors which had committed to the neuronal lineage was significantly decreased throughout embryonic brain development in the cortical SVZ of *Fbxw7$^{\Delta N}$* mice (**Figure 29c-f**). Next, I examined the expression of a marker for mature neurons, NeuN. Loss of Fbw7 led to a significantly decreased number of NeuN-positive neurons in the tectal ML and in the cortical IZ and CP (**Figure 30a-c**). To find out whether there is a block in neurogenesis in general or whether a specific subset of neurons is affected in particular, I performed IHC for various cortical layer neurons. As a result, the expression of all the different neuronal markers Tbr1, Ctip2 and Brn2 was reduced indicating that indeed, loss of Fbw7 leads to a general differentiation defect of neural stem cells into neurons (**Figure 30c-f**). Notably, the number of differentiated glia cells was not affected by Fbw7-deficiency. The expression of the astroglia markers GFAP and S100 and the oligodendroglia marker NG2 was similar in the wt and mutant cortex (**Figure 31**).

Taken together, the reduced cellularity in areas of differentiated cells accompanied by decreased expression of neuronal markers in these areas accounts for a severe reduction in neurons which is likely to contribute to the perinatal lethality of *Fbxw7$^{\Delta N}$* mice.

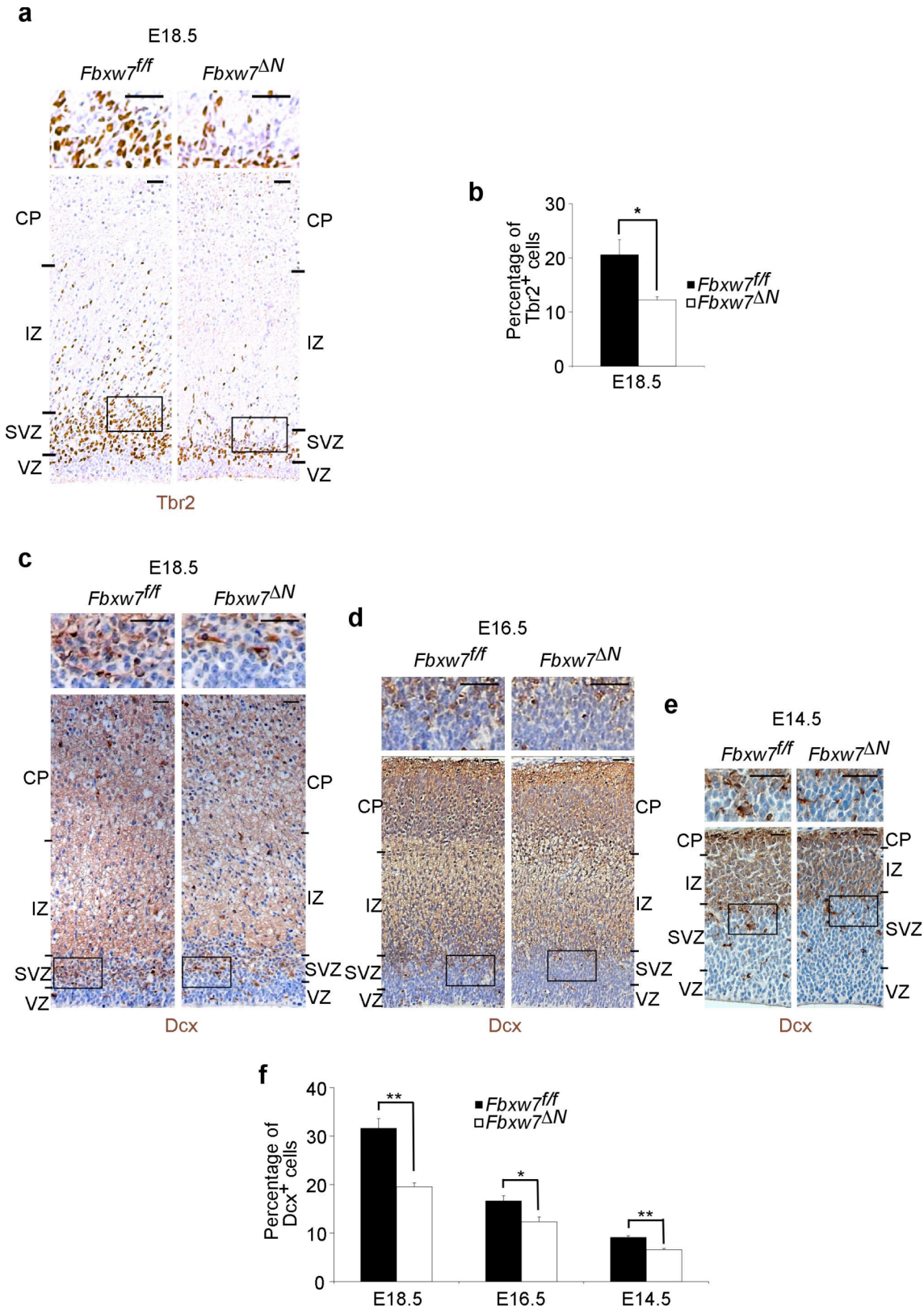

Figure 29 Reduced number of neuronal progenitors in the *Fbxw7$^{\Delta N}$* cortex.
(**a**) DAB staining for Tbr2 on the *Fbxw7$^{f/f}$* and *Fbxw7$^{\Delta N}$* E18.5 cortex. Black rectangles mark areas shown in high magnification in panels at the top. Cells are counterstained

with haematoxylin. Scale bars, 50 μm. (**b**) Quantification of Tbr2-positive cells in the IZ and the CP of the *Fbxw7*$^{f/f}$ and *Fbxw7*$^{\Delta N}$ E18.5 cortex. $n = 3$. (**c**-**e**) DAB staining for Doublecortin (Dcx) in the (**c**) E18.5, (**d**) E16.5 and (**e**) E14.5 *Fbxw7*$^{f/f}$ and *Fbxw7*$^{\Delta N}$ cortex. Black rectangles mark areas shown in high magnification in panels at the top. Cells are counterstained with haematoxylin. Scale bars: 50 μm. (**f**) Quantification of Dcx-positive cells in the SVZ of the E18.5 ($n = 4$), E16.5 ($n = 3$) and E14.5 ($n = 3$) *Fbxw7*$^{f/f}$ and *Fbxw7*$^{\Delta N}$ cortex.
Error bars, s.e.m.; $*P \leq 0.05$ (unpaired *t*-test); $**P \leq 0.01$. CP: cortical plate, IZ: intermediate zone, SVZ: subventricular zone, VZ: ventricular zone.

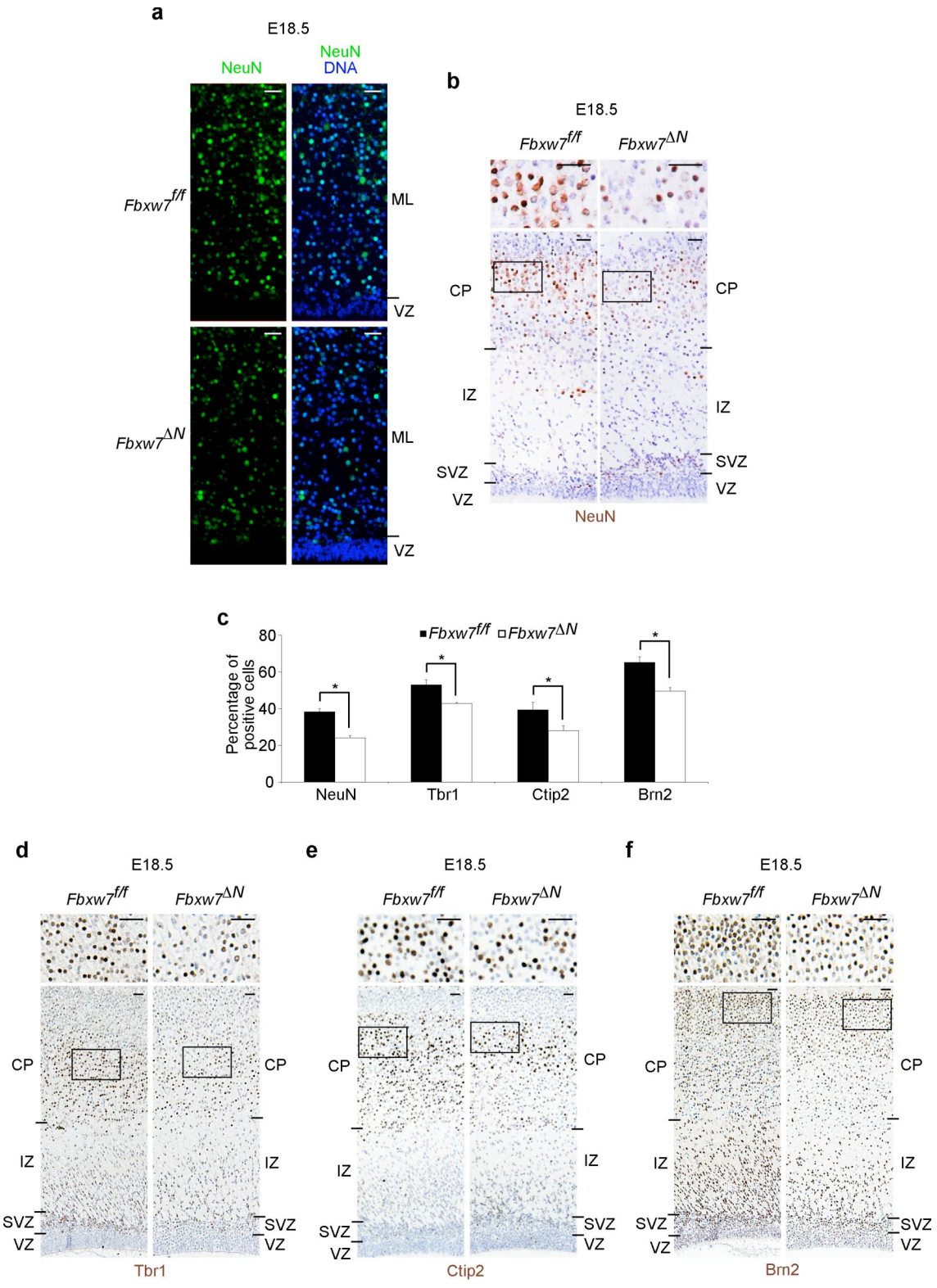

Figure 30 Decreased number of neurons in the *Fbxw7$^{\Delta N}$* brain.
(**a**) Immunohistochemistry for NeuN (green) on representative sections of the *Fbxw7$^{f/f}$* and *Fbxw7$^{\Delta N}$* E18.5 tectum. DNA (blue) is counterstained with DAPI. Scale bars: 50 µm. (**b**) DAB staining for NeuN on the *Fbxw7$^{f/f}$* and *Fbxw7$^{\Delta N}$* E18.5 cortex. Black

rectangles mark areas shown in high magnification in panels at the top. Cells are counterstained with haematoxylin. Scale bars, 50 μm. (**c**) Quantification of NeuN, Tbr1, Ctip2 and Brn2-positive cells in the IZ and the CP of the *Fbxw7*$^{f/f}$ and *Fbxw7*$^{\Delta N}$ E18.5 cortex. $n = 3$. (**d-f**) DAB staining for (**d**) Tbr1, (**e**) Ctip2 and (**f**) Brn2 on the *Fbxw7*$^{f/f}$ and *Fbxw7*$^{\Delta N}$ E18.5 cortex. Black rectangles mark areas shown in high magnification in panels at the top. Cells are counterstained with haematoxylin. Scale bars, 50 μm.
Error bars, s.e.m.; $*P \leq 0.05$ (unpaired *t*-test); CP: cortical plate, IZ: intermediate zone, ML: mantle layer, SVZ: subventricular zone, VZ: ventricular zone.

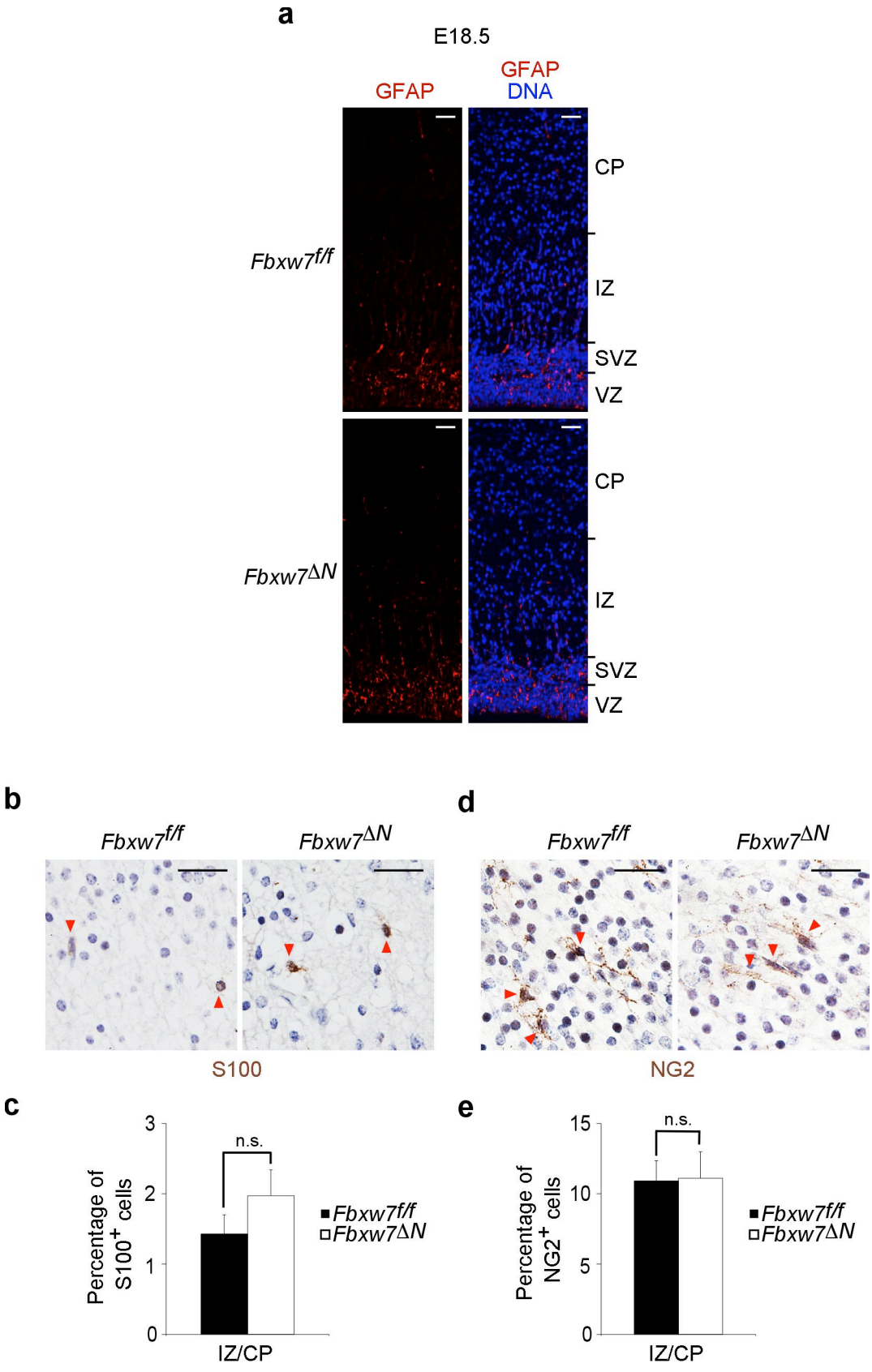
a
E18.5
GFAP
GFAP
DNA
CP
IZ
SVZ
VZ
Fbxw7f/f
Fbxw7ΔN
b
Fbxw7f/f
Fbxw7ΔN
S100
d
Fbxw7f/f
Fbxw7ΔN
NG2
c
Percentage of S100+ cells
n.s.
Fbxw7f/f
Fbxw7ΔN
IZ/CP
e
Percentage of NG2+ cells
n.s.
Fbxw7f/f
Fbxw7ΔN
IZ/CP

Figure 31 Loss of Fbw7 does not affect gliogenesis.
(**a**) Immunohistochemistry for GFAP (red) on representative sections of the *Fbxw7*$^{f/f}$ and *Fbxw7*$^{\Delta N}$ E18.5 cortex. DNA (blue) is counterstained with DAPI. Scale bars: 50 µm. (**b**,**d**) DAB staining for (**b**) S100 and (**d**) NG2 in the CP of the E18.5 *Fbxw7*$^{f/f}$ and *Fbxw7*$^{\Delta N}$ cortex. Red arrowheads denote positive cells. Cells are counterstained with haematoxylin. Scale bars: 50 µm. (**c**,**e**) Quantification of (**c**) S100-positive and (**e**) NG2-positive cells in the IZ and the CP of the E18.5 *Fbxw7*$^{f/f}$ and *Fbxw7*$^{\Delta N}$ cortex. n = 3.
Error bars, s.e.m.; n.s.: not significant (unpaired *t*-test). CP: cortical plate, IZ: intermediate zone, SVZ: subventricular zone, VZ: ventricular zone.

3.1.6 Fbw7 controls neural cell number *in vitro*

Having discovered Fbw7 function in the regulation of cell number and neural differentiation in the developing brain, I examined whether neural cells from *Fbxw7*$^{\Delta N}$ embryos show similar results to the observed *in vivo* phenotypes *in vitro*. I isolated neural cells from the wt and mutant E14.5 brain and cultured them in a medium conditioned with the growth factors EGF and FGF which is selective for neural stem cells (NSCs) and neural progenitor cells (NPCs). As a result, these cells form neurospheres which consist of NPCs and to a small extent of NSCs and more differentiated cells (Reynolds and Rietze, 2005). By light microscopy, it was clear that neurospheres in Fbw7 mutant cultures were significantly decreased in size and in number (**Figure 32**). The reduced number of neurosphere cells in the absence of Fbw7 *in vitro* might be similar to the *in vivo*-observation that loss of Fbw7 results in decreased numbers of progenitors.

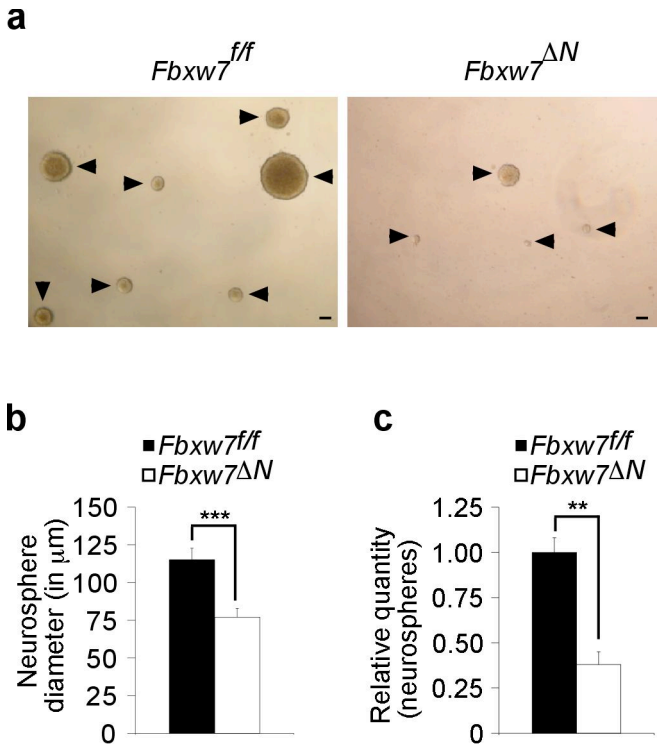

Figure 32 Absence of Fbw7 results in reduced cellularity *in vitro*.
(**a**) Phase contrast pictures of *Fbxw7*$^{f/f}$ and *Fbxw7*$^{\Delta N}$ neurosphere (arrowheads) cultures under self-renewal conditions. Scale bars, 100 µm. (**b**,**c**) Histograms showing (**b**) the diameter (in µm) and (**c**) the relative quantity of *Fbxw7*$^{f/f}$ and *Fbxw7*$^{\Delta N}$ neurospheres. Neurosphere numbers in *Fbxw7*$^{f/f}$ cultures are normalized to 1 (100%); $n = 4$.
Error bars, s.e.m.; $^{**}P \leq 0.01$; $^{***}P \leq 0.001$ (unpaired *t*-test).

3.1.7 Loss of Fbw7 does not affect proliferation but leads to increased progenitor apoptosis *in vitro*

To further investigate the decreased number of neurosphere cells in Fbw7 mutant cultures, I examined proliferation in wt and Fbw7-deficient neurospheres. By immunofluorescence staining for the mitotic marker pH3 on neurosphere sections, I could not detect a difference in the number of proliferative cells in wt and Fbw7 mutant neurospheres (**Figure 33a**). Furthermore, I performed carboxyfluorescein diacetate succinimidyl ester (CFSE) staining which labels all cellular proteins and is subsequently diluted out at each cell division, so that loss of CFSE intensity by cells over time can be used as a measure of their proliferation rate. FACS analysis of CFSE-stained cells revealed that proliferation rates of wt and mutant neurosphere cells were nearly identical, with a neurosphere cell dividing on average every 14 h independent of its Fbw7 status (**Figure 33b-d**).

Since proliferation was unchanged, I investigated whether differences in the level of apoptosis could explain the decreased cell number in Fbw7 mutant cultures. TdT-mediated dUTP-biotin nick end labeling (TUNEL) assay revealed that the number of apoptotic cells is significantly higher in Fbw7-deficient neurospheres in comparison to wt neurospheres (**Figure 34a,b**). Considering that neurospheres consist predominantly of neural progenitors, this indicated that the absence of Fbw7 leads to increased progenitor apoptosis.

As seen in the cortex, the expression of the astroglia marker S100 and the oligodendroglia marker NG2 was similar in wt and mutant neurospheres (**Figure 34c-f**).

Furthermore, the vast majority of neurosphere cells expressed the neural stem cell and progenitor marker Nestin (**Figure 34g**). However, the percentage of cells positive for the early stem cell marker Musashi 1 (Msi1) was significantly increased in mutant neurospheres (**Figure 34g,h**). This was the first indication that, as seen *in vivo*, Fbw7-deficiency leads to stem cell accumulation also *in vitro*.

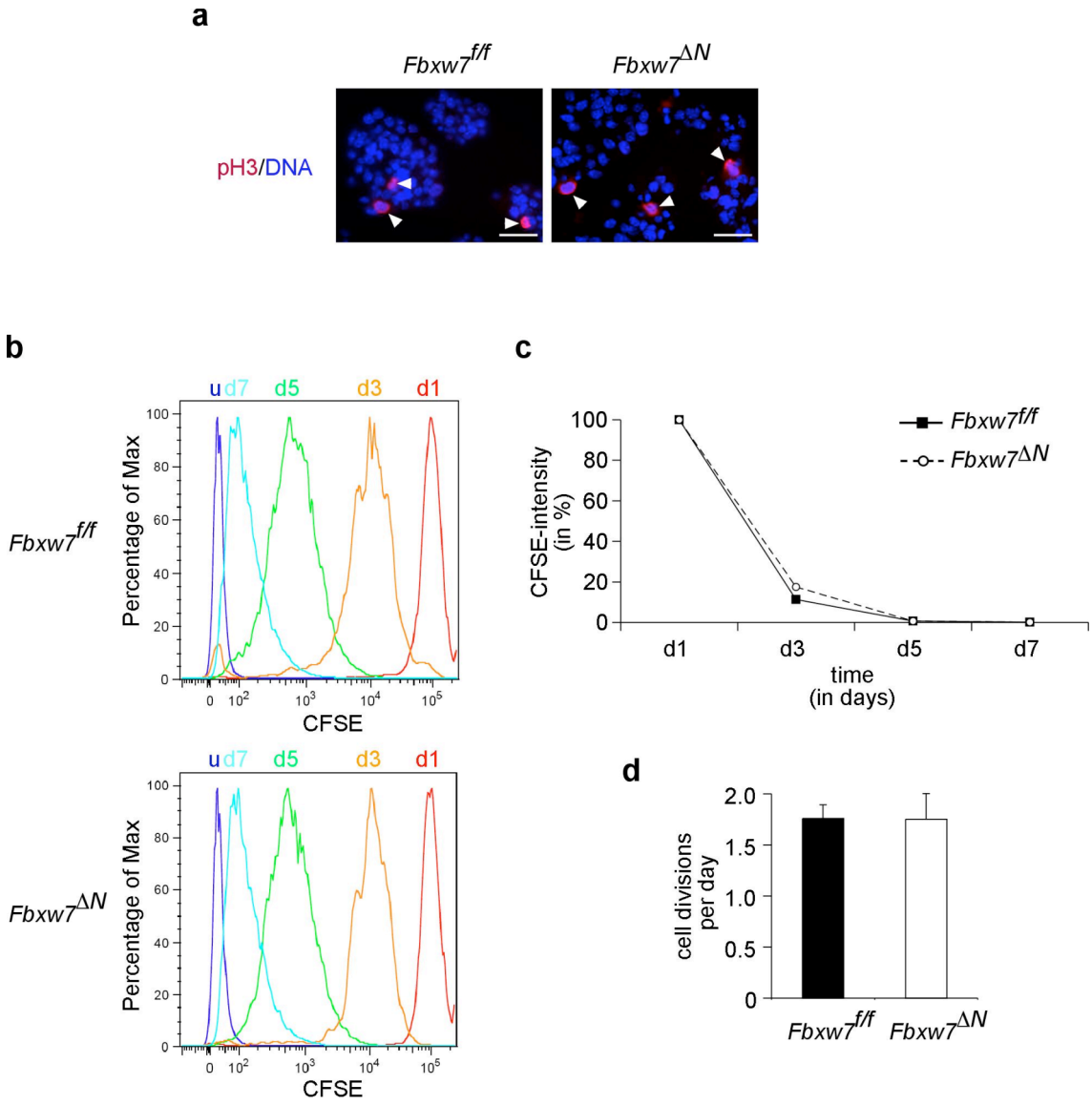

Figure 33 Loss of Fbw7 does not affect proliferation *in vitro*.
(**a**) Immunocytochemistry for phosphorylated histone H3 (pH3; red) on *Fbxw7*$^{f/f}$ and *Fbxw7*$^{\Delta N}$ neurosphere sections. DNA (blue) is counterstained with DAPI. Arrowheads denote pH3-positive cells. Scale bars: 50 µm. (**b**) FACS histograms showing carboxyfluorescein diacetate succinimidyl ester (CFSE) intensity in *Fbxw7*$^{f/f}$ and *Fbxw7*$^{\Delta N}$ neurosphere cultures 1 (d1), 3 (d3), 5 (d5) and 7 (d7) days after CFSE staining. u, unstained control. (**c**) Graph showing the loss of CFSE intensity (in %) over time (in days). (**d**) Histogram showing cell division rates of *Fbxw7*$^{f/f}$ and *Fbxw7*$^{\Delta N}$ neurosphere cells based on the loss of CFSE intensity. Error bars, s.e.m.

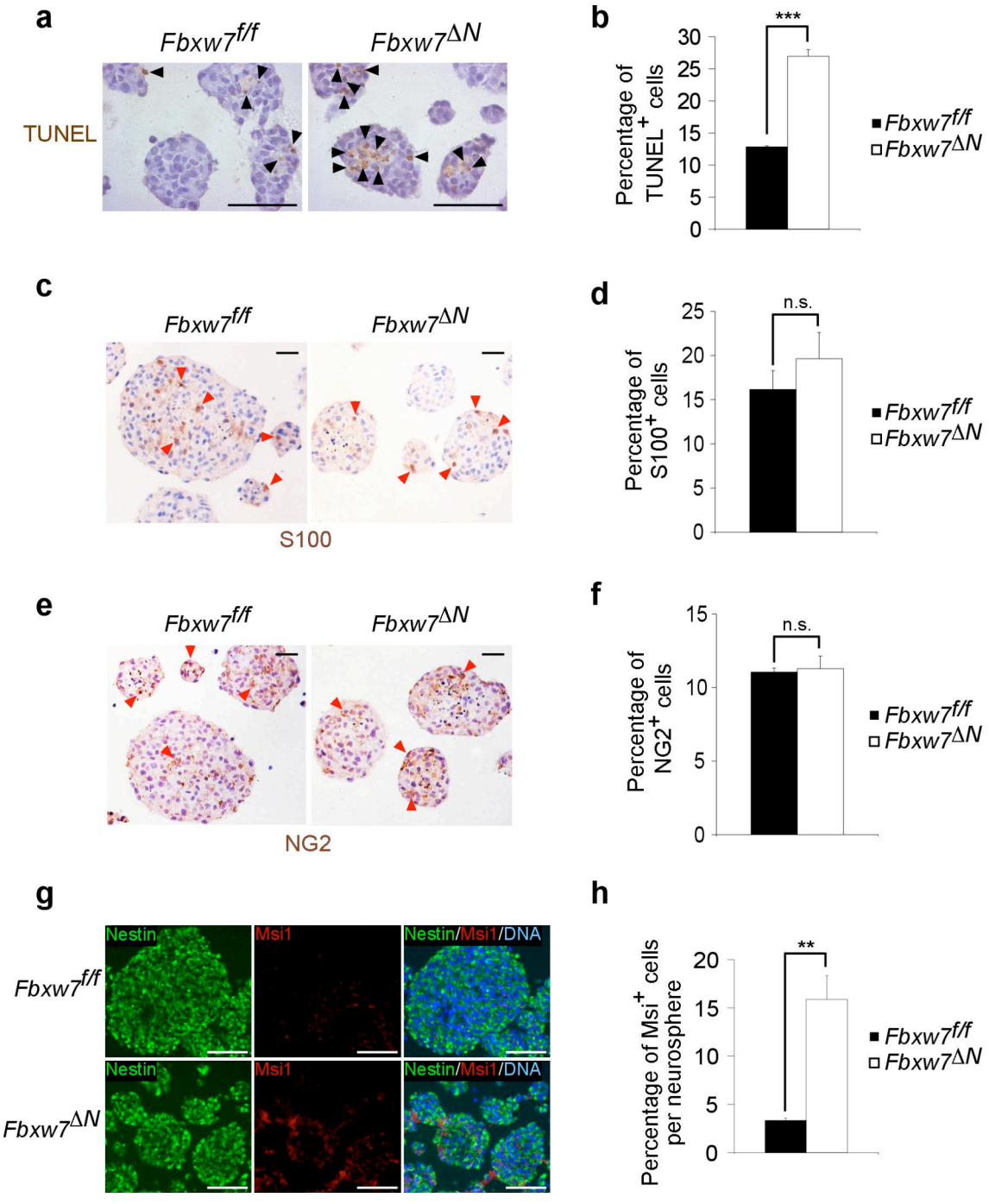

Figure 34 Increased apoptosis, unaffected gliogenesis and increased stem cell marker expression in *Fbxw7*$^{\Delta N}$ neurospheres.

(**a**) DAB staining for TUNEL (TdT-mediated dUTP-biotin nick end labeling)-positive cells (arrowheads) on *Fbxw7*$^{f/f}$ and *Fbxw7*$^{\Delta N}$ neurosphere sections. Cells are counterstained with haematoxylin. Scale bars, 100 µm. (**b**) Histogram showing the percentage of TUNEL-positive cells in *Fbxw7*$^{f/f}$ and *Fbxw7*$^{\Delta N}$ neurosphere cultures; n = 3. (**c**,**e**) DAB staining for (**c**) S100 and (**e**) NG2 on *Fbxw7*$^{f/f}$ and *Fbxw7*$^{\Delta N}$ neurosphere sections. Red arrowheads denote positive cells. Cells are counterstained with haematoxylin. Scale bars: 50 µm. (**d**,**f**) Quantification of (**d**) S100-positive and

(**f**) NG2-positive cells in *Fbxw7*$^{f/f}$ and *Fbxw7*$^{\Delta N}$ neurospheres. $n = 3$. (**g**) Immunocytochemistry for Nestin (green) and Musashi 1 (Msi1; red) on *Fbxw7*$^{f/f}$ and *Fbxw7*$^{\Delta N}$ neurosphere sections. DNA (blue) is counterstained with DAPI. Scale bars, 100 μm. (**e**) Quantification of Msi1-positive cells per neurosphere in *Fbxw7*$^{f/f}$ and *Fbxw7*$^{\Delta N}$ neurosphere cultures; $n = 3$.
Error bars, s.e.m.; n.s., not significant, $^{**}P \leq 0.01$; $^{***}P \leq 0.001$ (unpaired *t*-test).

3.1.8 Fbw7-deficiency blocks stem cell differentiation into neurons *in vitro*

To further study the role of Fbw7 in neural differentiation, wt and mutant neurospheres were cultured under differentiation conditions by withdrawal of growth factors and addition of a neural stem cell differentiation supplement (Stem Cell Technologies). Consequently, in wt neurosphere differentiation cultures, neurosphere cells became adherent, spread away from the neurospheres and differentiated into neurons, astrocytes and oligodendrocytes. By light microscopy and Hoechst DNA staining, I observed that many neurospheres in Fbw7-mutant differentiation cultures maintained the undifferentiated neurosphere-shape (**Figure 35a**,**b**). However, also in mutant cultures, some neurosphere cells were able to spread which made it possible to investigate the differentiation fate of these cells. After 5 days under differentiation conditions, the majority of cells have lost expression of the NSC/NPC marker Nestin and the radial glia stem cell marker RC2 in wt cultures (**Figure 35c**,**d**). On the contrary, a significantly higher percentage of neurosphere cells in Fbw7-mutant differentiation cultures retained stem cell marker expression after 5 days under differentiation conditions. Similarly, the expression of further radial glia markers BLBP and Vimentin were markedly elevated in Fbw7-mutant differentiation cultures (**Figure 36a**). Notably, also the number of cells positive for CD133 (Prominin 1), a marker for early neural stem cells, was increased in the absence of Fbw7 (**Figure 36b**). The next question to arise was whether the retention of stem cell marker expression after 5 days under differentiation conditions represents a block or only a delay in neural stem cell differentiation? To test this, I performed stainings for the NSC/NPC marker Nestin on neurosphere cultures after prolonged time (11 days) under differentiation conditions. As a result, Nestin reactivity was still

substantially increased in Fbw7 mutant cultures indicating that Fbw7-deficiency leads to a genuine block in neural stem cell differentiation (**Figure 36c**).

To investigate the differentiation potential of cells which had lost stem cell marker expression in mutant cultures, I performed immunofluorescence stainings for markers of neurons, astrocytes and oligodendrocytes. Notably, Fbw7-deficient neurospheres maintained multipotentiality since they were able to differentiate into Map2-positive neurons, Connexin-43-positive astrocytes and O4-positive oligodendrocytes (**Figure 37**). However, whereas the number of astrocytes and oligodendrocytes was not significantly altered, the number of Map2-positive neurons was significantly decreased in Fbw7-mutant differentiation cultures (**Figure 38a-c**). This confirmed the *in vivo*-observation that Fbw7-deficiency impairs neural stem cell differentiation into neurons but has no significant effect on neural stem cell differentiation into astro- and oligodendroglia.

To confirm that the stem cell differentiation defect also occurs in a culture of more homogenous and more immature neural stem cells, wt and Fbw7 mutant adherent NSC cultures were analysed. As seen in neurosphere cultures, Fbw7-deficient adherent NSCs also retained the expression of the NSC/NPC marker Nestin after 5 days under differentiation conditions indicative of a stem cell differentiation defect (**Figure 39**).

In conclusion, loss of Fbw7 results in increased neuronal progenitor apoptosis and in turn decreased numbers of neurons *in vitro* and *in vivo*. Furthermore, Fbw7-deficient neural stem cells exhibit a defect in differentiating into neurons which in addition contributes to the reduced neuronal numbers detected in the developing brain of $Fbxw7^{\Delta N}$ mice.

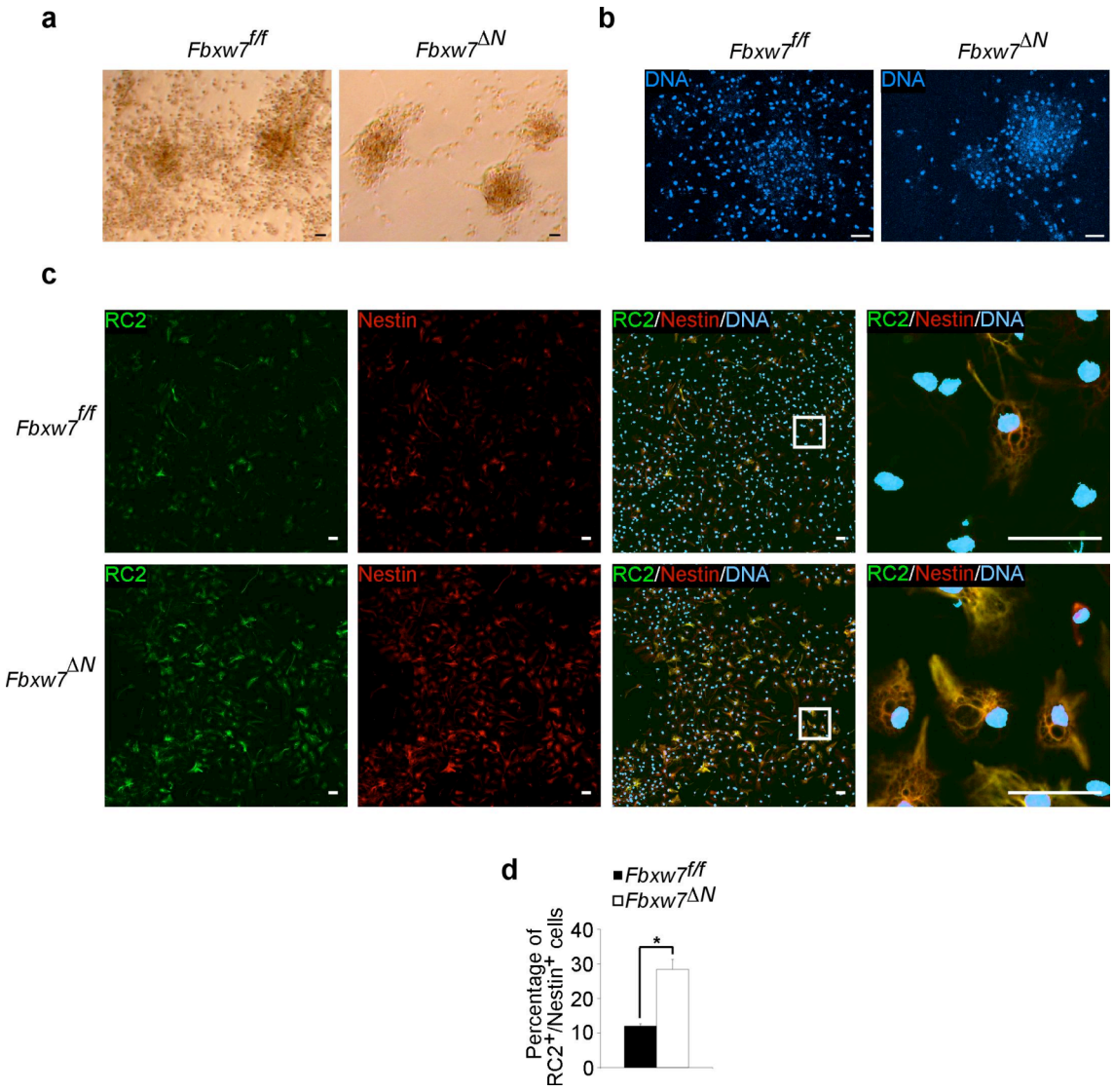

Figure 35 Loss of Fbw7 leads to retention of stem cell markers *in vitro*.
(**a**) Phase contrast pictures of *Fbxw7*$^{f/f}$ and *Fbxw7*$^{\Delta N}$ neurosphere cultures under differentiation conditions. (**b**) Stainings for DNA (blue) with Hoechst 33342 on *Fbxw7*$^{f/f}$ and *Fbxw7*$^{\Delta N}$ neurosphere cultures after 5 d of differentiation. Scale bars: 50 µm. (**c**) Immunocytochemistry for RC2 (green) and Nestin (red) on *Fbxw7*$^{f/f}$ and *Fbxw7*$^{\Delta N}$ neurosphere cultures after 5 d under differentiation conditions. White squares mark areas shown in high magnification in panels on the right. DNA (blue) was counterstained with Hoechst 33342. Scale bars, 50 µm. (**d**) Quantification of RC2/Nestin-double positive cells in *Fbxw7*$^{f/f}$ and *Fbxw7*$^{\Delta N}$ neurosphere cultures after 5 d under differentiation conditions. Error bars, s.e.m.; *$P \leq 0.05$ (unpaired *t*-test).

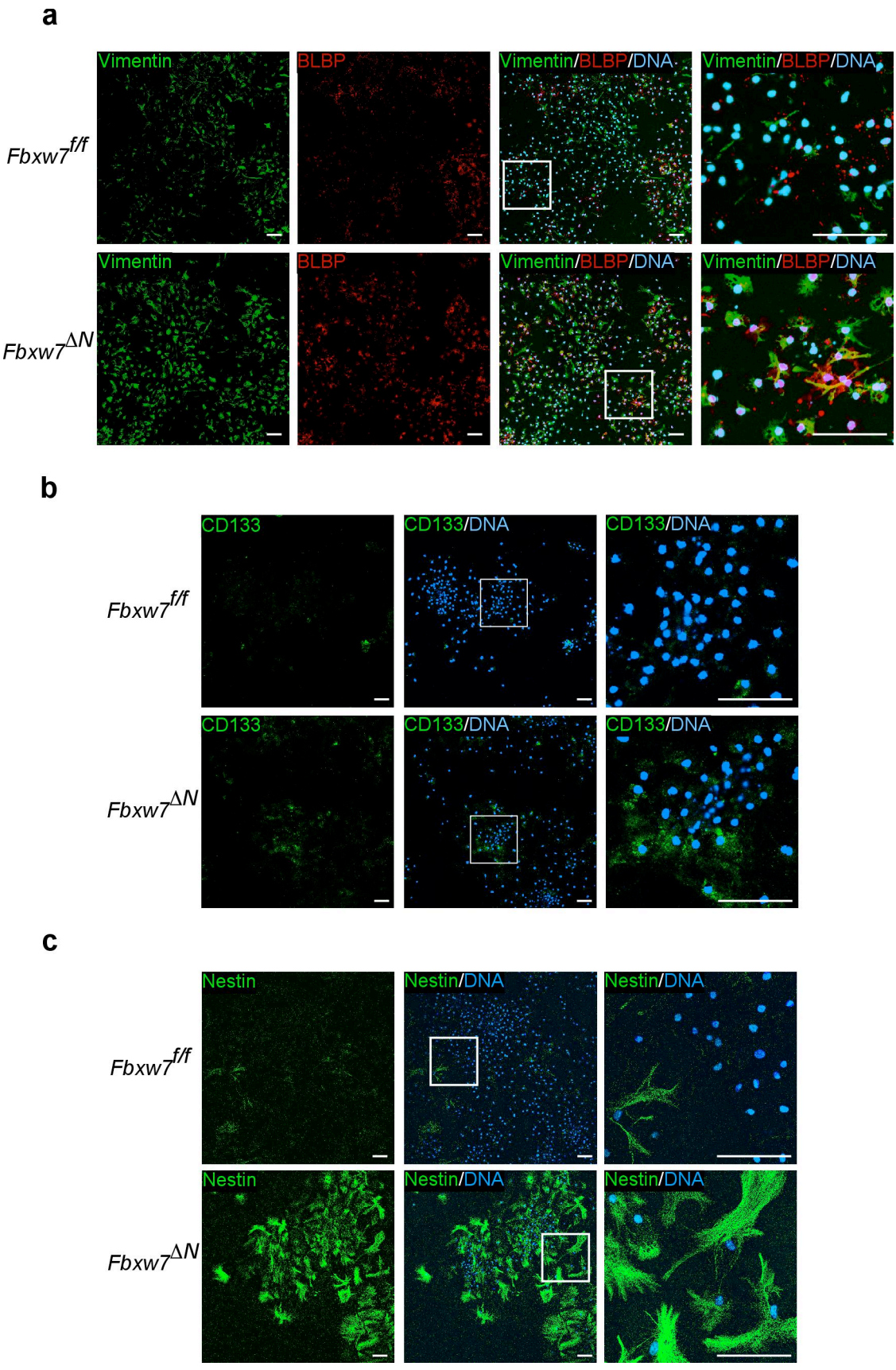
a
Vimentin
BLBP
Vimentin/BLBP/DNA
Vimentin/BLBP/DNA
Fbxw7f/f
Vimentin
BLBP
Vimentin/BLBP/DNA
Vimentin/BLBP/DNA
Fbxw7ΔN
b
CD133
CD133/DNA
CD133/DNA
Fbxw7f/f
CD133
CD133/DNA
CD133/DNA
Fbxw7ΔN
c
Nestin
Nestin/DNA
Nestin/DNA
Fbxw7f/f
Nestin
Nestin/DNA
Nestin/DNA
Fbxw7ΔN

Figure 36 Absence of Fbw7 blocks differentiation *in vitro*.
(**a,b**) Immunocytochemistry for (**a**) Vimentin (green) and BLBP (red) and (**b**) CD133 (green) on *Fbxw7*$^{f/f}$ and *Fbxw7*$^{\Delta N}$ neurosphere cultures after 5 d under differentiation conditions. White squares mark areas shown in high magnification in panels on the right. DNA (blue) is counterstained with Hoechst 33342. Scale bars: 100 µm. (**c**) Immunocytochemistry for Nestin (green) on *Fbxw7*$^{f/f}$ and *Fbxw7*$^{\Delta N}$ neurosphere cultures after 11 d of differentiation. White squares mark areas shown in high magnification in panels on the right. DNA (blue) is counterstained with Hoechst 33342. Scale bars: 100 µm.

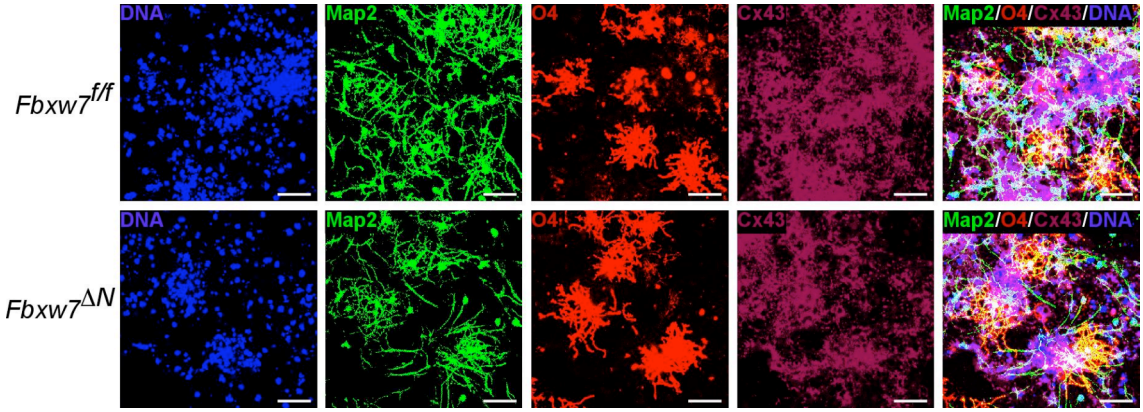

Figure 37 Absence of Fbw7 does not affect multipotentiality of neurospheres
Immunocytochemistry for Map2 (green), O4 (red) and Connexin 43 (Cx43; magenta) on *Fbxw7*$^{f/f}$ and *Fbxw7*$^{\Delta N}$ neurosphere cultures after 5 d of differentiation. DNA (blue) is counterstained with Hoechst 33342. Scale bars: 50 µm.

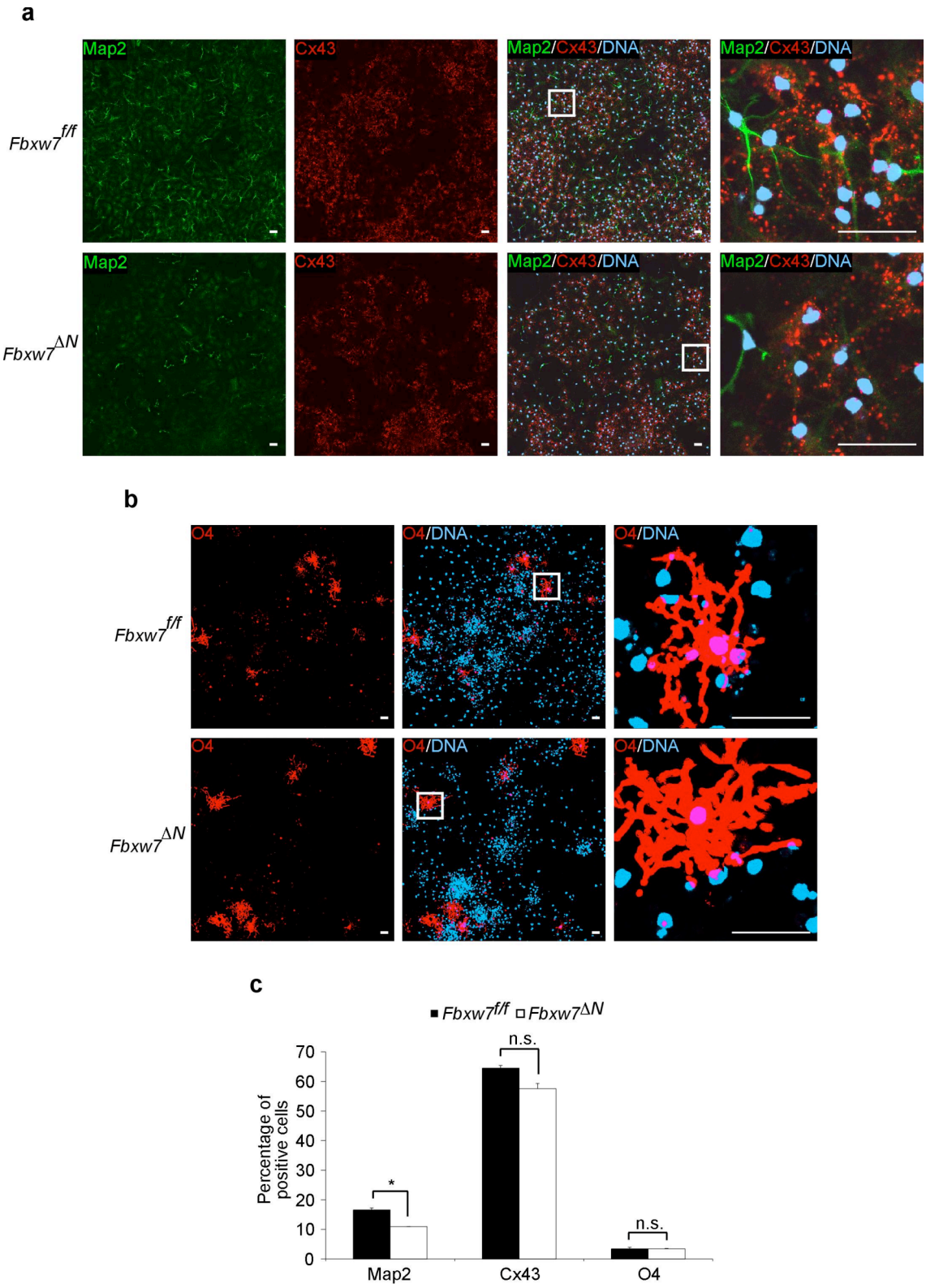

Figure 38 Loss of Fbw7 impairs neurogenesis *in vitro*.
(**a**,**b**) Immunocytochemistry for (**a**) Map2 (green) and Connexin 43 (Cx43; red) and (**b**) O4 on *Fbxw7*$^{f/f}$ and *Fbxw7*$^{\Delta N}$ neurosphere cultures after 5 d under differentiation conditions. White squares mark areas shown in high magnification in panels on the

right. DNA (blue) is counterstained with Hoechst 33342. Scale bars, 50 μm. (**c**) Quantification of Map2-, Cx43- and O4-positive cells in *Fbxw7*$^{f/f}$ and *Fbxw7*$^{\Delta N}$ neurosphere cultures after 5 d under differentiation conditions. Error bars, s.e.m.; n.s., not significant; *$P \leq 0.05$ (unpaired *t*-test).

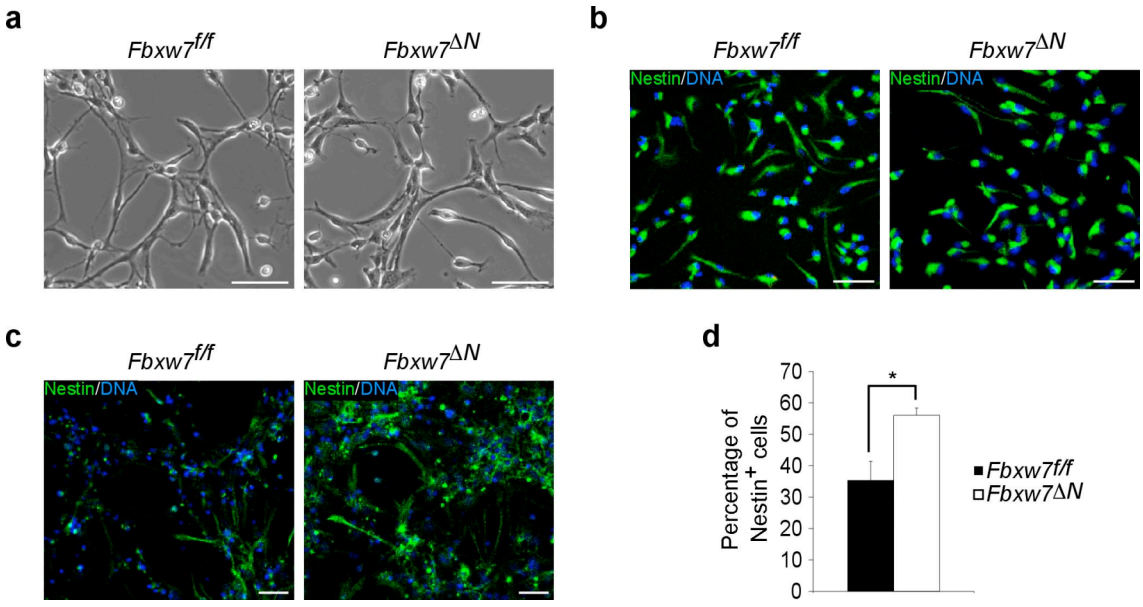

Figure 39 Loss of Fbw7 leads to a block in differentiation also in adherent NSC cultures.
(**a**) Phase contrast pictures of *Fbxw7*$^{f/f}$ and *Fbxw7*$^{\Delta N}$ adherent NSC cultures under growth conditions. Scale bars: 50 µm. (**b**,**c**) Immunocytochemistry for Nestin (green) on *Fbxw7*$^{f/f}$ and *Fbxw7*$^{\Delta N}$ adherent NSC cultures (**b**) under growth conditions and (**c**) after 5 d under differentiation conditions. DNA (blue) was counterstained with Hoechst 33342. Scale bars: 50 µm. (**d**) Quantification of Nestin-positive cells in *Fbxw7*$^{f/f}$ and *Fbxw7*$^{\Delta N}$ adherent NSC cultures after 5 d under differentiation conditions. $n = 3$. Error bars, s.e.m.; $^*P \leq 0.05$ (unpaired *t*-test).

3.1.9 Discussion: The function of Fbw7 in brain development

3.1.9.1 Fbw7 in neuronal differentiation

Immunohistochemical analysis of stem cell, progenitor and neuronal markers in the brain revealed that the number of stem cells is highly increased whereas the number of neuronal progenitors and differentiated neurons is significantly reduced in the absence of Fbw7 (**Figures 27-30**). Expression of the radial glia stem cell markers BLBP, GLAST and Nestin was greatly increased in the E18.5 *Fbxw7*$^{\Delta N}$ cortical and tectal ventricular zones. Also the number of more immature Musashi 1-positive stem cells was found to be elevated in the mutant brain. This was confirmed *in vitro* where *Fbxw7*$^{\Delta N}$ neurospheres exhibited an increase in Musashi-1 and CD133-positive early neural stem cells (**Figures 34** and **36**). This suggested that Fbw7 already plays a role in the differentiation of early neuroepithelial stem cells. However, the main population of cells accumulating in the Fbw7-knockout brain were radial glia stem cells (RGCs), which are the main subset of neural stem cells at later stages of embryonic development (**Figure 27**). Apart from the greatly augmented levels of RGCs in the cortical and tectal ventricular zones, ectopic expression of RGC markers was also detectable in the cortical subventricular zone, intermediate zone and cortical plate and in the tectal mantle layer.

On the contrary, the expression of markers for neuronal progenitors, such as Tbr2 and Doublecortin, and for differentiated neurons, such as NeuN, Tbr1, Ctip2 and Brn2, was significantly decreased in the *Fbxw7*$^{\Delta N}$ cortex (**Figures 29** and **30**). In addition to the already reduced cellularity detected in areas of differentiated cells, the decrease in the percentage of cells positive for markers of differentiated neurons accounts for a total loss of more than 50% of mature neurons in the *Fbxw7*$^{\Delta N}$ cortex. Furthermore, since markers of various cortical layer neurons were reduced, it seems that lack of Fbw7

affects neurogenesis in general and is not solely responsible for the differentiation of specific neurons. *In vitro*-experiments on neurosphere and adherent NSC cultures confirmed the defect in stem cell differentiation into neurons and the accumulation of cells expressing radial glia stem cell markers (**Figures 35-39**). Additionally, data on Nestin-expression in *Fbxw7*$^{\Delta N}$ neurosphere cultures showed that even at prolonged time under differentiation conditions, *Fbxw7*$^{\Delta N}$ neurosphere cells do not undergo differentiation. Thus, the absence of Fbw7 results not only in a delay but in a genuine block of stem cell differentiation. It is likely that the significant lack of mature neurons in the *Fbxw7*$^{\Delta N}$ brain contributes to the perinatal lethality of Fbw7-knockout mice.

3.1.9.2 Fbw7 in glial differentiation

In contrast to neurogenesis, glia differentiation was not affected by the absence of Fbw7. The number of S100-positive astrocytes and NG2-positive oligodendrocytes was not changed in the *Fbxw7*$^{\Delta N}$ E18.5 cortex (**Figure 31**). This was confirmed by *in vitro*-results showing that the percentage of Connexin-43-positive astrocytes and O4-positive oligodendrocytes generated in wt and *Fbxw7*$^{\Delta N}$ neurosphere differentiation cultures is similar (**Figure 38**). Thus, Fbw7 seems to be essential for neural stem cell differentiation into neurons but not for neural stem cell differentiation into glia cells.

Interestingly, the overall structure of the brain is not altered in *Fbxw7*$^{\Delta N}$ mouse embryos. The thickness of the *Fbxw7*$^{\Delta N}$ cortex is similar to the thickness of the wt cortex (**Figure 23**). Radial glia cells have been reported to be crucial for the structural integrity of the nervous system by forming the basal and apical barriers (Hatakeyama et al., 2004). Considering that the development of radial glia cells and differentiated glia,

as well as the cortical layering was not impaired in the absence of Fbw7, it seems that the general loss of mature neurons was not sufficient to perturb the overall brain structure.

3.1.9.3 Fbw7 in neural apoptosis

Whilst I could not detect a difference in the level of proliferation *in vivo* and *in vitro* in the absence of Fbw7, the number of apoptotic cells was significantly increased in the $Fbxw7^{\Delta N}$ brain and in $Fbxw7^{\Delta N}$ neurospheres (**Figures 25**,**26**,**33** and **34**). Thus, Fbw7 is not only required for differentiation during brain development, but also for preventing inappropriate cell death. Consequently, upon Fbw7 deletion, increased progenitor apoptosis in combination with defective stem cell differentiation leads to reduced numbers of differentiated cells. A peak in active Caspase-3-positive apoptotic cells was detectable in areas of progenitors at E14.5 in the cortex and at E16.5 in the tectum of $Fbxw7^{\Delta N}$ mice. Physiological programmed cell death is an important mechanism of specification in the developing brain and has been shown to be necessary for the generation of functional neuronal networks (Huang and Reichardt, 2001, Rabinowicz et al., 1996, Rakic and Zecevic, 2000). Furthermore, apoptosis is required for the clearance of cells exhibiting faulty differentiation (Buss and Oppenheim, 2004). Thus, Fbw7 could have two roles in programmed cell death during brain development. On the one hand, Fbw7 could inhibit physiological apoptosis of neural cells that successfully integrate into the neuronal network. On the other hand, Fbw7 could support the survival of neural cells that have undergone a molecularly correct differentiation programme. Consequently, Fbw7 expression does not only allow neural stem cells to differentiate but it also protects neuronal progenitors from undergoing apoptosis and is therefore a

safeguard for the survival of correctly integrating and differentiating cells in the developing brain.

Chapter 4. Results

4.1 Fbw7 antagonises Notch and JNK/c-Jun signalling to allow stem cell differentiation and progenitor survival in the brain

4.1.1 Loss of Fbw7 leads to increased levels of its substrates Notch and c-Jun in neurosphere cells

After describing the effects of Fbw7-deficiency on neurogenesis and brain development, I wanted to find out which target proteins of the E3 ubiquitin ligase Fbw7 are involved in the observed phenotypes.

The *Fbxw7* locus encodes three Fbw7 isoforms Fbw7α, β and γ which are generated by alternative splicing of the first exon. By qRT-PCR, it was shown that Fbw7α is the predominantly expressed isoform in neurosphere cells, whereas Fbw7β was expressed to a lower extent and Fbw7γ was not detectable (**Figure 40**). Similarly, Fbw7α and β expression were found in total brain RNA, although Fbw7β was the most abundant isoform in this case, and no Fbw7γ expression was detected in the brain in agreement with previous publications (Nateri et al., 2004, Strohmaier et al., 2001). Notably, other organs showed different Fbw7 isoform expression patterns (**Figure 40**).

Next, I performed immunoblotting for Fbw7 and the *bona fide* Fbw7-substrates phospho-c-Jun (p-c-Jun), Notch intracellular domain 1 (NICD1), phospho-c-Myc (p-c-Myc) and phospho-cyclin E (p-cyclin E) on protein extracts from wt and Fbw7-deficient neurosphere cells. Western blot analysis confirmed that neurosphere cells in $Fbxw7^{\Delta N}$ cultures lack Fbw7 (**Figure 41a**). The most abundant Fbw7 isoform Fbw7α

was detected at 110 kDa. Although Fbw7α has a predicted size of 80kDa, it has been previously reported that Fbw7α runs aberrantly on SDS gels at 110 kDa (Strohmaier et al., 2001). Furthermore, absence of Fbw7 resulted in significantly increased protein levels of the Fbw7-substrates p-c-Jun and NICD1 whereas levels of the other Fbw7 target proteins p-c-Myc and p-cyclin E were not substantially altered (**Figure 41a**). Notably, also unphosphorylated c-Jun levels were increased which is probably due to the fact that c-Jun autoregulates its expression in a positive feedback mechanism (Angel et al., 1988b). Similar results on Fbw7 and its substrate expression levels were obtained by Western blot analysis on protein extracts from adherent NSC cultures (**Figure 41b**).

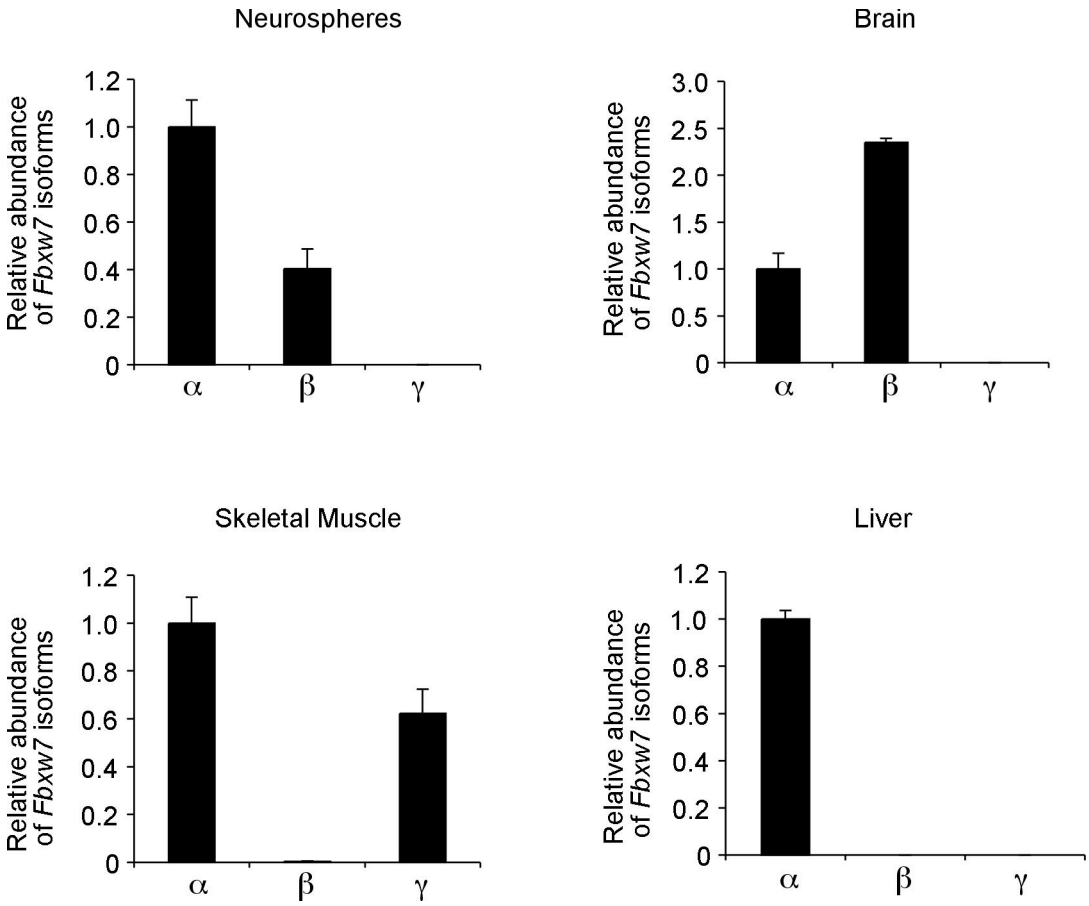

Figure 40 *Fbxw7* isoform expression
Quantitative real-time PCR analysis showing the relative abundance of *Fbxw7* isoforms α, β and γ in *Fbxw7*$^{f/f}$ neurospheres, adult brain, skeletal muscle and liver normalised to *Gapdh* (Glyceraldehyde-3-phosphate dehydrogenase) expression. Expression of *Fbxw7*α is set to 1. Error bars represent the standard deviation (s.d.).

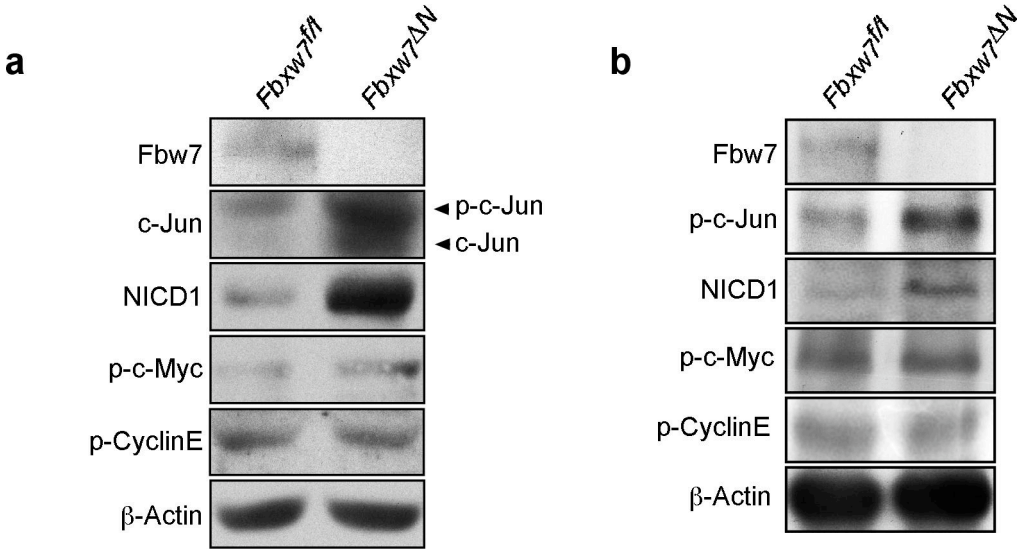

Figure 41 Loss of Fbw7 leads to increased c-Jun and Notch levels
(**a**) Western blot analysis of Fbw7 (α: 110 kDa), c-Jun (c-Jun: 39 kDa, p-c-Jun: 42 kDa), activated Notch1 (NICD1, 80 kDa), Thr58- and Ser62-phosphorylated c-Myc (p-c-Myc, 70 kDa), Thr395-phosphorylated cyclin E (p-Cyclin E, 55 kDa) and β-Actin (42 kDa) on protein lysates from *Fbxw7*$^{f/f}$ and *Fbxw7*$^{\Delta N}$ neurospheres. (**b**) Western blot analysis of Fbw7, serine 73 phosphorylated c-Jun (p-c-Jun), activated Notch1 (NICD1), Thr58- and Ser62-phosphorylated c-Myc (p-c-Myc), Thr395-phosphorylated cyclin E (p-Cyclin E) and β-Actin on protein lysates from *Fbxw7*$^{f/f}$ and *Fbxw7*$^{\Delta N}$ adherent NSC cultures.

4.1.2 Attenuation of c-Jun levels rescues cell number and progenitor apoptosis

After detecting increased p-c-Jun protein levels in neurosphere cells, I went on to examine p-c-Jun levels in the *Fbxw7*$^{\Delta N}$ brain. Immunofluorescence staining revealed that p-c-Jun levels were also elevated *in vivo* (**Figure 42a**). Interestingly, p-c-Jun was mainly increased in the tectal ML which harbours progenitors and differentiated cells. On the contrary, there was no increase detectable in the stem cell compartment, the VZ. To rescue p-c-Jun levels, I deleted one *Jun* allele in the *Fbxw7*$^{\Delta N}$ background by crossing in *Jun*$^{f/f}$ mice (*Fbxw7*$^{\Delta N}$; *Jun*$^{\Delta N/+}$). Indeed, immunofluorescence staining showed that this significantly attenuated p-c-Jun levels, even though p-c-Jun was still slightly increased in the *Fbxw7*$^{\Delta N}$; *Jun*$^{\Delta N/+}$ brain in comparison to wt levels (**Figure 42a**).

p-c-Jun has previously been reported to play a role in neuronal apoptosis (reviewed in Raivich and Behrens, 2006). Thus, I analysed the Fbw7; c-Jun double-mutant mice to see whether downregulation of p-c-Jun in the Fbw7-knockout background can rescue cell number and progenitor apoptosis in neurosphere cells and the developing brain. Histological analysis of H&E stainings revealed that in fact, the cellularity in the tectal ML was significantly increased in the E18.5 *Fbxw7*$^{\Delta N}$; *Jun*$^{\Delta N/+}$ brain in comparison to the E18.5 *Fbxw7*$^{\Delta N}$ brain (**Figure 42b,c**). On the contrary, attenuation of p-c-Jun levels had no effect on the number of stem cells in the tectal VZ which was similarly increased in *Fbxw7*$^{\Delta N}$; *Jun*$^{\Delta N/+}$ mice in comparison to *Fbxw7*$^{\Delta N}$ mice. This indicates that p-c-Jun plays a crucial role in the regulation of progenitors and differentiated cells by Fbw7. However, p-c-Jun is not involved in the observed stem cell accumulation in *Fbxw7*$^{\Delta N}$ mice. This was confirmed by *in vitro*-data which showed that similar to what was seen in *Fbxw7*$^{\Delta N}$ neurosphere differentiation cultures, also in *Fbxw7*$^{\Delta N}$; *Jun*$^{\Delta N/+}$ neurosphere

differentiation cultures, the number of cells expressing the NSC/NPC marker Nestin was highly increased after 5 days under differentiation conditions (**Figure 43a**). However, under growth conditions, neural cells isolated from E14.5 *Fbxw7*$^{\Delta N}$; *Jun*$^{\Delta N/+}$ mouse embryos showed a significantly higher ability to generate neurospheres in comparison to *Fbxw7*$^{\Delta N}$ neurosphere cultures (**Figure 43b**). This indicates that downregulation of c-Jun can rescue neurosphere formation. This would predict that attenuation of c-Jun levels can also prevent increased progenitor apoptosis which was identified to be responsible for the decreased cell number. Indeed, *Fbxw7*$^{\Delta N}$; *Jun*$^{\Delta N/+}$ neurospheres harboured a significantly lower number of TUNEL-positive apoptotic cells in comparison to *Fbxw7*$^{\Delta N}$ neurospheres (**Figure 43c**).

To study the role of Fbw7 and its substrate p-c-Jun in neural progenitor apoptosis further, I performed qRT-PCR for genes involved in c-Jun function in apoptosis. Pro-apoptotic members of the *Bcl2*-family of genes have been shown to be upregulated after JNK/c-Jun signalling activation (Bossy-Wetzel et al., 1997, Whitfield et al., 2001, Ma et al., 2007). By qRT-PCR, I confirmed that no *Fbxw7* expression was detectable in *Fbxw7*$^{\Delta N}$ and *Fbxw7*$^{\Delta N}$; *Jun*$^{\Delta N/+}$ neurosphere cells (**Figure 43d**). As a consequence of c-Jun autoregulation, *Jun* expression itself was increased in *Fbxw7*$^{\Delta N}$ neurosphere cells. Furthermore, the pro-apoptotic *Bcl2*-family member genes *Bcl2l11* [Bcl2-like 11 (apoptosis facilitator); *Bim*] and *Bad* (BCL2-associated agonist of cell death) were upregulated whereas expression levels of the anti-apoptotic *Bcl2* gene were not elevated in the absence of Fbw7 (**Figure 43d**). This indicates that increased progenitor apoptosis in the absence of Fbw7 is mediated via elevated p-c-Jun levels and in turn increased expression of pro-apoptotic members of the *Bcl2*-family of genes. Interestingly, attenuation of c-Jun levels in the *Fbxw7*$^{\Delta N}$; *Jun*$^{\Delta N/+}$ neurospheres led to downregulation

of the pro-apoptotic genes *Bcl2l11* (*Bim*) and *Bad* which explains molecularly how downregulation of c-Jun rescues the increased progenitor apoptosis detected in the absence of Fbw7 (**Figure 43d**). Since neurosphere cells with highest *Jun*, *Bcl2l11* (*Bim*) and *Bad* levels are expected to undergo apoptosis and consequently are cleared from neurosphere cultures during passaging, the qRT-PCR analysis might even underestimate the increase in *Jun*, *Bcl2l11* (*Bim*) and *Bad* expression.

In summary, the E3 ubiquitin ligase Fbw7 degrades c-Jun during neural development to allow neural progenitors to survive. In the absence of Fbw7, high p-c-Jun levels induce apoptosis via pro-apoptotic members of the *Bcl2*-family of genes. By regulating neural progenitor apoptosis during brain development, Fbw7 is a key switch to control neural cell number in the brain.

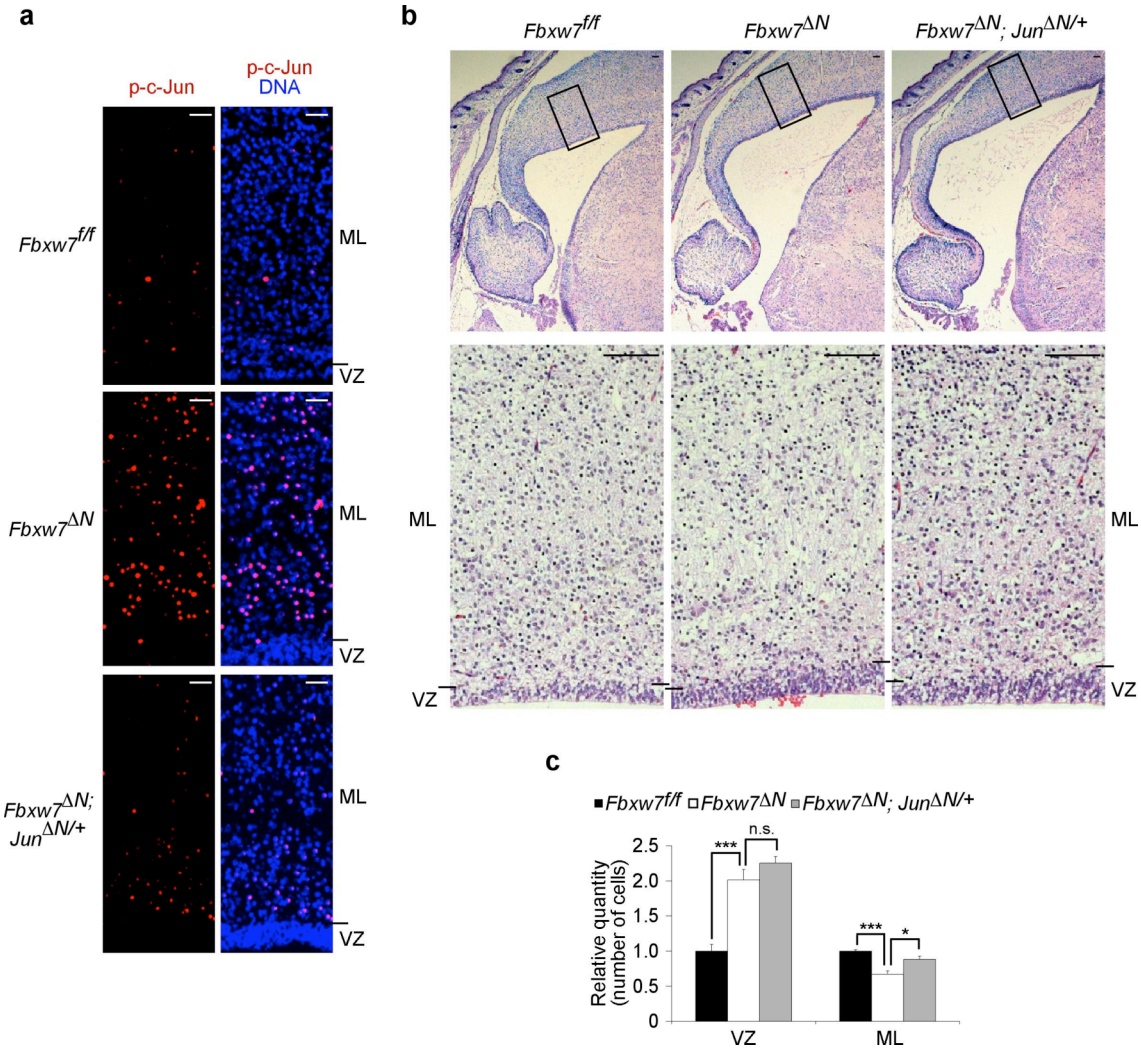

Figure 42 Fbw7 controls cell number in the brain via c-Jun

(**a**) Immunohistochemistry for Ser73-phosphorylated c-Jun (p-c-Jun; red) on representative sections of *Fbxw7*$^{f/f}$, *Fbxw7*$^{\Delta N}$ and *Fbxw7*$^{\Delta N}$; *Jun*$^{\Delta N/+}$ E18.5 tectum. DNA (blue) is counterstained with DAPI. Scale bars, 50 µm. (**b**) H&E staining of comparable regions of the *Fbxw7*$^{f/f}$, *Fbxw7*$^{\Delta N}$ and *Fbxw7*$^{\Delta N}$; *Jun*$^{\Delta N/+}$ E18.5 midbrain. Rectangles mark the area of the tectum shown below in high magnification. Scale bars: 200 µm. (**c**) Histogram showing the relative quantity of cells in the VZ and the ML of *Fbxw7*$^{f/f}$ (n = 5), *Fbxw7*$^{\Delta N}$ (n = 5) and *Fbxw7*$^{\Delta N}$; *Jun*$^{\Delta N/+}$ (n = 3) E18.5 tectum. Cell numbers in the *Fbxw7*$^{f/f}$ E18.5 tectum are normalized to 1 (100%).
Error bars, s.e.m.; n.s., not significant; *$P \leq 0.05$; ***$P \leq 0.001$ (unpaired t-test). ML: mantle layer, VZ: ventricular zone.

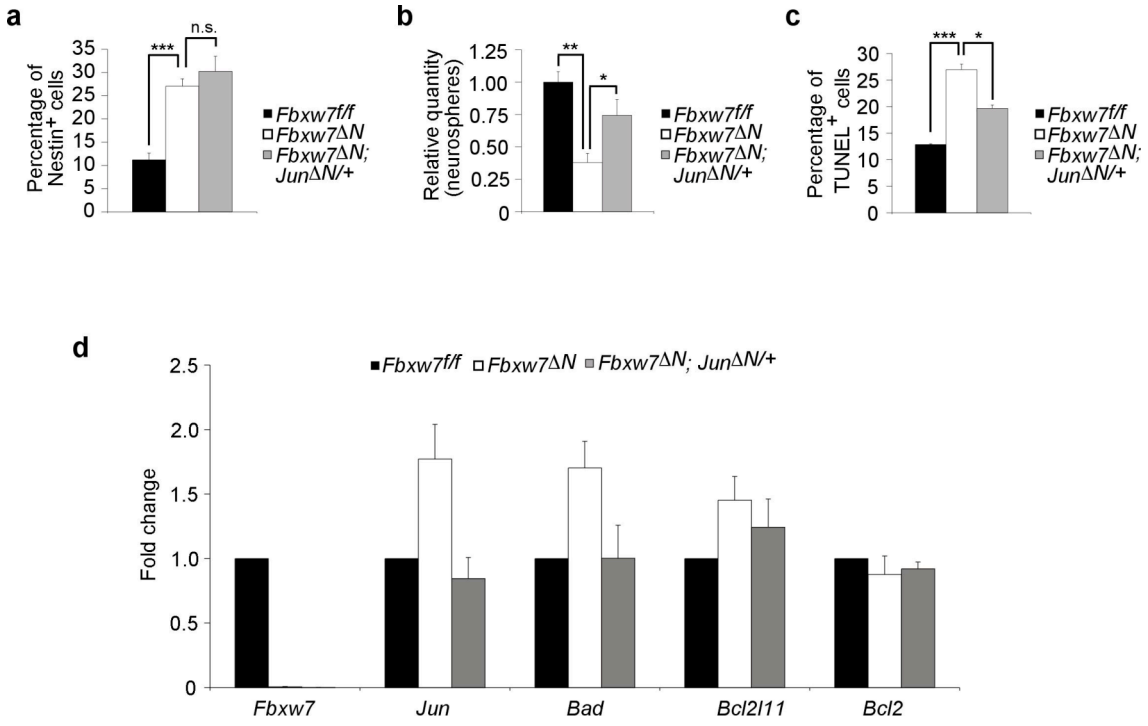

Figure 43 Negative regulation of c-Jun by Fbw7 controls neural cell viability.
(**a**) Histogram showing the percentage of Nestin-positive cells in *Fbxw7*$^{f/f}$ (n = 8), *Fbxw7*$^{\Delta N}$ (n = 11) and *Fbxw7*$^{\Delta N}$*; Jun*$^{\Delta N/+}$ (n = 2) neurosphere cultures after 5 d of differentiation. (**b**) Histogram showing the relative quantity of neurospheres in *Fbxw7*$^{f/f}$ (n = 4), *Fbxw7*$^{\Delta N}$ (n = 4) and *Fbxw7*$^{\Delta N}$; *Jun*$^{\Delta N/+}$ (n = 2) neurosphere cultures after 2 weeks under growth conditions. Neurosphere numbers in *Fbxw7*$^{f/f}$ neurosphere cultures are normalized to 1 (100%). (**c**) Histogram showing the percentage of TUNEL-positive cells in *Fbxw7*$^{f/f}$ (n = 3), *Fbxw7*$^{\Delta N}$ (n = 3) and *Fbxw7*$^{\Delta N}$; *Jun*$^{\Delta N/+}$ (n = 2) neurosphere cultures. (**d**) Quantitative real-time PCR analysis of *Fbxw7, Jun, Bad, Bcl2l11* and *Bcl2* transcripts in *Fbxw7*$^{f/f}$, *Fbxw7*$^{\Delta N}$ and *Fbxw7*$^{\Delta N}$; *Jun*$^{\Delta N/+}$ neurosphere cells. The data are normalised to *Gapdh* and represented as fold change relative to RNA levels in *Fbxw7*$^{f/f}$ neurosphere cells, which are set to 1.
Error bars, s.e.m.; n.s., not significant; *$P \leq 0.05$; **$P \leq 0.01$; ***$P \leq 0.001$ (unpaired t-test).

4.1.3 Attenuation of Notch levels rescues neural stem cell differentiation

Since downregulation of c-Jun levels did not rescue neural stem cell differentiation, I examined whether the increase in Notch levels detected in Fbw7 mutant neurosphere cells is involved in this phenotype. Notch1 has previously been reported to play an essential role in the maintenance of radial glia stem cells (reviewed in Yoon and Gaiano, 2005, Louvi and Artavanis-Tsakonas, 2006). As seen *in vitro*, NICD1 levels were also highly elevated in the E18.5 $Fbxw7^{\Delta N}$ brain (**Figure 44a**). Similar to the genetic rescue experiments using $Fbxw7^{\Delta N}$; $Jun^{\Delta N/+}$ mice, I deleted one *Notch1* allele in the $Fbxw7^{\Delta N}$ background by crossing in $Notch1^{\Delta/+}$ mice. Indeed, E18.5 $Fbxw7^{\Delta N}$; $Notch1^{\Delta/+}$ brains showed significantly reduced levels of NICD1, although there was still a slight increase in NICD1 levels detectable in comparison to the E18.5 wt brain (**Figure 44a**). To investigate whether downregulation of Notch can rescue the stem cell differentiation defect caused by Fbw7 deficiency, I compared the E18.5 $Fbxw7^{\Delta N}$; $Notch1^{\Delta/+}$ brain with the $Fbxw7^{\Delta N}$ brain. As seen before, Nestin reactivity was highly increased in the E18.5 $Fbxw7^{\Delta N}$ brain in comparison to the wt E18.5 brain (**Figure 44b**). Attenuation of Notch1 levels however led to markedly reduced levels of Nestin in the E18.5 $Fbxw7^{\Delta N}$; $Notch1^{\Delta/+}$ brain in comparison to the E18.5 $Fbxw7^{\Delta N}$ brain. Furthermore, downregulation of Notch partially rescued the increased number of cells expressing the radial glia stem cell marker BLBP in the E18.5 cortex (**Figure 44c**,**d**). This indicated that attenuation of Notch1 in the absence of Fbw7 can prevent stem cell accumulation in the brain.

To confirm these results *in vitro*, I analysed neurospheres generated from neural cells from the E14.5 $Fbxw7^{f/f}$, $Fbxw7^{\Delta N}$ and $Fbxw7^{\Delta N}$; $Notch1^{\Delta/+}$ brain. As described before, Fbw7 deficiency resulted in stem cell accumulation in neurosphere cultures after 5 days

under differentiation condition (**Figure 45**). Both pharmacological inhibition of Notch signalling as well as genetic attenuation of Notch levels was able to rescue stem cell differentiation in the *Fbxw7*$^{\Delta N}$ background. Treatment of Fbw7 mutant neurosphere cultures with *N*-[*N*-(3,5-difluorophenacetyl-l-alanyl)]-*S*-phenylglycine *t*-butyl ester (DAPT), which prevents Notch cleavage and activation by inhibition of γ-secretase, led to a significant downregulation of Nestin-positive cells in *Fbxw7*$^{\Delta N}$ neurosphere cultures (**Figure 45a**,**b**). Similarly, specific genetic attenuation of Notch1 levels resulted in a decrease of Nestin-positive cells in *Fbxw7*$^{\Delta N}$; *Notch1*$^{\Delta/+}$ neurosphere differentiation cultures in comparison to *Fbxw7*$^{\Delta N}$ differentiation cultures (**Figure 45c**,**d**).

To study this further on a molecular level, I performed qRT-PCR analysis for *bona fide* Notch target genes *Hes1*, *Hes5* and *Hey1* on cDNA from *Fbxw7*$^{f/f}$ ± DAPT, *Fbxw7*$^{\Delta N}$ ± DAPT, *Fbxw7*$^{f/f}$; *Notch1*$^{\Delta/+}$ and *Fbxw7*$^{\Delta N}$; *Notch1*$^{\Delta/+}$ neurosphere cells (**Figure 46**). DAPT treatment significantly reduced *Hes5* and *Hey1* levels which were highly upregulated in *Fbxw7*$^{\Delta N}$ neurospheres whereas *Hes1* expression was not substantially altered (**Figure 46a**). Similarly, attenuation of Notch1 levels in *Fbxw7*$^{\Delta N}$; *Notch1*$^{\Delta/+}$ neurospheres markedly reduced the elevated *Hes5* and *Hey1* levels in the *Fbxw7*$^{\Delta N}$ background while having no significant effect on *Hes1* (**Figure 46b**). This indicates that Fbw7 is responsible for Notch degradation during neural differentiation. In the absence of Fbw7, increased Notch levels maintain the radial glia stem cell state via its downstream targets Hes5 and Hey1. Notably, similar results were observed in adherent NSCs where the c-Jun target gene *Jun* itself and the Notch target gene *Hes5* were upregulated in the *Fbxw7*$^{\Delta N}$ background (**Figure 46c**).

After showing that attenuation of Notch signalling can decrease the elevated number of stem cells in the absence of Fbw7, I wanted to find out whether neuronal differentiation is also rescued by downregulation of Notch. Indeed, immunohistochemistry on the E18.5 *Fbxw7*$^{f/f}$, *Fbxw7*$^{\Delta N}$ and *Fbxw7*$^{\Delta N}$; *Notch1*$^{\Delta/+}$ cortex revealed that attenuation of Notch results in a significantly increased number of cells expressing the neuronal marker NeuN (**Figure 47a**,**b**). Similarly, the number of Map2-positive neurons were significantly increased in *Fbxw7*$^{\Delta N}$; *Notch1*$^{\Delta/+}$ neurosphere differentiation cultures in comparison to *Fbxw7*$^{\Delta N}$ differentiation cultures (**Figure 47c**,**d**). This indicates, that downregulation of Notch can rescue neurogenesis in the *Fbxw7*$^{\Delta N}$ background. Thus, Fbw7 antagonises Notch to allow radial glia stem cells to differentiate into neurons.

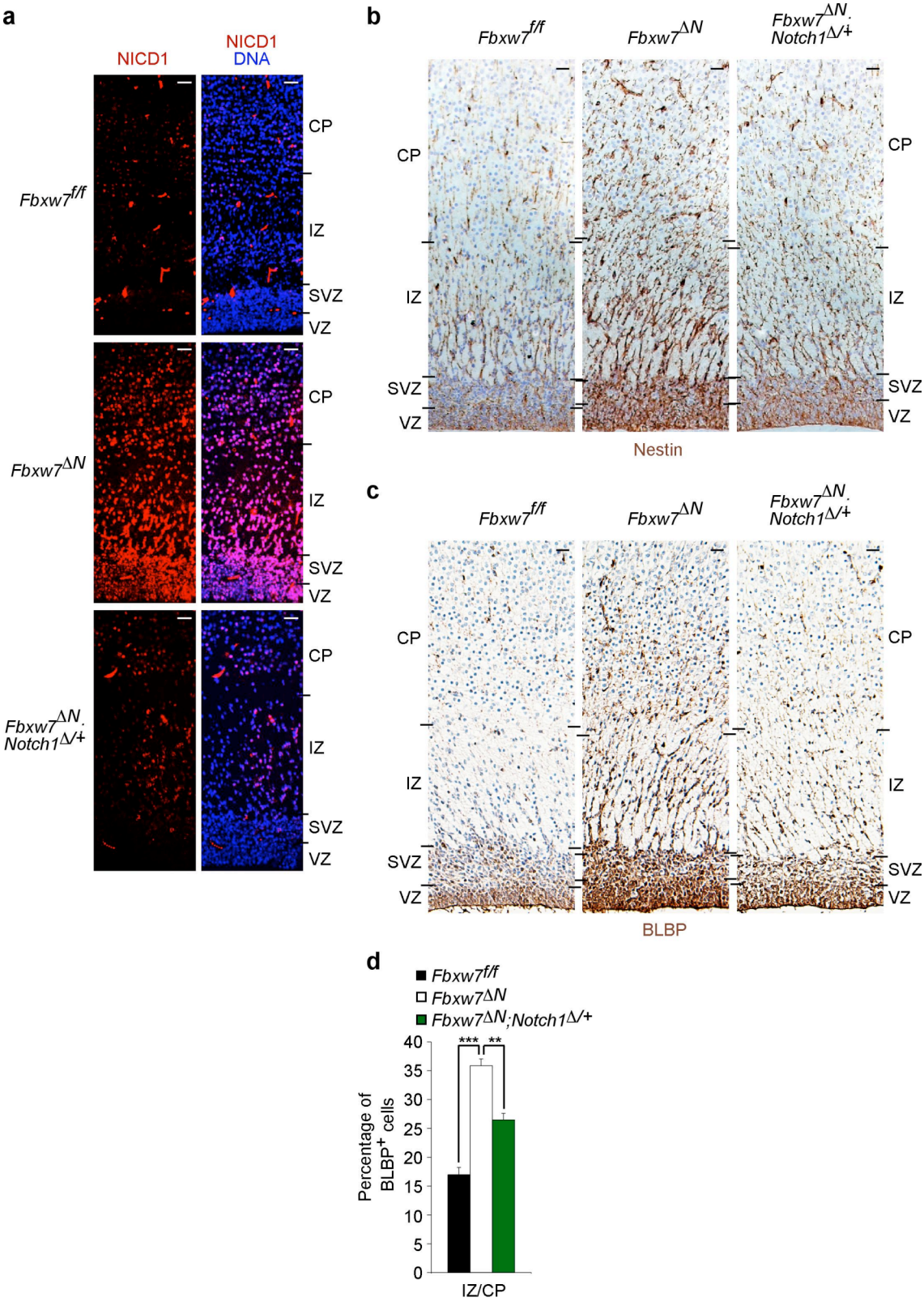

Figure 44 Fbw7 controls stem cell differentiation by antagonising Notch
(**a**) Immunohistochemistry for activated Notch1 (NICD1; red) on representative sections of the *Fbxw7*$^{f/f}$, *Fbxw7*$^{\Delta N}$ and *Fbxw7*$^{\Delta N}$; *Notch1*$^{\Delta/+}$ E18.5 cortex. DNA (blue) is

counterstained with DAPI. Scale bars, 50 μm. (**b**,**c**) DAB staining for (**b**) Nestin and (**c**) BLBP on the *Fbxw7*$^{f/f}$, *Fbxw7*$^{\Delta N}$ and *Fbxw7*$^{\Delta N}$; *Notch1*$^{\Delta/+}$ E18.5 cortex. Cells are counterstained with haematoxylin. Scale bars, 50 μm. (**d**) Quantification of BLBP-positive cells in the IZ and the CP of the *Fbxw7*$^{f/f}$, *Fbxw7*$^{\Delta N}$ and *Fbxw7*$^{\Delta N}$; *Notch1*$^{\Delta/+}$ E18.5 cortex. $n = 3$.
Error bars, s.e.m.; $^{**}P \leq 0.01$; $^{***}P \leq 0.001$ (unpaired *t*-test). CP: cortical plate, IZ: intermediate zone, SVZ: subventricular zone, VZ: ventricular zone.

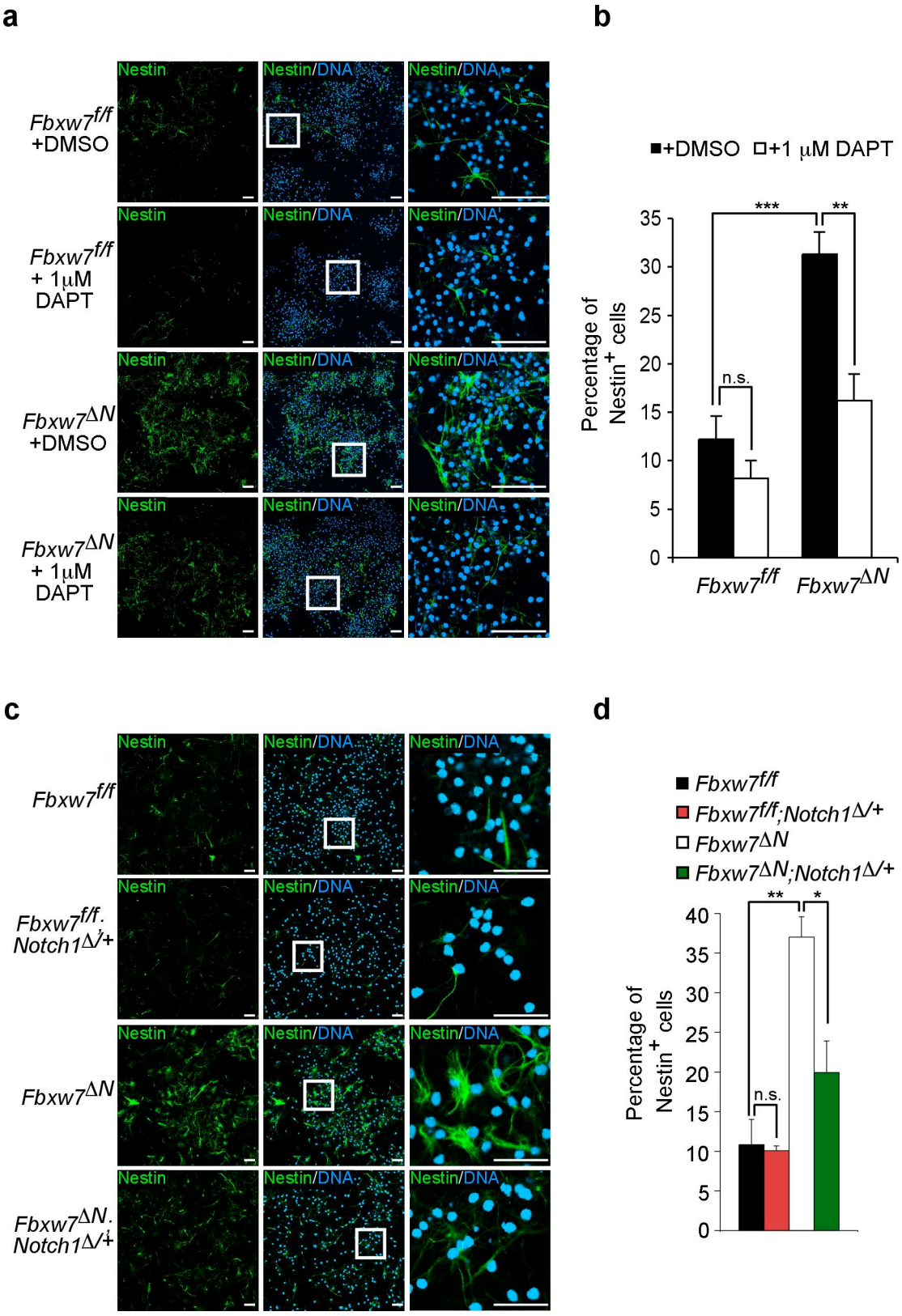

Figure 45 Inhibition of Notch signalling alleviates the block in stem cell differentiation *in vitro*.

(**a**) Immunocytochemistry for Nestin (green) on *Fbxw7*$^{f/f}$ and *Fbxw7*$^{\Delta N}$ neurosphere cultures after 5 d under differentiation conditions treated with DMSO (control) or 1 μM

DAPT. White squares mark areas shown in high magnification in panels on the right. DNA (blue) is counterstained with Hoechst 33342. Scale bars, 100 μm. (**b**) Histogram showing the percentage of Nestin-positive cells in *Fbxw7*$^{f/f}$ and *Fbxw7*$^{\Delta N}$ neurosphere cultures after 5 d under differentiation conditions treated with DMSO (control) or 1 μM DAPT. n = 5. (**c**) Immunocytochemistry for Nestin (green) on *Fbxw7*$^{f/f}$, *Fbxw7*$^{f/f}$; *Notch1*$^{\Delta/+}$, *Fbxw7*$^{\Delta N}$ and *Fbxw7*$^{\Delta N}$; *Notch1*$^{\Delta/+}$ neurosphere cultures after 5 d under differentiation conditions. White squares mark areas shown in high magnification in panels on the right. DNA (blue) is counterstained with Hoechst 33342. Scale bars, 50 μm. (**d**) Histogram showing the percentage of Nestin-positive cells in *Fbxw7*$^{f/f}$, *Fbxw7*$^{f/f}$; *Notch1*$^{\Delta/+}$, *Fbxw7*$^{\Delta N}$ and *Fbxw7*$^{\Delta N}$; *Notch1*$^{\Delta/+}$ neurosphere cultures after 5 d under differentiation conditions. n = 3. Error bars, s.e.m.; n.s., not significant; $*P \leq 0.05$; $**P \leq 0.01$; $***P \leq 0.001$ (unpaired t-test).

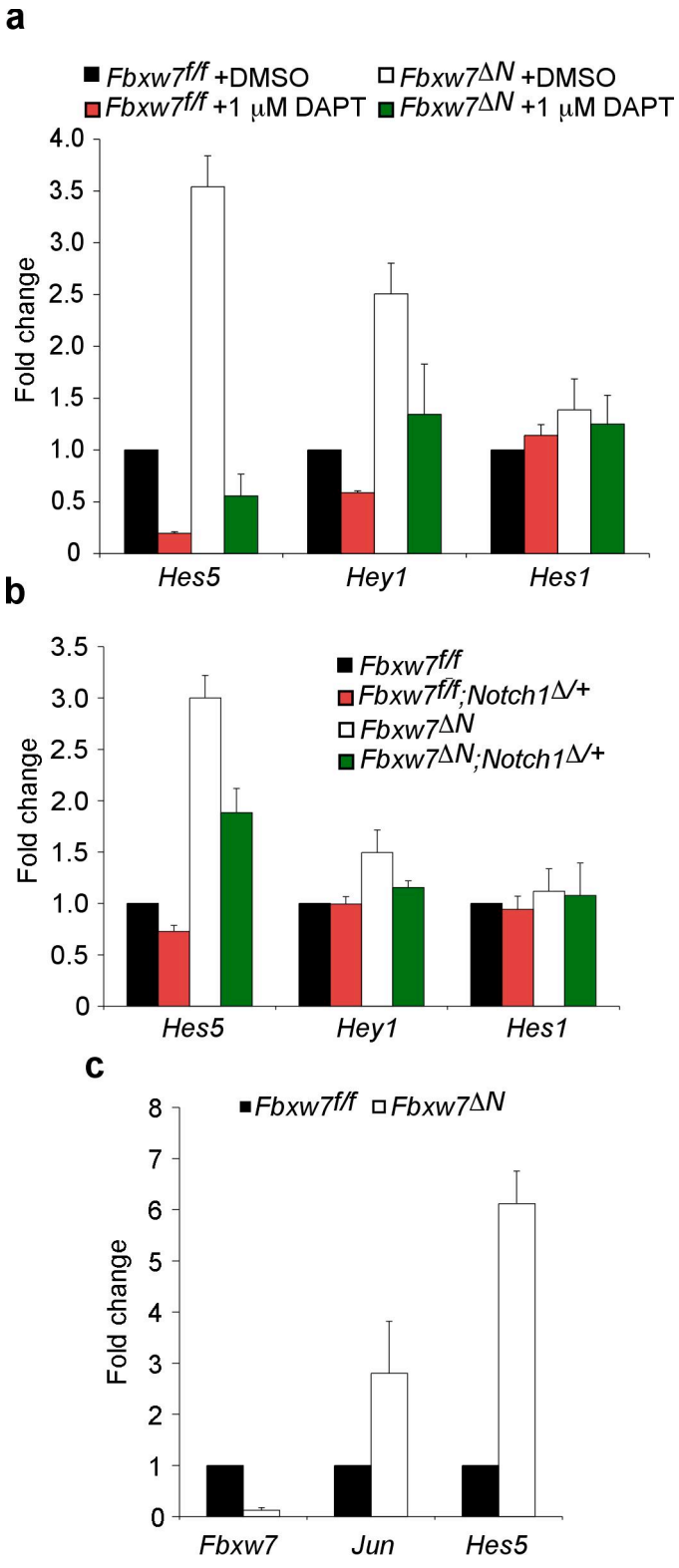

Figure 46 Fbw7 controls stem cell differentiation via Notch targets *Hes5* and *Hey1*
(**a**) Quantitative real-time PCR analysis of *Hes5, Hey1* and *Hes1* transcripts in $Fbxw7^{f/f}$ and $Fbxw7^{\Delta N}$ neurospheres treated with DMSO (control) or 1 μM DAPT. The data are normalised to *Gapdh* and represented as fold change over RNA levels in $Fbxw7^{f/f}$ + DMSO neurospheres, which is set to 1. (**b**) Quantitative real-time PCR analysis of

Hes5, Hey1 and *Hes1* transcripts in *Fbxw7*$^{f/f}$, *Fbxw7*$^{f/f}$; *Notch1*$^{\Delta/+}$, *Fbxw7*$^{\Delta N}$ and *Fbxw7*$^{\Delta N}$; *Notch1*$^{\Delta/+}$ neurospheres. The data are normalized to *Gapdh* and represented as fold change relative to RNA levels in *Fbxw7*$^{f/f}$ neurospheres, which is set to 1. **(c)** Quantitative real-time PCR analysis of *Fbxw7, Jun* and *Hes5* transcripts in cells from *Fbxw7*$^{f/f}$ and *Fbxw7*$^{\Delta N}$ adherent NSC cultures. The data are normalised to *Gapdh* and represented as fold change over RNA levels in *Fbxw7*$^{f/f}$ adherent NSCs, which is set to 1. Error bars, s.e.m.

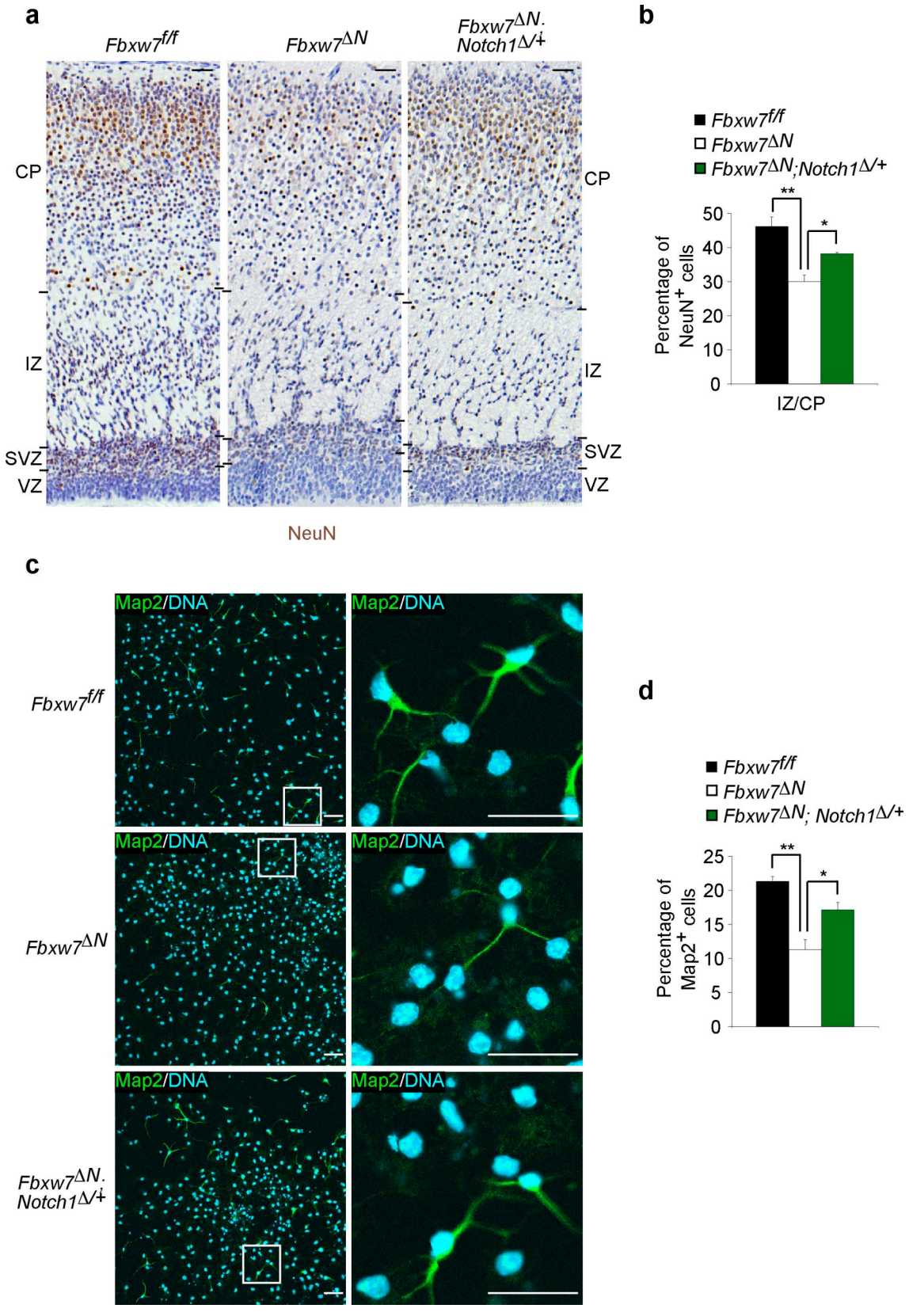
a
Fbxw7f/f
Fbxw7ΔN
Fbxw7ΔN. Notch1Δ/+
CP
IZ
SVZ
VZ
NeuN
b
Fbxw7f/f
Fbxw7ΔN
Fbxw7ΔN;Notch1Δ/+
Percentage of NeuN+ cells
IZ/CP
c
Map2/DNA
Fbxw7f/f
Fbxw7ΔN
Fbxw7ΔN. Notch1Δ/+
d
Fbxw7f/f
Fbxw7ΔN
Fbxw7ΔN; Notch1Δ/+
Percentage of Map2+ cells

Figure 47 Notch downregulation in the Fbxw7$^{\Delta N}$ background rescues neuronal numbers

(**a**) DAB staining for NeuN on the E18.5 *Fbxw7$^{f/f}$*, *Fbxw7$^{\Delta N}$* and *Fbxw7$^{\Delta N}$*; *Notch1$^{\Delta/+}$* cortex. Cells are counterstained with haematoxylin. Scale bars: 50 μm. (**b**) Quantification of NeuN-positive cells in the IZ and the CP of the E18.5 *Fbxw7$^{f/f}$*, *Fbxw7$^{\Delta N}$* and *Fbxw7$^{\Delta N}$*; *Notch1$^{\Delta/+}$* cortex (n = 3). (**c**) Immunocytochemistry for Map2 (green) on *Fbxw7$^{f/f}$*, *Fbxw7$^{\Delta N}$* and *Fbxw7$^{\Delta N}$*; *Notch1$^{\Delta/+}$* neurosphere cultures after 5 d under differentiation conditions. White squares mark areas shown in high magnification in panels on the right. DNA (blue) is counterstained with Hoechst 33342. Scale bars: 50 μm. (**d**) Histogram showing the percentage of Map2-positive cells in *Fbxw7$^{f/f}$* (n = 3), *Fbxw7$^{\Delta N}$* (n = 4) and *Fbxw7$^{\Delta N}$*; *Notch1$^{\Delta/+}$* (n = 5) neurosphere cultures after 5 d under differentiation conditions.

Error bars, s.e.m.; *$P \leq 0.05$; **$P \leq 0.01$ (unpaired t-test). CP: cortical plate, IZ: intermediate zone, SVZ: subventricular zone, VZ: ventricular zone.

4.1.4 Discussion: Fbw7 controls c-Jun and Notch levels in the developing brain

4.1.4.1 Fbw7 and c-Jun in neuronal progenitor apoptosis

Whereas the levels of the prominent Fbw7-substrates c-Myc and cyclin E were not altered in *Fbxw7*$^{\Delta N}$ neural cells, Notch and c-Jun were highly upregulated in the absence of Fbw7 (**Figure 41**).

JNK/c-Jun signalling has been reported to be involved in neuronal apoptosis both during development and after excitotoxic stress (reviewed in Raivich and Behrens, 2006). Factors antagonising pro-apoptotic JNK/c-Jun action in the brain have not been fully described. I could show that Fbw7-deficiency resulted in increased neuronal progenitor apoptosis *in vivo* and *in vitro* which was accompanied by increased levels of phosphorylated c-Jun. Genetic deletion of one *Jun* allele significantly downregulated the elevated p-c-Jun levels in the Fbw7-knockout background (**Figure 42**). Attenuation of JNK/c-Jun signalling was able to reduce the elevated number of apoptotic progenitors indicating that the increased progenitor apoptosis observed in the absence of Fbw7 is c-Jun dependent. It has been described that transcriptional regulation of pro-apoptotic members of the Bcl2-family of proteins by c-Jun is involved in c-Jun function in neuronal apoptosis (Bossy-Wetzel et al., 1997, Ma et al., 2007, Whitfield et al., 2001). As a consequence of increased c-Jun levels in the absence of Fbw7, mRNA levels of the pro-apoptotic *Bcl2*-family members *Bad* and *Bcl2l11* (*Bim*) were markedly increased, whereas the expression of the anti-apoptotic member *Bcl2* was not changed. Furthermore, attenuation of c-Jun levels by genetic deletion of one *Jun* allele was able to reduce the increased levels of the pro-apoptotic genes *Bad* and *Bcl2l11* (*Bim*).

Taken together, Fbw7 antagonises JNK/c-Jun signalling during neural development to protect neuronal progenitors from undergoing apoptosis. Interestingly, JNK activity has been shown to be very high in the brain, but it is not only involved in apoptosis but also in neuronal migration and the maintenance of cytoskeletal integrity (Chang et al., 2003, Wang et al., 2007). Thus, Fbw7 could act as a survival factor antagonising pro-apoptotic JNK signalling via c-Jun whereas c-Jun-independent JNK activity is required for migration and cytoskeletal integrity of neural cells. This might explain why in the absence of Fbw7, cortical layering and neuronal migration is normal.

4.1.4.2 Fbw7 and Notch in neural stem cell differentiation

Notch levels were highly elevated in the absence of Fbw7 and Notch signalling has been reported to be involved in radial glia stem cell maintenance (Hitoshi et al., 2002), thus making it a possible target involved in the stem cell differentiation defect observed in the *Fbxw7*$^{\Delta N}$ brain. Indeed, genetic downregulation of Notch by deletion of one *Notch1* allele in the Fbw7-knockout background rescued stem cell differentiation *in vivo* and *in vitro* (**Figures 44** and **45**). Attenuation of Notch levels reduced the elevated number of stem cells and increased the percentage of cells expressing markers of mature neurons. Also pharmacological inhibition of Notch activation by the γ-secretase inhibitor DAPT, which acts upstream of the Fbw7-NICD interaction can revert the accumulation of neural stem cells in the absence of Fbw7 (**Figure 45**). Considering that Fbw7 also targets Presenilin, which is an essential part of the γ-secretase complex, this result suggests that apart from impaired NICD-degradation, also enhanced Notch cleavage might contribute to Notch signalling hyperactivation in the absence of Fbw7.

Furthermore, the rescue by DAPT treatment indicates that other E3 ubiquitin ligases which target the Notch intracellular domain (NICD) such as the Itch/NEDD4/Su(dx) family contribute to NICD degradation. However, deletion of these E3 ubiquitin ligases have been described to only result in mild phenotypes (Lai, 2002, Qiu et al., 2000, Sakata et al., 2004). Thus, I could show that during brain development, Fbw7 is the crucial E3 ubiquitin ligase for Notch degradation, a process pivotal for neurogenesis.

Downstream of increased NICD levels, the Notch target genes *Hes5* and *Hey1* were upregulated in the absence of Fbw7, whereas *Hes1* levels were not substantially altered (**Figure 46**). *Hes1* and *Hes5* are prominent Notch targets which have been reported to mediate Notch signalling in the brain (Ohtsuka et al., 1999). Attenuation of Notch signalling in *Notch1*-, *Rbpj*-, *Delta1*- and *Hes1* single mutants as well as in *Hes1* and *Hes5* double mutants has been reported to result in precocious neuronal differentiation (Corbin et al., 2008, Yoon and Gaiano, 2005). However, deletion of Notch1 and Rbpj only lead to a decrease in *Hes5* but not in *Hes1* levels (de la Pompa et al., 1997, Yoon and Gaiano, 2005). Moreover, DAPT-treatment of neural progenitors results in a much stronger decrease in *Hes5* levels compared to *Hes1* levels (Nelson et al., 2007), which is consistent with my qRT-PCR results on cDNA from neurosphere cultures (**Figure 46**). In *Fbxw7*$^{\Delta N}$ neural cells, elevated stem cell maintenance due to high Notch levels was mediated by increased *Hes5* levels which could be rescued by genetic or pharmacological attenuation of Notch signalling. Another Fbw7-substrate c-Myc, which has been shown to be a direct Notch1 target in T-cell acute lymphoblastic leukaemia (T-ALL) (Weng et al., 2006), does not seem to be activated by Notch during brain development since no significant increase in c-Myc protein levels were detectable in the absence of Fbw7 (**Figure 41**).

Whereas the role of Notch in neural stem cell maintenance is well established, the role of Notch in neural stem cell proliferation is incompletely understood. Notch signalling has been implicated in both promoting neural stem cell self-renewal and inducing neural stem cell quiescence (reviewed in Pierfelice et al., 2011). At various time points of embryonic mouse development as well as in neurosphere cultures, I could not detect a difference in proliferation in the absence of Fbw7 (**Figures 25** and **33**). Interestingly, Gaiano *et al*. describe that NICD1-overexpression in cortical radial glia stem cells results in an accumulation of mainly quiescent radial glia stem cells (Gaiano et al., 2000). This is consistent with my finding that, although stem cell numbers were increased, the level of proliferation was not elevated in the *Fbxw7*$^{\Delta N}$ cortex. Thus, it seems that increased Notch levels in the absence of Fbw7 prevent radial glia stem cells from entering differentiation but they do not promote radial glia stem cell self-renewal.

4.1.4.3 Fbw7 substrate-specificity

Fbw7 seems to use distinct substrates to control various biological mechanisms in different tissues. As described before, Fbw7 regulates vascular development via Notch, controls haematopoietic stem cell quiescence and progenitor proliferation via c-Myc and cyclin E and is involved in intestinal progenitor proliferation and differentiation via c-Jun and Notch (Sancho et al., 2010, Thompson et al., 2008, Tsunematsu et al., 2004). By *in situ* hybridisation, I could show that *Fbxw7* expression during brain development peaks around E14.5 in the ventricular zone and the subventricular zone of the cortex whereas there is only low expression detectable in areas of differentiated cells (**Figure 27a).** This is consistent with a role of Fbw7 in stem and progenitor cells during brain development.

A way of generating substrate-specificity for Fbw7 is tissue- and cell-type-specific expression of *Fbxw7* isoforms α, β and γ. This is possible because all three isoforms have their own promoter which can be differentially regulated in distinct tissues and cell types (**Figure 40**; reviewed in Welcker and Clurman, 2008). Furthermore, all three isoforms are localised to different cellular compartments. *Fbxw7*α, which is ubiquitously expressed, is found in the nucleus, *Fbxw7*β, which is highly expressed in the brain, is localised to the cytoplasm and *Fbxw7*γ, which was detected in muscle tissue and the haematopoietic system is contained within nucleoli (reviewed in Welcker and Clurman, 2008). Interestingly, it has been reported that *Fbxw7*γ targets cyclin E and c-Myc (van Drogen et al., 2006, Welcker et al., 2004a). However, *Fbxw7*γ expression was neither detectable in neurosphere cells nor in the brain which might explain why Fbw7 does not regulate these substrates in this tissue (**Figure 40**). *Fbxw7*α and β are the most abundant isoforms in undifferentiated neurosphere cells and in the brain suggesting that these isoforms are mainly responsible for p-c-Jun and NICD degradation in neural stem cells and progenitors. Consistent with previous reports that the E3 ubiquitin ligase Fbw7 targets p-c-Jun and NICD for subsequent proteasomal degradation (Gupta-Rossi et al., 2001, Hubbard et al., 1997, Nateri et al., 2004, Oberg et al., 2001, Sundaram and Greenwald, 1993, Wei et al., 2005, Wu et al., 2001), the increased levels of p-c-Jun and NICD in $Fbxw7^{\Delta N}$ neurospheres and the Fbw7-deficient brain are likely due to p-c-Jun and NICD stabilisation. One way to confirm this would be to assess protein turnover for example by cycloheximide chase experiments.

Varying Fbw7 substrate-specificity might also explain the opposite biological effects of Fbw7 deletion in distinct tissues. Whereas loss of Fbw7 results in depletion of quiescent stem cells and increased progenitor proliferation in the haematopoietic system mediated

via c-Myc and cyclin E stabilisation (Thompson et al., 2008), loss of Fbw7 in the brain leads to accumulation of radial glia stem cells and increased progenitor apoptosis via elevated Notch and c-Jun levels (Hoeck et al., 2010).

Chapter 5. Results

5.1 JNK/c-Jun signalling in the nervous system and development

5.1.1 Targeting strategy for the generation of the *Jun*4A mouse

To further study the role of the transcription factor c-Jun in the nervous system and development, I generated two transgenic mouse lines to be able to either inhibit (*Jun*4A mouse) or activate (ROSA26-LSL-JNKK2-JNK1 mouse) JNK/c-Jun signalling and function.

In the *Jun*4A mouse, the *Jun* gene has the four main JNK-phosphorylation sites located in the N-terminal transactivation domain mutated to alanines: Ser63Ala, Ser73Ala, Thr91Ala, Thr93Ala. Consequently, c-Jun cannot be phosphorylated and activated by JNK and phospho-c-Jun (p-c-Jun) target gene expression is impaired.

To generate the *Jun*4A mouse, I inserted a genomic 10 kb fragment containing the *Jun* locus from a bacterial artificial chromosome (BAC) into a minimal vector (Gene Bridges) via homologous recombination (**Figure 48a**). To achieve this, I amplified the minimal vector by PCR adding *Jun* locus homology regions and unique restriction sites for PmeI at the 5' end and for MluI at the 3' end of the minimal vector. After homologous recombination, correct insertion was verified by restriction digest. A 0.6 kb fragment containing the four N-terminal JNK-phosphorylation sites was then excised making use of the two unique RsrII and SfiI restriction sites which flank this region of

the *Jun* gene (**Figure 48a**). Next, I cloned a RsrII-SfiI fragment excised from a pMSCV-*Jun*4A vector into the targeting construct.

As a consequence of the mutations at serine 63 and serine 73, two new SfoI/EheI restriction sites are introduced into the *Jun* gene. Indeed, SfoI/EheI test digest of the *Jun*4A targeting construct showed the fragment pattern expected after correct insertion of the 4A mutations (**Figure 48b**). To be able to identify correctly targeted ES cell clones for the subsequent blastocyst injection, a 1.6 kb neomycin-resistance cassette flanked by loxP-sites (neoR) was inserted into a unique AscI restriction site 0.2 kb 3' of the *Jun* gene in the short homology arm of the targeting construct (**Figures 48** and **49**). By PCR, I added a AscI restriction site to the 5'- and the 3'-end of the neomycin-resistance cassette and thus was able to clone it into the AscI site in the *Jun*4A targeting construct. Correct orientation of the inserted neomycin-resistance cassette was verified by EcoRI restriction digest since there is a single EcoRI restriction site at 5.4 kb in the *Jun* locus and a single EcoRI restriction site at 1.5 kb in the neomycin-resistance cassette. The presence of the mutations at the four JNK-phosphorylation sites in the *Jun*4A targeting construct was confirmed by DNA sequencing.

After that, the targeting construct was linearised by restriction digest with XmnI which has a single restriction site at 0.4 kb in the minimal vector (Gene Bridges) and a single restriction site at 10.1 kb in the targeting construct (**Figures 48** and **49**). The resulting 12.4 kb fragment contains a 8.5 kb homology region with the genomic *Jun* locus including the four mutations. Furthermore, it contains the 1.6 kb neoR-cassette and 2.3 kb of the minimal vector. Only homologous recombination between the targeting construct and the genomic *Jun* locus occurring 5' of the mutation sites and 3' of the

neoR-cassette results in correctly targeted ES cell clones. As a positive control for genomic insertion, the minimal vector containing the *Jun*4A targeting construct was linearised by MluI (unique restriction site) restriction digest.

Next, the 12.4 kb targeting construct and the positive control were electroporated into ES cells (strain 129) by the LRI Transgenic Service. I screened the ES cell clones for correct insertion by PCR with the forward primer sequence located in the neomycin-resistance cassette and the reverse primer sequence located in the genomic *Jun* locus behind the XmnI restriction site which was used to linearise the *Jun*4A targeting construct (**Figure 49**). Random insertion of the entire positive control construct into the mouse genome always resulted in the amplification of a 1.7 kb fragment, because the positive construct contains both, the forward primer sequence in the neoR-cassette and the reverse primer sequence in the genomic *Jun* locus behind the XmnI restriction site. However, solely correct insertion of the *Jun*4A targeting construct specifically into the mouse genomic *Jun* locus results in a 1.7 kb PCR-product because the *Jun*4A targeting construct only contains the forward primer sequence in the neoR-cassette whereas the reverse primer sequence in the genomic *Jun* locus is outside of the *Jun*4A targeting construct. Out of 384 screened ES cell clones, 5 clones were identified to carry the correctly inserted *Jun*4A construct in the genomic *Jun* locus. One of these clones was injected into blastocysts from C57BL/6 mice by the LRI Transgenic Service to obtain chimeras. $Jun^{4A/+}$ chimeras were confirmed to carry the mutations by amplification of the *Jun* 5'-end and restriction digest with SfoI/EheI (**Figure 50a**). Subsequently, $Jun^{4A/4A}$ mice were verified to carry the mutations by DNA sequencing (**Figure 50b**). $Jun^{4A/+}$ chimeras were crossed to PGK-Cre mice ubiquitously expressing Cre recombinase to excise the neoR-cassette which is flanked by loxP-sites. I took

advantage of the remaining 50 bp loxP-site after excision of the neoR-cassette to design genotyping primers flanking this region (**Figure 50c**).

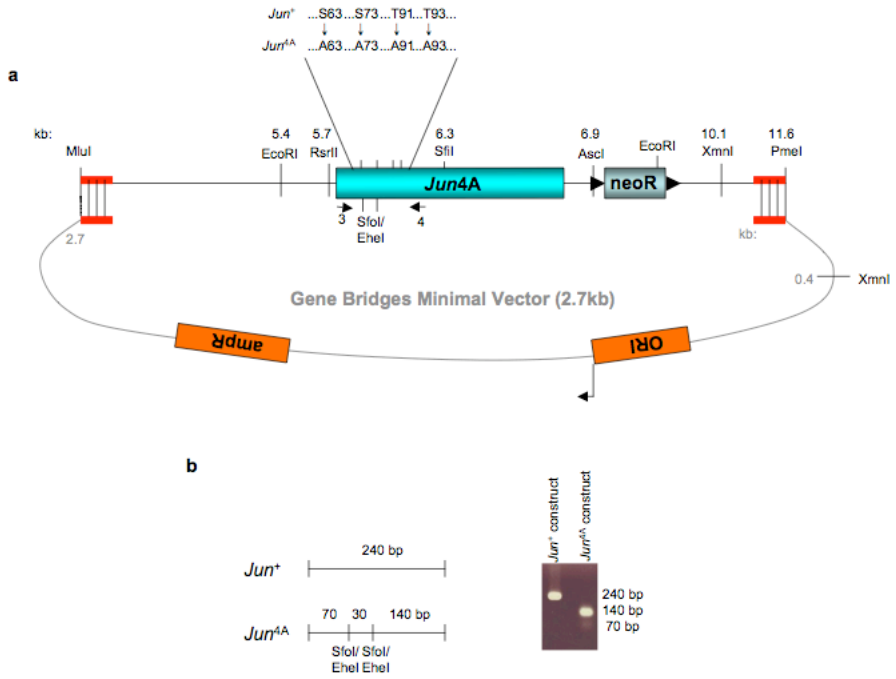

Figure 48 Generation of the *Jun*4A targeting construct
(**a**) Schematic representation of the *Jun*4A targeting construct in a minimal vector (Gene Bridges) carrying an ampicillin-resistance gene (ampR). After cloning of the *Jun* locus from a BAC into the minimal vector via homologous recombination, a RsrII-SfiI fragment carrying the four mutations (Ser63Ala, Ser73Ala, Thr91Ala, Thr93Ala) was inserted into the equivalent region of the *Jun* gene. For the identification of targeted ES cell clones, a neomycin-resistance cassette (neoR) was inserted into an AscI restriction site 0.2 kb 3' of the *Jun* gene. The targeting construct was linearised by XmnI restriction digest. Red lines represent homology regions between the targeting construct and the minimal vector. ORI, origin of replication. Arrowheads indicate loxP-sites. (**b**) Correct insertion of the *Jun*4A RsrII-SfiI fragment leads to the addition of two SfoI/EheI restriction sites created by the mutations at Ser63 and Ser73. SfoI/EheI restriction digest of the *Jun*4A 5'-end amplified by PCR using primers indicated by arrows 3 and 4 in (**a**) results in a 140 bp, 70 bp and 30 bp (30 bp band not visible in the gel picture on the right) DNA band.

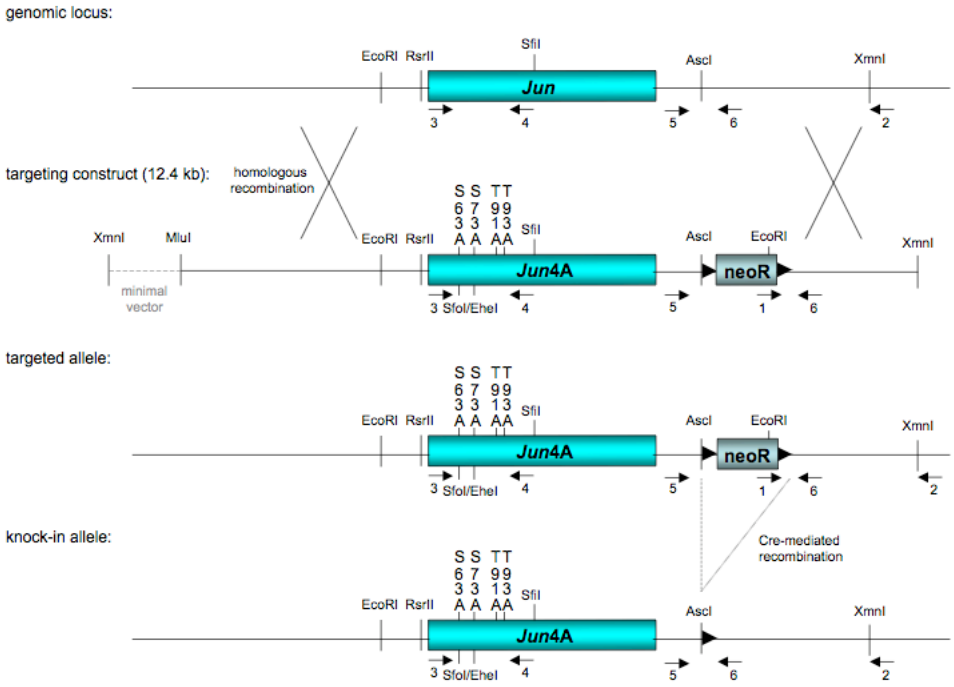

Figure 49 Targeting of the genomic *Jun* locus with the *Jun*4A construct
Schematic representation of the *Jun*4A construct targeting the genomic *Jun* locus in ES cells via homologous recombination mediated by a long homology arm 5' of the *Jun* gene and a short homology arm 3' of the *Jun* gene. Successfully targeted ES cell clones were identified by screening PCR using a forward primer indicated by arrow 1 in the neomycin-resistance cassette (neoR) and a reverse primer indicated by arrow 2 in the genomic *Jun* locus 3' of the targeting construct. To confirm the presence of the four mutations, DNA sequencing was performed using primers indicated by arrows 3 and 4 flanking the *Jun* 5'-end. After Cre-mediated excision of the neoR-cassette, a 50 bp loxP-site remained in the *Jun*4A locus 0.2 kb 3' of the *Jun*4A gene. For genotyping, primers indicated by arrows 5 and 6 flanking this region were used. Arrowheads indicate loxP-sites.

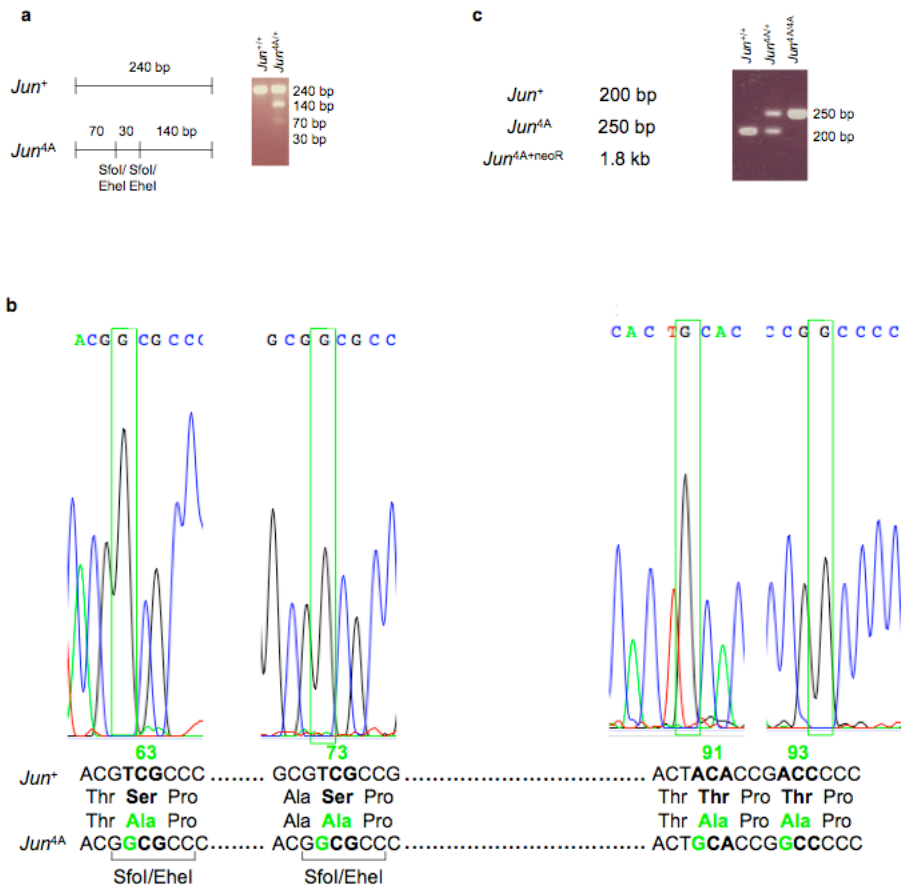

Figure 50 Verification and genotyping of *Jun*4A mice
(**a**) DNA from *Jun*$^{4A/+}$ chimeras showed the characteristic band pattern after PCR-amplification using primers indicated by arrows 3 and 4 in **Figure 48** and restriction digest with SfoI/EheI (240 bp, 140 bp, 70 bp and 30 bp) whereas SfoI/EheI restriction digest of amplified DNA from *Jun*$^{+/+}$ mice only result in a 240 bp DNA fragment. (**b**) The presence of the four mutations Ser63Ala, Ser73Ala, Thr91Ala and Thr93Ala (green rectangles) in *Jun*$^{4A/4A}$ mice was confirmed by DNA sequencing using primers indicated by arrows 3 and 4 in **Figure 48**. (**c**) After excision of the neoR-cassette, genotyping PCR using primers indicated by arrows 5 and 6 in **Figure 49** led to a 200 bp *Jun* wt (*Jun*$^{+}$) band and due to the remaining 50 bp loxP-site a 250 bp *Jun*^{4A} band.

5.1.2 Targeting strategy for the generation of the ROSA26-LSL-JNKK2-JNK1 mouse

As a counterpart of the *Jun*4A mouse, I generated the ROSA26-LSL-JNKK2-JNK1 mouse which expresses constitutively active JNK1. To achieve constitutive activation of JNK/c-Jun signalling, I inserted an HA-tagged human JNKK2-JNK1 fusion construct into the mouse genome. JNKK2 (also known as MKK7) is an upstream kinase of JNK1. Transgenic expression of both proteins should lead to increased levels of active phospho-JNK1 (p-JNK1) which consequently phosphorylates and activates c-Jun.

To guarantee controlled and efficient monosite insertion of the JNKK2-JNK1 construct into the ubiquitously expressed ROSA26 locus, I used the Gateway Entry system (Nyabi et al., 2009). Firstly, I excised the toxin-encoding *ccd*B gene from the pENTR1A vector (Invitrogen) by EcoR1 restriction digest (**Figure 51**). Secondly, a 2.8 kb human cDNA JNKK2-JNK1 fusion construct was excised from a pBabe-JNKK2-JNK1 vector by BamHI restriction digest (one BamHI site located 5' and one BamHI site located 3' of the construct) and inserted into the BamHI site of the pENTR1A-vector. Correct orientation of the inserted construct was confirmed by NotI restriction digest. Apart from the NotI restriction site in the pENTR1A multiple cloning site 3' of the BamHI site, there is a NotI site at 0.8 kb in the human JNKK2 cDNA. Consequently, correct orientation of the JNKK2-JNK1 construct resulted in a 1.9 kb DNA fragment by NotI restriction digest. Furthermore, correct insertion was confirmed by DNA sequencing.

In collaboration with Lieven Haenebalcke and Dr Jody Haigh at Ghent University, Belgium, the JNKK2-JNK1 construct was inserted into a targeting vector via *in vitro* recombination. Since the JNKK2-JNK1 construct in the pENTR1A vector is flanked by

specific lambda phage integrase recognition sites (*att*L), the JNKK2-JNK1 construct can be efficiently transferred to a targeting vector carrying the corresponding heterotypic sites (*att*R) (**Figure 52a**). The targeting vector contains a 5' homology region to the mouse ROSA26 genomic locus, a splice acceptor (SA) site, a PGK-neo-3 x pA stop cassette flanked by loxP-sites (LSL), the JNKK2-JNK1 construct, an IRES-eGFP reporter gene, a 3' homology region to the mouse ROSA26 genomic sequence and a Diphteria Toxin A (DTA) selection cassette. It was electroporated into G4 F1 hybrid ES cells and screening for positive clones with correct insertion was performed by PCR using a forward primer in the genomic ROSA26 locus 5' of the targeting vector and a reverse primer in the 5' region of the targeting vector (**Figure 52**). Correctly targeted clones showed a 1.3 kb band as a result of the screening PCR. Out of 96 tested ES cell clones, 5 were identified as carrying the correct insertion. This was confirmed by Southern Blot analysis, in which BamHI digest resulted in a 5.8 kb wt band and a 3 kb mutant band (5'-probe), whereas KpnI digest showed a 37 kb wt band and a 8.8 kb mutant band (3'-probe) (**Figure 52**). One of the positive ES cell clones was injected into blastocysts from C57BL/6 mice performed by the LRI Transgenic Service. Genotyping of the chimeras was performed using primers to detect the eGFP reporter gene.

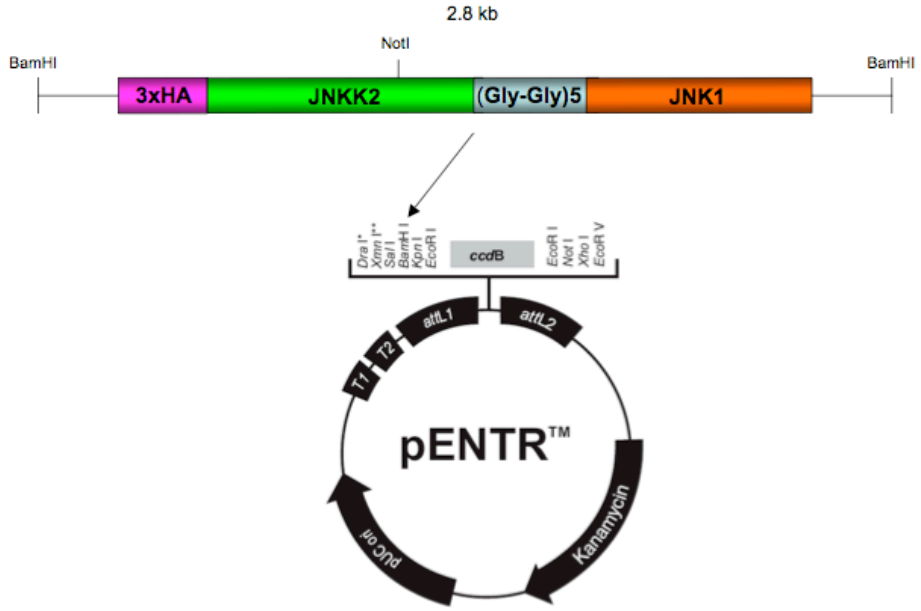

Figure 51 Insertion of the JNKK2-JNK1 fusion construct into the pENTR-vector
The JNKK2-JNK1 fusion construct consisting of a 3xHA tag, the human JNKK2 cDNA, (Gly-Gly)5 repeats and the human JNK1 cDNA was excised from a pBabe-JNKK2-JNK1 vector by BamHI restriction digest. After removal of the *ccd*B toxin gene from the pENTR1A-vector by EcoRI digest, the JNKK2-JNK1 fusion construct was inserted into the BamHI-site located in the multiple cloning site of the pENTR1A-vector.

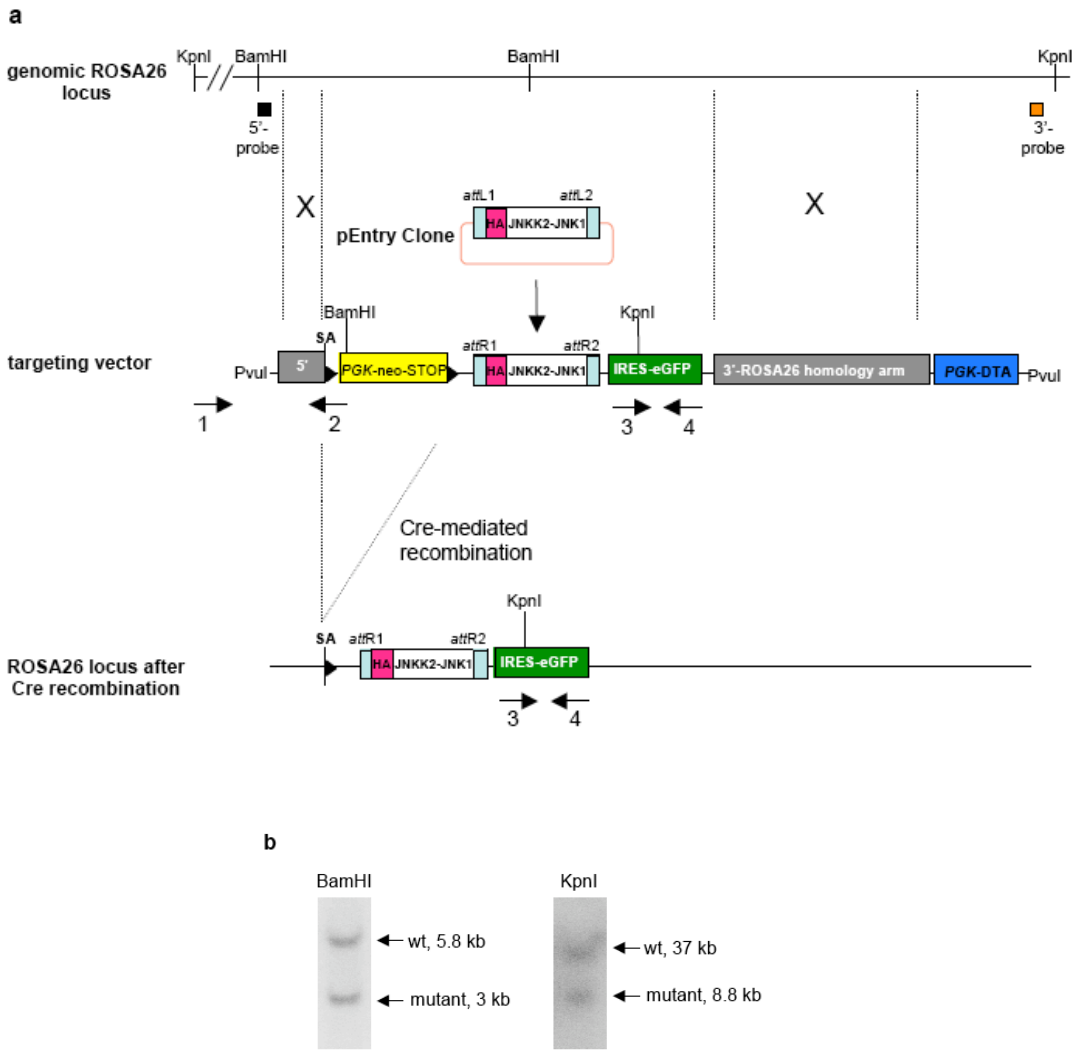

Figure 52 Targeting of the genomic ROSA26 locus with the JNKK2-JNK1 vector
(**a**) In the pEntry clone, the JNKK2-JNK1 construct is flanked by lambda phage integrase recognition sites (*att*L) and thus can be efficiently inserted into the targeting vector carrying the corresponding heterotypic sites (*att*R). The targeting construct consists of a 5'-ROSA26 homology arm, a splice acceptor (SA) site, a PGK-neo-STOP cassette flanked by loxP-sites (LSL), the JNKK2-JNK1 fusion construct, an IRES-eGFP reporter gene, a 3'-ROSA26 homology arm and a PGK-DTA selection cassette. Screening PCR was performed using a forward primer indicated by arrow 1 5' of the targeting construct and a reverse primer indicated by arrow 2 in the 5' region of the targeting construct. After Cre-mediated recombination, the LSL-cassette is excised and the JNKK2-JNK1 fusion construct is expressed in the genomic ROSA26 locus. For genotyping PCR, primers indicated by arrows 3 and 4 located in the eGFP reporter gene were used. Arrowheads indicate loxP-sites. (**b**) Southern Blot analysis performed by Lieven Haenebalcke resulted in a 5.8 kb wt band and a 3.0 kb mutant band after BamHI restriction digest [5'-probe indicated by black square in (**a**)] and a 37 kb wt band and a

8.8 kb mutant band after KpnI restriction digest [3'-probe indicated by orange square in (**a**)].

5.1.3 JNK signalling via c-Jun is dispensable for mouse development and gut regeneration

Crossing two heterozygous *Jun*$^{4A/+}$ mice revealed that *Jun*$^{4A/4A}$ mice are viable and are generated at normal Mendelian ratio. *Jun*$^{4A/4A}$ mice are fertile and they are indistinguishable from their wt littermates. Histological analysis of various tissues taken from *Jun*$^{4A/4A}$ mice such as the brain, liver, spleen, pancreas and lung showed no obvious structural differences (**Figure 53**). However, the villi in the small bowel seemed to be slightly smaller in length in the *Jun*$^{4A/4A}$ gut in comparison to the *Jun*$^{+/+}$ gut (**Figure 54a**,**b**). Although this decrease did not reach statistical significance, this observation is consistent with previous data showing that activation of JNK/c-Jun signalling results in increased villi length due to increased proliferation in the gut (Sancho et al., 2009). Immunohistochemistry for p-c-Jun confirmed the absence of N-terminally phosphorylated c-Jun in the *Jun*$^{4A/4A}$ gut whereas in the *Jun*$^{+/+}$ gut, p-c-Jun is expressed in immature cells in the crypt and in some enterocytes at the top of the villus (**Figure 54c**). I analysed numbers of proliferating cells in the gut of BrdU injected *Jun*$^{+/+}$ and *Jun*$^{4A/4A}$ mice. Although not significantly, numbers of BrdU-positive proliferative cells were slightly decreased in the *Jun*$^{4A/4A}$ gut in comparison to the *Jun*$^{+/+}$ gut (**Figure 54d**,**e**). The number of TUNEL-positive cells was similar in the *Jun*$^{+/+}$ and the *Jun*$^{4A/4A}$ gut suggesting that JNK/c-Jun signalling is not involved in apoptosis in the gut (**Figure 54f**,**g**). Moreover, differentiation of intestinal cells was not affected by loss of N-terminally phosphorylated c-Jun since the percentage of Alcian-Blue (AB)/Periodic Acid-Schiff (PAS)-positive goblet cells, Chromogranin-positive

enteroendocrine cells and Lysozyme-positive paneth cells was not significantly different in the *Jun*$^{4A/4A}$ gut when compared to the *Jun*$^{+/+}$ gut (**Figure 55a-f**). Also staining for alkaline phosphatase-positive enterocytes was similar in the *Jun*$^{+/+}$ and *Jun*$^{4A/4A}$ gut (**Figure 55g**).

Considering that p-c-Jun has been reported to positively regulate proliferation of intestinal cells but the number of proliferative cells in the *Jun*$^{4A/4A}$ gut was not significantly altered during physiological gut development, I investigated whether the JNK/c-Jun stress signalling pathway is necessary for gut regeneration. Therefore, *Jun*$^{4A/4A}$ mice and control mice were given drinking water containing dextran sodium sulfate (DSS) for one week to induce colitis in the large bowel. Next, mice were put back on normal drinking water to recover for three days and after that, the mice were sacrificed and analysed. Histologically, I could not detect an obvious difference in the regenerated guts from *Jun*$^{+/+}$ and *Jun*$^{4A/4A}$ mice (**Figure 56a**). Furthermore, the percentage of BrdU-positive proliferative cells and the percentage of TUNEL-positive apoptotic cells was not significantly altered in the *Jun*$^{+/+}$ and *Jun*$^{4A/4A}$ guts taken from DSS treated mice (**Figure 56b-e**).

Taken together, these data suggest that c-Jun N-terminal phosphorylation is not necessary for physiological mouse development since *Jun*$^{4A/4A}$ mice show no significant phenotypes and are indistinguishable from *Jun*$^{+/+}$ littermates. Furthermore, gut regeneration after induced colitis is not impaired in *Jun*$^{4A/4A}$ mice indicating that c-Jun N-terminal phosphorylation is not needed for recovery from this pathological condition.

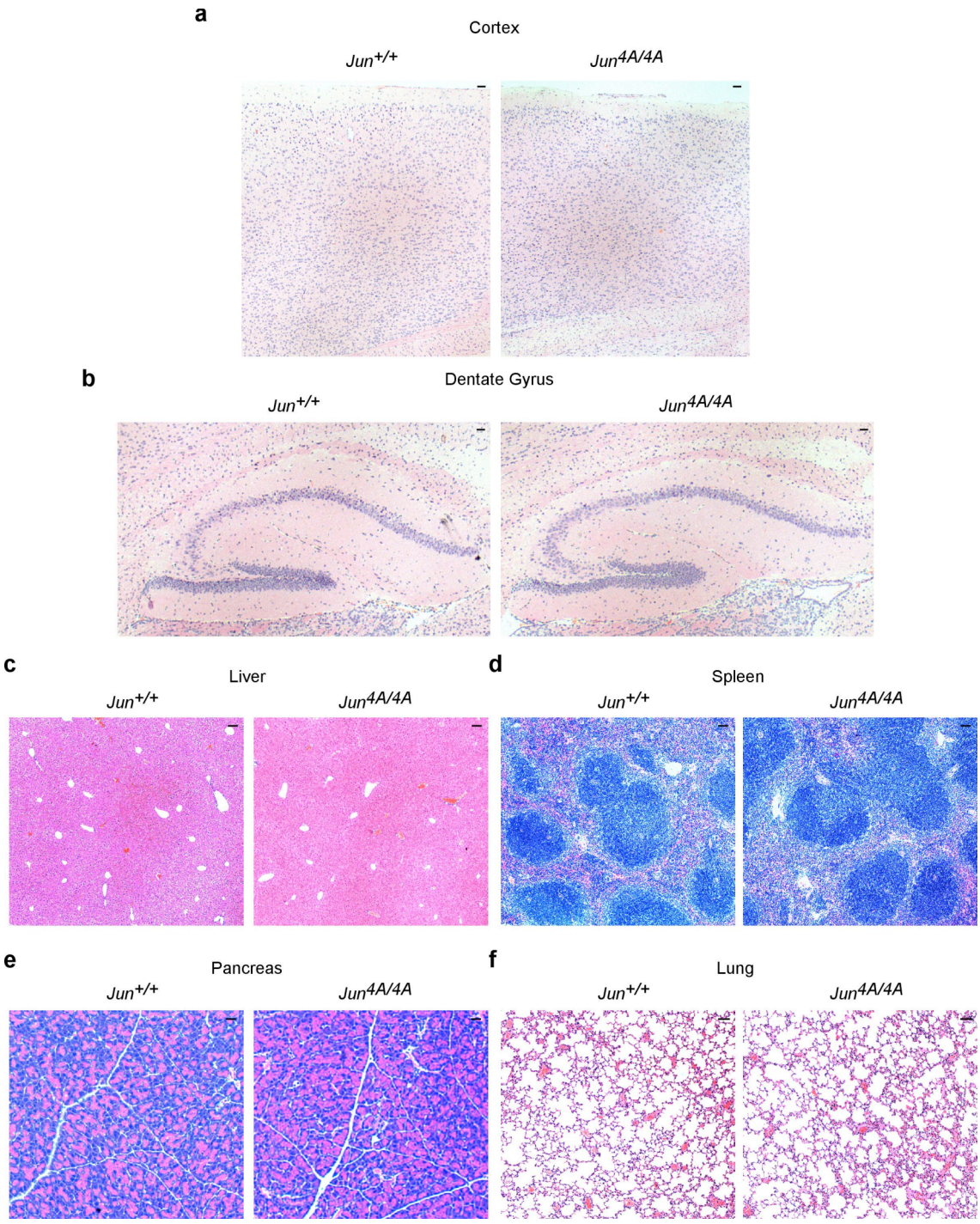

Figure 53 Inhibition of JNK/c-Jun signalling does not affect physiological development

(**a-f**) H&E staining on representative sections of the *Jun*$^{+/+}$ and *Jun*$^{4A/4A}$ (**a**) cortex, (**b**) dentate gyrus, (**c**) liver, (**d**) spleen, (**e**) pancreas and (**f**) lung. Scale bars, in (**a**,**b**,**e**) 50 μm, in (**c**,**d**,**f**) 100 μm.

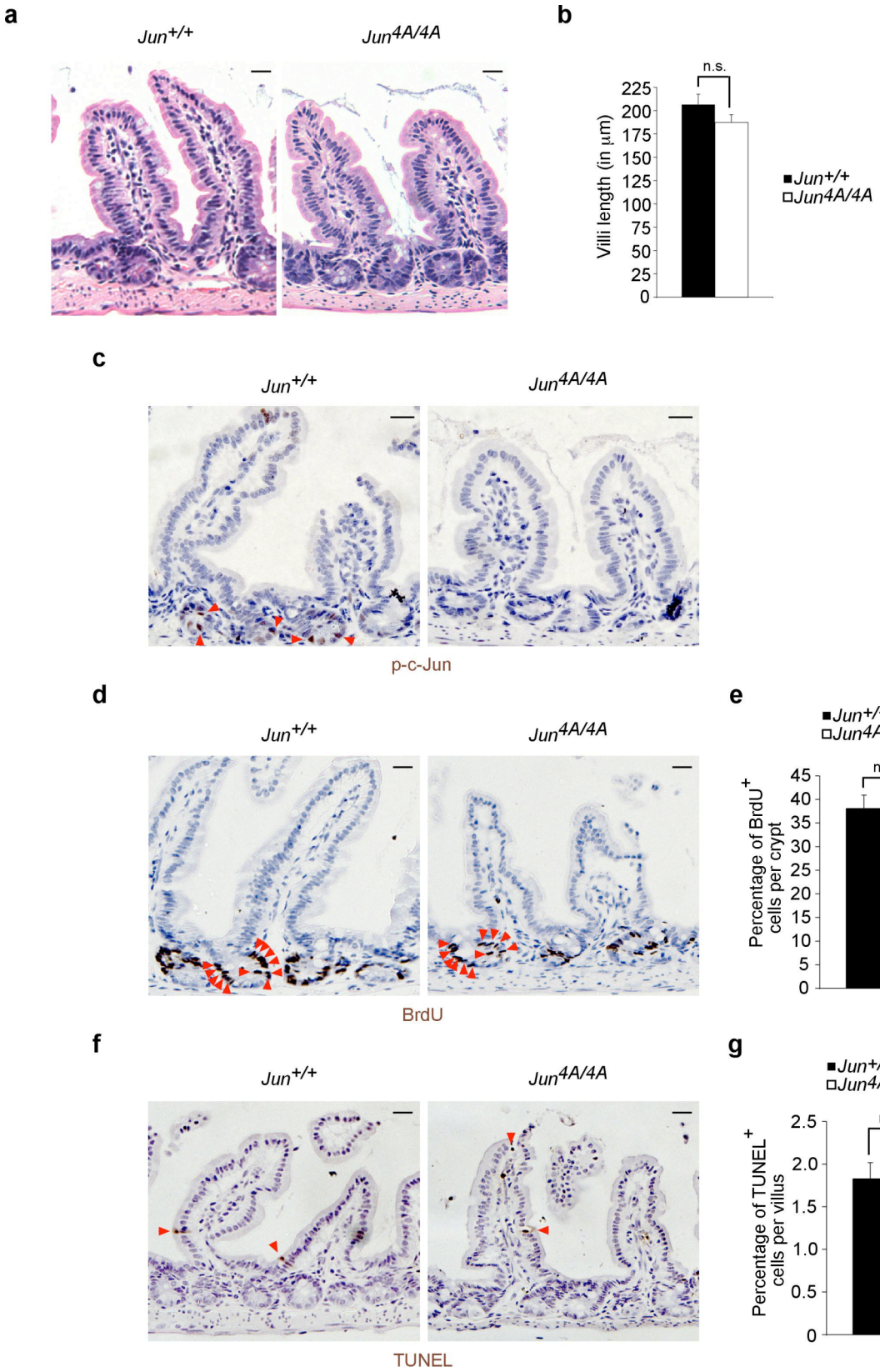
a
Jun+/+
Jun4A/4A
b
n.s.
Villi length (in µm)
225
200
175
150
125
100
75
50
25
0
Jun+/+
Jun4A/4A
c
Jun+/+
Jun4A/4A
p-c-Jun
d
Jun+/+
Jun4A/4A
BrdU
e
Jun+/+
Jun4A/4A
n.s.
Percentage of BrdU+ cells per crypt
45
40
35
30
25
20
15
10
5
0
f
Jun+/+
Jun4A/4A
TUNEL
g
Jun+/+
Jun4A/4A
n.s.
Percentage of TUNEL+ cells per villus
2.5
2.0
1.5
1.0
0.5
0

Figure 54 Absence of N-terminally phosphorylated c-Jun does not significantly alter gut development

(**a**) H&E staining on representative sections of the $Jun^{+/+}$ and $Jun^{4A/4A}$ small bowel. (**b**) Histogram showing the villi length in μm in the ileum of the small bowel of the $Jun^{+/+}$ and $Jun^{4A/4A}$ gut. The length of at least 50 villi was measured per mouse. $n = 3$. (**c**,**d**,**f**) DAB-staining for (**c**) serine 63 phosphorylated c-Jun-, (**d**) BrdU- and (**f**) TUNEL-positive cells in the $Jun^{+/+}$ and $Jun^{4A/4A}$ small bowel. Cells are counterstained with haematoxylin. Red arrowheads denote positive cells. (**e**,**g**) Quantification of (**e**) BrdU-positive cells per crypt and (**g**) TUNEL-positive cells per villus of the $Jun^{+/+}$ and $Jun^{4A/4A}$ small bowel. Positive cells in 10 crypts or villi were counted per mouse. $n = 3$.

Scale bars, 50 μm. Error bars, s.e.m.; n.s., not significant (unpaired *t* test).

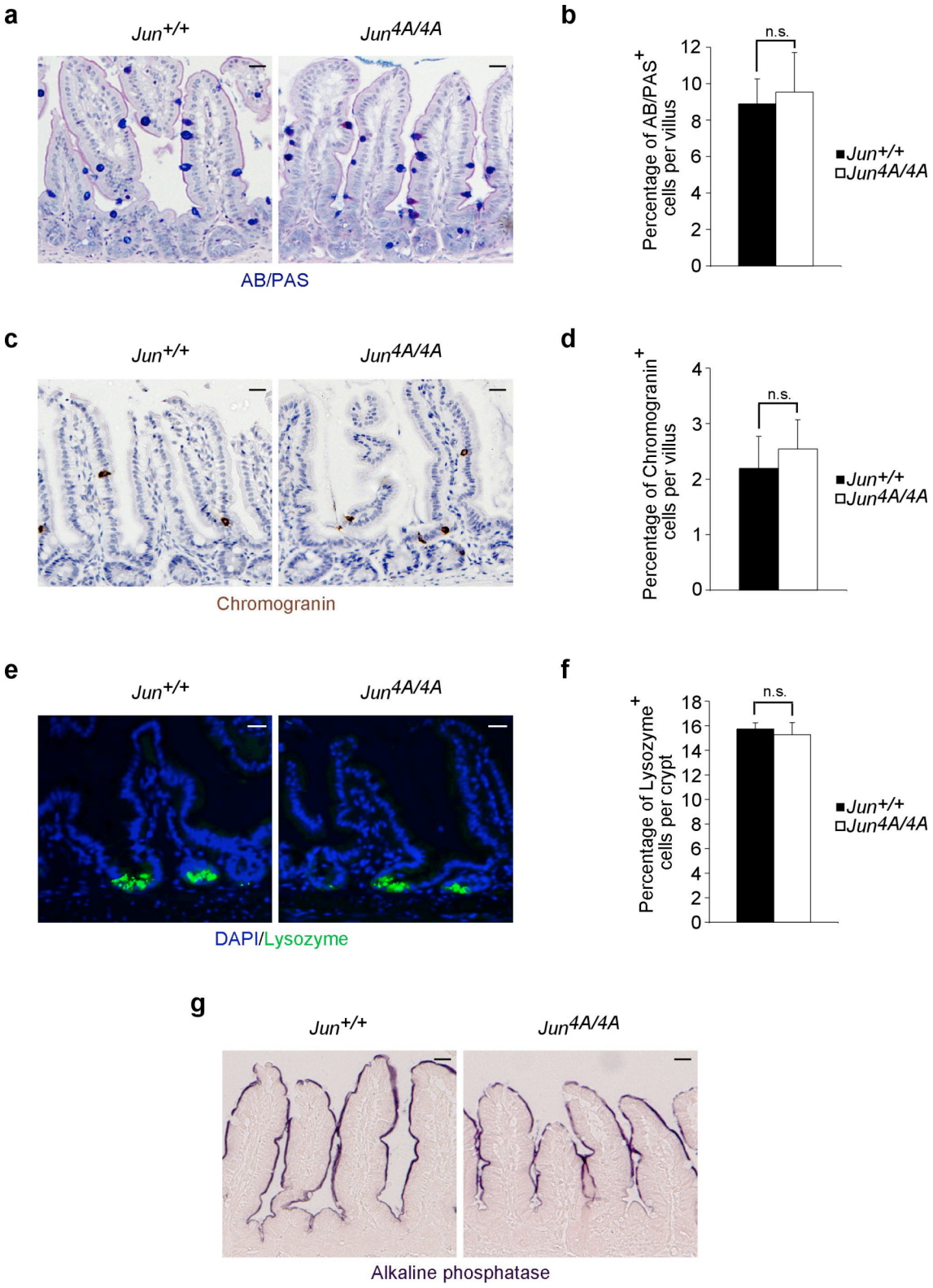
a
Jun+/+
Jun4A/4A
AB/PAS
b
n.s.
Percentage of AB/PAS+ cells per villus
12
10
8
6
4
2
0
Jun+/+
Jun4A/4A
c
Jun+/+
Jun4A/4A
Chromogranin
d
n.s.
Percentage of Chromogranin+ cells per villus
4
3
2
1
0
Jun+/+
Jun4A/4A
e
Jun+/+
Jun4A/4A
DAPI/Lysozyme
f
n.s.
Percentage of Lysozyme+ cells per crypt
18
16
14
12
10
8
6
4
2
0
Jun+/+
Jun4A/4A
g
Jun+/+
Jun4A/4A
Alkaline phosphatase

Figure 55 Inhibition of JNK/c-Jun signalling does not change differentiation in the gut

(**a**,**c**,**e**,**g**) Immunohistochemistry for (**a**) AB/PAS-positive goblet cells, (**c**) Chromogranin-positive enteroendocrine cells, (**e**) Lysozyme-positive paneth cells and (**g**) Alkaline phosphatase-positive enterocytes in the small bowel of the $Jun^{+/+}$ and $Jun^{4A/4A}$ gut. Cells are counterstained with (**a**,**c**) haematoxylin, (**e**) DAPI and (**g**) nuclear fast red. (**b**,**d**,**f**) Quantification of (**b**) AB/PAS-positive, (**d**) Chromogranin-positive and (**f**) Lysozyme-positive cells (**b**,**d**) per villi and (**e**) per crypt. Positive cells in 10 villi or crypts were counted per mouse. $n = 3$.

Scale bars, 50 μm. Error bars, s.e.m.; n.s., not significant (unpaired *t* test).

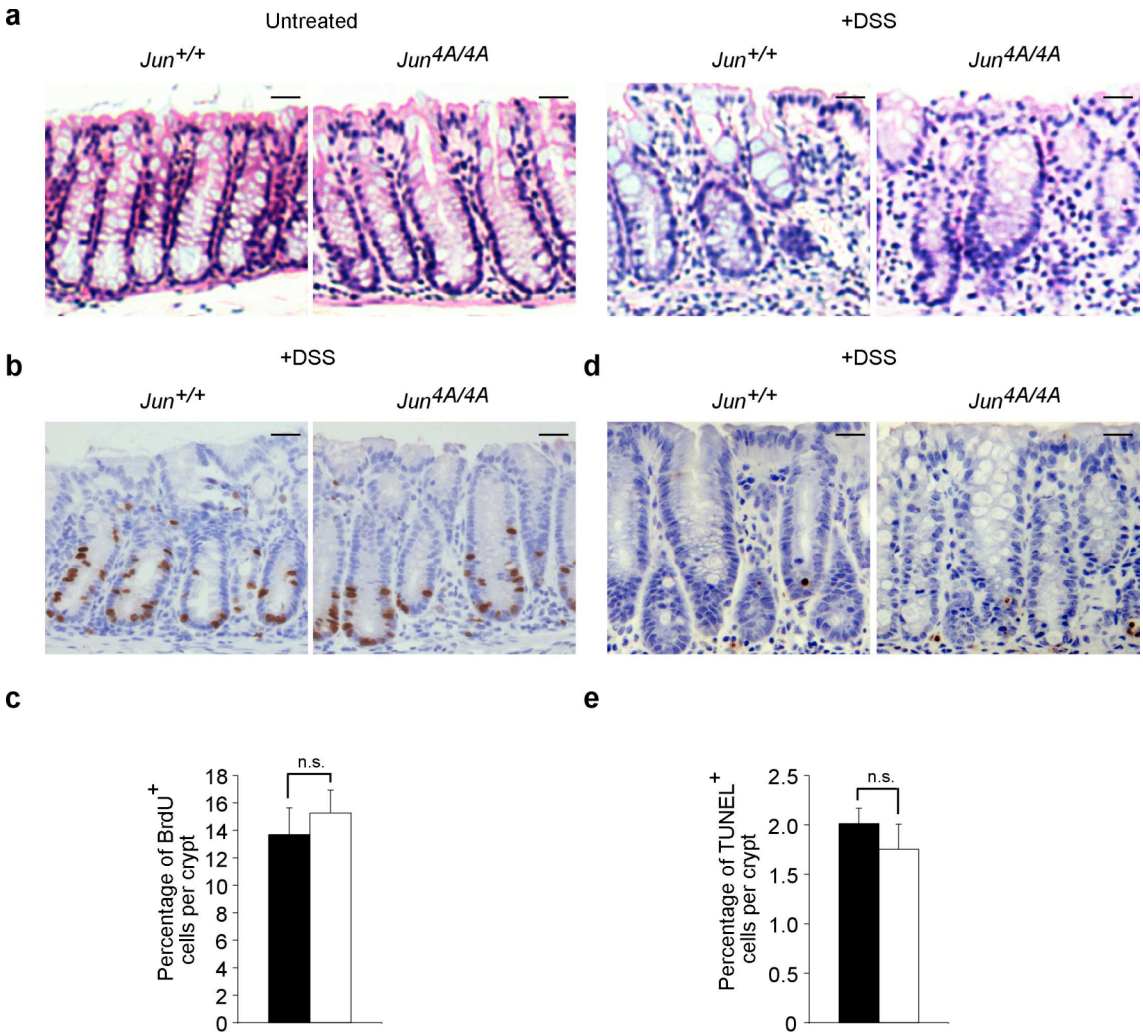

Figure 56 Absence of N-terminally phosphorylated c-Jun does not affect gut regeneration

(**a**) H&E staining on representative sections of the untreated or DSS-treated $Jun^{+/+}$ and $Jun^{4A/4A}$ large bowel. DSS-treated colons exhibited disorganisation of crypts and cell infiltration indicative of colitis. (**b**,**d**) DAB-staining for (**b**) BrdU-positive and (**d**) TUNEL positive cells in the crypts of the large bowel of DSS-treated $Jun^{+/+}$ and $Jun^{4A/4A}$ mice. Cells are counterstained with haematoxylin. (**c**,**e**) Quantification of (**c**) BrdU- and (**e**) TUNEL-positive cells in the crypts of the large bowel of DSS-treated $Jun^{+/+}$ ($n = 4$) and $Jun^{4A/4A}$ ($n = 5$) mice.

Scale bars, 50 μm. Error bars, s.e.m.; n.s., not significant (unpaired *t*-test).

5.1.4 Increased JNK/c-Jun signalling does not significantly alter brain development but slightly improves nerve regeneration

Having observed that inhibition of JNK/c-Jun signalling does not significantly impair mouse development, I went on to investigate whether enhanced JNK/c-Jun signalling affects development. Since my work as well as previous publications showed that p-c-Jun is involved in the apoptosis of neural cells (**Chapter 3 and 4**; Raivich and Behrens, 2006), I crossed the ROSA26-LSL-JNKK2-JNK1$^{LSL/+}$ mice to Nestin-Cre transgenic mice providing tissue-specific expression of the JNKK2-JNK1 fusion protein in the nervous system. ROSA26-LSL-JNKK2-JNK1$^{LSL/+}$; Nestin-Cre (LSL-JNKK2-JNK1$^{\Delta N/+}$) mice are viable and fertile and were generated at normal Mendelian ratio. Furthermore, LSL-JNKK2-JNK1$^{\Delta N/+}$ mice showed no obvious phenotypes and were indistinguishable from wt (LSL-JNKK2-JNK1$^{LSL/+}$) littermates. Histological analysis of the LSL-JNKK2-JNK1$^{LSL/+}$ and LSL-JNKK2-JNK1$^{\Delta N/+}$ brain showed no overall structural differences (**Figure 57a**). Immunohistochemistry for GFP confirmed the deletion of the Lox-STOP-Lox (LSL) cassette and reporter gene expression in the LSL-JNKK2-JNK1$^{\Delta N/+}$ brain (**Figure 57b**). Western Blot analysis exhibited expression of the HA-tagged JNKK2-JNK1 fusion protein at the expected molecular weight (~97 kDa) and a mild upregulation of p-c-Jun levels in the LSL-JNKK2-JNK1$^{\Delta N/+}$ brain (**Figure 57c**,**d**). Since I was able to show that highly elevated p-c-Jun levels in the Fbw7-knockout background lead to increased neural progenitor apoptosis during brain development (**Chapter 3 and 4**), I examined the effects of p-c-Jun upregulation in the LSL-JNKK2-JNK1$^{\Delta N/+}$ adult brain in areas of progenitors, i.e. the rostral migratory stream (RMS). Immunostaining for progenitor markers GFAP and Nestin in the adult brain revealed that although not significantly, the number of GFAP/Nestin-positive cells was slightly reduced in the LSL-JNKK2-JNK1$^{\Delta N/+}$ RMS (**Figure 58a**,**b**). When

examining the number of active Caspase-3-positive apoptotic cells, I could hardly detect any active Caspase-3-positive cells in the LSL-JNKK2-JNK1$^{LSL/+}$ as well as the LSL-JNKK2-JNK1$^{\Delta N/+}$ adult brain (**Figure 58c**). Also the number of BrdU-positive proliferative cells was similar in the LSL-JNKK2-JNK1$^{\Delta N/+}$ adult brain in comparison to the LSL-JNKK2-JNK1$^{LSL/+}$ brain (**Figure 58d**,**e**). Furthermore, the percentage of progenitors committed to the neuronal lineage (Doublecortin-positive) was not affected by the activation of JNK/c-Jun signalling whereas the percentage of astroglia progenitors (S100-positive) was slightly but not significantly decreased in the LSL-JNKK2-JNK1$^{\Delta N/+}$ adult brain (**Figure 58f-i**).

Since the mild activation of JNK/c-Jun signalling in the LSL-JNKK2-JNK1$^{\Delta N/+}$ brain did not significantly affect brain development, I investigated whether stress stimuli could lead to distinct JNK-dependent biological effects in the nervous system of mice with altered JNK/c-Jun signalling. c-Jun has previously been shown to be essential for nerve regeneration (Raivich et al., 2004). Thus, facial axotomy was performed on *Jun*$^{+/+}$, *Jun*$^{4A/4A}$, LSL-JNKK2-JNK1$^{LSL/+}$ and LSL-JNKK2-JNK1$^{\Delta N/+}$ mice. During this procedure, the facial nerve of the mouse is crushed unilaterally so that whisker movement is paralysed on one side. Wt mice re-innervate their whiskers within one month and thus regain whisker movement. The improvement in whisker mobility over time can be used as a measure for nerve regeneration. Indeed, although not significantly, nerve regeneration assessed by whisker movement test was slightly improved in LSL-JNKK2-JNK1$^{\Delta N/+}$ mice whereas *Jun*$^{4A/4A}$ mice showed slightly impaired nerve regeneration 26 days after facial axotomy (**Figure 59a**,**b**).

Taken together, these data suggest that a mild activation of JNK/c-Jun signalling in the nervous system does not significantly alter brain development, but it might have the potential to improve nerve regeneration.

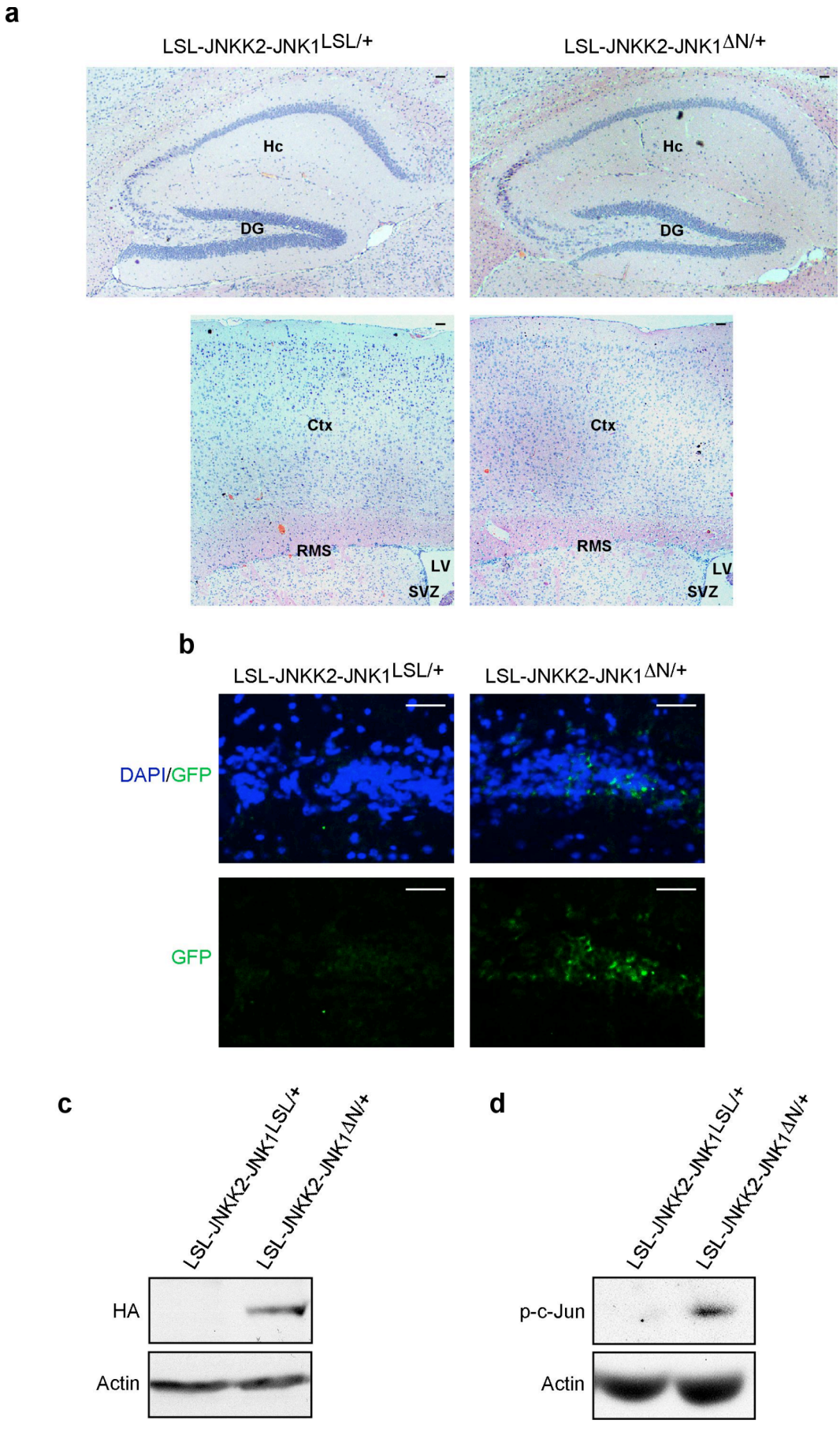
a
LSL-JNKK2-JNK1LSL/+
LSL-JNKK2-JNK1ΔN/+
Hc
DG
Ctx
RMS
LV
SVZ
b
LSL-JNKK2-JNK1LSL/+
LSL-JNKK2-JNK1ΔN/+
DAPI/GFP
GFP
c
LSL-JNKK2-JNK1LSL/+
LSL-JNKK2-JNK1ΔN/+
HA
Actin
d
LSL-JNKK2-JNK1LSL/+
LSL-JNKK2-JNK1ΔN/+
p-c-Jun
Actin

Figure 57 Expression of the JNKK2-JNK1 fusion protein in the brain leads to a mild increase in p-c-Jun levels

(**a**) H&E staining on representative sections of the LSL-JNKK2-JNK1$^{LSL/+}$ and LSL-JNKK2-JNK1$^{\Delta N/+}$ brain showing the hippocampus (Hc) and the dentate gyrus (DG) in panels at the top, cortex (Ctx), rostral migratory stream (RMS), subventricular zone (SVZ) and lateral ventricle (LV) in panels at the bottom. Scale bars, 50 μm. (**b**) Immunohistochemistry for GFP (green) on the LSL-JNKK2-JNK1$^{LSL/+}$ and LSL-JNKK2-JNK1$^{\Delta N/+}$ RMS. DNA (blue) is counterstained with DAPI. Scale bars, 50 μm. (**c**,**d**) Western Blot analysis for (**c**) the HA-tagged JNKK2-JNK1 fusion protein (97 kDa) and β-Actin (42 kDa), (**d**) for serine 73 phosphorylated c-Jun (42 kDa) and β-Actin (42 kDa) on protein extracts from the LSL-JNKK2-JNK1$^{LSL/+}$ and LSL-JNKK2-JNK1$^{\Delta N/+}$ brain.

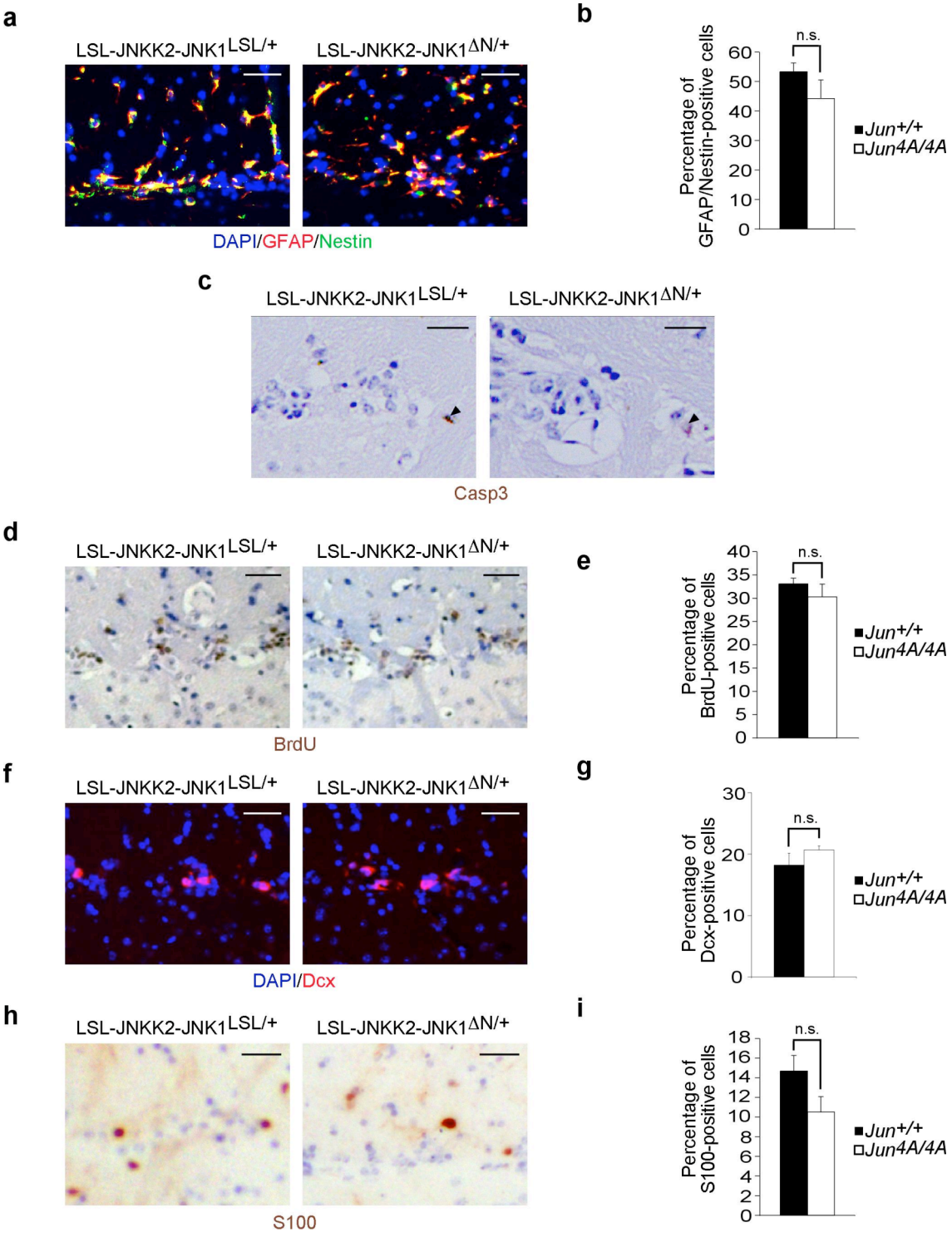

Figure 58 Increased JNK/c-Jun signalling does not significantly alter brain development

(**a**,**c**,**d**,**f**,**h**) Immunohistochemistry for (**a**) GFAP (red)/Nestin (green), (**c**) active Caspase 3 (Casp3; arrowheads denote Casp3-positive cells), (**d**) BrdU, (**f**) Doublecortin (Dcx; red) and (**h**) S100 in the LSL-JNKK2-JNK1$^{LSL/+}$ and LSL-JNKK2-JNK1$^{\Delta N/+}$ RMS. Cells are counterstained with (**a**,**f**) DAPI and (**c**,**d**,**h**) haematoxylin.

(**b**,**e**,**g**,**i**) Quantification of (**b**) GFAP/Nestin-, (**e**) BrdU-, (**g**) Dcx- and (**i**) S100-positive cells in the LSL-JNKK2-JNK1$^{LSL/+}$ and LSL-JNKK2-JNK1$^{\Delta N/+}$ RMS. In (**b**) LSL-JNKK2-JNK1$^{LSL/+}$ $n = 4$ and LSL-JNKK2-JNK1$^{\Delta N/+}$ $n = 5$, in (**e**,**g**,**i**) $n = 3$ per genotype. Scale bars, 50 μm. Error bars, s.e.m.; n.s., not significant (unpaired *t* test).

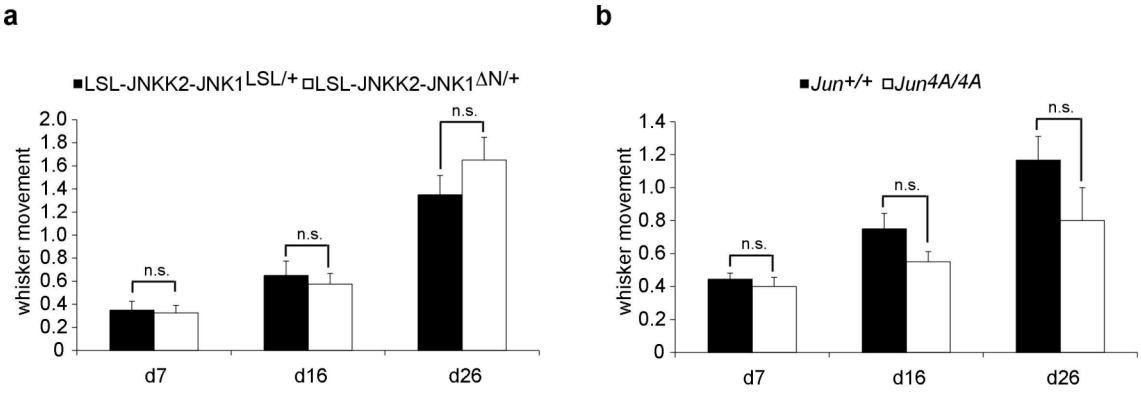

Figure 59 Alterations in JNK/c-Jun signalling activity slightly affect nerve regeneration

(**a**,**b**) Whisker movement was assessed in a double blind experiment independently by two researchers 7, 16 and 26 days after facial axotomy of (**a**) LSL-JNKK2-JNK1$^{LSL/+}$ (n = 10) and LSL-JNKK2-JNK1$^{\Delta N/+}$ (n = 10) mice and (**b**) *Jun*$^{+/+}$ (n = 9) and *Jun*$^{4A/4A}$ (n = 10) mice. Whisker movement was classified in 0.5 point steps from "0 = no movement" to "3.0 = normal movement" in comparison to the uninjured side.
Error bars, s.e.m.; n.s., not significant (unpaired t test).

5.1.5 Inhibition of JNK/c-Jun signalling induces premature senescence in mouse embryonic fibroblasts

Another cellular context in which JNK/c-Jun signalling has been described to play a major role is in fibroblasts. c-Jun-deficient mouse embryonic fibroblasts (MEFs) exhibit a severe proliferation defect and undergo premature senescence (Johnson et al., 1993). To investigate whether c-Jun function in MEF proliferation and senescence is JNK-dependent, I isolated MEFs from *Jun*$^{4A/4A}$ mice. Immunostaining and immunoblotting for p-c-Jun revealed that no N-terminally phosphorylated c-Jun was detectable in untreated and anisomycin (JNK signalling activating agent) treated *Jun*$^{4A/4A}$ MEFs (**Figure 60a**,**b**). By light microscopy, I observed that at late passage (>p5), cell numbers were highly reduced in *Jun*$^{4A/+}$ and *Jun*$^{4A/4A}$ MEF cultures in comparison to wt cultures. Furthermore, cells in *Jun*$^{4A/+}$ and *Jun*$^{4A/4A}$ MEF cultures exhibited a flatter morphology similar to senescent fibroblasts (**Figure 60c**). Interestingly, this phenotype was not due to increased oxidative stress in cultures at atmospheric O_2 because it also occurred when culturing *Jun*$^{4A/4A}$ MEFs at physiological oxygen levels (3% O_2).

To examine proliferation in the absence of N-terminally phosphorylated c-Jun, I performed growth curve analyses at early passage (p3) which revealed a mild reduction in proliferation in *Jun*$^{4A/+}$ and *Jun*$^{4A/4A}$ cultures in comparison to wt cultures (**Figure 61a**). Furthermore, cell cycle analysis showed a slightly decreased number of cells progressing through the cell cycle in *Jun*$^{4A/+}$ and *Jun*$^{4A/4A}$ MEF cultures in comparison to wt MEFs (**Figure 61b**,**c**). These data are consistent with previous data for c-Jun$^{AA/AA}$ MEFs which have two (Ser63, Ser73) of the four main JNK-phosphorylation sites mutated to alanine (Behrens et al., 1999). It has been described that c-Jun$^{AA/AA}$ MEFs only exhibit a mild proliferation defect, much less severe than

c-Jun-deficient MEFs. The data from *Jun*$^{4A/4A}$ MEFs confirmed that c-Jun function in fibroblast proliferation is only partially JNK-dependent.

To examine the decreased numbers of cells at later passages, I did growth curve analyses also at p7 (**Figure 62a**). At this stage, *Jun*$^{4A/+}$ and *Jun*$^{4A/4A}$ MEFs cannot efficiently repopulate their cultures any longer in contrast to *Jun*$^{+/+}$ MEFs. Furthermore, cell cycle analysis revealed that the vast majority of *Jun*$^{4A/4A}$ MEFs were stuck in G1 phase at this stage and do no longer enter the cell cycle (**Figure 62b**,**c**). This indicated that they might have undergone premature senescence. Indeed, when I performed a β-galactosidase (β-gal) senescence assay on *Jun*$^{4A/4A}$ MEF cultures at late passage, the number of senescent cells was highly increased in the absence of N-terminally phosphorylated c-Jun, both at atmospheric O_2 or physiological O_2 (**Figure 63a-d**). Interestingly, heterozygous *Jun*$^{4A/+}$ MEFs showed the same increase in premature senescence than homozygous *Jun*$^{4A/4A}$ MEFs at atmospheric O_2 whereas at physiological O_2, the increase in the number of senescent cells seemed to be inversely dosage-dependent on p-c-Jun levels (**Figure 63a-d**). The data from *Jun*$^{4A/4A}$ MEF cultures suggest that in contrast to its function in proliferation, c-Jun function in senescence is highly JNK-dependent. Since premature senescence was not observed in a previous study using c-Jun$^{AA/AA}$ MEFs (Behrens et al., 1999), it might be that the two additionally mutated JNK-phosphorylation sites in *Jun*$^{4A/4A}$ MEFs play an important role in c-Jun function in senescence.

Induction of p53 is the main event responsible for fibroblasts undergoing senescence (Atadja et al., 1995, Bond et al., 1996, Kulju and Lehman, 1995) and c-Jun has been implicated in the transcriptional repression of p53 (Schreiber et al., 1999). To

investigate how lack of N-terminally phosphorylated c-Jun triggers premature senescence molecularly, I did Western Blot analysis for p53. Surprisingly, p53 was downregulated in $Jun^{4A/4A}$ MEFs indicating that senescence in $Jun^{4A/4A}$ MEF cultures is p53-independent (**Figure 64**).

Taken together, these data suggest that whereas c-Jun function in fibroblast proliferation is only partially JNK-dependent, c-Jun function in senescence is highly JNK-dependent. Interestingly, oxidative stress is seemingly not the main stimulus for the observed premature senescence in $Jun^{4A/4A}$ MEFs suggesting that an intrinsic mechanism triggered by lack of N-terminally phosphorylated c-Jun induces senescence. Strikingly, the observed senescence appears to be p53-independent.

Oncogenic stress can induce senescence in tumour cells and thus limit tumour growth. The apparent absence of detrimental effects of lacking N-terminally phosphorylated c-Jun in development and regeneration in combination with its role in triggering p53-independent senescence in fibroblasts makes the JNK/c-Jun signalling pathway an interesting target for cancer therapy.

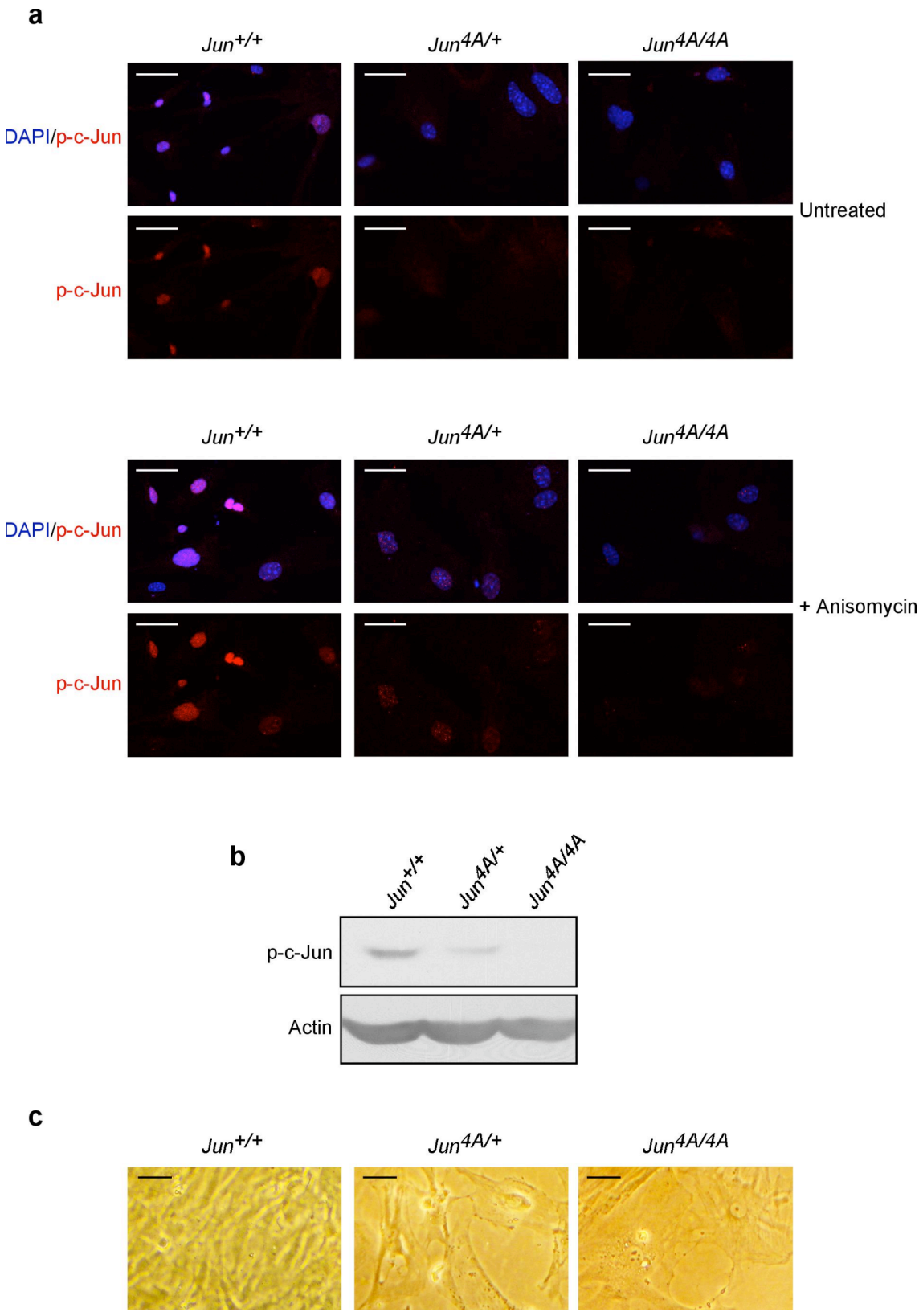
a
Jun+/+
Jun4A/+
Jun4A/4A
DAPI/p-c-Jun
p-c-Jun
Untreated
+ Anisomycin
b
p-c-Jun
Actin
c

Figure 60 Absence of N-terminally phosphorylated c-Jun results in decreased cell numbers in MEF cultures
(**a**) Immunohistochemistry for serine 63 phosphorylated c-Jun (red) on untreated and anisomycin-treated (25 ng/ml, 12 h) $Jun^{+/+}$, $Jun^{4A/+}$ and $Jun^{4A/4A}$ MEF cultures. DNA (blue) is counterstained with DAPI. (**b**) Western blot analysis for serine 73 phosphorylated c-Jun and β-Actin on protein extracts from $Jun^{+/+}$, $Jun^{4A/+}$ and $Jun^{4A/4A}$ MEF cultures. (**c**) Phase contrast pictures of $Jun^{+/+}$, $Jun^{4A/+}$ and $Jun^{4A/4A}$ MEF cultures at passage 7.
Scale bars, 20 μm.

a

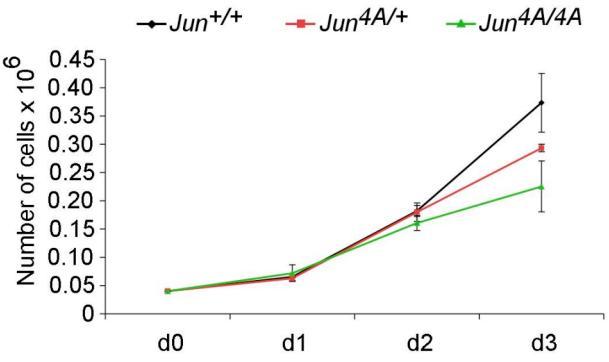

b

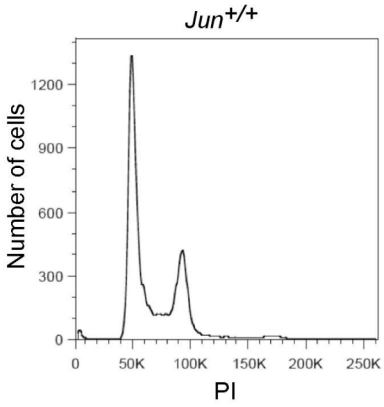

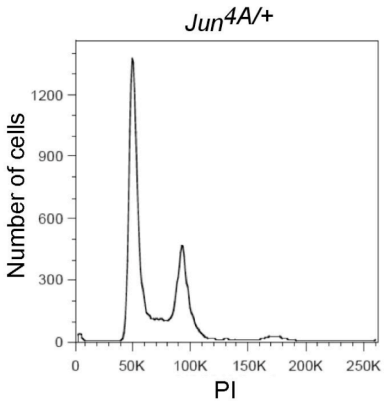

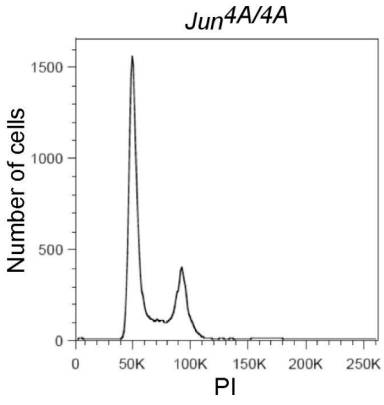

c

	$Jun^{+/+}$	$Jun^{4A/+}$	$Jun^{4A/4A}$
G1	42.9%	49.1%	51.8%
S	31.9%	25.2%	26.3%
G2	25.2%	25.7%	21.9%

Figure 61 Inhibition of JNK/c-Jun signalling leads to a mild proliferation defect in MEF cultures at early passage

(**a**) Growth curve analysis for three days on $Jun^{+/+}$, $Jun^{4A/+}$ and $Jun^{4A/4A}$ MEF cultures at passage 3. Initial number of plated cells: 0.04 x 10^6. n = 3. Error bars, s.e.m. (**b**) Cell cycle profiles of propidium iodide (PI) stained $Jun^{+/+}$, $Jun^{4A/+}$ and $Jun^{4A/4A}$ MEFs at passage 3. (**c**) Percentages of $Jun^{+/+}$, $Jun^{4A/+}$ and $Jun^{4A/4A}$ MEFs in G1-, S- and G2-phase of the cell cycle at passage 3 based on the cell cycle profiles depicted in (**b**). Percentages were determined using the Watson Pragmatic algorithm and normalised to a total percentage of 100%.

a

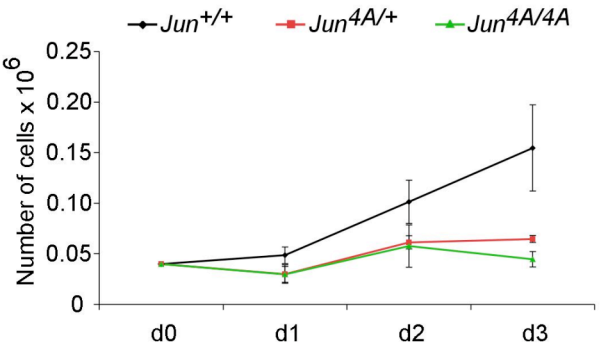

b

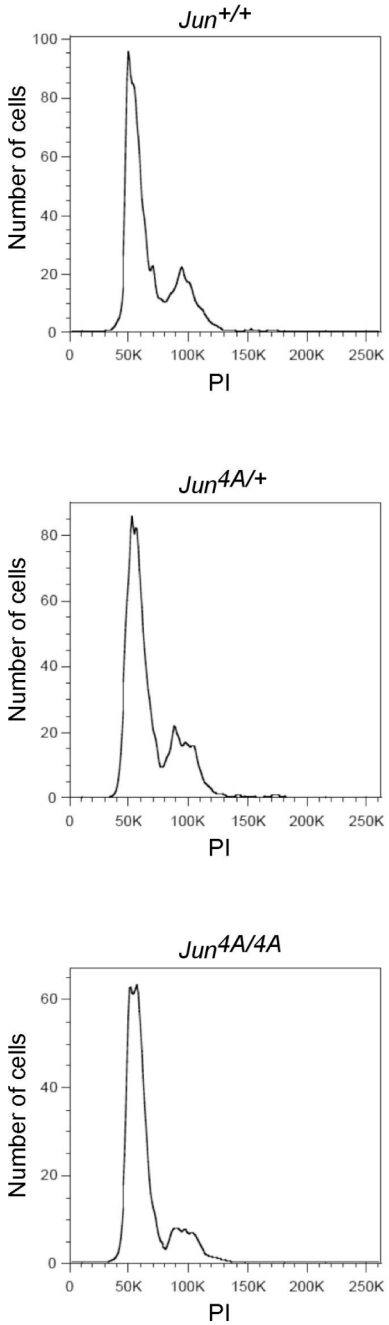

c

	Jun$^{+/+}$	*Jun*$^{4A/+}$	*Jun*$^{4A/4A}$
G1	37.3%	58.3%	72.9%
S	45.0%	28.1%	23.8%
G2	17.7%	13.6%	3.3%

Figure 62 Absence of N-terminally phosphorylated c-Jun blocks cell cycle progression of MEFs at late passage

(**a**) Growth curve analysis for three days on *Jun*$^{+/+}$, *Jun*$^{4A/+}$ and *Jun*$^{4A/4A}$ MEF cultures at passage 7. Initial number of plated cells: 0.04 x 10^6. n = 3. Error bars, s.e.m. (**b**) Cell cycle profiles of propidium iodide (PI) stained *Jun*$^{+/+}$, *Jun*$^{4A/+}$ and *Jun*$^{4A/4A}$ MEFs at passage 7. (**c**) Percentages of *Jun*$^{+/+}$, *Jun*$^{4A/+}$ and *Jun*$^{4A/4A}$ MEFs in G1-, S- and G2-phase of the cell cycle at passage 7 based on the cell cycle profiles depicted in (**b**). Percentages were determined using the Watson Pragmatic algorithm and normalised to a total percentage of 100%.

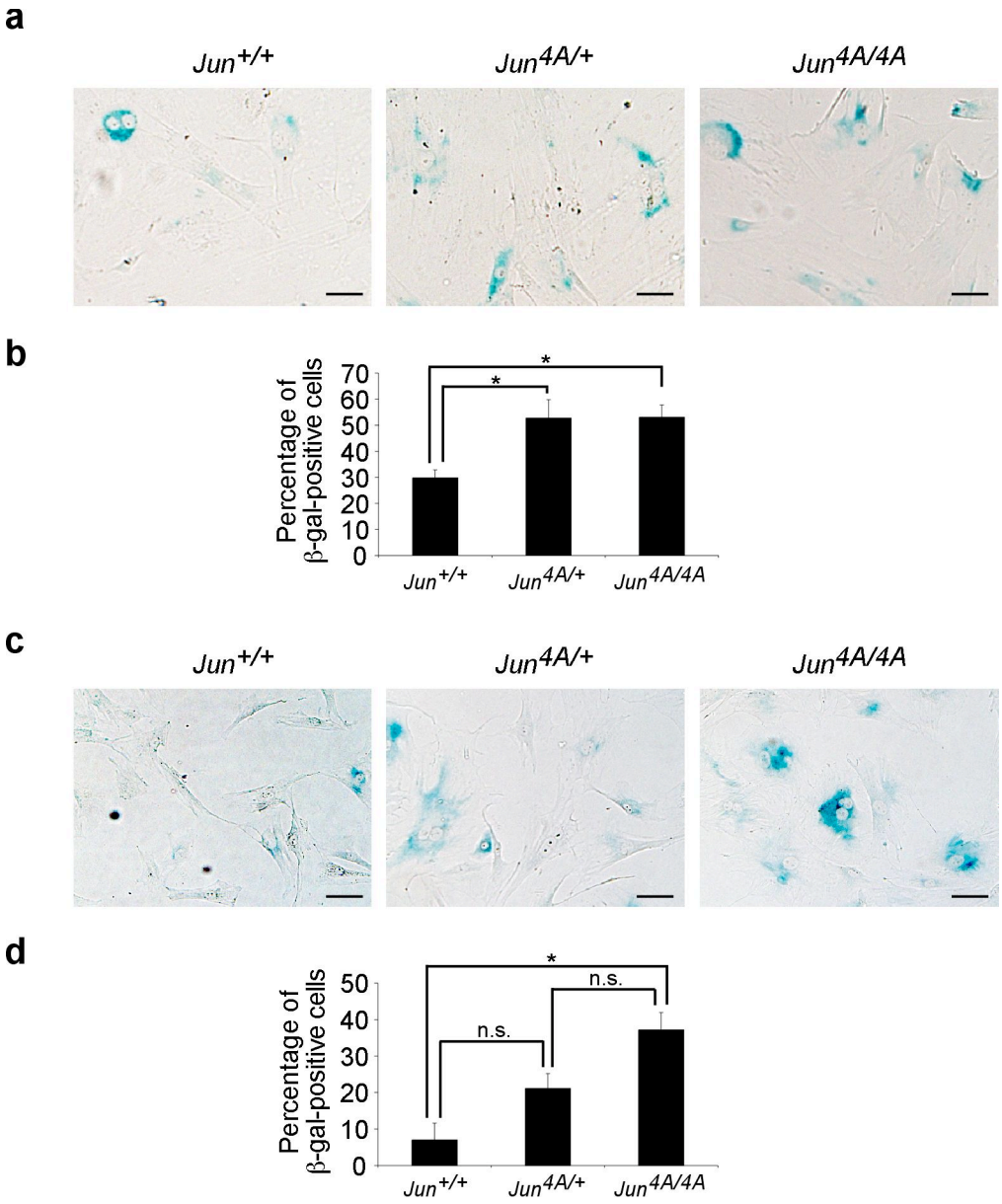

Figure 63 Inhibition of JNK/c-Jun signalling leads to premature senescence independent of oxygen levels

(**a**,**c**) Phase contrast pictures of β-galactosidase (β-gal; blue)-positive senescent cells in *Jun*$^{+/+}$, *Jun*$^{4A/+}$ and *Jun*$^{4A/4A}$ MEF cultures at passage 7 at (**a**) atmospheric (~21%) and (**c**) at physiological O_2 (3%). (**b**,**d**) Quantification of β-gal-positive senescent cells in *Jun*$^{+/+}$, *Jun*$^{4A/+}$ and *Jun*$^{4A/4A}$ MEF cultures at passage 7 (**b**) at atmospheric (~21%) and (**d**) at physiological O_2 (3%). $n = 3$.

Scale bars, 20 μm. Error bars, s.e.m.; n.s., not significant; *$P \leq 0.05$ (unpaired *t* test).

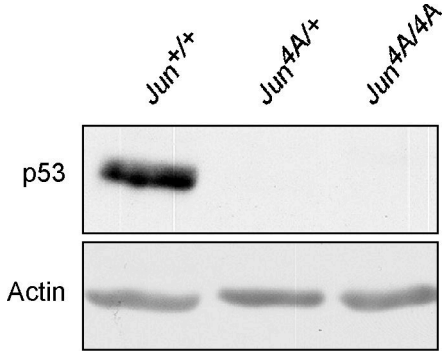

Figure 64 Absence of N-terminally phosphorylated c-Jun leads to highly decreased p53 levels
Western blot analysis for total p53 (53 kDa) and β-Actin (42 kDa) on protein extracts from *Jun*$^{+/+}$, *Jun*$^{4A/+}$ and *Jun*$^{4A/4A}$ MEFs at passage 5.

5.1.6 Discussion: The role of JNK/c-Jun signalling in development and pathology

5.1.6.1 JNK/c-Jun signalling in the nervous system

JNK signalling components show particularly high expression in the nervous system indicating that JNK signalling is of major importance in this tissue (reviewed in Haeusgen et al., 2009, Raivich and Behrens, 2006). Consequently, *JNK1*$^{-/-}$; *JNK2*$^{-/-}$ double mutant mice die at E11.5 due to defects in neural tube closure, in part linked to abnormal programmed cell death during brain development. Interestingly, this phenotype was not recapitulated in c-Jun deficient mice, which die around E15.5 due to defects in hepatogenesis (Hilberg et al., 1993). This suggests that the role of JNK signalling in neural tube closure is either not mediated by c-Jun, or other JNK signalling targets can compensate for the loss of c-Jun. Furthermore, ablation of c-Jun phosphorylation by JNK at serine 63 and serine 73 as well as conditional deletion of c-Jun in the CNS does not lead to abnormal brain histology indicating that c-Jun is not required for brain development (Behrens et al., 1999, Raivich et al., 2004). Whereas the crucial role of p-c-Jun in stress-induced neuronal apoptosis has been described before, the importance of p-c-Jun degradation during brain development was unknown (Raivich and Behrens, 2006). I could show that elevated p-c-Jun levels as a consequence of Fbw7 deletion results in increased progenitor apoptosis and reduced neuronal numbers in the developing brain (Hoeck et al., 2010).

Consistent with previous data, ablation of c-Jun phosphorylation by JNK at the four main sites in *Jun*$^{4A/4A}$ mice did not affect brain development, as brain histology of *Jun*$^{4A/4A}$ mice was normal (**Figure 53**). Furthermore, mild activation of JNK/c-Jun signalling through expression of a JNKK2-JNK1 fusion protein under the control of the

endogenous ROSA26-promoter in LSL-JNKK2-JNK1$^{\Delta N/+}$ mice did not impair brain development. The moderate upregulation of p-c-Jun detected in the LSL-JNKK2-JNK1$^{\Delta N/+}$ brain did not lead to significant structural or cellular abnormalities in the adult brain of these mice (**Figures 57** and **58**). There are several reasons which might explain why the LSL-JNKK2-JNK1$^{\Delta N/+}$ mice do not recapitulate the c-Jun-dependent *Fbxw7*$^{\Delta N}$ phenotype. Considering the essential role of Fbw7 during brain development, it could be that p-c-Jun stabilisation in the *Fbxw7*$^{\Delta N}$ brain led to a higher increase in p-c-Jun levels than that in LSL-JNKK2-JNK1$^{\Delta N/+}$ mice where the JNKK2-JNK1 fusion protein is expressed to moderate levels under the endogenous ROSA26 promoter. Furthermore, Fbw7, which is highly expressed in the developing brain, might be able to efficiently reduce p-c-Jun levels in the LSL-JNKK2-JNK1$^{\Delta N/+}$ brain during development.

All in all, my data suggests that neither ablation of JNK/c-Jun signalling nor moderate activation of JNK/c-Jun signalling has a significant impact on brain development and the histology of the adult brain.

5.1.6.2 JNK/c-Jun signalling in nerve regeneration

Whilst being dispensable for the physiological development of the nervous system, JNK/c-Jun signalling has been shown to be important under certain pathological conditions. JNK/c-Jun signalling has been reported to mediate the detrimental effects of neuronal apoptosis after kainate-induced seizures, because *Jun*$^{AA/AA}$ mice are protected from this excitotoxic stress-induced neuronal death (Behrens et al., 1999). Furthermore, loss of neurons in neurodegenerative diseases such as amyotrophic lateral sclerosis (ALS), Alzheimer's dementia and Parkinson's Disease has been linked to upregulation

of p-c-Jun levels (reviewed in Raivich, 2008). On the contrary, conditional deletion of c-Jun in the nervous system has shown that c-Jun is essential for nerve regeneration after facial nerve crush injury (Raivich et al., 2004). Absence of c-Jun led to atrophy of axotomised nerves due to reduced apoptosis and clearance of damaged neurons. Taken together, absence of N-terminal c-Jun phosphorylation at serine 63 and 73 protects mice from excitotoxic stress-induced loss of neurons, but c-Jun is essential for nerve regeneration.

In order to uncouple the regenerative and detrimental c-Jun actions in the nervous system from each other, I analysed nerve regeneration after facial axotomy in $Jun^{4A/4A}$ mice. Although, nerve regeneration seemed to be delayed in $Jun^{4A/4A}$ mice, it was not significantly impaired unlike what was seen by Raivich *et al*. in $Jun^{\Delta N}$ mice (**Figure 59**; (Raivich et al., 2004).

All in all, whilst the detrimental c-Jun action in stress-induced neuronal apoptosis in the brain has been reported to be JNK-dependent, the positive c-Jun function in the removal of damaged motoneurons during nerve regeneration was only partially JNK-dependent. Furthermore, although not significantly, constitutively active JNK/c-Jun signalling in LSL-JNKK2-JNK1$^{\Delta N/+}$ mice was able to slightly improve nerve regeneration (**Figure 59**). These findings might be interesting for targeting JNK/c-Jun signalling in neurodegenerative diseases and after nerve injuries.

5.1.6.3 JNK/c-Jun signalling in the intestine

Ablation of JNK-mediated c-Jun N-terminal phosphorylation at serine 63, serine 73, threonine 91 and threonine 93 did not affect mouse development, since *Jun*$^{4A/4A}$ mice were viable and fertile and did not show histological abnormalities in the brain, the liver, the lungs, the spleen and the pancreas (**Figure 53**). This is consistent with previous data showing that inactivating mutations at serine 63 and serine 73 does not impair embryogenesis (Behrens et al., 1999). However, activation of JNK signalling has recently been reported to increase progenitor proliferation and villus length in the intestine (Sancho et al., 2009). Thus, I investigated whether ablation of c-Jun N-terminal phosphorylation in *Jun*$^{4A/4A}$ mice has an effect on physiological gut development. Although the villus length in *Jun*$^{4A/4A}$ mice seemed to be slightly decreased, I could not detect a significant difference in proliferation, apoptosis and differentiation in the absence of c-Jun N-terminal phosphorylation (**Figures 54** and **55**). This indicates that whereas constitutive activation of JNK/c-Jun signalling leads to increased proliferation in the intestine, JNK/c-Jun signalling is not required for normal intestinal development.

5.1.6.4 JNK/c-Jun signalling in gut regeneration

Due to the increased progenitor proliferation after JNK signalling activation detected by Sancho *et al*. (Sancho et al., 2009) and the absence of proliferative defects in the *Jun*$^{4A/4A}$ gut under physiological conditions, I examined whether under pathological conditions, gut regeneration requires JNK/c-Jun signalling. Therefore, I induced colitis in wt and *Jun*$^{4A/4A}$ mice by addition of dextran sodium sulfate (DSS) salt to their drinking water and analysed gut regeneration after this treatment. I could not detect a

histological difference between wt and *Jun*$^{4A/4A}$ regenerated guts (**Figure 56**). Furthermore, the number of proliferative and apoptotic cells was similar in *Jun*$^{4A/4A}$ and control guts. This indicates that JNK/c-Jun signalling is dispensable for normal gut development as well as for regeneration after gut pathology. Considering that JNK signalling activation has been shown to promote gut tumour development (Sancho et al., 2009), these findings might be interesting for the establishment of JNK/c-Jun signalling as a promising target for anti-cancer therapy in the gut with possibly insignificant side effects in this tissue.

5.1.6.5 JNK/c-Jun signalling in fibroblasts

c-Jun deficiency has been reported to result in severely impaired proliferation and premature senescence of mouse embryonic fibroblasts (MEFs) (Johnson et al., 1993). Ablation of c-Jun N-terminal phosphorylation by JNK at serine 63 and serine 73 in *Jun*$^{AA/AA}$ mice only showed a mild defect in MEF proliferation (Behrens et al., 1999). Furthermore, Ras-induced transformation was inhibited in *Jun*$^{AA/AA}$ MEFs (Behrens et al., 2000). These data suggests that c-Jun function in promoting transformation depends on c-Jun phosphorylation by JNK at serine 63 and serine 73, whereas c-Jun function in promoting proliferation is only partially dependent on these phosphorylations. The role of c-Jun N-terminal phosphorylation in senescence is unclear because it has been reported in two different studies that c-Jun function in preventing premature senescence is JNK-independent and JNK-dependent (Behrens et al., 1999, Wada et al., 2004). To further dissect the dependency of c-Jun actions on phosphorylation by JNK and to study the role of the importance of c-Jun phosphorylation at threonine 91 and threonine 93, I analysed *Jun*$^{4A/4A}$ MEFs in culture. Similar to *Jun*$^{AA/AA}$ MEFs, but unlike c-Jun-

deficient MEFs, *Jun*$^{4A/4A}$ MEFs only showed a mild proliferation defect at early passage (**Figure 61**; Behrens et al., 1999, Johnson et al., 1993). This confirmed that c-Jun function in MEF proliferation is only partially dependent on N-terminal phosphorylation by JNK. In contrast, similar to c-Jun deficient MEFs, a significantly increased amount of *Jun*$^{4A/4A}$ MEFs underwent premature senescence (**Figures 62** and **63**; Johnson et al., 1993). In comparison to Behrens *et al*. who did not detect increased premature senescence in *Jun*$^{AA/AA}$ MEF cultures, this indicated that c-Jun function in preventing senescence is JNK-dependent, particularly with respect to c-Jun phosphorylation by JNK at threonine 91 and threonine 93 (Behrens et al., 1999). In comparison to Wada *et al*. who suggested that premature senescence in *Mkk7*(*Jnkk2*)$^{-/-}$ and *Jun*$^{AA/AA}$ MEF cultures is increased, my results confirm JNK-dependency of c-Jun action in premature senescence (Wada et al., 2004). Wada *et al*. detected a block in G2/M cell cycle progression of *Mkk7*$^{-/-}$ and *Jun*$^{AA/AA}$ MEFs due to reduced levels of the c-Jun target cell cycle kinase Cdc2 (cell division control protein 2; also known as Cdk1). However, senescence is usually associated with accumulation of cells in G1 which I could detect in *Jun*$^{4A/4A}$ MEF cultures (**Figure 62**; Sherwood et al., 1988). Thus, it seems that ablation of c-Jun phosphorylation in *Jun*$^{AA/AA}$ and *Jun*$^{4A/4A}$ MEFs leads to different biological effects on the cell cycle.

Interestingly, *Jun*$^{4A/4A}$ MEFs also underwent premature senescence when cultured at physiological oxygen levels suggesting that extrinsic oxidative stress is not the main reason for this phenotype. However, Wada *et al*. show that oxidative stress triggers G2/M block and senescence in *Mkk7*$^{-/-}$ MEFs (Wada et al., 2004). Instead, the G1 block and the premature senescence detected in *Jun*$^{4A/4A}$ MEF cultures might be due to an intrinsic mechanism triggered by absence of c-Jun N-terminal phosphorylation.

To study the increased senescence in *Jun*$^{4A/4A}$ MEF cultures molecularly, I examined protein levels of the main inducer of senescence, p53, which has been reported to be negatively regulated by c-Jun (Schreiber et al., 1999). Strikingly, p53 levels were drastically reduced in the absence of c-Jun N-terminal phosphorylation (**Figure 64**). From this result, two questions arose which will have to be addressed:

1. If not via p53, how does absence of N-terminally phosphorylated c-Jun trigger senescence?

2. How does c-Jun regulate p53?

With regard to the first question, Wada *et al*. showed that *Mkk7*$^{-/-}$ MEFs undergo premature senescence due to decreased levels of the cell cycle kinase Cdc2 which is required for G2/M cell cycle progression (Wada et al., 2004). The authors reported that the *Cdc2* gene is a direct transcriptional target of c-Jun and that p53 levels are not altered in *Mkk7*$^{-/-}$ MEFs. Since I could detect increased premature senescence due to a G1 arrest in *Jun*$^{4A/4A}$ MEFs, it is unlikely that reduced Cdc2 expression accounts for this phenotype. Apart from the c-Jun target p53, a second prominent inducer of senescence is the retinoblastoma (Rb) tumour suppressor. In contrast to reduced Cdc2 levels which lead to G2/M block, Rb induces G1 arrest (Shapiro et al., 2000). Interestingly, phosphorylation and consequently inactivation of Rb is mediated by the *bona fide* c-Jun transcriptional target cyclin D1 (Sellers and Kaelin, 1997). Thus, absence of c-Jun N-terminal phosphorylation in *Jun*$^{4A/4A}$ MEFs might result in decreased cyclin D1 levels, Rb activation, G1 arrest and premature senescence. This hypothesis will need to be tested by qRT-PCR, immunoblotting, *etc*. in the future.

Secondly, how does c-Jun regulate p53? Schreiber *et al*. identified c-Jun as a negative regulator of p53 transcription in MEFs (Schreiber et al., 1999). Recent work by Aguilera *et al*. revealed that unphosphorylated but not phosphorylated c-Jun is recruited via Mbd3 (Methyl-CpG binding domain protein 3) to nucleosome remodelling and histone deacetylation (NuRD) complexes which repress transcription (Aguilera et al., 2011). It is tempting to speculate that in the absence of N-terminal c-Jun phosphorylation, the unphosphorylated-c-Jun/Mbd3/NuRD complex represses p53 transcription in $Jun^{4A/4A}$ MEFs, a hypothesis which will have to be tested by chromatin immunoprecipitation (ChIP) in the future.

Taken together, my data on $Jun^{4A/4A}$ MEFs suggests that inhibition of c-Jun N-terminal phosphorylation by JNK at serine 63, serine 73, threonine 91 and threonine 93 triggers premature senescence which is independent of extrinsic oxidative stress. Furthermore, absence of c-Jun N-terminal phosphorylation leads to a drastic decrease in p53 levels, and premature senescence in $Jun^{4A/4A}$ MEFs is induced in a p53-independent manner. Considering that c-Jun N-terminal phosphorylation can promote tumourigenesis, these findings could prove to be interesting for targeting p53 null tumours in cancer therapy.

Chapter 6. Discussion

6.1 Fbw7 and its substrates Notch and c-Jun in brain development

Fbw7 function during mouse embryonic development is crucial around mid-gestation. Fbw7-knockout mice die at E10.5 due to vascular defects, accompanied by increased levels of the Fbw7-substrate Notch, and placental defects which are associated with high cyclin E levels in the extra-embryonic tissue (Tetzlaff et al., 2004, Tsunematsu et al., 2004). Furthermore, conditional deletion of Fbw7 in the haematopoietic system results in a loss of quiescent haematopoietic stem cells which is caused by increased c-Myc levels (Thompson et al., 2008). These data point towards a tissue-specific function of Fbw7 in the degradation of distinct substrates. Due to the embryonic lethality of Fbw7-knockout mice at E10.5, it had not been possible to examine Fbw7 function in the developing brain yet, since brain development only starts around mid-gestation. To address this, conditional Fbw7-knockout mice were generated in our laboratory which show tissue-specific deletion of Fbw7 in the nervous system (*Fbxw7*$^{f/f}$; Nestin-Cre or *Fbxw7*$^{\Delta N}$).

The fact that *Fbxw7*$^{\Delta N}$ mice die perinatally was the first indication for an essential role of Fbw7 in the development of the nervous system. Histological analysis of E18.5 *Fbxw7*$^{\Delta N}$ mouse embryos revealed a significant reduction in cellularity in areas of differentiated cells throughout the brain, for example in the cerebellum, the thalamus, the midbrain tectum and the forebrain cortex (**Figure 24**). In contrast, cell numbers in areas harbouring stem cells were either unaffected, as seen in the cortical ventricular zone, or increased, as observed in the tectal ventricular zone. I could show that Fbw7 is

a key molecular switch antagonising Notch and JNK/c-Jun signalling during neural development. On the one hand, Fbw7 degrades phosphorylated c-Jun to prevent neuronal progenitors from undergoing apoptosis and to regulate neural cell numbers. On the other hand, Fbw7 degrades Notch to allow radial glia stem cells to undergo differentiation and to control neurogenesis. Loss of Fbw7 led to increased Notch levels in the developing brain which was responsible for the accumulation of radial glia stem cells and the differentiation defect of these cells. Cells progressing to a neuronal progenitor state despite high Notch levels underwent apoptosis which was mediated by high p-c-Jun levels, the other Fbw7 substrate upregulated in the *Fbxw7*$^{\Delta N}$ brain. Whereas neuronal differentiation is incompatible with high Notch levels, Notch seems to play a permissive role in glia differentiation (Cau and Blader, 2009), which explains why glia differentiation was not affected in the absence of Fbw7. The observation that radial glia cells were also localised ectopically might be explained by an intermediate state of these cells in which they have entered neuronal differentiation and show normal JNK signalling-mediated migration but maintain stem cell characteristics due to increased Notch levels. The more than 50% reduction in differentiated neurons in the *Fbxw7*$^{\Delta N}$ brain could be responsible for the lack of suckling behaviour of new-born *Fbxw7*$^{\Delta N}$ mice which has recently been reported as cause of death of these mice (Matsumoto et al., 2011). The fact that neither attenuation of c-Jun nor Notch alone was able to rescue perinatal lethality of Fbw7-deficient mice suggests that both, the p-c-Jun-mediated progenitor apoptosis and the Notch-mediated stem cell differentiation defect contribute to the perinatal lethality of these mice. In future breedings, we would expect that genetic downregulation of both p-c-Jun and Notch can lead to the survival of *Fbxw7*$^{\Delta N}$ mice.

6.2 Recent publications on Fbw7 function in the brain

Shortly after our publication on Fbw7 function in neural stem cell differentiation and progenitor apoptosis by antagonising Notch and JNK/c-Jun signalling (Hoeck et al., 2010), another group published results from CNS-specific conditional Fbw7-knockout mice (Matsumoto et al., 2011). Matsumoto *et al*. confirmed my results on Notch-dependent neural stem cell accumulation and decreased numbers of differentiated cells in the Fbw7-knockout brain. However, Matsumoto *et al*. come to different conclusions in some crucial aspects.

Firstly, the authors of this article report that they could not detect an upregulation of c-Jun in the absence of Fbw7. Remarkably, this claim is not supported by their own data, since there is a clear increase in c-Jun levels seen in their immunoblotting results on protein extracts from the Fbw7-mutant brain (Figure 3A in Matsumoto et al., 2011). Strikingly, c-Jun levels were highest in the Fbw7-knockout brain at E16.5 when we describe a peak in progenitor apoptosis (Hoeck et al., 2010). Furthermore, a recent paper by Jandke *et al*. reports highly upregulated p-c-Jun levels in progenitors in the cerebellum of mice with conditional inactivation of Fbw7 in the cerebellum (Jandke et al., 2011).

Secondly, Matsumoto *et al*. report that they could not detect increased apoptosis in the absence of Fbw7. However, it is not mentioned how apoptosis was assessed and this assumption is not substantiated with any data (Matsumoto et al., 2011). Furthermore, they claim that there is an increase in the number of proliferative pH3-positive cells in the VZ and a decrease in the SVZ in the Fbw7-mutant brain. I have analysed the percentage of pH3 and Ki67-expressing cells at various time points during embryonic

brain development and could not detect a significant difference in proliferation. Furthermore, pH3 staining of neurosphere cells and a CFSE cell proliferation assay revealed that also *in vitro*, the number of proliferative cells and the proliferation rate is the same in wt and Fbw7-mutant cultures (Hoeck et al., 2010). This is in line with a previous publication reporting that NICD1-overexpression in radial glia stem cells in the VZ results in the accumulation of mainly quiescent radial glia stem cells in the cortex (Gaiano et al., 2000). The fact that I could not detect a difference in Ki67-positive progenitors in the SVZ despite reduced progenitor numbers suggests that the p-c-Jun-mediated progenitor apoptosis only occurs after the proliferative stage and upon entry into neuronal differentiation of these cells which is incompatible with the observed increase in Notch levels.

Thirdly, Matsumoto *et al*. report that absence of Fbw7 promotes differentiation of neural stem cells into astrocytes (Matsumoto et al., 2011). This assumption is solely based on immunostaining for the astroglia marker GFAP *in vitro* and in the P0.5 brain. The generation of differentiated glia cells only slowly starts at late-gestation (Qian et al., 2000). I could show that the number of S100-positive astrocytes and NG2-positive oligodendrocytes is similar in the wt and the *Fbxw7*$^{\Delta N}$ brain (**Figure 31**). Also in *in vitro*-differentiation assays, absence of Fbw7 did not result in increased formation of Connexin-43-positive astrocytes and O4-positive oligodendrocytes (**Figure 38**). The marker Matsumoto *et al*. use to identify astroglia, GFAP, is postnatally not only a marker of astrocytes, but also of radial glia cells (reviewed in Pinto and Gotz, 2007). Also the morphology of the GFAP-positive cells they show at P0.5 resembles very much the morphology of radial glia cells (Figure 4E in Matsumoto et al., 2011). Thus, what Matsumoto *et al*. have confirmed with this data is just the accumulation of radial

glia stem cells, but they do not show a skewed differentiation into the astroglia lineage. It is noteworthy that whereas the role of Notch in neural stem cell maintenance is undisputed, Notch function in astrogenesis remains elusive. Whereas some studies come to the conclusion that Notch is not involved in the lineage decision between neurons and glia (Hitoshi et al., 2002, Nyfeler et al., 2005, Yoon et al., 2004), others have reported that Notch promotes astrocyte differentiation (Chambers et al., 2001, Ge et al., 2002, Grandbarbe et al., 2003). Recent publications suggest that the role of Notch in glia differentiation is rather permissive than instructive (reviewed in Cau and Blader, 2009). This model fits well with my data showing that increased Notch signalling in the absence of Fbw7 does not interfere with gliogenesis, but it does not actively promote glia differentiation.

6.3 Future directions: Fbw7 in the nervous system

After elucidating the role of Fbw7 in the developing brain, it will be interesting to investigate the function of Fbw7 in the adult brain. Due to the perinatal lethality of *Fbxw7*$^{\Delta N}$ mice, I have crossed *Fbxw7*$^{f/f}$ mice to inducible Nestin-CreER transgenic mice which express Cre recombinase in the nervous system after tamoxifen administration. Together with other colleagues in the lab, I have established adult neurosphere cultures from cells isolated from the subventricular zone of the adult brain. It will be interesting to see whether Fbw7 deletion also leads to alterations in the subventricular zone and the dentate gyrus, which are the stem cell compartments of the adult brain, whether it will influence differentiation and apoptosis and which Fbw7-substrates will be affected.

Due to its potential role as a tumour suppressor in glioma (Hagedorn et al., 2007) and its newly discovered role in stem cell differentiation in the brain, it is worth investigating whether deletion of Fbw7 leads to the development of more stem-cell-like and more aggressive brain tumours. Therefore, I have crossed *Fbxw7*$^{f/f}$ mice with a brain tumour model mouse carrying deletions of the tumour suppressors pten and p53 which has recently been reported to result in brain tumour formation (Zheng et al., 2008). It will be interesting to see whether deletion of Fbw7 in the pten; p53 null background promotes development of glioblastoma, in which regions of the brain the tumours arise and if Fbw7-deficiency can promote maintenance of cancer stem cells.

After establishing Fbw7 as a differentiation and survival factor of neural stem and progenitor cells, it would be worth investigating whether in regenerative medicine, increased levels of Fbw7 can make the *in vitro*-differentiation of stem cells into neurons more efficient.

Moreover, due to the fact that c-Jun and Notch in Schwann cells are required for nerve regeneration after injury (Mirsky et al., 2008), a colleague in our laboratory is currently investigating whether deletion of Fbw7 specifically in Schwann cells can promote nerve regeneration after facial axotomy and spinal cord injury.

6.4 JNK/c-Jun signalling in physiology and pathology

In physiological development, the absence of obvious phenotypes in *JNK1*$^{-/-}$, *JNK2*$^{-/-}$ and *JNK3*$^{-/-}$ single mutant mice as well as in *JNK1*$^{-/-}$; *JNK3*$^{-/-}$ and *JNK2*$^{-/-}$; *JNK3*$^{-/-}$ double mutants suggests that loss of JNK1 or JNK2 can be compensated by each other and that either JNK1 or JNK2 can compensate for lack of JNK3 (Chang and Karin, 2001, Dong et al., 1998, Kuan et al., 1999, Yang et al., 1998, Yang et al., 1997). Only *JNK1*$^{-/-}$; *JNK2*$^{-/-}$ double mutants show embryonic lethality around mid-gestation due to impaired neural tube closure which was associated with abnormal apoptosis (Kuan et al., 1999). Deletion of the JNK target c-Jun has been shown to result in embryonic lethality around mid- and late-gestation due to severe defects in liver development (Hilberg et al., 1993). Interestingly, ablation of c-Jun N-terminal phosphorylation by JNK at serine 63 and serine 73 does not impair embryonic development but is required for Ras-induced transformation of mouse embryonic fibroblasts (MEFs) and protects neurons from undergoing apoptosis after kainate-induced seizures (Behrens et al., 2000, Behrens et al., 1999). Recent publications have suggested that apart from serine 63 and serine 73 phosphorylation, also c-Jun phosphorylation at threonine 91 and threonine 93 by JNK is involved in the stress-induced augmentation of c-Jun transactivation function (Morton et al., 2003, Vinciguerra et al., 2008). The question arose whether JNK-dependent c-Jun functions are dispensable in physiology but are important under pathological conditions? To study this, I have generated two mouse models to be able to either constitutively activate JNK/c-Jun signalling (ROSA26-LSL-JNKK2-JNK1) or to ablate JNK signalling via c-Jun (*Jun4A*; Ser63Ala, Ser73Ala, Thr91Ala, Thr93Ala). I could show that JNK-dependent c-Jun phosphorylation is not required for physiological mouse development and regenerative events after pathology, i.e. colitis and nerve injury

whereas JNK/c-Jun activation could slightly improve nerve regeneration. Furthermore, the prevention of cells to become senescent mediated by c-Jun seems to be highly JNK-dependent. Interestingly, the levels of p53, the main inducer of senescence, were highly decreased in *Jun*$^{4A/4A}$ MEF cultures. c-Jun has been described as a transcriptional repressor of p53 (Schreiber et al., 1999). As a consequence of my results, it is tempting to speculate that c-Jun N-terminal phosphorylation by JNK is involved in p53 regulation and that unphosphorylated c-Jun can repress p53 transcription. Since senescence in the absence of p-c-Jun is p53-independent, it could be mediated by the alternative p16/Rb senescence pathway. Furthermore, extrinsic oxidative stress does not seem to be the main cause of senescence in *Jun*$^{4A/4A}$ MEF cultures which suggests that, in the absence of p-c-Jun, there might be an intrinsic mechanism that triggers senescence. Since tumour cell growth can be limited by senescence, these findings might be interesting for targeting JNK/c-Jun signalling in tumour therapy.

6.5 Future directions: JNK/c-Jun signalling in tumourigenesis

The absence of obvious detrimental effects by the loss of c-Jun N-terminal phosphorylation in *Jun*$^{4A/4A}$ mice supports the establishment of JNK/c-Jun signalling as a promising target for cancer therapy. Hyperactivation of the pathway has been shown to promote tumour growth in various tissues, for example in the intestine, the skin and the haematopoietic system (reviewed in Eferl and Wagner, 2003). Ras-induced skin tumourigenesis and c-Fos-induced osteosarcoma development have been reported to be impaired in *Jun*$^{AA/AA}$ mice. Furthermore, *Jun*$^{AA/AA}$ mice have been reported to show decreased tumourigenesis and prolonged survival in the APCmin intestinal tumour

model background (Nateri et al., 2005). To further study the role of c-Jun N-terminal phosphorylation in gut tumour development, $Jun^{4A/4A}$ mice are currently being crossed to two animal models of intestinal tumourigenesis (LSL-RasG12D; VillinCreERT and APCmin mice). It will be interesting to see whether ablation of c-Jun N-terminal phosphorylation by JNK at serine 63, serine 73, threonine 91 and threonine 93 in $Jun^{4A/4A}$ mice can impair intestinal tumour development to a greater extent than the $Jun^{AA/AA}$ mice.

The tumour suppressor p53 has been found to be mutated in more than 50% of human tumours and correlates with poor prognosis in many cancers (reviewed in Levine, 1997). $Jun^{4A/4A}$ MEFs underwent premature senescence independent of p53. Thus, $Jun^{4A/4A}$ mice are being crossed to $p53^{\Delta/+}$ mice, which develop tumours in various tissues, to investigate whether lack of c-Jun N-terminal phosphorylation can inhibit tumour development induced by reduced p53 levels.

It will be exciting to see whether upon oncogenic stress, lack of c-Jun N-terminal phosphorylation can induce senescence in tumour cells in a p53-independent manner and thus can limit tumour growth.

6.6 Concluding remarks

In my PhD studies, I could show that the E3 ubiquitin ligase Fbw7 is a key regulator of neural stem cell differentiation and progenitor apoptosis during brain development. Fbw7 is essential for the degradation of the stem cell factor Notch to allow radial glia stem cells to enter the differentiation programme. Furthermore, Fbw7 negatively regulates pro-apoptotic c-Jun in the developing brain to prevent differentiating neuronal progenitors from undergoing apoptosis. Consequently, Fbw7 controls differentiation and neuronal number in the developing brain by Notch and c-Jun degradation (**Figure 65**).

Furthermore, I could show that N-terminal c-Jun phosphorylation at the four main JNK-phosphorylation sites (serine 63, serine 73, threonine 91 and threonine 93) is dispensable for mouse development. Moreover, lack of p-c-Jun does not significantly impair gut and nerve regeneration. Due to its role in tumourigenesis, JNK/c-Jun signalling has been suggested as a target for cancer therapy. I could show that loss of p-c-Jun induces premature senescence in mouse embryonic fibroblasts at physiological oxygen levels in a p53-independent manner (**Figure 66**). Hence, inhibition of JNK/c-Jun signalling might be a promising way to induce senescence in tumour cells independent of p53 and thus limit tumour growth with possibly limited side effects.

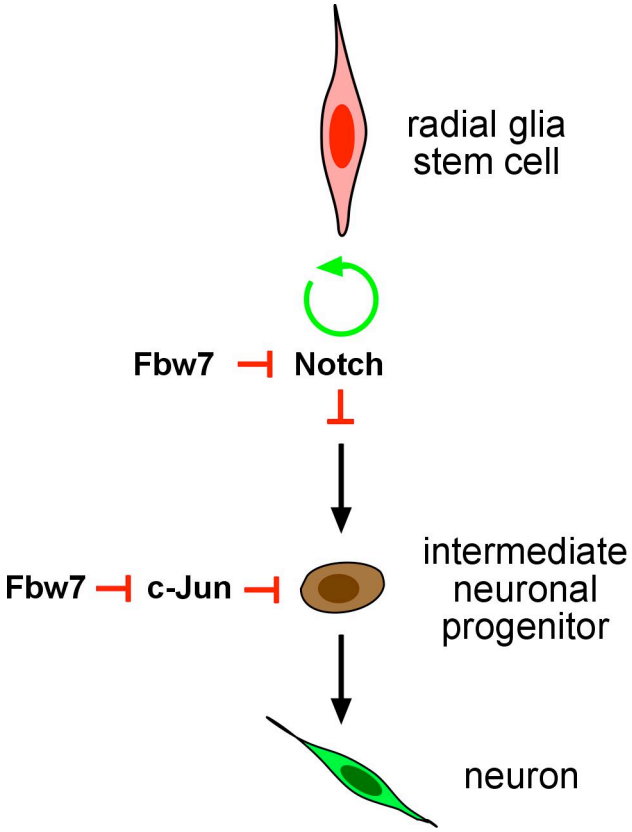

Figure 65 Fbw7 in neurogenesis
Schematic representation of neuronal differentiation and Fbw7 function in antagonising Notch, which promotes radial glia stem cell maintenance, and c-Jun, which induces apoptosis in neuronal progenitors.

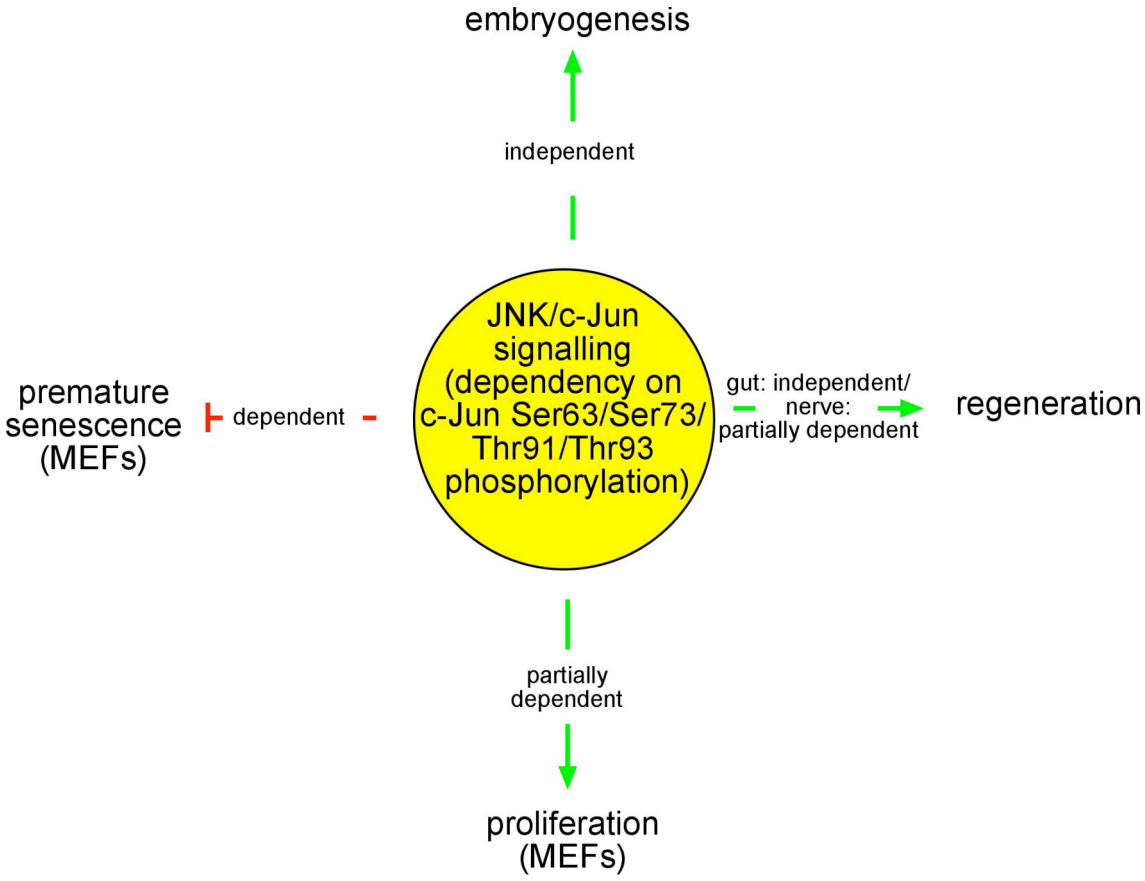

Figure 66 Dependency of c-Jun functions on Ser63/Ser73/Thr91/Thr93 phosphorylation by JNK
Schematic representation of c-Jun functions and their dependency on N-terminal phosphorylation of c-Jun at serine 63, serine 73, threonine 91 and threonine 93 by JNK. Green lines point towards actions promoted by JNK/c-Jun, red lines point towards actions inhibited by JNK/c-Jun.

Reference List

ABLES, J. L., DECAROLIS, N. A., JOHNSON, M. A., RIVERA, P. D., GAO, Z., COOPER, D. C., RADTKE, F., HSIEH, J. & EISCH, A. J. (2010) Notch1 is required for maintenance of the reservoir of adult hippocampal stem cells. *J Neurosci,* 30**,** 10484-92.

ABOITIZ, F. & MONTIEL, J. (2007) Co-option of signaling mechanisms from neural induction to telencephalic patterning. *Rev Neurosci,* 18**,** 311-42.

AGUILERA, C., NAKAGAWA, K., SANCHO, R., CHAKRABORTY, A., HENDRICH, B. & BEHRENS, A. (2011) c-Jun N-terminal phosphorylation antagonises recruitment of the Mbd3/NuRD repressor complex. *Nature,* 469**,** 231-5.

AGUIRRE, V., UCHIDA, T., YENUSH, L., DAVIS, R. & WHITE, M. F. (2000) The c-Jun NH(2)-terminal kinase promotes insulin resistance during association with insulin receptor substrate-1 and phosphorylation of Ser(307). *J Biol Chem,* 275**,** 9047-54.

AKHOONDI, S., SUN, D., VON DER LEHR, N., APOSTOLIDOU, S., KLOTZ, K., MALJUKOVA, A., CEPEDA, D., FIEGL, H., DAFOU, D., MARTH, C., MUELLER-HOLZNER, E., CORCORAN, M., DAGNELL, M., NEJAD, S. Z., NAYER, B. N., ZALI, M. R., HANSSON, J., EGYHAZI, S., PETERSSON, F., SANGFELT, P., NORDGREN, H., GRANDER, D., REED, S. I., WIDSCHWENDTER, M., SANGFELT, O. & SPRUCK, C. (2007) FBXW7/hCDC4 is a general tumor suppressor in human cancer. *Cancer Res,* 67**,** 9006-12.

ALPER, J. (2009) Geron gets green light for human trial of ES cell-derived product. *Nat Biotechnol,* 27**,** 213-4.

ANDERSON, S. A., MARIN, O., HORN, C., JENNINGS, K. & RUBENSTEIN, J. L. (2001) Distinct cortical migrations from the medial and lateral ganglionic eminences. *Development,* 128**,** 353-63.

ANGEL, P., ALLEGRETTO, E. A., OKINO, S. T., HATTORI, K., BOYLE, W. J., HUNTER, T. & KARIN, M. (1988a) Oncogene jun encodes a sequence-specific trans-activator similar to AP-1. *Nature,* 332**,** 166-71.

ANGEL, P., HATTORI, K., SMEAL, T. & KARIN, M. (1988b) The jun proto-oncogene is positively autoregulated by its product, Jun/AP-1. *Cell,* 55**,** 875-85.

ANGEL, P., IMAGAWA, M., CHIU, R., STEIN, B., IMBRA, R. J., RAHMSDORF, H. J., JONAT, C., HERRLICH, P. & KARIN, M. (1987) Phorbol ester-inducible genes contain a common cis element recognized by a TPA-modulated trans-acting factor. *Cell,* 49**,** 729-39.

ANTHONY, T. E., MASON, H. A., GRIDLEY, T., FISHELL, G. & HEINTZ, N. (2005) Brain lipid-binding protein is a direct target of Notch signaling in radial glial cells. *Genes Dev,* 19**,** 1028-33.

APELQVIST, A., LI, H., SOMMER, L., BEATUS, P., ANDERSON, D. J., HONJO, T., HRABE DE ANGELIS, M., LENDAHL, U. & EDLUND, H. (1999) Notch signalling controls pancreatic cell differentiation. *Nature,* 400**,** 877-81.

ARTAVANIS-TSAKONAS, S., MATSUNO, K. & FORTINI, M. E. (1995) Notch signaling. *Science,* 268**,** 225-32.

ARTAVANIS-TSAKONAS, S., MUSKAVITCH, M. A. & YEDVOBNICK, B. (1983) Molecular cloning of Notch, a locus affecting neurogenesis in Drosophila melanogaster. *Proc Natl Acad Sci U S A,* 80**,** 1977-81.

ARTAVANIS-TSAKONAS, S., RAND, M. D. & LAKE, R. J. (1999) Notch signaling: cell fate control and signal integration in development. *Science,* 284**,** 770-6.

ASCANO, J. M., BEVERLY, L. J. & CAPOBIANCO, A. J. (2003) The C-terminal PDZ-ligand of JAGGED1 is essential for cellular transformation. *J Biol Chem,* 278**,** 8771-9.

ATADJA, P., WONG, H., GARKAVTSEV, I., VEILLETTE, C. & RIABOWOL, K. (1995) Increased activity of p53 in senescing fibroblasts. *Proc Natl Acad Sci U S A,* 92**,** 8348-52.

AXELROD, J. D., MATSUNO, K., ARTAVANIS-TSAKONAS, S. & PERRIMON, N. (1996) Interaction between Wingless and Notch signaling pathways mediated by dishevelled. *Science,* 271**,** 1826-32.

BAHRAM, F., VON DER LEHR, N., CETINKAYA, C. & LARSSON, L. G. (2000) c-Myc hot spot mutations in lymphomas result in inefficient ubiquitination and decreased proteasome-mediated turnover. *Blood,* 95**,** 2104-10.

BAI, C., SEN, P., HOFMANN, K., MA, L., GOEBL, M., HARPER, J. W. & ELLEDGE, S. J. (1996) SKP1 connects cell cycle regulators to the ubiquitin proteolysis machinery through a novel motif, the F-box. *Cell,* 86**,** 263-74.

BAIN, G., RAY, W. J., YAO, M. & GOTTLIEB, D. I. (1996) Retinoic acid promotes neural and represses mesodermal gene expression in mouse embryonic stem cells in culture. *Biochem Biophys Res Commun,* 223**,** 691-4.

BARBERI, T., KLIVENYI, P., CALINGASAN, N. Y., LEE, H., KAWAMATA, H., LOONAM, K., PERRIER, A. L., BRUSES, J., RUBIO, M. E., TOPF, N., TABAR, V., HARRISON, N. L., BEAL, M. F., MOORE, M. A. & STUDER, L. (2003) Neural subtype specification of fertilization and nuclear transfer embryonic stem cells and application in parkinsonian mice. *Nat Biotechnol,* 21**,** 1200-7.

BAROLO, S., WALKER, R. G., POLYANOVSKY, A. D., FRESCHI, G., KEIL, T. & POSAKONY, J. W. (2000) A notch-independent activity of suppressor of hairless is required for normal mechanoreceptor physiology. *Cell,* 103**,** 957-69.

BASAK, O. & TAYLOR, V. (2007) Identification of self-replicating multipotent progenitors in the embryonic nervous system by high Notch activity and Hes5 expression. *Eur J Neurosci,* 25**,** 1006-22.

BEGLEY, C. G., APLAN, P. D., DENNING, S. M., HAYNES, B. F., WALDMANN, T. A. & KIRSCH, I. R. (1989) The gene SCL is expressed during early hematopoiesis and encodes a differentiation-related DNA-binding motif. *Proc Natl Acad Sci U S A,* 86**,** 10128-32.

BEHRENS, A., JOCHUM, W., SIBILIA, M. & WAGNER, E. F. (2000) Oncogenic transformation by ras and fos is mediated by c-Jun N-terminal phosphorylation. *Oncogene,* 19**,** 2657-63.

BEHRENS, A., SABAPATHY, K., GRAEF, I., CLEARY, M., CRABTREE, G. R. & WAGNER, E. F. (2001) Jun N-terminal kinase 2 modulates thymocyte apoptosis and T cell activation through c-Jun and nuclear factor of activated T cell (NF-AT). *Proc Natl Acad Sci U S A,* 98**,** 1769-74.

BEHRENS, A., SIBILIA, M. & WAGNER, E. F. (1999) Amino-terminal phosphorylation of c-Jun regulates stress-induced apoptosis and cellular proliferation. *Nat Genet,* 21**,** 326-9.

BEN-HUR, T., IDELSON, M., KHANER, H., PERA, M., REINHARTZ, E., ITZIK, A. & REUBINOFF, B. E. (2004) Transplantation of human embryonic stem cell-derived neural progenitors improves behavioral deficit in Parkinsonian rats. *Stem Cells,* 22**,** 1246-55.

BENBROOK, D. M. & JONES, N. C. (1990) Heterodimer formation between CREB and JUN proteins. *Oncogene,* 5**,** 295-302.

BENNETT, G. D., LAU, F., CALVIN, J. A. & FINNELL, R. H. (1997) Phenytoin-induced teratogenesis: a molecular basis for the observed developmental delay during neurulation. *Epilepsia,* 38**,** 415-23.

BERDNIK, D., TOROK, T., GONZALEZ-GAITAN, M. & KNOBLICH, J. A. (2002) The endocytic protein alpha-Adaptin is required for numb-mediated asymmetric cell division in Drosophila. *Dev Cell,* 3**,** 221-31.

BEREZOVSKA, O., MCLEAN, P., KNOWLES, R., FROSH, M., LU, F. M., LUX, S. E. & HYMAN, B. T. (1999) Notch1 inhibits neurite outgrowth in postmitotic primary neurons. *Neuroscience,* 93**,** 433-9.

BERNSTEIN, B. E., MIKKELSEN, T. S., XIE, X., KAMAL, M., HUEBERT, D. J., CUFF, J., FRY, B., MEISSNER, A., WERNIG, M., PLATH, K., JAENISCH, R., WAGSCHAL, A., FEIL, R., SCHREIBER, S. L. & LANDER, E. S. (2006) A bivalent chromatin structure marks key developmental genes in embryonic stem cells. *Cell,* 125**,** 315-26.

BLANK, J. L., GERWINS, P., ELLIOTT, E. M., SATHER, S. & JOHNSON, G. L. (1996) Molecular cloning of mitogen-activated protein/ERK kinase kinases (MEKK) 2 and 3. Regulation of sequential phosphorylation pathways involving mitogen-activated protein kinase and c-Jun kinase. *J Biol Chem,* 271**,** 5361-8.

BOGOYEVITCH, M. A., BOEHM, I., OAKLEY, A., KETTERMAN, A. J. & BARR, R. K. (2004) Targeting the JNK MAPK cascade for inhibition: basic science and therapeutic potential. *Biochim Biophys Acta,* 1697**,** 89-101.

BOHMANN, D., BOS, T. J., ADMON, A., NISHIMURA, T., VOGT, P. K. & TJIAN, R. (1987) Human proto-oncogene c-jun encodes a DNA binding protein with structural and functional properties of transcription factor AP-1. *Science,* 238**,** 1386-92.

BOLLI, R., CHUGH, A. R., D'AMARIO, D., LOUGHRAN, J. H., STODDARD, M. F., IKRAM, S., BEACHE, G. M., WAGNER, S. G., LERI, A., HOSODA, T., SANADA, F., ELMORE, J. B., GOICHBERG, P., CAPPETTA, D., SOLANKHI, N. K., FAHSAH, I., ROKOSH, D. G., SLAUGHTER, M. S., KAJSTURA, J. & ANVERSA, P. (2011) Cardiac stem cells in patients with ischaemic cardiomyopathy (SCIPIO): initial results of a randomised phase 1 trial. *Lancet,* 378**,** 1847-57.

BOND, J., HAUGHTON, M., BLAYDES, J., GIRE, V., WYNFORD-THOMAS, D. & WYLLIE, F. (1996) Evidence that transcriptional activation by p53 plays a direct role in the induction of cellular senescence. *Oncogene,* 13**,** 2097-104.

BORSELLO, T. & FORLONI, G. (2007) JNK signalling: a possible target to prevent neurodegeneration. *Curr Pharm Des,* 13**,** 1875-86.

BOSSY-WETZEL, E., BAKIRI, L. & YANIV, M. (1997) Induction of apoptosis by the transcription factor c-Jun. *EMBO J,* 16**,** 1695-709.

BOYER, L. A., PLATH, K., ZEITLINGER, J., BRAMBRINK, T., MEDEIROS, L. A., LEE, T. I., LEVINE, S. S., WERNIG, M., TAJONAR, A., RAY, M. K., BELL, G. W., OTTE, A. P., VIDAL, M., GIFFORD, D. K., YOUNG, R. A. & JAENISCH, R. (2006) Polycomb complexes repress developmental regulators in murine embryonic stem cells. *Nature,* 441**,** 349-53.

BOZTUG, K., SCHMIDT, M., SCHWARZER, A., BANERJEE, P. P., DIEZ, I. A., DEWEY, R. A., BOHM, M., NOWROUZI, A., BALL, C. R., GLIMM, H., NAUNDORF, S., KUHLCKE, K., BLASCZYK, R., KONDRATENKO, I., MARODI, L., ORANGE, J. S., VON KALLE, C. & KLEIN, C. (2010) Stem-cell gene therapy for the Wiskott-Aldrich syndrome. *N Engl J Med,* 363**,** 1918-27.

BRAY, S. J. (2006) Notch signalling: a simple pathway becomes complex. *Nat Rev Mol Cell Biol,* 7**,** 678-89.

BRENNAN, K., TATESON, R., LEWIS, K. & ARIAS, A. M. (1997) A functional analysis of Notch mutations in Drosophila. *Genetics,* 147**,** 177-88.

BREUNIG, J. J., SILBEREIS, J., VACCARINO, F. M., SESTAN, N. & RAKIC, P. (2007) Notch regulates cell fate and dendrite morphology of newborn neurons in the postnatal dentate gyrus. *Proc Natl Acad Sci U S A,* 104**,** 20558-63.

BROLEN, G. K., HEINS, N., EDSBAGGE, J. & SEMB, H. (2005) Signals from the embryonic mouse pancreas induce differentiation of human embryonic stem cells into insulin-producing beta-cell-like cells. *Diabetes,* 54**,** 2867-74.

BROU, C., LOGEAT, F., GUPTA, N., BESSIA, C., LEBAIL, O., DOEDENS, J. R., CUMANO, A., ROUX, P., BLACK, R. A. & ISRAEL, A. (2000) A novel proteolytic cleavage involved in Notch signaling: the role of the disintegrin-metalloprotease TACE. *Mol Cell,* 5**,** 207-16.

BRUCKNER, K., PEREZ, L., CLAUSEN, H. & COHEN, S. (2000) Glycosyltransferase activity of Fringe modulates Notch-Delta interactions. *Nature,* 406**,** 411-5.

BUSS, R. R. & OPPENHEIM, R. W. (2004) Role of programmed cell death in normal neuronal development and function. *Anat Sci Int,* 79**,** 191-7.

CALHOUN, E. S., JONES, J. B., ASHFAQ, R., ADSAY, V., BAKER, S. J., VALENTINE, V., HEMPEN, P. M., HILGERS, W., YEO, C. J., HRUBAN, R. H. & KERN, S. E. (2003) BRAF and FBXW7 (CDC4, FBW7, AGO, SEL10) mutations in distinct subsets of pancreatic cancer: potential therapeutic targets. *Am J Pathol,* 163**,** 1255-60.

CALVI, L. M., ADAMS, G. B., WEIBRECHT, K. W., WEBER, J. M., OLSON, D. P., KNIGHT, M. C., MARTIN, R. P., SCHIPANI, E., DIVIETI, P., BRINGHURST, F. R., MILNER, L. A., KRONENBERG, H. M. & SCADDEN, D. T. (2003) Osteoblastic cells regulate the haematopoietic stem cell niche. *Nature,* 425**,** 841-6.

CAMPOS, L. S., DUARTE, A. J., BRANCO, T. & HENRIQUE, D. (2001) mDll1 and mDll3 expression in the developing mouse brain: role in the establishment of the early cortex. *J Neurosci Res,* 64**,** 590-8.

CAPELLO, E., VUOLO, L., GUALANDI, F., VAN LINT, M. T., ROCCATAGLIATA, L., BONZANO, L., PARDINI, M., UCCELLI, A. & MANCARDI, G. (2009) Autologous haematopoietic stem-cell transplantation in multiple sclerosis: benefits and risks. *Neurol Sci,* 30 Suppl 2**,** S175-7.

CARPENTER, M. K., INOKUMA, M. S., DENHAM, J., MUJTABA, T., CHIU, C. P. & RAO, M. S. (2001) Enrichment of neurons and neural precursors from human embryonic stem cells. *Exp Neurol,* 172**,** 383-97.

CASANOVA, E., GARATE, C., OVALLE, S., CALVO, P. & CHINCHETRU, M. A. (1996) Identification of four splice variants of the mouse stress-activated protein kinase JNK/SAPK alpha-isoform. *Neuroreport,* 7**,** 1320-4.

CASTRO, B., BAROLO, S., BAILEY, A. M. & POSAKONY, J. W. (2005) Lateral inhibition in proneural clusters: cis-regulatory logic and default repression by Suppressor of Hairless. *Development,* 132**,** 3333-44.

CAU, E. & BLADER, P. (2009) Notch activity in the nervous system: to switch or not switch? *Neural Dev,* 4**,** 36.

CHAMBERS, C. B., PENG, Y., NGUYEN, H., GAIANO, N., FISHELL, G. & NYE, J. S. (2001) Spatiotemporal selectivity of response to Notch1 signals in mammalian forebrain precursors. *Development,* 128**,** 689-702.

CHAMBERS, I., COLBY, D., ROBERTSON, M., NICHOLS, J., LEE, S., TWEEDIE, S. & SMITH, A. (2003) Functional expression cloning of Nanog, a pluripotency sustaining factor in embryonic stem cells. *Cell,* 113**,** 643-55.

CHANAS-SACRE, G., THIRY, M., PIRARD, S., ROGISTER, B., MOONEN, G., MBEBI, C., VERDIERE-SAHUQUE, M. & LEPRINCE, P. (2000) A 295-kDA intermediate filament-associated protein in radial glia and developing muscle cells in vivo and in vitro. *Dev Dyn,* 219**,** 514-25.

CHANG, L., JONES, Y., ELLISMAN, M. H., GOLDSTEIN, L. S. & KARIN, M. (2003) JNK1 is required for maintenance of neuronal microtubules and controls phosphorylation of microtubule-associated proteins. *Dev Cell,* 4**,** 521-33.

CHANG, L. & KARIN, M. (2001) Mammalian MAP kinase signalling cascades. *Nature,* 410**,** 37-40.

CHAZAUD, C., YAMANAKA, Y., PAWSON, T. & ROSSANT, J. (2006) Early lineage segregation between epiblast and primitive endoderm in mouse blastocysts through the Grb2-MAPK pathway. *Dev Cell,* 10**,** 615-24.

CHEN, N. & GREENWALD, I. (2004) The lateral signal for LIN-12/Notch in C. elegans vulval development comprises redundant secreted and transmembrane DSL proteins. *Dev Cell,* 6**,** 183-92.

CHENG, J., YANG, J., XIA, Y., KARIN, M. & SU, B. (2000) Synergistic interaction of MEK kinase 2, c-Jun N-terminal kinase (JNK) kinase 2, and JNK1 results in efficient and specific JNK1 activation. *Mol Cell Biol,* 20**,** 2334-42.

CHITNIS, A., HENRIQUE, D., LEWIS, J., ISH-HOROWICZ, D. & KINTNER, C. (1995) Primary neurogenesis in Xenopus embryos regulated by a homologue of the Drosophila neurogenic gene Delta. *Nature,* 375**,** 761-6.

CIANI, L. & SALINAS, P. C. (2005) WNTs in the vertebrate nervous system: from patterning to neuronal connectivity. *Nat Rev Neurosci,* 6**,** 351-62.

CIOFANI, M., SCHMITT, T. M., CIOFANI, A., MICHIE, A. M., CUBURU, N., AUBLIN, A., MARYANSKI, J. L. & ZUNIGA-PFLUCKER, J. C. (2004) Obligatory role for cooperative signaling by pre-TCR and Notch during thymocyte differentiation. *J Immunol,* 172**,** 5230-9.

CLURMAN, B. E., SHEAFF, R. J., THRESS, K., GROUDINE, M. & ROBERTS, J. M. (1996) Turnover of cyclin E by the ubiquitin-proteasome pathway is regulated by cdk2 binding and cyclin phosphorylation. *Genes Dev,* 10**,** 1979-90.

COHEN, D. R. & CURRAN, T. (1988) fra-1: a serum-inducible, cellular immediate-early gene that encodes a fos-related antigen. *Mol Cell Biol,* 8**,** 2063-9.

COHEN, P. & FRAME, S. (2001) The renaissance of GSK3. *Nat Rev Mol Cell Biol,* 2**,** 769-76.

CONLON, R. A., REAUME, A. G. & ROSSANT, J. (1995) Notch1 is required for the coordinate segmentation of somites. *Development,* 121**,** 1533-45.

CORBIN, J. G., GAIANO, N., JULIANO, S. L., POLUCH, S., STANCIK, E. & HAYDAR, T. F. (2008) Regulation of neural progenitor cell development in the nervous system. *J Neurochem,* 106**,** 2272-87.

CORBIN, J. G., NERY, S. & FISHELL, G. (2001) Telencephalic cells take a tangent: non-radial migration in the mammalian forebrain. *Nat Neurosci,* 4 Suppl**,** 1177-82.

CROSSLEY, P. H., MARTINEZ, S. & MARTIN, G. R. (1996) Midbrain development induced by FGF8 in the chick embryo. *Nature,* 380**,** 66-8.

CRUSIO, K. M., KING, B., REAVIE, L. B. & AIFANTIS, I. (2010) The ubiquitous nature of cancer: the role of the SCF(Fbw7) complex in development and transformation. *Oncogene,* 29**,** 4865-73.

CURRAN, T., PETERS, G., VAN BEVEREN, C., TEICH, N. M. & VERMA, I. M. (1982) FBJ murine osteosarcoma virus: identification and molecular cloning of biologically active proviral DNA. *J Virol,* 44**,** 674-82.

CURRAN, T. & TEICH, N. M. (1982a) Candidate product of the FBJ murine osteosarcoma virus oncogene: characterization of a 55,000-dalton phosphoprotein. *J Virol,* 42**,** 114-22.

CURRAN, T. & TEICH, N. M. (1982b) Identification of a 39,000-dalton protein in cells transformed by the FBJ murine osteosarcoma virus. *Virology,* 116**,** 221-35.

D'AMOUR, K. A., BANG, A. G., ELIAZER, S., KELLY, O. G., AGULNICK, A. D., SMART, N. G., MOORMAN, M. A., KROON, E., CARPENTER, M. K. & BAETGE, E. E. (2006) Production of pancreatic hormone-expressing endocrine cells from human embryonic stem cells. *Nat Biotechnol,* 24**,** 1392-401.

DAHL, D., RUEGER, D. C., BIGNAMI, A., WEBER, K. & OSBORN, M. (1981) Vimentin, the 57 000 molecular weight protein of fibroblast filaments, is the major cytoskeletal component in immature glia. *Eur J Cell Biol,* 24**,** 191-6.

DAVIS, R. J. (1995) Transcriptional regulation by MAP kinases. *Mol Reprod Dev,* 42**,** 459-67.

DAVIS, R. J. (2000) Signal transduction by the JNK group of MAP kinases. *Cell,* 103**,** 239-52.

DAVIS, R. P., NG, E. S., COSTA, M., MOSSMAN, A. K., SOURRIS, K., ELEFANTY, A. G. & STANLEY, E. G. (2008) Targeting a GFP reporter gene to the MIXL1 locus of human embryonic stem cells identifies human primitive streak-like cells and enables isolation of primitive hematopoietic precursors. *Blood,* 111**,** 1876-84.

DE JOUSSINEAU, C., SOULE, J., MARTIN, M., ANGUILLE, C., MONTCOURRIER, P. & ALEXANDRE, D. (2003) Delta-promoted filopodia mediate long-range lateral inhibition in Drosophila. *Nature,* 426**,** 555-9.

DE LA POMPA, J. L., WAKEHAM, A., CORREIA, K. M., SAMPER, E., BROWN, S., AGUILERA, R. J., NAKANO, T., HONJO, T., MAK, T. W., ROSSANT, J. & CONLON, R. A. (1997) Conservation of the Notch signalling pathway in mammalian neurogenesis. *Development,* 124**,** 1139-48.

DE LA ROSA, E. J. & DE PABLO, F. (2000) Cell death in early neural development: beyond the neurotrophic theory. *Trends Neurosci,* 23**,** 454-8.

DEL BARCO BARRANTES, I., DAVIDSON, G., GRONE, H. J., WESTPHAL, H. & NIEHRS, C. (2003) Dkk1 and noggin cooperate in mammalian head induction. *Genes Dev,* 17**,** 2239-44.

DERIJARD, B., HIBI, M., WU, I. H., BARRETT, T., SU, B., DENG, T., KARIN, M. & DAVIS, R. J. (1994) JNK1: a protein kinase stimulated by UV light and Ha-Ras that binds and phosphorylates the c-Jun activation domain. *Cell,* 76**,** 1025-37.

DESAI, A. R. & MCCONNELL, S. K. (2000) Progressive restriction in fate potential by neural progenitors during cerebral cortical development. *Development,* 127**,** 2863-72.

DEXTER, J. S. (1914) The analysis of a case of continuous variation in Drosophila by a study of its linkage relations. [Salem, Mass.,, Columbia university, 1914.

DHARA, S. K. & STICE, S. L. (2008) Neural differentiation of human embryonic stem cells. *J Cell Biochem,* 105**,** 633-40.

DOE, C. Q. & GOODMAN, C. S. (1985) Early events in insect neurogenesis. II. The role of cell interactions and cell lineage in the determination of neuronal precursor cells. *Dev Biol,* 111**,** 206-19.

DOLGIN, E. (2011) Flaw in induced-stem-cell model. *Nature,* 470**,** 13.

DOMENGA, V., FARDOUX, P., LACOMBE, P., MONET, M., MACIAZEK, J., KREBS, L. T., KLONJKOWSKI, B., BERROU, E., MERICSKAY, M., LI, Z., TOURNIER-LASSERVE, E., GRIDLEY, T. & JOUTEL, A. (2004) Notch3 is required for arterial identity and maturation of vascular smooth muscle cells. *Genes Dev,* 18**,** 2730-5.

DONG, C., YANG, D. D., WYSK, M., WHITMARSH, A. J., DAVIS, R. J. & FLAVELL, R. A. (1998) Defective T cell differentiation in the absence of Jnk1. *Science,* 282**,** 2092-5.

DRAGUNOW, M., XU, R., WALTON, M., WOODGATE, A., LAWLOR, P., MACGIBBON, G. A., YOUNG, D., GIBBONS, H., LIPSKI, J., MURAVLEV, A., PEARSON, A. & DURING, M. (2000) c-Jun promotes neurite outgrowth and survival in PC12 cells. *Brain Res Mol Brain Res,* 83**,** 20-33.

DUARTE, A., HIRASHIMA, M., BENEDITO, R., TRINDADE, A., DINIZ, P., BEKMAN, E., COSTA, L., HENRIQUE, D. & ROSSANT, J. (2004) Dosage-sensitive requirement for mouse Dll4 in artery development. *Genes Dev,* 18**,** 2474-8.

DUNCAN, A. W., RATTIS, F. M., DIMASCIO, L. N., CONGDON, K. L., PAZIANOS, G., ZHAO, C., YOON, K., COOK, J. M., WILLERT, K., GAIANO, N. & REYA, T. (2005) Integration of Notch and Wnt signaling in hematopoietic stem cell maintenance. *Nat Immunol,* 6**,** 314-22.

DUNN, C., WILTSHIRE, C., MACLAREN, A. & GILLESPIE, D. A. (2002) Molecular mechanism and biological functions of c-Jun N-terminal kinase signalling via the c-Jun transcription factor. *Cell Signal,* 14**,** 585-93.

DZIERZAK, E. & SPECK, N. A. (2008) Of lineage and legacy: the development of mammalian hematopoietic stem cells. *Nat Immunol,* 9**,** 129-36.

EDWARDS, M. A., YAMAMOTO, M. & CAVINESS, V. S., JR. (1990) Organization of radial glia and related cells in the developing murine CNS. An analysis based upon a new monoclonal antibody marker. *Neuroscience,* 36**,** 121-44.

EFERL, R. & WAGNER, E. F. (2003) AP-1: a double-edged sword in tumorigenesis. *Nat Rev Cancer,* 3**,** 859-68.

EHM, O., GORITZ, C., COVIC, M., SCHAFFNER, I., SCHWARZ, T. J., KARACA, E., KEMPKES, B., KREMMER, E., PFRIEGER, F. W., ESPINOSA, L., BIGAS, A., GIACHINO, C., TAYLOR, V., FRISEN, J. & LIE, D. C. (2010) RBPJkappa-dependent signaling is essential for long-term maintenance of neural stem cells in the adult hippocampus. *J Neurosci,* 30**,** 13794-807.

ELKABETZ, Y., PANAGIOTAKOS, G., AL SHAMY, G., SOCCI, N. D., TABAR, V. & STUDER, L. (2008) Human ES cell-derived neural rosettes reveal a functionally distinct early neural stem cell stage. *Genes Dev,* 22**,** 152-65.

ENGLISH, J. M., VANDERBILT, C. A., XU, S., MARCUS, S. & COBB, M. H. (1995) Isolation of MEK5 and differential expression of alternatively spliced forms. *J Biol Chem,* 270**,** 28897-902.

ENGLUND, C., FINK, A., LAU, C., PHAM, D., DAZA, R. A., BULFONE, A., KOWALCZYK, T. & HEVNER, R. F. (2005) Pax6, Tbr2, and Tbr1 are expressed sequentially by radial glia, intermediate progenitor cells, and postmitotic neurons in developing neocortex. *J Neurosci,* 25**,** 247-51.

ESCUDERO, L. M., WEI, S. Y., CHIU, W. H., MODOLELL, J. & HSU, J. C. (2003) Echinoid synergizes with the Notch signaling pathway in Drosophila mesothorax bristle patterning. *Development,* 130**,** 6305-16.

EVANS, M. J. & KAUFMAN, M. H. (1981) Establishment in culture of pluripotential cells from mouse embryos. *Nature,* 292**,** 154-6.

FELDMAN, R. M., CORRELL, C. C., KAPLAN, K. B. & DESHAIES, R. J. (1997) A complex of Cdc4p, Skp1p, and Cdc53p/cullin catalyzes ubiquitination of the phosphorylated CDK inhibitor Sic1p. *Cell,* 91**,** 221-30.

FENG, L., HATTEN, M. E. & HEINTZ, N. (1994) Brain lipid-binding protein (BLBP): a novel signaling system in the developing mammalian CNS. *Neuron,* 12**,** 895-908.

FISCHER, A., SCHUMACHER, N., MAIER, M., SENDTNER, M. & GESSLER, M. (2004) The Notch target genes Hey1 and Hey2 are required for embryonic vascular development. *Genes Dev,* 18**,** 901-11.

FOLETTA, V. C., SONOBE, M. H., SUZUKI, T., ENDO, T., IBA, H. & COHEN, D. R. (1994) Cloning and characterisation of the mouse fra-2 gene. *Oncogene,* 9**,** 3305-11.

FORTINI, M. E. (2001) Notch and presenilin: a proteolytic mechanism emerges. *Curr Opin Cell Biol,* 13**,** 627-34.

FORTINI, M. E. (2002) Gamma-secretase-mediated proteolysis in cell-surface-receptor signalling. *Nat Rev Mol Cell Biol,* 3**,** 673-84.

FRANTZ, G. D. & MCCONNELL, S. K. (1996) Restriction of late cerebral cortical progenitors to an upper-layer fate. *Neuron,* 17**,** 55-61.

FRANZA, B. R., JR., RAUSCHER, F. J., 3RD, JOSEPHS, S. F. & CURRAN, T. (1988) The Fos complex and Fos-related antigens recognize sequence elements that contain AP-1 binding sites. *Science,* 239**,** 1150-3.

FRE, S., HUYGHE, M., MOURIKIS, P., ROBINE, S., LOUVARD, D. & ARTAVANIS-TSAKONAS, S. (2005) Notch signals control the fate of immature progenitor cells in the intestine. *Nature,* 435**,** 964-8.

FREED, C. R., GREENE, P. E., BREEZE, R. E., TSAI, W. Y., DUMOUCHEL, W., KAO, R., DILLON, S., WINFIELD, H., CULVER, S., TROJANOWSKI, J. Q.,

EIDELBERG, D. & FAHN, S. (2001) Transplantation of embryonic dopamine neurons for severe Parkinson's disease. *N Engl J Med,* 344**,** 710-9.

FRYER, C. J., LAMAR, E., TURBACHOVA, I., KINTNER, C. & JONES, K. A. (2002) Mastermind mediates chromatin-specific transcription and turnover of the Notch enhancer complex. *Genes Dev,* 16**,** 1397-411.

FRYER, C. J., WHITE, J. B. & JONES, K. A. (2004) Mastermind recruits CycC:CDK8 to phosphorylate the Notch ICD and coordinate activation with turnover. *Mol Cell,* 16**,** 509-20.

FURUKAWA, T., MUKHERJEE, S., BAO, Z. Z., MORROW, E. M. & CEPKO, C. L. (2000) rax, Hes1, and notch1 promote the formation of Muller glia by postnatal retinal progenitor cells. *Neuron,* 26**,** 383-94.

GADUE, P., HUBER, T. L., NOSTRO, M. C., KATTMAN, S. & KELLER, G. M. (2005) Germ layer induction from embryonic stem cells. *Exp Hematol,* 33**,** 955-64.

GAIANO, N. & FISHELL, G. (2002) The role of notch in promoting glial and neural stem cell fates. *Annu Rev Neurosci,* 25**,** 471-90.

GAIANO, N., NYE, J. S. & FISHELL, G. (2000) Radial glial identity is promoted by Notch1 signaling in the murine forebrain. *Neuron,* 26**,** 395-404.

GALE, N. W., DOMINGUEZ, M. G., NOGUERA, I., PAN, L., HUGHES, V., VALENZUELA, D. M., MURPHY, A. J., ADAMS, N. C., LIN, H. C., HOLASH, J., THURSTON, G. & YANCOPOULOS, G. D. (2004) Haploinsufficiency of delta-like 4 ligand results in embryonic lethality due to major defects in arterial and vascular development. *Proc Natl Acad Sci U S A,* 101**,** 15949-54.

GALIC, Z., KITCHEN, S. G., KACENA, A., SUBRAMANIAN, A., BURKE, B., CORTADO, R. & ZACK, J. A. (2006) T lineage differentiation from human embryonic stem cells. *Proc Natl Acad Sci U S A,* 103**,** 11742-7.

GALL, C., LAUTERBORN, J., ISACKSON, P. & WHITE, J. (1990) Seizures, neuropeptide regulation, and mRNA expression in the hippocampus. *Prog Brain Res,* 83**,** 371-90.

GAO, M., LABUDA, T., XIA, Y., GALLAGHER, E., FANG, D., LIU, Y. C. & KARIN, M. (2004) Jun turnover is controlled through JNK-dependent phosphorylation of the E3 ligase Itch. *Science,* 306**,** 271-5.

GASPARD, N., BOUSCHET, T., HOUREZ, R., DIMIDSCHSTEIN, J., NAEIJE, G., VAN DEN AMEELE, J., ESPUNY-CAMACHO, I., HERPOEL, A., PASSANTE, L., SCHIFFMANN, S. N., GAILLARD, A. & VANDERHAEGHEN, P. (2008) An intrinsic mechanism of corticogenesis from embryonic stem cells. *Nature,* 455**,** 351-7.

GASS, P., HERDEGEN, T., BRAVO, R. & KIESSLING, M. (1993) Spatiotemporal induction of immediate early genes in the rat brain after limbic seizures: effects of NMDA receptor antagonist MK-801. *Eur J Neurosci,* 5**,** 933-43.

GE, W., MARTINOWICH, K., WU, X., HE, F., MIYAMOTO, A., FAN, G., WEINMASTER, G. & SUN, Y. E. (2002) Notch signaling promotes astrogliogenesis via direct CSL-mediated glial gene activation. *J Neurosci Res,* 69**,** 848-60.

GERWINS, P., BLANK, J. L. & JOHNSON, G. L. (1997) Cloning of a novel mitogen-activated protein kinase kinase kinase, MEKK4, that selectively regulates the c-Jun amino terminal kinase pathway. *J Biol Chem,* 272**,** 8288-95.

GINIGER, E. (1998) A role for Abl in Notch signaling. *Neuron,* 20**,** 667-81.

GIUDICELLI, F. & LEWIS, J. (2004) The vertebrate segmentation clock. *Curr Opin Genet Dev,* 14**,** 407-14.

GLISE, B., BOURBON, H. & NOSELLI, S. (1995) hemipterous encodes a novel Drosophila MAP kinase kinase, required for epithelial cell sheet movement. *Cell,* 83**,** 451-61.

GOLDSMITH, E. J. & COBB, M. H. (1994) Protein kinases. *Curr Opin Struct Biol,* 4**,** 833-40.

GOMEZ-ROMAN, N., FELTON-EDKINS, Z. A., KENNETH, N. S., GOODFELLOW, S. J., ATHINEOS, D., ZHANG, J., RAMSBOTTOM, B. A., INNES, F., KANTIDAKIS, T., KERR, E. R., BRODIE, J., GRANDORI, C. & WHITE, R. J. (2006) Activation by c-Myc of transcription by RNA polymerases I, II and III. *Biochem Soc Symp***,** 141-54.

GOTZ, M. & HUTTNER, W. B. (2005) The cell biology of neurogenesis. *Nat Rev Mol Cell Biol,* 6**,** 777-88.

GOUON-EVANS, V., BOUSSEMART, L., GADUE, P., NIERHOFF, D., KOEHLER, C. I., KUBO, A., SHAFRITZ, D. A. & KELLER, G. (2006) BMP-4 is required for hepatic specification of mouse embryonic stem cell-derived definitive endoderm. *Nat Biotechnol,* 24**,** 1402-11.

GRAICHEN, R., XU, X., BRAAM, S. R., BALAKRISHNAN, T., NORFIZA, S., SIEH, S., SOO, S. Y., THAM, S. C., MUMMERY, C., COLMAN, A., ZWEIGERDT, R. & DAVIDSON, B. P. (2008) Enhanced cardiomyogenesis of human embryonic stem cells by a small molecular inhibitor of p38 MAPK. *Differentiation,* 76**,** 357-70.

GRANDBARBE, L., BOUISSAC, J., RAND, M., HRABE DE ANGELIS, M., ARTAVANIS-TSAKONAS, S. & MOHIER, E. (2003) Delta-Notch signaling controls the generation of neurons/glia from neural stem cells in a stepwise process. *Development,* 130**,** 1391-402.

GRANDORI, C., GOMEZ-ROMAN, N., FELTON-EDKINS, Z. A., NGOUENET, C., GALLOWAY, D. A., EISENMAN, R. N. & WHITE, R. J. (2005) c-Myc binds to human ribosomal DNA and stimulates transcription of rRNA genes by RNA polymerase I. *Nat Cell Biol,* 7**,** 311-8.

GREGORY, M. A. & HANN, S. R. (2000) c-Myc proteolysis by the ubiquitin-proteasome pathway: stabilization of c-Myc in Burkitt's lymphoma cells. *Mol Cell Biol,* 20**,** 2423-35.

GUPTA, S., BARRETT, T., WHITMARSH, A. J., CAVANAGH, J., SLUSS, H. K., DERIJARD, B. & DAVIS, R. J. (1996) Selective interaction of JNK protein kinase isoforms with transcription factors. *EMBO J,* 15**,** 2760-70.

GUPTA-ROSSI, N., LE BAIL, O., GONEN, H., BROU, C., LOGEAT, F., SIX, E., CIECHANOVER, A. & ISRAEL, A. (2001) Functional interaction between SEL-10, an F-box protein, and the nuclear form of activated Notch1 receptor. *J Biol Chem,* 276**,** 34371-8.

HADLAND, B. K., HUPPERT, S. S., KANUNGO, J., XUE, Y., JIANG, R., GRIDLEY, T., CONLON, R. A., CHENG, A. M., KOPAN, R. & LONGMORE, G. D. (2004) A requirement for Notch1 distinguishes 2 phases of definitive hematopoiesis during development. *Blood,* 104**,** 3097-105.

HADLAND, B. K., MANLEY, N. R., SU, D., LONGMORE, G. D., MOORE, C. L., WOLFE, M. S., SCHROETER, E. H. & KOPAN, R. (2001) Gamma -secretase

inhibitors repress thymocyte development. *Proc Natl Acad Sci U S A,* 98**,** 7487-91.

HAEUSGEN, W., BOEHM, R., ZHAO, Y., HERDEGEN, T. & WAETZIG, V. (2009) Specific activities of individual c-Jun N-terminal kinases in the brain. *Neuroscience,* 161**,** 951-9.

HAGEDORN, E. J., BAYRAKTAR, J. L., KANDACHAR, V. R., BAI, T., ENGLERT, D. M. & CHANG, H. C. (2006) Drosophila melanogaster auxilin regulates the internalization of Delta to control activity of the Notch signaling pathway. *J Cell Biol,* 173**,** 443-52.

HAGEDORN, M., DELUGIN, M., ABRALDES, I., ALLAIN, N., BELAUD-ROTUREAU, M. A., TURMO, M., PRIGENT, C., LOISEAU, H., BIKFALVI, A. & JAVERZAT, S. (2007) FBXW7/hCDC4 controls glioma cell proliferation in vitro and is a prognostic marker for survival in glioblastoma patients. *Cell Div,* 2**,** 9.

HAGELL, P., PICCINI, P., BJORKLUND, A., BRUNDIN, P., REHNCRONA, S., WIDNER, H., CRABB, L., PAVESE, N., OERTEL, W. H., QUINN, N., BROOKS, D. J. & LINDVALL, O. (2002) Dyskinesias following neural transplantation in Parkinson's disease. *Nat Neurosci,* 5**,** 627-8.

HAGEMANN, C. & BLANK, J. L. (2001) The ups and downs of MEK kinase interactions. *Cell Signal,* 13**,** 863-75.

HAI, T. & CURRAN, T. (1991) Cross-family dimerization of transcription factors Fos/Jun and ATF/CREB alters DNA binding specificity. *Proc Natl Acad Sci U S A,* 88**,** 3720-4.

HAINES, N. & IRVINE, K. D. (2003) Glycosylation regulates Notch signalling. *Nat Rev Mol Cell Biol,* 4**,** 786-97.

HALAZONETIS, T. D., GEORGOPOULOS, K., GREENBERG, M. E. & LEDER, P. (1988) c-Jun dimerizes with itself and with c-Fos, forming complexes of different DNA binding affinities. *Cell,* 55**,** 917-24.

HAM, J., BABIJ, C., WHITFIELD, J., PFARR, C. M., LALLEMAND, D., YANIV, M. & RUBIN, L. L. (1995) A c-Jun dominant negative mutant protects sympathetic neurons against programmed cell death. *Neuron,* 14**,** 927-39.

HAMADA, Y., KADOKAWA, Y., OKABE, M., IKAWA, M., COLEMAN, J. R. & TSUJIMOTO, Y. (1999) Mutation in ankyrin repeats of the mouse Notch2 gene induces early embryonic lethality. *Development,* 126**,** 3415-24.

HANASHIMA, C., LI, S. C., SHEN, L., LAI, E. & FISHELL, G. (2004) Foxg1 suppresses early cortical cell fate. *Science,* 303**,** 56-9.

HAO, B., OEHLMANN, S., SOWA, M. E., HARPER, J. W. & PAVLETICH, N. P. (2007) Structure of a Fbw7-Skp1-cyclin E complex: multisite-phosphorylated substrate recognition by SCF ubiquitin ligases. *Mol Cell,* 26**,** 131-43.

HARTFUSS, E., GALLI, R., HEINS, N. & GOTZ, M. (2001) Characterization of CNS precursor subtypes and radial glia. *Dev Biol,* 229**,** 15-30.

HARTWELL, L. H., MORTIMER, R. K., CULOTTI, J. & CULOTTI, M. (1973) Genetic Control of the Cell Division Cycle in Yeast: V. Genetic Analysis of cdc Mutants. *Genetics,* 74**,** 267-86.

HATAKEYAMA, J., BESSHO, Y., KATOH, K., OOKAWARA, S., FUJIOKA, M., GUILLEMOT, F. & KAGEYAMA, R. (2004) Hes genes regulate size, shape and histogenesis of the nervous system by control of the timing of neural stem cell differentiation. *Development,* 131**,** 5539-50.

HAUBENSAK, W., ATTARDO, A., DENK, W. & HUTTNER, W. B. (2004) Neurons arise in the basal neuroepithelium of the early mammalian telencephalon: a major site of neurogenesis. *Proc Natl Acad Sci U S A,* 101**,** 3196-201.

HAYDEN, E. C. (2011) Stem cells: The growing pains of pluripotency. *Nature,* 473**,** 272-4.

HAYWARD, P., BRENNAN, K., SANDERS, P., BALAYO, T., DASGUPTA, R., PERRIMON, N. & MARTINEZ ARIAS, A. (2005) Notch modulates Wnt signalling by associating with Armadillo/beta-catenin and regulating its transcriptional activity. *Development,* 132**,** 1819-30.

HENRIQUE, D., ADAM, J., MYAT, A., CHITNIS, A., LEWIS, J. & ISH-HOROWICZ, D. (1995) Expression of a Delta homologue in prospective neurons in the chick. *Nature,* 375**,** 787-90.

HENRIQUE, D., HIRSINGER, E., ADAM, J., LE ROUX, I., POURQUIE, O., ISH-HOROWICZ, D. & LEWIS, J. (1997) Maintenance of neuroepithelial progenitor cells by Delta-Notch signalling in the embryonic chick retina. *Curr Biol,* 7**,** 661-70.

HERDEGEN, T., KUMMER, W., FIALLOS, C. E., LEAH, J. & BRAVO, R. (1991) Expression of c-JUN, JUN B and JUN D proteins in rat nervous system following transection of vagus nerve and cervical sympathetic trunk. *Neuroscience,* 45**,** 413-22.

HERSHKO, A. (1983) Ubiquitin: roles in protein modification and breakdown. *Cell,* 34**,** 11-2.

HERZOG, K. H., CHEN, S. C. & MORGAN, J. I. (1999) c-jun Is dispensable for developmental cell death and axogenesis in the retina. *J Neurosci,* 19**,** 4349-59.

HIBI, M., LIN, A., SMEAL, T., MINDEN, A. & KARIN, M. (1993) Identification of an oncoprotein- and UV-responsive protein kinase that binds and potentiates the c-Jun activation domain. *Genes Dev,* 7**,** 2135-48.

HICKS, C., LADI, E., LINDSELL, C., HSIEH, J. J., HAYWARD, S. D., COLLAZO, A. & WEINMASTER, G. (2002) A secreted Delta1-Fc fusion protein functions both as an activator and inhibitor of Notch1 signaling. *J Neurosci Res,* 68**,** 655-67.

HILBERG, F., AGUZZI, A., HOWELLS, N. & WAGNER, E. F. (1993) c-jun is essential for normal mouse development and hepatogenesis. *Nature,* 365**,** 179-81.

HIRAI, S., IZAWA, M., OSADA, S., SPYROU, G. & OHNO, S. (1996) Activation of the JNK pathway by distantly related protein kinases, MEKK and MUK. *Oncogene,* 12**,** 641-50.

HIROSUMI, J., TUNCMAN, G., CHANG, L., GORGUN, C. Z., UYSAL, K. T., MAEDA, K., KARIN, M. & HOTAMISLIGIL, G. S. (2002) A central role for JNK in obesity and insulin resistance. *Nature,* 420**,** 333-6.

HITOSHI, S., ALEXSON, T., TROPEPE, V., DONOVIEL, D., ELIA, A. J., NYE, J. S., CONLON, R. A., MAK, T. W., BERNSTEIN, A. & VAN DER KOOY, D. (2002) Notch pathway molecules are essential for the maintenance, but not the generation, of mammalian neural stem cells. *Genes Dev,* 16**,** 846-58.

HOECK, J. D., JANDKE, A., BLAKE, S. M., NYE, E., SPENCER-DENE, B., BRANDNER, S. & BEHRENS, A. (2010) Fbw7 controls neural stem cell differentiation and progenitor apoptosis via Notch and c-Jun. *Nat Neurosci,* 13**,** 1365-72.

HOPE, I. A. & STRUHL, K. (1985) GCN4 protein, synthesized in vitro, binds HIS3 regulatory sequences: implications for general control of amino acid biosynthetic genes in yeast. *Cell,* 43**,** 177-88.

HORI, K., FOSTIER, M., ITO, M., FUWA, T. J., GO, M. J., OKANO, H., BARON, M. & MATSUNO, K. (2004) Drosophila deltex mediates suppressor of Hairless-independent and late-endosomal activation of Notch signaling. *Development,* 131**,** 5527-37.

HOTAMISLIGIL, G. S. (2003) Inflammatory pathways and insulin action. *Int J Obes Relat Metab Disord,* 27 Suppl 3**,** S53-5.

HOU, X. S., GOLDSTEIN, E. S. & PERRIMON, N. (1997) Drosophila Jun relays the Jun amino-terminal kinase signal transduction pathway to the Decapentaplegic signal transduction pathway in regulating epithelial cell sheet movement. *Genes Dev,* 11**,** 1728-37.

HRABE DE ANGELIS, M., MCINTYRE, J., 2ND & GOSSLER, A. (1997) Maintenance of somite borders in mice requires the Delta homologue DII1. *Nature,* 386**,** 717-21.

HSIEH, J. J., ZHOU, S., CHEN, L., YOUNG, D. B. & HAYWARD, S. D. (1999) CIR, a corepressor linking the DNA binding factor CBF1 to the histone deacetylase complex. *Proc Natl Acad Sci U S A,* 96**,** 23-8.

HUANG, E. J. & REICHARDT, L. F. (2001) Neurotrophins: roles in neuronal development and function. *Annu Rev Neurosci,* 24**,** 677-736.

HUBALEK, M. M., WIDSCHWENDTER, A., ERDEL, M., GSCHWENDTNER, A., FIEGL, H. M., MULLER, H. M., GOEBEL, G., MUELLER-HOLZNER, E., MARTH, C., SPRUCK, C. H., REED, S. I. & WIDSCHWENDTER, M. (2004) Cyclin E dysregulation and chromosomal instability in endometrial cancer. *Oncogene,* 23**,** 4187-92.

HUBBARD, E. J., WU, G., KITAJEWSKI, J. & GREENWALD, I. (1997) sel-10, a negative regulator of lin-12 activity in Caenorhabditis elegans, encodes a member of the CDC4 family of proteins. *Genes Dev,* 11**,** 3182-93.

HUDSON, C., LOTITO, S. & YASUO, H. (2007) Sequential and combinatorial inputs from Nodal, Delta2/Notch and FGF/MEK/ERK signalling pathways establish a grid-like organisation of distinct cell identities in the ascidian neural plate. *Development,* 134**,** 3527-37.

HUNOT, S., VILA, M., TEISMANN, P., DAVIS, R. J., HIRSCH, E. C., PRZEDBORSKI, S., RAKIC, P. & FLAVELL, R. A. (2004) JNK-mediated induction of cyclooxygenase 2 is required for neurodegeneration in a mouse model of Parkinson's disease. *Proc Natl Acad Sci U S A,* 101**,** 665-70.

ICHIJO, H., NISHIDA, E., IRIE, K., TEN DIJKE, P., SAITOH, M., MORIGUCHI, T., TAKAGI, M., MATSUMOTO, K., MIYAZONO, K. & GOTOH, Y. (1997) Induction of apoptosis by ASK1, a mammalian MAPKKK that activates SAPK/JNK and p38 signaling pathways. *Science,* 275**,** 90-4.

IMAYOSHI, I., SAKAMOTO, M., YAMAGUCHI, M., MORI, K. & KAGEYAMA, R. (2010) Essential roles of Notch signaling in maintenance of neural stem cells in developing and adult brains. *J Neurosci,* 30**,** 3489-98.

IRIUCHISHIMA, H., TAKUBO, K., MATSUOKA, S., ONOYAMA, I., NAKAYAMA, K. I., NOJIMA, Y. & SUDA, T. (2011) Ex vivo maintenance of hematopoietic stem cells by quiescence induction through Fbxw7α overexpression. *Blood,* 117**,** 2373-7.

IRVINE, K. D. (1999) Fringe, Notch, and making developmental boundaries. *Curr Opin Genet Dev,* 9**,** 434-41.

ISHIBASHI, M., ANG, S. L., SHIOTA, K., NAKANISHI, S., KAGEYAMA, R. & GUILLEMOT, F. (1995) Targeted disruption of mammalian hairy and Enhancer of split homolog-1 (HES-1) leads to up-regulation of neural helix-loop-helix factors, premature neurogenesis, and severe neural tube defects. *Genes Dev,* 9**,** 3136-48.

ISO, T., HAMAMORI, Y. & KEDES, L. (2003) Notch signaling in vascular development. *Arterioscler Thromb Vasc Biol,* 23**,** 543-53.

IVASHKIV, L. B., LIOU, H. C., KARA, C. J., LAMPH, W. W., VERMA, I. M. & GLIMCHER, L. H. (1990) mXBP/CRE-BP2 and c-Jun form a complex which binds to the cyclic AMP, but not to the 12-O-tetradecanoylphorbol-13-acetate, response element. *Mol Cell Biol,* 10**,** 1609-21.

JAESCHKE, A., CZECH, M. P. & DAVIS, R. J. (2004) An essential role of the JIP1 scaffold protein for JNK activation in adipose tissue. *Genes Dev,* 18**,** 1976-80.

JANDKE, A., DA COSTA, C., SANCHO, R., NYE, E., SPENCER-DENE, B. & BEHRENS, A. (2011) The F-box protein Fbw7 is required for cerebellar development. *Dev Biol*.

JARRIAULT, S. & GREENWALD, I. (2005) Evidence for functional redundancy between C. elegans ADAM proteins SUP-17/Kuzbanian and ADM-4/TACE. *Dev Biol,* 287**,** 1-10.

JENKINS, R. & HUNT, S. P. (1991) Long-term increase in the levels of c-jun mRNA and jun protein-like immunoreactivity in motor and sensory neurons following axon damage. *Neurosci Lett,* 129**,** 107-10.

JENSEN, J., HELLER, R. S., FUNDER-NIELSEN, T., PEDERSEN, E. E., LINDSELL, C., WEINMASTER, G., MADSEN, O. D. & SERUP, P. (2000) Independent development of pancreatic alpha- and beta-cells from neurogenin3-expressing precursors: a role for the notch pathway in repression of premature differentiation. *Diabetes,* 49**,** 163-76.

JIANG, R., LAN, Y., CHAPMAN, H. D., SHAWBER, C., NORTON, C. R., SERREZE, D. V., WEINMASTER, G. & GRIDLEY, T. (1998) Defects in limb, craniofacial, and thymic development in Jagged2 mutant mice. *Genes Dev,* 12**,** 1046-57.

JIANG, W., SHI, Y., ZHAO, D., CHEN, S., YONG, J., ZHANG, J., QING, T., SUN, X., ZHANG, P., DING, M., LI, D. & DENG, H. (2007) In vitro derivation of functional insulin-producing cells from human embryonic stem cells. *Cell Res,* 17**,** 333-44.

JOHNSON, M. H. & ZIOMEK, C. A. (1981) The foundation of two distinct cell lineages within the mouse morula. *Cell,* 24**,** 71-80.

JOHNSON, R. S., VAN LINGEN, B., PAPAIOANNOU, V. E. & SPIEGELMAN, B. M. (1993) A null mutation at the c-jun locus causes embryonic lethality and retarded cell growth in culture. *Genes Dev,* 7**,** 1309-17.

KAGEYAMA, R. & OHTSUKA, T. (1999) The Notch-Hes pathway in mammalian neural development. *Cell Res,* 9**,** 179-88.

KAGEYAMA, R., OHTSUKA, T., SHIMOJO, H. & IMAYOSHI, I. (2008) Dynamic Notch signaling in neural progenitor cells and a revised view of lateral inhibition. *Nat Neurosci,* 11**,** 1247-51.

KAMAKURA, S., OISHI, K., YOSHIMATSU, T., NAKAFUKU, M., MASUYAMA, N. & GOTOH, Y. (2004) Hes binding to STAT3 mediates crosstalk between Notch and JAK-STAT signalling. *Nat Cell Biol,* 6**,** 547-54.

KAO, H. Y., ORDENTLICH, P., KOYANO-NAKAGAWA, N., TANG, Z., DOWNES, M., KINTNER, C. R., EVANS, R. M. & KADESCH, T. (1998) A histone deacetylase corepressor complex regulates the Notch signal transduction pathway. *Genes Dev,* 12**,** 2269-77.

KAWAGUCHI, A., IKAWA, T., KASUKAWA, T., UEDA, H. R., KURIMOTO, K., SAITOU, M. & MATSUZAKI, F. (2008a) Single-cell gene profiling defines differential progenitor subclasses in mammalian neurogenesis. *Development,* 135**,** 3113-24.

KAWAGUCHI, D., YOSHIMATSU, T., HOZUMI, K. & GOTOH, Y. (2008b) Selection of differentiating cells by different levels of delta-like 1 among neural precursor cells in the developing mouse telencephalon. *Development,* 135**,** 3849-58.

KAWASAKI, H., MIZUSEKI, K., NISHIKAWA, S., KANEKO, S., KUWANA, Y., NAKANISHI, S., NISHIKAWA, S. I. & SASAI, Y. (2000) Induction of midbrain dopaminergic neurons from ES cells by stromal cell-derived inducing activity. *Neuron,* 28**,** 31-40.

KEARNS-JONKER, M., DAI, W. & KLONER, R. A. (2010) Stem cells for the treatment of heart failure. *Curr Opin Mol Ther,* 12**,** 432-41.

KEIRSTEAD, H. S., NISTOR, G., BERNAL, G., TOTOIU, M., CLOUTIER, F., SHARP, K. & STEWARD, O. (2005) Human embryonic stem cell-derived oligodendrocyte progenitor cell transplants remyelinate and restore locomotion after spinal cord injury. *J Neurosci,* 25**,** 4694-705.

KELLER, G. (2005) Embryonic stem cell differentiation: emergence of a new era in biology and medicine. *Genes Dev,* 19**,** 1129-55.

KENNEDY, M., D'SOUZA, S. L., LYNCH-KATTMAN, M., SCHWANTZ, S. & KELLER, G. (2007) Development of the hemangioblast defines the onset of hematopoiesis in human ES cell differentiation cultures. *Blood,* 109**,** 2679-87.

KIM, I. J., LEE, K. W., PARK, B. Y., LEE, J. K., PARK, J., CHOI, I. Y., EOM, S. J., CHANG, T. S., KIM, M. J., YEOM, Y. I., CHANG, S. K., LEE, Y. D., CHOI, E. J. & HAN, P. L. (1999) Molecular cloning of multiple splicing variants of JIP-1 preferentially expressed in brain. *J Neurochem,* 72**,** 1335-43.

KIM, J. H., AUERBACH, J. M., RODRIGUEZ-GOMEZ, J. A., VELASCO, I., GAVIN, D., LUMELSKY, N., LEE, S. H., NGUYEN, J., SANCHEZ-PERNAUTE, R., BANKIEWICZ, K. & MCKAY, R. (2002) Dopamine neurons derived from embryonic stem cells function in an animal model of Parkinson's disease. *Nature,* 418**,** 50-6.

KIM, K., DOI, A., WEN, B., NG, K., ZHAO, R., CAHAN, P., KIM, J., ARYEE, M. J., JI, H., EHRLICH, L. I., YABUUCHI, A., TAKEUCHI, A., CUNNIFF, K. C., HONGGUANG, H., MCKINNEY-FREEMAN, S., NAVEIRAS, O., YOON, T. J., IRIZARRY, R. A., JUNG, N., SEITA, J., HANNA, J., MURAKAMI, P., JAENISCH, R., WEISSLEDER, R., ORKIN, S. H., WEISSMAN, I. L., FEINBERG, A. P. & DALEY, G. Q. (2010) Epigenetic memory in induced pluripotent stem cells. *Nature,* 467**,** 285-90.

KIMURA, T., GOTOH, M., NAKAMURA, Y. & ARAKAWA, H. (2003) hCDC4b, a regulator of cyclin E, as a direct transcriptional target of p53. *Cancer Sci,* 94**,** 431-6.

KINDY, M. S., CARNEY, J. P., DEMPSEY, R. J. & CARNEY, J. M. (1991) Ischemic induction of protooncogene expression in gerbil brain. *J Mol Neurosci,* 2**,** 217-28.

KISHI, M., MIZUSEKI, K., SASAI, N., YAMAZAKI, H., SHIOTA, K., NAKANISHI, S. & SASAI, Y. (2000) Requirement of Sox2-mediated signaling for differentiation of early Xenopus neuroectoderm. *Development,* 127**,** 791-800.

KITAGAWA, K., KOTAKE, Y., HIRAMATSU, Y., LIU, N., SUZUKI, S., NAKAMURA, S., KIKUCHI, A. & KITAGAWA, M. (2010) GSK3 regulates the expressions of human and mouse c-Myb via different mechanisms. *Cell Div,* 5**,** 27.

KLINAKIS, A., SZABOLCS, M., POLITI, K., KIARIS, H., ARTAVANIS-TSAKONAS, S. & EFSTRATIADIS, A. (2006) Myc is a Notch1 transcriptional target and a requisite for Notch1-induced mammary tumorigenesis in mice. *Proc Natl Acad Sci U S A,* 103**,** 9262-7.

KLUEG, K. M., PARODY, T. R. & MUSKAVITCH, M. A. (1998) Complex proteolytic processing acts on Delta, a transmembrane ligand for Notch, during Drosophila development. *Mol Biol Cell,* 9**,** 1709-23.

KOCKEL, L., ZEITLINGER, J., STASZEWSKI, L. M., MLODZIK, M. & BOHMANN, D. (1997) Jun in Drosophila development: redundant and nonredundant functions and regulation by two MAPK signal transduction pathways. *Genes Dev,* 11**,** 1748-58.

KOELZER, S. & KLEIN, T. (2003) A Notch-independent function of Suppressor of Hairless during the development of the bristle sensory organ precursor cell of Drosophila. *Development,* 130**,** 1973-88.

KOEPP, D. M., SCHAEFER, L. K., YE, X., KEYOMARSI, K., CHU, C., HARPER, J. W. & ELLEDGE, S. J. (2001) Phosphorylation-dependent ubiquitination of cyclin E by the SCFFbw7 ubiquitin ligase. *Science,* 294**,** 173-7.

KOMINAMI, K., OCHOTORENA, I. & TODA, T. (1998) Two F-box/WD-repeat proteins Pop1 and Pop2 form hetero- and homo-complexes together with cullin-1 in the fission yeast SCF (Skp1-Cullin-1-F-box) ubiquitin ligase. *Genes Cells,* 3**,** 721-35.

KOPAN, R., NYE, J. S. & WEINTRAUB, H. (1994) The intracellular domain of mouse Notch: a constitutively activated repressor of myogenesis directed at the basic helix-loop-helix region of MyoD. *Development,* 120**,** 2385-96.

KRAMER, E. R., KNOTT, L., SU, F., DESSAUD, E., KRULL, C. E., HELMBACHER, F. & KLEIN, R. (2006) Cooperation between GDNF/Ret and ephrinA/EphA4 signals for motor-axon pathway selection in the limb. *Neuron,* 50**,** 35-47.

KREBS, L. T., SHUTTER, J. R., TANIGAKI, K., HONJO, T., STARK, K. L. & GRIDLEY, T. (2004) Haploinsufficient lethality and formation of arteriovenous malformations in Notch pathway mutants. *Genes Dev,* 18**,** 2469-73.

KREBS, L. T., XUE, Y., NORTON, C. R., SHUTTER, J. R., MAGUIRE, M., SUNDBERG, J. P., GALLAHAN, D., CLOSSON, V., KITAJEWSKI, J., CALLAHAN, R., SMITH, G. H., STARK, K. L. & GRIDLEY, T. (2000) Notch

signaling is essential for vascular morphogenesis in mice. *Genes Dev,* 14**,** 1343-52.

KREBS, L. T., XUE, Y., NORTON, C. R., SUNDBERG, J. P., BEATUS, P., LENDAHL, U., JOUTEL, A. & GRIDLEY, T. (2003) Characterization of Notch3-deficient mice: normal embryonic development and absence of genetic interactions with a Notch1 mutation. *Genesis,* 37**,** 139-43.

KRIEGSTEIN, A. R. & GOTZ, M. (2003) Radial glia diversity: a matter of cell fate. *Glia,* 43**,** 37-43.

KUAN, C. Y., WHITMARSH, A. J., YANG, D. D., LIAO, G., SCHLOEMER, A. J., DONG, C., BAO, J., BANASIAK, K. J., HADDAD, G. G., FLAVELL, R. A., DAVIS, R. J. & RAKIC, P. (2003) A critical role of neural-specific JNK3 for ischemic apoptosis. *Proc Natl Acad Sci U S A,* 100**,** 15184-9.

KUAN, C. Y., YANG, D. D., SAMANTA ROY, D. R., DAVIS, R. J., RAKIC, P. & FLAVELL, R. A. (1999) The Jnk1 and Jnk2 protein kinases are required for regional specific apoptosis during early brain development. *Neuron,* 22**,** 667-76.

KULJU, K. S. & LEHMAN, J. M. (1995) Increased p53 protein associated with aging in human diploid fibroblasts. *Exp Cell Res,* 217**,** 336-45.

KUMANO, K., CHIBA, S., KUNISATO, A., SATA, M., SAITO, T., NAKAGAMI-YAMAGUCHI, E., YAMAGUCHI, T., MASUDA, S., SHIMIZU, K., TAKAHASHI, T., OGAWA, S., HAMADA, Y. & HIRAI, H. (2003) Notch1 but not Notch2 is essential for generating hematopoietic stem cells from endothelial cells. *Immunity,* 18**,** 699-711.

KURODA, K., HAN, H., TANI, S., TANIGAKI, K., TUN, T., FURUKAWA, T., TANIGUCHI, Y., KUROOKA, H., HAMADA, Y., TOYOKUNI, S. & HONJO, T. (2003) Regulation of marginal zone B cell development by MINT, a suppressor of Notch/RBP-J signaling pathway. *Immunity,* 18**,** 301-12.

KWAK, E. L., MOBERG, K. H., WAHRER, D. C., QUINN, J. E., GILMORE, P. M., GRAHAM, C. A., HARIHARAN, I. K., HARKIN, D. P., HABER, D. A. & BELL, D. W. (2005) Infrequent mutations of Archipelago (hAGO, hCDC4, Fbw7) in primary ovarian cancer. *Gynecol Oncol,* 98**,** 124-8.

KYRIAKIS, J. M., BANERJEE, P., NIKOLAKAKI, E., DAI, T., RUBIE, E. A., AHMAD, M. F., AVRUCH, J. & WOODGETT, J. R. (1994) The stress-activated protein kinase subfamily of c-Jun kinases. *Nature,* 369**,** 156-60.

LAFLAMME, M. A., CHEN, K. Y., NAUMOVA, A. V., MUSKHELI, V., FUGATE, J. A., DUPRAS, S. K., REINECKE, H., XU, C., HASSANIPOUR, M., POLICE, S., O'SULLIVAN, C., COLLINS, L., CHEN, Y., MINAMI, E., GILL, E. A., UENO, S., YUAN, C., GOLD, J. & MURRY, C. E. (2007) Cardiomyocytes derived from human embryonic stem cells in pro-survival factors enhance function of infarcted rat hearts. *Nat Biotechnol,* 25**,** 1015-24.

LAFLAMME, M. A., GOLD, J., XU, C., HASSANIPOUR, M., ROSLER, E., POLICE, S., MUSKHELI, V. & MURRY, C. E. (2005) Formation of human myocardium in the rat heart from human embryonic stem cells. *Am J Pathol,* 167**,** 663-71.

LAI, E. C. (2002) Protein degradation: four E3s for the notch pathway. *Curr Biol,* 12**,** R74-8.

LAMPH, W. W., WAMSLEY, P., SASSONE-CORSI, P. & VERMA, I. M. (1988) Induction of proto-oncogene JUN/AP-1 by serum and TPA. *Nature,* 334**,** 629-31.

LANDSCHULZ, W. H., JOHNSON, P. F. & MCKNIGHT, S. L. (1988) The leucine zipper: a hypothetical structure common to a new class of DNA binding proteins. *Science,* 240**,** 1759-64.

LAURENT, L. C., ULITSKY, I., SLAVIN, I., TRAN, H., SCHORK, A., MOREY, R., LYNCH, C., HARNESS, J. V., LEE, S., BARRERO, M. J., KU, S., MARTYNOVA, M., SEMECHKIN, R., GALAT, V., GOTTESFELD, J., IZPISUA BELMONTE, J. C., MURRY, C., KEIRSTEAD, H. S., PARK, H. S., SCHMIDT, U., LASLETT, A. L., MULLER, F. J., NIEVERGELT, C. M., SHAMIR, R. & LORING, J. F. (2011) Dynamic changes in the copy number of pluripotency and cell proliferation genes in human ESCs and iPSCs during reprogramming and time in culture. *Cell Stem Cell,* 8**,** 106-18.

LE BORGNE, R., REMAUD, S., HAMEL, S. & SCHWEISGUTH, F. (2005) Two distinct E3 ubiquitin ligases have complementary functions in the regulation of delta and serrate signaling in Drosophila. *PLoS Biol,* 3**,** e96.

LE GALL, M., DE MATTEI, C. & GINIGER, E. (2008) Molecular separation of two signaling pathways for the receptor, Notch. *Dev Biol,* 313**,** 556-67.

LE-NICULESCU, H., BONFOCO, E., KASUYA, Y., CLARET, F. X., GREEN, D. R. & KARIN, M. (1999) Withdrawal of survival factors results in activation of the JNK pathway in neuronal cells leading to Fas ligand induction and cell death. *Mol Cell Biol,* 19**,** 751-63.

LEE, J. K., HWANG, W. S., LEE, Y. D. & HAN, P. L. (1999) Dynamic expression of SEK1 suggests multiple roles of the gene during embryogenesis and in adult brain of mice. *Brain Res Mol Brain Res,* 66**,** 133-40.

LEE, S. M., DANIELIAN, P. S., FRITZSCH, B. & MCMAHON, A. P. (1997) Evidence that FGF8 signalling from the midbrain-hindbrain junction regulates growth and polarity in the developing midbrain. *Development,* 124**,** 959-69.

LEE, W., MITCHELL, P. & TJIAN, R. (1987) Purified transcription factor AP-1 interacts with TPA-inducible enhancer elements. *Cell,* 49**,** 741-52.

LEONE, D. P., SRINIVASAN, K., CHEN, B., ALCAMO, E. & MCCONNELL, S. K. (2008) The determination of projection neuron identity in the developing cerebral cortex. *Curr Opin Neurobiol,* 18**,** 28-35.

LEPPA, S., SAFFRICH, R., ANSORGE, W. & BOHMANN, D. (1998) Differential regulation of c-Jun by ERK and JNK during PC12 cell differentiation. *EMBO J,* 17**,** 4404-13.

LÉVESQUE, M. F., NEUMAN, T. & REZAK, M. (2009) Therapeutic Microinjection of Autologous Adult Human Neural Stem Cells and Differentiated Neurons for Parkinson's Disease: Five-Year Post-Operative Outcome. *The Open Stem Cell Journal,* 1**,** 20-9.

LEVI-MONTALCINI, R. (1964) The Nerve Growth Factor. *Ann N Y Acad Sci,* 118**,** 149-70.

LEVINE, A. J. (1997) p53, the cellular gatekeeper for growth and division. *Cell,* 88**,** 323-31.

LEVKOVITZ, Y. & BARABAN, J. M. (2002) A dominant negative Egr inhibitor blocks nerve growth factor-induced neurite outgrowth by suppressing c-Jun activation: role of an Egr/c-Jun complex. *J Neurosci,* 22**,** 3845-54.

LI, J., PAULEY, A. M., MYERS, R. L., SHUANG, R., BRASHLER, J. R., YAN, R., BUHL, A. E., RUBLE, C. & GURNEY, M. E. (2002) SEL-10 interacts with

presenilin 1, facilitates its ubiquitination, and alters A-beta peptide production. *J Neurochem,* 82**,** 1540-8.

LI, X. J., DU, Z. W., ZARNOWSKA, E. D., PANKRATZ, M., HANSEN, L. O., PEARCE, R. A. & ZHANG, S. C. (2005) Specification of motoneurons from human embryonic stem cells. *Nat Biotechnol,* 23**,** 215-21.

LI, Y., ZHANG, Q., YIN, X., YANG, W., DU, Y., HOU, P., GE, J., LIU, C., ZHANG, W., ZHANG, X., WU, Y., LI, H., LIU, K., WU, C., SONG, Z., ZHAO, Y., SHI, Y. & DENG, H. (2011) Generation of iPSCs from mouse fibroblasts with a single gene, Oct4, and small molecules. *Cell Res,* 21**,** 196-204.

LINDVALL, O. & HAGELL, P. (2001) Cell therapy and transplantation in Parkinson's disease. *Clin Chem Lab Med,* 39**,** 356-61.

LISTER, R., PELIZZOLA, M., KIDA, Y. S., HAWKINS, R. D., NERY, J. R., HON, G., ANTOSIEWICZ-BOURGET, J., O'MALLEY, R., CASTANON, R., KLUGMAN, S., DOWNES, M., YU, R., STEWART, R., REN, B., THOMSON, J. A., EVANS, R. M. & ECKER, J. R. (2011) Hotspots of aberrant epigenomic reprogramming in human induced pluripotent stem cells. *Nature,* 471**,** 68-73.

LOUVI, A. & ARTAVANIS-TSAKONAS, S. (2006) Notch signalling in vertebrate neural development. *Nat Rev Neurosci,* 7**,** 93-102.

LUCCHINI, G., HINNEBUSCH, A. G., CHEN, C. & FINK, G. R. (1984) Positive regulatory interactions of the HIS4 gene of Saccharomyces cerevisiae. *Mol Cell Biol,* 4**,** 1326-33.

LUTOLF, S., RADTKE, F., AGUET, M., SUTER, U. & TAYLOR, V. (2002) Notch1 is required for neuronal and glial differentiation in the cerebellum. *Development,* 129**,** 373-85.

MA, C., YING, C., YUAN, Z., SONG, B., LI, D., LIU, Y., LAI, B., LI, W., CHEN, R., CHING, Y. P. & LI, M. (2007) dp5/HRK is a c-Jun target gene and required for apoptosis induced by potassium deprivation in cerebellar granule neurons. *J Biol Chem,* 282**,** 30901-9.

MADEN, M. (2007) Retinoic acid in the development, regeneration and maintenance of the nervous system. *Nat Rev Neurosci,* 8**,** 755-65.

MAKI, Y., BOS, T. J., DAVIS, C., STARBUCK, M. & VOGT, P. K. (1987) Avian sarcoma virus 17 carries the jun oncogene. *Proc Natl Acad Sci U S A,* 84**,** 2848-52.

MALATESTA, P., HARTFUSS, E. & GOTZ, M. (2000) Isolation of radial glial cells by fluorescent-activated cell sorting reveals a neuronal lineage. *Development,* 127**,** 5253-63.

MAO, J. H., KIM, I. J., WU, D., CLIMENT, J., KANG, H. C., DELROSARIO, R. & BALMAIN, A. (2008) FBXW7 targets mTOR for degradation and cooperates with PTEN in tumor suppression. *Science,* 321**,** 1499-502.

MAO, J. H., PEREZ-LOSADA, J., WU, D., DELROSARIO, R., TSUNEMATSU, R., NAKAYAMA, K. I., BROWN, K., BRYSON, S. & BALMAIN, A. (2004) Fbxw7/Cdc4 is a p53-dependent, haploinsufficient tumour suppressor gene. *Nature,* 432**,** 775-9.

MARUYAMA, S., HATAKEYAMA, S., NAKAYAMA, K., ISHIDA, N. & KAWAKAMI, K. (2001) Characterization of a mouse gene (Fbxw6) that encodes a homologue of Caenorhabditis elegans SEL-10. *Genomics,* 78**,** 214-22.

MASER, R. S., CHOUDHURY, B., CAMPBELL, P. J., FENG, B., WONG, K. K., PROTOPOPOV, A., O'NEIL, J., GUTIERREZ, A., IVANOVA, E., PERNA, I., LIN, E., MANI, V., JIANG, S., MCNAMARA, K., ZAGHLUL, S., EDKINS, S., STEVENS, C., BRENNAN, C., MARTIN, E. S., WIEDEMEYER, R., KABBARAH, O., NOGUEIRA, C., HISTEN, G., ASTER, J., MANSOUR, M., DUKE, V., FORONI, L., FIELDING, A. K., GOLDSTONE, A. H., ROWE, J. M., WANG, Y. A., LOOK, A. T., STRATTON, M. R., CHIN, L., FUTREAL, P. A. & DEPINHO, R. A. (2007) Chromosomally unstable mouse tumours have genomic alterations similar to diverse human cancers. *Nature,* 447**,** 966-71.

MASON, S. L., STEWART, R. M., KEARNS, V. R., WILLIAMS, R. L. & SHERIDAN, C. M. (2011) Ocular epithelial transplantation: current uses and future potential. *Regen Med,* 6**,** 767-82.

MATSUMOTO, A., ONOYAMA, I. & NAKAYAMA, K. I. (2006) Expression of mouse Fbxw7 isoforms is regulated in a cell cycle- or p53-dependent manner. *Biochem Biophys Res Commun,* 350**,** 114-9.

MATSUMOTO, A., ONOYAMA, I., SUNABORI, T., KAGEYAMA, R., OKANO, H. & NAKAYAMA, K. I. (2011) Fbxw7-dependent degradation of Notch is required for control of "stemness" and neuronal-glial differentiation in neural stem cells. *J Biol Chem,* 286**,** 13754-64.

MATSUNO, K., DIEDERICH, R. J., GO, M. J., BLAUMUELLER, C. M. & ARTAVANIS-TSAKONAS, S. (1995) Deltex acts as a positive regulator of Notch signaling through interactions with the Notch ankyrin repeats. *Development,* 121**,** 2633-44.

MATSUOKA, S., OIKE, Y., ONOYAMA, I., IWAMA, A., ARAI, F., TAKUBO, K., MASHIMO, Y., OGURO, H., NITTA, E., ITO, K., MIYAMOTO, K., YOSHIWARA, H., HOSOKAWA, K., NAKAMURA, Y., GOMEI, Y., IWASAKI, H., HAYASHI, Y., MATSUZAKI, Y., NAKAYAMA, K., IKEDA, Y., HATA, A., CHIBA, S., NAKAYAMA, K. I. & SUDA, T. (2008) Fbxw7 acts as a critical fail-safe against premature loss of hematopoietic stem cells and development of T-ALL. *Genes Dev,* 22**,** 986-91.

MCCONNELL, S. K. & KAZNOWSKI, C. E. (1991) Cell cycle dependence of laminar determination in developing neocortex. *Science,* 254**,** 282-5.

MCGILL, M. A. & MCGLADE, C. J. (2003) Mammalian numb proteins promote Notch1 receptor ubiquitination and degradation of the Notch1 intracellular domain. *J Biol Chem,* 278**,** 23196-203.

MIGHELI, A., PIVA, R., ATZORI, C., TROOST, D. & SCHIFFER, D. (1997) c-Jun, JNK/SAPK kinases and transcription factor NF-kappa B are selectively activated in astrocytes, but not motor neurons, in amyotrophic lateral sclerosis. *J Neuropathol Exp Neurol,* 56**,** 1314-22.

MILAN, M. & COHEN, S. M. (2010) Notch signaling: filopodia dynamics confer robustness. *Curr Biol,* 20**,** R802-4.

MILANO, J., MCKAY, J., DAGENAIS, C., FOSTER-BROWN, L., POGNAN, F., GADIENT, R., JACOBS, R. T., ZACCO, A., GREENBERG, B. & CIACCIO, P. J. (2004) Modulation of notch processing by gamma-secretase inhibitors causes intestinal goblet cell metaplasia and induction of genes known to specify gut secretory lineage differentiation. *Toxicol Sci,* 82**,** 341-58.

MILLER, F. D. & GAUTHIER, A. S. (2007) Timing is everything: making neurons versus glia in the developing cortex. *Neuron,* 54**,** 357-69.

MINDEN, A., LIN, A., MCMAHON, M., LANGE-CARTER, C., DERIJARD, B., DAVIS, R. J., JOHNSON, G. L. & KARIN, M. (1994) Differential activation of ERK and JNK mitogen-activated protein kinases by Raf-1 and MEKK. *Science,* 266**,** 1719-23.

MINELLA, A. C., GRIM, J. E., WELCKER, M. & CLURMAN, B. E. (2007) p53 and SCFFbw7 cooperatively restrain cyclin E-associated genome instability. *Oncogene,* 26**,** 6948-53.

MINELLA, A. C., LOEB, K. R., KNECHT, A., WELCKER, M., VARNUM-FINNEY, B. J., BERNSTEIN, I. D., ROBERTS, J. M. & CLURMAN, B. E. (2008) Cyclin E phosphorylation regulates cell proliferation in hematopoietic and epithelial lineages in vivo. *Genes Dev,* 22**,** 1677-89.

MIRSKY, R., WOODHOO, A., PARKINSON, D. B., ARTHUR-FARRAJ, P., BHASKARAN, A. & JESSEN, K. R. (2008) Novel signals controlling embryonic Schwann cell development, myelination and dedifferentiation. *J Peripher Nerv Syst,* 13**,** 122-35.

MISHRA-GORUR, K., RAND, M. D., PEREZ-VILLAMIL, B. & ARTAVANIS-TSAKONAS, S. (2002) Down-regulation of Delta by proteolytic processing. *J Cell Biol,* 159**,** 313-24.

MISSON, J. P., EDWARDS, M. A., YAMAMOTO, M. & CAVINESS, V. S., JR. (1988) Identification of radial glial cells within the developing murine central nervous system: studies based upon a new immunohistochemical marker. *Brain Res Dev Brain Res,* 44**,** 95-108.

MITSUI, K., TOKUZAWA, Y., ITOH, H., SEGAWA, K., MURAKAMI, M., TAKAHASHI, K., MARUYAMA, M., MAEDA, M. & YAMANAKA, S. (2003) The homeoprotein Nanog is required for maintenance of pluripotency in mouse epiblast and ES cells. *Cell,* 113**,** 631-42.

MIYATA, T., KAWAGUCHI, A., OKANO, H. & OGAWA, M. (2001) Asymmetric inheritance of radial glial fibers by cortical neurons. *Neuron,* 31**,** 727-41.

MIYATA, T., KAWAGUCHI, A., SAITO, K., KAWANO, M., MUTO, T. & OGAWA, M. (2004) Asymmetric production of surface-dividing and non-surface-dividing cortical progenitor cells. *Development,* 131**,** 3133-45.

MIZUGUCHI, R., KRIKS, S., CORDES, R., GOSSLER, A., MA, Q. & GOULDING, M. (2006) Ascl1 and Gsh1/2 control inhibitory and excitatory cell fate in spinal sensory interneurons. *Nat Neurosci,* 9**,** 770-8.

MIZUTANI, K., YOON, K., DANG, L., TOKUNAGA, A. & GAIANO, N. (2007) Differential Notch signalling distinguishes neural stem cells from intermediate progenitors. *Nature,* 449**,** 351-5.

MOBERG, K. H., BELL, D. W., WAHRER, D. C., HABER, D. A. & HARIHARAN, I. K. (2001) Archipelago regulates Cyclin E levels in Drosophila and is mutated in human cancer cell lines. *Nature,* 413**,** 311-6.

MOHR, O. L. (1919) Character Changes Caused by Mutation of an Entire Region of a Chromosome in Drosophila. *Genetics,* 4**,** 275-82.

MOLONEY, D. J., PANIN, V. M., JOHNSTON, S. H., CHEN, J., SHAO, L., WILSON, R., WANG, Y., STANLEY, P., IRVINE, K. D., HALTIWANGER, R. S. & VOGT, T. F. (2000) Fringe is a glycosyltransferase that modifies Notch. *Nature,* 406**,** 369-75.

MOLYNEAUX, B. J., ARLOTTA, P., MENEZES, J. R. & MACKLIS, J. D. (2007) Neuronal subtype specification in the cerebral cortex. *Nat Rev Neurosci,* 8**,** 427-37.

MOREL, V., LECOURTOIS, M., MASSIANI, O., MAIER, D., PREISS, A. & SCHWEISGUTH, F. (2001) Transcriptional repression by suppressor of hairless involves the binding of a hairless-dCtBP complex in Drosophila. *Curr Biol,* 11**,** 789-92.

MOREL, V. & SCHWEISGUTH, F. (2000) Repression by suppressor of hairless and activation by Notch are required to define a single row of single-minded expressing cells in the Drosophila embryo. *Genes Dev,* 14**,** 377-88.

MORGAN, J. I. & CURRAN, T. (1988) Calcium as a modulator of the immediate-early gene cascade in neurons. *Cell Calcium,* 9**,** 303-11.

MORGAN, T. H. & BRIDGES, C. B. (1916) *Sex-linked inheritance in Drosophila,* Washington,, Carnegie Institution of Washington.

MORRISON, D. K. & DAVIS, R. J. (2003) Regulation of MAP kinase signaling modules by scaffold proteins in mammals. *Annu Rev Cell Dev Biol,* 19**,** 91-118.

MORRISON, S. J., PEREZ, S. E., QIAO, Z., VERDI, J. M., HICKS, C., WEINMASTER, G. & ANDERSON, D. J. (2000) Transient Notch activation initiates an irreversible switch from neurogenesis to gliogenesis by neural crest stem cells. *Cell,* 101**,** 499-510.

MORTON, S., DAVIS, R. J., MCLAREN, A. & COHEN, P. (2003) A reinvestigation of the multisite phosphorylation of the transcription factor c-Jun. *EMBO J,* 22**,** 3876-86.

MOTOYAMA, J., MILENKOVIC, L., IWAMA, M., SHIKATA, Y., SCOTT, M. P. & HUI, C. C. (2003) Differential requirement for Gli2 and Gli3 in ventral neural cell fate specification. *Dev Biol,* 259**,** 150-61.

MUKHERJEE, A., VERAKSA, A., BAUER, A., ROSSE, C., CAMONIS, J. & ARTAVANIS-TSAKONAS, S. (2005) Regulation of Notch signalling by non-visual beta-arrestin. *Nat Cell Biol,* 7**,** 1191-201.

MUKHOPADHYAY, D. & RIEZMAN, H. (2007) Proteasome-independent functions of ubiquitin in endocytosis and signaling. *Science,* 315**,** 201-5.

MUMM, J. S. & KOPAN, R. (2000) Notch signaling: from the outside in. *Dev Biol,* 228**,** 151-65.

MUMM, J. S., SCHROETER, E. H., SAXENA, M. T., GRIESEMER, A., TIAN, X., PAN, D. J., RAY, W. J. & KOPAN, R. (2000) A ligand-induced extracellular cleavage regulates gamma-secretase-like proteolytic activation of Notch1. *Mol Cell,* 5**,** 197-206.

NAGEL, A. C., KREJCI, A., TENIN, G., BRAVO-PATINO, A., BRAY, S., MAIER, D. & PREISS, A. (2005) Hairless-mediated repression of notch target genes requires the combined activity of Groucho and CtBP corepressors. *Mol Cell Biol,* 25**,** 10433-41.

NAITO, A. T., SHIOJIMA, I., AKAZAWA, H., HIDAKA, K., MORISAKI, T., KIKUCHI, A. & KOMURO, I. (2006) Developmental stage-specific biphasic roles of Wnt/beta-catenin signaling in cardiomyogenesis and hematopoiesis. *Proc Natl Acad Sci U S A,* 103**,** 19812-7.

NAKABEPPU, Y., RYDER, K. & NATHANS, D. (1988) DNA binding activities of three murine Jun proteins: stimulation by Fos. *Cell,* 55**,** 907-15.

NAM, Y., SLIZ, P., SONG, L., ASTER, J. C. & BLACKLOW, S. C. (2006) Structural basis for cooperativity in recruitment of MAML coactivators to Notch transcription complexes. *Cell,* 124**,** 973-83.

NASH, P., TANG, X., ORLICKY, S., CHEN, Q., GERTLER, F. B., MENDENHALL, M. D., SICHERI, F., PAWSON, T. & TYERS, M. (2001) Multisite phosphorylation of a CDK inhibitor sets a threshold for the onset of DNA replication. *Nature,* 414**,** 514-21.

NATERI, A. S., RIERA-SANS, L., DA COSTA, C. & BEHRENS, A. (2004) The ubiquitin ligase SCFFbw7 antagonizes apoptotic JNK signaling. *Science,* 303**,** 1374-8.

NATERI, A. S., SPENCER-DENE, B. & BEHRENS, A. (2005) Interaction of phosphorylated c-Jun with TCF4 regulates intestinal cancer development. *Nature,* 437**,** 281-5.

NELSON, B. R., HARTMAN, B. H., GEORGI, S. A., LAN, M. S. & REH, T. A. (2007) Transient inactivation of Notch signaling synchronizes differentiation of neural progenitor cells. *Dev Biol,* 304**,** 479-98.

NERY, S., FISHELL, G. & CORBIN, J. G. (2002) The caudal ganglionic eminence is a source of distinct cortical and subcortical cell populations. *Nat Neurosci,* 5**,** 1279-87.

NG, E. S., DAVIS, R. P., AZZOLA, L., STANLEY, E. G. & ELEFANTY, A. G. (2005) Forced aggregation of defined numbers of human embryonic stem cells into embryoid bodies fosters robust, reproducible hematopoietic differentiation. *Blood,* 106**,** 1601-3.

NIETO, M., SCHUURMANS, C., BRITZ, O. & GUILLEMOT, F. (2001) Neural bHLH genes control the neuronal versus glial fate decision in cortical progenitors. *Neuron,* 29**,** 401-13.

NIWA, H., TOYOOKA, Y., SHIMOSATO, D., STRUMPF, D., TAKAHASHI, K., YAGI, R. & ROSSANT, J. (2005) Interaction between Oct3/4 and Cdx2 determines trophectoderm differentiation. *Cell,* 123**,** 917-29.

NOCTOR, S. C., FLINT, A. C., WEISSMAN, T. A., DAMMERMAN, R. S. & KRIEGSTEIN, A. R. (2001) Neurons derived from radial glial cells establish radial units in neocortex. *Nature,* 409**,** 714-20.

NOCTOR, S. C., MARTINEZ-CERDENO, V., IVIC, L. & KRIEGSTEIN, A. R. (2004) Cortical neurons arise in symmetric and asymmetric division zones and migrate through specific phases. *Nat Neurosci,* 7**,** 136-44.

NOFZIGER, D., MIYAMOTO, A., LYONS, K. M. & WEINMASTER, G. (1999) Notch signaling imposes two distinct blocks in the differentiation of C2C12 myoblasts. *Development,* 126**,** 1689-702.

NOSTRO, M. C., CHENG, X., KELLER, G. M. & GADUE, P. (2008) Wnt, activin, and BMP signaling regulate distinct stages in the developmental pathway from embryonic stem cells to blood. *Cell Stem Cell,* 2**,** 60-71.

NOWAK, D., MOSSNER, M., BALDUS, C. D., HOPFER, O., THIEL, E. & HOFMANN, W. K. (2006) Mutation analysis of hCDC4 in AML cells identifies a new intronic polymorphism. *Int J Med Sci,* 3**,** 148-51.

NYABI, O., NAESSENS, M., HAIGH, K., GEMBARSKA, A., GOOSSENS, S., MAETENS, M., DE CLERCQ, S., DROGAT, B., HAENEBALCKE, L., BARTUNKOVA, S., DE VOS, I., DE CRAENE, B., KARIMI, M., BERX, G., NAGY, A., HILSON, P., MARINE, J. C. & HAIGH, J. J. (2009) Efficient

mouse transgenesis using Gateway-compatible ROSA26 locus targeting vectors and F1 hybrid ES cells. *Nucleic Acids Res,* 37**,** e55.

NYE, J. S., KOPAN, R. & AXEL, R. (1994) An activated Notch suppresses neurogenesis and myogenesis but not gliogenesis in mammalian cells. *Development,* 120**,** 2421-30.

NYFELER, Y., KIRCH, R. D., MANTEI, N., LEONE, D. P., RADTKE, F., SUTER, U. & TAYLOR, V. (2005) Jagged1 signals in the postnatal subventricular zone are required for neural stem cell self-renewal. *EMBO J,* 24**,** 3504-15.

O'LEARY, D. D., CHOU, S. J. & SAHARA, S. (2007) Area patterning of the mammalian cortex. *Neuron,* 56**,** 252-69.

O'LEARY, D. D. & NAKAGAWA, Y. (2002) Patterning centers, regulatory genes and extrinsic mechanisms controlling arealization of the neocortex. *Curr Opin Neurobiol,* 12**,** 14-25.

O'LEARY, D. D. & SAHARA, S. (2008) Genetic regulation of arealization of the neocortex. *Curr Opin Neurobiol,* 18**,** 90-100.

OBERG, C., LI, J., PAULEY, A., WOLF, E., GURNEY, M. & LENDAHL, U. (2001) The Notch intracellular domain is ubiquitinated and negatively regulated by the mammalian Sel-10 homolog. *J Biol Chem,* 276**,** 35847-53.

OCHIAI, W., NAKATANI, S., TAKAHARA, T., KAINUMA, M., MASAOKA, M., MINOBE, S., NAMIHIRA, M., NAKASHIMA, K., SAKAKIBARA, A., OGAWA, M. & MIYATA, T. (2009) Periventricular notch activation and asymmetric Ngn2 and Tbr2 expression in pair-generated neocortical daughter cells. *Mol Cell Neurosci,* 40**,** 225-33.

OHTSUKA, T., ISHIBASHI, M., GRADWOHL, G., NAKANISHI, S., GUILLEMOT, F. & KAGEYAMA, R. (1999) Hes1 and Hes5 as notch effectors in mammalian neuronal differentiation. *EMBO J,* 18**,** 2196-207.

OKABE, S., FORSBERG-NILSSON, K., SPIRO, A. C., SEGAL, M. & MCKAY, R. D. (1996) Development of neuronal precursor cells and functional postmitotic neurons from embryonic stem cells in vitro. *Mech Dev,* 59**,** 89-102.

OKAJIMA, T. & IRVINE, K. D. (2002) Regulation of notch signaling by o-linked fucose. *Cell,* 111**,** 893-904.

OKAJIMA, T., XU, A., LEI, L. & IRVINE, K. D. (2005) Chaperone activity of protein O-fucosyltransferase 1 promotes notch receptor folding. *Science,* 307**,** 1599-603.

ONOYAMA, I. & NAKAYAMA, K. I. (2008) Fbxw7 in cell cycle exit and stem cell maintenance: insight from gene-targeted mice. *Cell Cycle,* 7**,** 3307-13.

ONOYAMA, I., TSUNEMATSU, R., MATSUMOTO, A., KIMURA, T., DE ALBORAN, I. M., NAKAYAMA, K. & NAKAYAMA, K. I. (2007) Conditional inactivation of Fbxw7 impairs cell-cycle exit during T cell differentiation and results in lymphomatogenesis. *J Exp Med,* 204**,** 2875-88.

OO, T. F., HENCHCLIFFE, C., JAMES, D. & BURKE, R. E. (1999) Expression of c-fos, c-jun, and c-jun N-terminal kinase (JNK) in a developmental model of induced apoptotic death in neurons of the substantia nigra. *J Neurochem,* 72**,** 557-64.

ORLICKY, S., TANG, X., WILLEMS, A., TYERS, M. & SICHERI, F. (2003) Structural basis for phosphodependent substrate selection and orientation by the SCFCdc4 ubiquitin ligase. *Cell,* 112**,** 243-56.

OSTERTAG, D., AMUNDSON, K. K., LOPEZ ESPINOZA, F., MARTIN, B., BUCKLEY, T., DA SILVA, A. P., LIN, A. H., VALENTA, D. T., PEREZ, O.

D., IBANEZ, C. E., CHEN, C. I., PETTERSSON, P. L., BURNETT, R., DAUBLEBSKY, V., HLAVATY, J., GUNZBURG, W., KASAHARA, N., GRUBER, H. E., JOLLY, D. J. & ROBBINS, J. M. (2011) Brain tumor eradication and prolonged survival from intratumoral conversion of 5-fluorocytosine to 5-fluorouracil using a nonlytic retroviral replicating vector. *Neuro Oncol*.

OSWALD, F., WINKLER, M., CAO, Y., ASTRAHANTSEFF, K., BOURTEELE, S., KNOCHEL, W. & BORGGREFE, T. (2005) RBP-Jkappa/SHARP recruits CtIP/CtBP corepressors to silence Notch target genes. *Mol Cell Biol,* 25**,** 10379-90.

PALOMERO, T., LIM, W. K., ODOM, D. T., SULIS, M. L., REAL, P. J., MARGOLIN, A., BARNES, K. C., O'NEIL, J., NEUBERG, D., WENG, A. P., ASTER, J. C., SIGAUX, F., SOULIER, J., LOOK, A. T., YOUNG, R. A., CALIFANO, A. & FERRANDO, A. A. (2006) NOTCH1 directly regulates c-MYC and activates a feed-forward-loop transcriptional network promoting leukemic cell growth. *Proc Natl Acad Sci U S A,* 103**,** 18261-6.

PARK, C. H., MINN, Y. K., LEE, J. Y., CHOI, D. H., CHANG, M. Y., SHIM, J. W., KO, J. Y., KOH, H. C., KANG, M. J., KANG, J. S., RHIE, D. J., LEE, Y. S., SON, H., MOON, S. Y., KIM, K. S. & LEE, S. H. (2005) In vitro and in vivo analyses of human embryonic stem cell-derived dopamine neurons. *J Neurochem,* 92**,** 1265-76.

PASQUINI, M. C., GRIFFITH, L. M., ARNOLD, D. L., ATKINS, H. L., BOWEN, J. D., CHEN, J. T., FREEDMAN, M. S., KRAFT, G. H., MANCARDI, G. L., MARTIN, R., MURARO, P. A., NASH, R. A., RACKE, M. K., STOREK, J. & SACCARDI, R. (2010) Hematopoietic stem cell transplantation for multiple sclerosis: collaboration of the CIBMTR and EBMT to facilitate international clinical studies. *Biol Blood Marrow Transplant,* 16**,** 1076-83.

PAVLOPOULOS, E., PITSOULI, C., KLUEG, K. M., MUSKAVITCH, M. A., MOSCHONAS, N. K. & DELIDAKIS, C. (2001) neuralized Encodes a peripheral membrane protein involved in delta signaling and endocytosis. *Dev Cell,* 1**,** 807-16.

PEARSON, A. G., BYRNE, U. T., MACGIBBON, G. A., FAULL, R. L. & DRAGUNOW, M. (2006) Activated c-Jun is present in neurofibrillary tangles in Alzheimer's disease brains. *Neurosci Lett,* 398**,** 246-50.

PENG, C. Y., YAJIMA, H., BURNS, C. E., ZON, L. I., SISODIA, S. S., PFAFF, S. L. & SHARMA, K. (2007) Notch and MAML signaling drives Scl-dependent interneuron diversity in the spinal cord. *Neuron,* 53**,** 813-27.

PERA, E. M., IKEDA, A., EIVERS, E. & DE ROBERTIS, E. M. (2003) Integration of IGF, FGF, and anti-BMP signals via Smad1 phosphorylation in neural induction. *Genes Dev,* 17**,** 3023-8.

PERRIER, A. L., TABAR, V., BARBERI, T., RUBIO, M. E., BRUSES, J., TOPF, N., HARRISON, N. L. & STUDER, L. (2004) Derivation of midbrain dopamine neurons from human embryonic stem cells. *Proc Natl Acad Sci U S A,* 101**,** 12543-8.

PETCHERSKI, A. G. & KIMBLE, J. (2000) Mastermind is a putative activator for Notch. *Curr Biol,* 10**,** R471-3.

PFISTER, S., PRZEMECK, G. K., GERBER, J. K., BECKERS, J., ADAMSKI, J. & HRABE DE ANGELIS, M. (2003) Interaction of the MAGUK family member

Acvrinp1 and the cytoplasmic domain of the Notch ligand Delta1. *J Mol Biol,* 333**,** 229-35.

PICK, M., AZZOLA, L., MOSSMAN, A., STANLEY, E. G. & ELEFANTY, A. G. (2007) Differentiation of human embryonic stem cells in serum-free medium reveals distinct roles for bone morphogenetic protein 4, vascular endothelial growth factor, stem cell factor, and fibroblast growth factor 2 in hematopoiesis. *Stem Cells,* 25**,** 2206-14.

PICKART, C. M. & EDDINS, M. J. (2004) Ubiquitin: structures, functions, mechanisms. *Biochim Biophys Acta,* 1695**,** 55-72.

PIERFELICE, T., ALBERI, L. & GAIANO, N. (2011) Notch in the vertebrate nervous system: an old dog with new tricks. *Neuron,* 69**,** 840-55.

PINTO, L. & GOTZ, M. (2007) Radial glial cell heterogeneity--the source of diverse progeny in the CNS. *Prog Neurobiol,* 83**,** 2-23.

POLLARD, S. M., CONTI, L., SUN, Y., GOFFREDO, D. & SMITH, A. (2006) Adherent neural stem (NS) cells from fetal and adult forebrain. *Cereb Cortex,* 16 Suppl 1**,** i112-20.

POLO, J. M., LIU, S., FIGUEROA, M. E., KULALERT, W., EMINLI, S., TAN, K. Y., APOSTOLOU, E., STADTFELD, M., LI, Y., SHIODA, T., NATESAN, S., WAGERS, A. J., MELNICK, A., EVANS, T. & HOCHEDLINGER, K. (2010) Cell type of origin influences the molecular and functional properties of mouse induced pluripotent stem cells. *Nat Biotechnol,* 28**,** 848-55.

POPOV, N., HEROLD, S., LLAMAZARES, M., SCHULEIN, C. & EILERS, M. (2007) Fbw7 and Usp28 regulate myc protein stability in response to DNA damage. *Cell Cycle,* 6**,** 2327-31.

POULSON, D. F. (1940) The effects of certain X-chromosome deficiencies on the embryonic development of Drosophila melanogaster. *Journal of Experimental Zoology,* 83**,** 271-325.

POURQUIE, O. (2003) The segmentation clock: converting embryonic time into spatial pattern. *Science,* 301**,** 328-30.

POWELL, L. M. & JARMAN, A. P. (2008) Context dependence of proneural bHLH proteins. *Curr Opin Genet Dev,* 18**,** 411-7.

PUI, J. C., ALLMAN, D., XU, L., DEROCCO, S., KARNELL, F. G., BAKKOUR, S., LEE, J. Y., KADESCH, T., HARDY, R. R., ASTER, J. C. & PEAR, W. S. (1999) Notch1 expression in early lymphopoiesis influences B versus T lineage determination. *Immunity,* 11**,** 299-308.

PULVERER, B. J., HUGHES, K., FRANKLIN, C. C., KRAFT, A. S., LEEVERS, S. J. & WOODGETT, J. R. (1993) Co-purification of mitogen-activated protein kinases with phorbol ester-induced c-Jun kinase activity in U937 leukaemic cells. *Oncogene,* 8**,** 407-15.

QI, H., RAND, M. D., WU, X., SESTAN, N., WANG, W., RAKIC, P., XU, T. & ARTAVANIS-TSAKONAS, S. (1999) Processing of the notch ligand delta by the metalloprotease Kuzbanian. *Science,* 283**,** 91-4.

QIAN, X., SHEN, Q., GODERIE, S. K., HE, W., CAPELA, A., DAVIS, A. A. & TEMPLE, S. (2000) Timing of CNS cell generation: a programmed sequence of neuron and glial cell production from isolated murine cortical stem cells. *Neuron,* 28**,** 69-80.

QIU, L., JOAZEIRO, C., FANG, N., WANG, H. Y., ELLY, C., ALTMAN, Y., FANG, D., HUNTER, T. & LIU, Y. C. (2000) Recognition and ubiquitination of Notch by Itch, a hect-type E3 ubiquitin ligase. *J Biol Chem,* 275**,** 35734-7.

RABINOWICZ, T., DE COURTEN-MYERS, G. M., PETETOT, J. M., XI, G. & DE LOS REYES, E. (1996) Human cortex development: estimates of neuronal numbers indicate major loss late during gestation. *J Neuropathol Exp Neurol,* 55**,** 320-8.

RADTKE, F., WILSON, A., STARK, G., BAUER, M., VAN MEERWIJK, J., MACDONALD, H. R. & AGUET, M. (1999) Deficient T cell fate specification in mice with an induced inactivation of Notch1. *Immunity,* 10**,** 547-58.

RAIVICH, G. (2008) c-Jun expression, activation and function in neural cell death, inflammation and repair. *J Neurochem,* 107**,** 898-906.

RAIVICH, G. & BEHRENS, A. (2006) Role of the AP-1 transcription factor c-Jun in developing, adult and injured brain. *Prog Neurobiol,* 78**,** 347-63.

RAIVICH, G., BOHATSCHEK, M., DA COSTA, C., IWATA, O., GALIANO, M., HRISTOVA, M., NATERI, A. S., MAKWANA, M., RIERA-SANS, L., WOLFER, D. P., LIPP, H. P., AGUZZI, A., WAGNER, E. F. & BEHRENS, A. (2004) The AP-1 transcription factor c-Jun is required for efficient axonal regeneration. *Neuron,* 43**,** 57-67.

RAKIC, P. (1972) Mode of cell migration to the superficial layers of fetal monkey neocortex. *J Comp Neurol,* 145**,** 61-83.

RAKIC, S. & ZECEVIC, N. (2000) Programmed cell death in the developing human telencephalon. *Eur J Neurosci,* 12**,** 2721-34.

RANGAPPA, S., MAKKAR, R. & FORRESTER, J. (2010) Review article: current status of myocardial regeneration: new cell sources and new strategies. *J Cardiovasc Pharmacol Ther,* 15**,** 338-43.

RAUSCHER, F. J., 3RD, COHEN, D. R., CURRAN, T., BOS, T. J., VOGT, P. K., BOHMANN, D., TJIAN, R. & FRANZA, B. R., JR. (1988a) Fos-associated protein p39 is the product of the jun proto-oncogene. *Science,* 240**,** 1010-6.

RAUSCHER, F. J., 3RD, SAMBUCETTI, L. C., CURRAN, T., DISTEL, R. J. & SPIEGELMAN, B. M. (1988b) Common DNA binding site for Fos protein complexes and transcription factor AP-1. *Cell,* 52**,** 471-80.

REAVIE, L., DELLA GATTA, G., CRUSIO, K., ARANDA-ORGILLES, B., BUCKLEY, S. M., THOMPSON, B., LEE, E., GAO, J., BREDEMEYER, A. L., HELMINK, B. A., ZAVADIL, J., SLECKMAN, B. P., PALOMERO, T., FERRANDO, A. & AIFANTIS, I. (2010) Regulation of hematopoietic stem cell differentiation by a single ubiquitin ligase-substrate complex. *Nat Immunol,* 11**,** 207-15.

REDMOND, L., OH, S. R., HICKS, C., WEINMASTER, G. & GHOSH, A. (2000) Nuclear Notch1 signaling and the regulation of dendritic development. *Nat Neurosci,* 3**,** 30-40.

REYNOLDS, B. A. & RIETZE, R. L. (2005) Neural stem cells and neurospheres--re-evaluating the relationship. *Nat Methods,* 2**,** 333-6.

RIESGO-ESCOVAR, J. R. & HAFEN, E. (1997a) Common and distinct roles of DFos and DJun during Drosophila development. *Science,* 278**,** 669-72.

RIESGO-ESCOVAR, J. R. & HAFEN, E. (1997b) Drosophila Jun kinase regulates expression of decapentaplegic via the ETS-domain protein Aop and the AP-1 transcription factor DJun during dorsal closure. *Genes Dev,* 11**,** 1717-27.

RINCON, M., WHITMARSH, A., YANG, D. D., WEISS, L., DERIJARD, B., JAYARAJ, P., DAVIS, R. J. & FLAVELL, R. A. (1998) The JNK pathway regulates the In vivo deletion of immature CD4(+)CD8(+) thymocytes. *J Exp Med,* 188**,** 1817-30.

ROFFLER-TARLOV, S., BROWN, J. J., TARLOV, E., STOLAROV, J., CHAPMAN, D. L., ALEXIOU, M. & PAPAIOANNOU, V. E. (1996) Programmed cell death in the absence of c-Fos and c-Jun. *Development,* 122**,** 1-9.

ROY, N. S., CLEREN, C., SINGH, S. K., YANG, L., BEAL, M. F. & GOLDMAN, S. A. (2006) Functional engraftment of human ES cell-derived dopaminergic neurons enriched by coculture with telomerase-immortalized midbrain astrocytes. *Nat Med,* 12**,** 1259-68.

RYDER, K., LAU, L. F. & NATHANS, D. (1988) A gene activated by growth factors is related to the oncogene v-jun. *Proc Natl Acad Sci U S A,* 85**,** 1487-91.

SABAPATHY, K., HOCHEDLINGER, K., NAM, S. Y., BAUER, A., KARIN, M. & WAGNER, E. F. (2004) Distinct roles for JNK1 and JNK2 in regulating JNK activity and c-Jun-dependent cell proliferation. *Mol Cell,* 15**,** 713-25.

SABAPATHY, K., JOCHUM, W., HOCHEDLINGER, K., CHANG, L., KARIN, M. & WAGNER, E. F. (1999) Defective neural tube morphogenesis and altered apoptosis in the absence of both JNK1 and JNK2. *Mech Dev,* 89**,** 115-24.

SABAPATHY, K., KALLUNKI, T., DAVID, J. P., GRAEF, I., KARIN, M. & WAGNER, E. F. (2001) c-Jun NH2-terminal kinase (JNK)1 and JNK2 have similar and stage-dependent roles in regulating T cell apoptosis and proliferation. *J Exp Med,* 193**,** 317-28.

SAITO, T., CHIBA, S., ICHIKAWA, M., KUNISATO, A., ASAI, T., SHIMIZU, K., YAMAGUCHI, T., YAMAMOTO, G., SEO, S., KUMANO, K., NAKAGAMI-YAMAGUCHI, E., HAMADA, Y., AIZAWA, S. & HIRAI, H. (2003) Notch2 is preferentially expressed in mature B cells and indispensable for marginal zone B lineage development. *Immunity,* 18**,** 675-85.

SAKATA, T., SAKAGUCHI, H., TSUDA, L., HIGASHITANI, A., AIGAKI, T., MATSUNO, K. & HAYASHI, S. (2004) Drosophila Nedd4 regulates endocytosis of notch and suppresses its ligand-independent activation. *Curr Biol,* 14**,** 2228-36.

SANCHO, R., JANDKE, A., DAVIS, H., DIEFENBACHER, M. E., TOMLINSON, I. & BEHRENS, A. (2010) F-box and WD repeat domain-containing 7 regulates intestinal cell lineage commitment and is a haploinsufficient tumor suppressor. *Gastroenterology,* 139**,** 929-41.

SANCHO, R., NATERI, A. S., DE VINUESA, A. G., AGUILERA, C., NYE, E., SPENCER-DENE, B. & BEHRENS, A. (2009) JNK signalling modulates intestinal homeostasis and tumourigenesis in mice. *EMBO J,* 28**,** 1843-54.

SAPIR, A., ASSA-KUNIK, E., TSRUYA, R., SCHEJTER, E. & SHILO, B. Z. (2005) Unidirectional Notch signaling depends on continuous cleavage of Delta. *Development,* 132**,** 123-32.

SAPORITO, M. S., THOMAS, B. A. & SCOTT, R. W. (2000) MPTP activates c-Jun NH(2)-terminal kinase (JNK) and its upstream regulatory kinase MKK4 in nigrostriatal neurons in vivo. *J Neurochem,* 75**,** 1200-8.

SASAMURA, T., SASAKI, N., MIYASHITA, F., NAKAO, S., ISHIKAWA, H. O., ITO, M., KITAGAWA, M., HARIGAYA, K., SPANA, E., BILDER, D., PERRIMON, N. & MATSUNO, K. (2003) neurotic, a novel maternal

neurogenic gene, encodes an O-fucosyltransferase that is essential for Notch-Delta interactions. *Development,* 130**,** 4785-95.

SASSONE-CORSI, P., LAMPH, W. W., KAMPS, M. & VERMA, I. M. (1988) fos-associated cellular p39 is related to nuclear transcription factor AP-1. *Cell,* 54**,** 553-60.

SATO, Y., YASUDA, K. & TAKAHASHI, Y. (2002) Morphological boundary forms by a novel inductive event mediated by Lunatic fringe and Notch during somitic segmentation. *Development,* 129**,** 3633-44.

SCHMITT, T. M., DE POOTER, R. F., GRONSKI, M. A., CHO, S. K., OHASHI, P. S. & ZUNIGA-PFLUCKER, J. C. (2004) Induction of T cell development and establishment of T cell competence from embryonic stem cells differentiated in vitro. *Nat Immunol,* 5**,** 410-7.

SCHMITT, T. M. & ZUNIGA-PFLUCKER, J. C. (2002) Induction of T cell development from hematopoietic progenitor cells by delta-like-1 in vitro. *Immunity,* 17**,** 749-56.

SCHNITZER, J., FRANKE, W. W. & SCHACHNER, M. (1981) Immunocytochemical demonstration of vimentin in astrocytes and ependymal cells of developing and adult mouse nervous system. *J Cell Biol,* 90**,** 435-47.

SCHREIBER, M., KOLBUS, A., PIU, F., SZABOWSKI, A., MOHLE-STEINLEIN, U., TIAN, J., KARIN, M., ANGEL, P. & WAGNER, E. F. (1999) Control of cell cycle progression by c-Jun is p53 dependent. *Genes Dev,* 13**,** 607-19.

SCHULDINER, M., EIGES, R., EDEN, A., YANUKA, O., ITSKOVITZ-ELDOR, J., GOLDSTEIN, R. S. & BENVENISTY, N. (2001) Induced neuronal differentiation of human embryonic stem cells. *Brain Res,* 913**,** 201-5.

SCHULMAN, B. A., CARRANO, A. C., JEFFREY, P. D., BOWEN, Z., KINNUCAN, E. R., FINNIN, M. S., ELLEDGE, S. J., HARPER, J. W., PAGANO, M. & PAVLETICH, N. P. (2000) Insights into SCF ubiquitin ligases from the structure of the Skp1-Skp2 complex. *Nature,* 408**,** 381-6.

SCHWARTZ, A. L. & CIECHANOVER, A. (2009) Targeting proteins for destruction by the ubiquitin system: implications for human pathobiology. *Annu Rev Pharmacol Toxicol,* 49**,** 73-96.

SCHWOB, E., BOHM, T., MENDENHALL, M. D. & NASMYTH, K. (1994) The B-type cyclin kinase inhibitor p40SIC1 controls the G1 to S transition in S. cerevisiae. *Cell,* 79**,** 233-44.

SELKOE, D. & KOPAN, R. (2003) Notch and Presenilin: regulated intramembrane proteolysis links development and degeneration. *Annu Rev Neurosci,* 26**,** 565-97.

SELLERS, W. R. & KAELIN, W. G., JR. (1997) Role of the retinoblastoma protein in the pathogenesis of human cancer. *J Clin Oncol,* 15**,** 3301-12.

SESTAN, N., ARTAVANIS-TSAKONAS, S. & RAKIC, P. (1999) Contact-dependent inhibition of cortical neurite growth mediated by notch signaling. *Science,* 286**,** 741-6.

SEYDOUX, G. & GREENWALD, I. (1989) Cell autonomy of lin-12 function in a cell fate decision in C. elegans. *Cell,* 57**,** 1237-45.

SGAMBATO, A., CITTADINI, A., MASCIULLO, V., DI SALVATORE, M., GRAZIANI, C., RETTINO, A., VALDIVIESO, P., SCAMBIA, G., BIANCHINO, G., ZUPA, A., IMPROTA, G. & CIFARELLI, R. A. (2007) Low

frequency of hCDC4 mutations in human primary ovarian cancer. *Gynecol Oncol,* 105**,** 553-5.

SHAPIRO, G. I., EDWARDS, C. D. & ROLLINS, B. J. (2000) The physiology of p16(INK4A)-mediated G1 proliferative arrest. *Cell Biochem Biophys,* 33**,** 189-97.

SHAWBER, C., NOFZIGER, D., HSIEH, J. J., LINDSELL, C., BOGLER, O., HAYWARD, D. & WEINMASTER, G. (1996) Notch signaling inhibits muscle cell differentiation through a CBF1-independent pathway. *Development,* 122**,** 3765-73.

SHEN, Q., WANG, Y., DIMOS, J. T., FASANO, C. A., PHOENIX, T. N., LEMISCHKA, I. R., IVANOVA, N. B., STIFANI, S., MORRISEY, E. E. & TEMPLE, S. (2006) The timing of cortical neurogenesis is encoded within lineages of individual progenitor cells. *Nat Neurosci,* 9**,** 743-51.

SHERWOOD, S. W., RUSH, D., ELLSWORTH, J. L. & SCHIMKE, R. T. (1988) Defining cellular senescence in IMR-90 cells: a flow cytometric analysis. *Proc Natl Acad Sci U S A,* 85**,** 9086-90.

SHI, S., STAHL, M., LU, L. & STANLEY, P. (2005) Canonical Notch signaling is dispensable for early cell fate specifications in mammals. *Mol Cell Biol,* 25**,** 9503-8.

SHI, S. & STANLEY, P. (2003) Protein O-fucosyltransferase 1 is an essential component of Notch signaling pathways. *Proc Natl Acad Sci U S A,* 100**,** 5234-9.

SHIBATA, T., YAMADA, K., WATANABE, M., IKENAKA, K., WADA, K., TANAKA, K. & INOUE, Y. (1997) Glutamate transporter GLAST is expressed in the radial glia-astrocyte lineage of developing mouse spinal cord. *J Neurosci,* 17**,** 9212-9.

SHIM, J. H., KIM, S. E., WOO, D. H., KIM, S. K., OH, C. H., MCKAY, R. & KIM, J. H. (2007) Directed differentiation of human embryonic stem cells towards a pancreatic cell fate. *Diabetologia,* 50**,** 1228-38.

SHIN, S., DALTON, S. & STICE, S. L. (2005) Human motor neuron differentiation from human embryonic stem cells. *Stem Cells Dev,* 14**,** 266-9.

SILVA, R. M., KUAN, C. Y., RAKIC, P. & BURKE, R. E. (2005) Mixed lineage kinase-c-jun N-terminal kinase signaling pathway: a new therapeutic target in Parkinson's disease. *Mov Disord,* 20**,** 653-64.

SKAAR, J. R. & PAGANO, M. (2009) Control of cell growth by the SCF and APC/C ubiquitin ligases. *Curr Opin Cell Biol,* 21**,** 816-24.

SKOWYRA, D., CRAIG, K. L., TYERS, M., ELLEDGE, S. J. & HARPER, J. W. (1997) F-box proteins are receptors that recruit phosphorylated substrates to the SCF ubiquitin-ligase complex. *Cell,* 91**,** 209-19.

SMEAL, T., ANGEL, P., MEEK, J. & KARIN, M. (1989) Different requirements for formation of Jun: Jun and Jun: Fos complexes. *Genes Dev,* 3**,** 2091-100.

SMEAL, T., BINETRUY, B., MERCOLA, D. A., BIRRER, M. & KARIN, M. (1991) Oncogenic and transcriptional cooperation with Ha-Ras requires phosphorylation of c-Jun on serines 63 and 73. *Nature,* 354**,** 494-6.

SONG, J. K. & GINIGER, E. (2011) Noncanonical Notch function in motor axon guidance is mediated by Rac GTPase and the GEF1 domain of Trio. *Dev Dyn,* 240**,** 324-32.

SPRINZAK, D., LAKHANPAL, A., LEBON, L., SANTAT, L. A., FONTES, M. E., ANDERSON, G. A., GARCIA-OJALVO, J. & ELOWITZ, M. B. (2010) Cis-interactions between Notch and Delta generate mutually exclusive signalling states. *Nature,* 465**,** 86-90.

SPRUCK, C. H., STROHMAIER, H., SANGFELT, O., MULLER, H. M., HUBALEK, M., MULLER-HOLZNER, E., MARTH, C., WIDSCHWENDTER, M. & REED, S. I. (2002) hCDC4 gene mutations in endometrial cancer. *Cancer Res,* 62**,** 4535-9.

SRINIVAS, S., WATANABE, T., LIN, C. S., WILLIAM, C. M., TANABE, Y., JESSELL, T. M. & COSTANTINI, F. (2001) Cre reporter strains produced by targeted insertion of EYFP and ECFP into the ROSA26 locus. *BMC Dev Biol,* 1**,** 4.

STILES, J. & JERNIGAN, T. L. (2010) The basics of brain development. *Neuropsychol Rev,* 20**,** 327-48.

STREIT, A., BERLINER, A. J., PAPANAYOTOU, C., SIRULNIK, A. & STERN, C. D. (2000) Initiation of neural induction by FGF signalling before gastrulation. *Nature,* 406**,** 74-8.

STROHMAIER, H., SPRUCK, C. H., KAISER, P., WON, K. A., SANGFELT, O. & REED, S. I. (2001) Human F-box protein hCdc4 targets cyclin E for proteolysis and is mutated in a breast cancer cell line. *Nature,* 413**,** 316-22.

STRUHL, G. & ADACHI, A. (2000) Requirements for presenilin-dependent cleavage of notch and other transmembrane proteins. *Mol Cell,* 6**,** 625-36.

STRUHL, K. (1987) The DNA-binding domains of the jun oncoprotein and the yeast GCN4 transcriptional activator protein are functionally homologous. *Cell,* 50**,** 841-6.

SUN, L., ZHANG, T., LAN, X. & DU, G. (2010) Effects of stem cell therapy on left ventricular remodeling after acute myocardial infarction: a meta-analysis. *Clin Cardiol,* 33**,** 296-302.

SUN, W., GOULD, T. W., NEWBERN, J., MILLIGAN, C., CHOI, S. Y., KIM, H. & OPPENHEIM, R. W. (2005) Phosphorylation of c-Jun in avian and mammalian motoneurons in vivo during programmed cell death: an early reversible event in the apoptotic cascade. *J Neurosci,* 25**,** 5595-603.

SUN, X. & ARTAVANIS-TSAKONAS, S. (1997) Secreted forms of DELTA and SERRATE define antagonists of Notch signaling in Drosophila. *Development,* 124**,** 3439-48.

SUNDARAM, M. & GREENWALD, I. (1993) Suppressors of a lin-12 hypomorph define genes that interact with both lin-12 and glp-1 in Caenorhabditis elegans. *Genetics,* 135**,** 765-83.

SUNDQVIST, A., BENGOECHEA-ALONSO, M. T., YE, X., LUKIYANCHUK, V., JIN, J., HARPER, J. W. & ERICSSON, J. (2005) Control of lipid metabolism by phosphorylation-dependent degradation of the SREBP family of transcription factors by SCF(Fbw7). *Cell Metab,* 1**,** 379-91.

SUZUKI, T. & CHIBA, S. (2005) Notch signaling in hematopoietic stem cells. *Int J Hematol,* 82**,** 285-94.

SWIATEK, P. J., LINDSELL, C. E., DEL AMO, F. F., WEINMASTER, G. & GRIDLEY, T. (1994) Notch1 is essential for postimplantation development in mice. *Genes Dev,* 8**,** 707-19.

TAKAHASHI, K., TANABE, K., OHNUKI, M., NARITA, M., ICHISAKA, T., TOMODA, K. & YAMANAKA, S. (2007) Induction of pluripotent stem cells from adult human fibroblasts by defined factors. *Cell,* 131**,** 861-72.

TAKAHASHI, K. & YAMANAKA, S. (2006) Induction of pluripotent stem cells from mouse embryonic and adult fibroblast cultures by defined factors. *Cell,* 126**,** 663-76.

TAMAMAKI, N., NAKAMURA, K., OKAMOTO, K. & KANEKO, T. (2001) Radial glia is a progenitor of neocortical neurons in the developing cerebral cortex. *Neurosci Res,* 41**,** 51-60.

TANG, X., ORLICKY, S., LIN, Z., WILLEMS, A., NECULAI, D., CECCARELLI, D., MERCURIO, F., SHILTON, B. H., SICHERI, F. & TYERS, M. (2007) Suprafacial orientation of the SCFCdc4 dimer accommodates multiple geometries for substrate ubiquitination. *Cell,* 129**,** 1165-76.

TANIGAKI, K., HAN, H., YAMAMOTO, N., TASHIRO, K., IKEGAWA, M., KURODA, K., SUZUKI, A., NAKANO, T. & HONJO, T. (2002) Notch-RBP-J signaling is involved in cell fate determination of marginal zone B cells. *Nat Immunol,* 3**,** 443-50.

TETZLAFF, M. T., YU, W., LI, M., ZHANG, P., FINEGOLD, M., MAHON, K., HARPER, J. W., SCHWARTZ, R. J. & ELLEDGE, S. J. (2004) Defective cardiovascular development and elevated cyclin E and Notch proteins in mice lacking the Fbw7 F-box protein. *Proc Natl Acad Sci U S A,* 101**,** 3338-45.

THAKUR, A., WANG, X., SIEDLAK, S. L., PERRY, G., SMITH, M. A. & ZHU, X. (2007) c-Jun phosphorylation in Alzheimer disease. *J Neurosci Res,* 85**,** 1668-73.

THIREOS, G., PENN, M. D. & GREER, H. (1984) 5' untranslated sequences are required for the translational control of a yeast regulatory gene. *Proc Natl Acad Sci U S A,* 81**,** 5096-100.

THOMPSON, B. J., JANKOVIC, V., GAO, J., BUONAMICI, S., VEST, A., LEE, J. M., ZAVADIL, J., NIMER, S. D. & AIFANTIS, I. (2008) Control of hematopoietic stem cell quiescence by the E3 ubiquitin ligase Fbw7. *J Exp Med,* 205**,** 1395-408.

THOMPSON, B. J., MATHIEU, J., SUNG, H. H., LOESER, E., RORTH, P. & COHEN, S. M. (2005) Tumor suppressor properties of the ESCRT-II complex component Vps25 in Drosophila. *Dev Cell,* 9**,** 711-20.

THOMSON, J. A., ITSKOVITZ-ELDOR, J., SHAPIRO, S. S., WAKNITZ, M. A., SWIERGIEL, J. J., MARSHALL, V. S. & JONES, J. M. (1998) Embryonic stem cell lines derived from human blastocysts. *Science,* 282**,** 1145-7.

TIBBLES, L. A., ING, Y. L., KIEFER, F., CHAN, J., ISCOVE, N., WOODGETT, J. R. & LASSAM, N. J. (1996) MLK-3 activates the SAPK/JNK and p38/RK pathways via SEK1 and MKK3/6. *EMBO J,* 15**,** 7026-35.

TROPEPE, V., HITOSHI, S., SIRARD, C., MAK, T. W., ROSSANT, J. & VAN DER KOOY, D. (2001) Direct neural fate specification from embryonic stem cells: a primitive mammalian neural stem cell stage acquired through a default mechanism. *Neuron,* 30**,** 65-78.

TROUNSON, A., THAKAR, R. G., LOMAX, G. & GIBBONS, D. (2011) Clinical trials for stem cell therapies. *BMC Med,* 9**,** 52.

TSUNEMATSU, R., NAKAYAMA, K., OIKE, Y., NISHIYAMA, M., ISHIDA, N., HATAKEYAMA, S., BESSHO, Y., KAGEYAMA, R., SUDA, T. &

NAKAYAMA, K. I. (2004) Mouse Fbw7/Sel-10/Cdc4 is required for notch degradation during vascular development. *J Biol Chem,* 279**,** 9417-23.

UENO, S., WEIDINGER, G., OSUGI, T., KOHN, A. D., GOLOB, J. L., PABON, L., REINECKE, H., MOON, R. T. & MURRY, C. E. (2007) Biphasic role for Wnt/beta-catenin signaling in cardiac specification in zebrafish and embryonic stem cells. *Proc Natl Acad Sci U S A,* 104**,** 9685-90.

VACCARI, T. & BILDER, D. (2005) The Drosophila tumor suppressor vps25 prevents nonautonomous overproliferation by regulating notch trafficking. *Dev Cell,* 9**,** 687-98.

VAN DROGEN, F., SANGFELT, O., MALYUKOVA, A., MATSKOVA, L., YEH, E., MEANS, A. R. & REED, S. I. (2006) Ubiquitylation of cyclin E requires the sequential function of SCF complexes containing distinct hCdc4 isoforms. *Mol Cell,* 23**,** 37-48.

VAN ES, J. H., VAN GIJN, M. E., RICCIO, O., VAN DEN BORN, M., VOOIJS, M., BEGTHEL, H., COZIJNSEN, M., ROBINE, S., WINTON, D. J., RADTKE, F. & CLEVERS, H. (2005) Notch/gamma-secretase inhibition turns proliferative cells in intestinal crypts and adenomas into goblet cells. *Nature,* 435**,** 959-63.

VERMA, R., ANNAN, R. S., HUDDLESTON, M. J., CARR, S. A., REYNARD, G. & DESHAIES, R. J. (1997a) Phosphorylation of Sic1p by G1 Cdk required for its degradation and entry into S phase. *Science,* 278**,** 455-60.

VERMA, R., FELDMAN, R. M. & DESHAIES, R. J. (1997b) SIC1 is ubiquitinated in vitro by a pathway that requires CDC4, CDC34, and cyclin/CDK activities. *Mol Biol Cell,* 8**,** 1427-37.

VINCIGUERRA, M., ESPOSITO, I., SALZANO, S., MADEO, A., NAGEL, G., MAGGIOLINI, M., GALLO, A. & MUSTI, A. M. (2008) Negative charged threonine 95 of c-Jun is essential for c-Jun N-terminal kinase-dependent phosphorylation of threonine 91/93 and stress-induced c-Jun biological activity. *Int J Biochem Cell Biol,* 40**,** 307-16.

VISVADER, J. E., ELEFANTY, A. G., STRASSER, A. & ADAMS, J. M. (1992) GATA-1 but not SCL induces megakaryocytic differentiation in an early myeloid line. *EMBO J,* 11**,** 4557-64.

VOGT, P. K. (2001) Jun, the oncoprotein. *Oncogene,* 20**,** 2365-77.

VOGT, P. K., BOS, T. J. & DOOLITTLE, R. F. (1987) Homology between the DNA-binding domain of the GCN4 regulatory protein of yeast and the carboxyl-terminal region of a protein coded for by the oncogene jun. *Proc Natl Acad Sci U S A,* 84**,** 3316-9.

WADA, T., JOZA, N., CHENG, H. Y., SASAKI, T., KOZIERADZKI, I., BACHMAIER, K., KATADA, T., SCHREIBER, M., WAGNER, E. F., NISHINA, H. & PENNINGER, J. M. (2004) MKK7 couples stress signalling to G2/M cell-cycle progression and cellular senescence. *Nat Cell Biol,* 6**,** 215-26.

WALLBERG, A. E., PEDERSEN, K., LENDAHL, U. & ROEDER, R. G. (2002) p300 and PCAF act cooperatively to mediate transcriptional activation from chromatin templates by notch intracellular domains in vitro. *Mol Cell Biol,* 22**,** 7812-9.

WANG, S. W. & SPECK, N. A. (1992) Purification of core-binding factor, a protein that binds the conserved core site in murine leukemia virus enhancers. *Mol Cell Biol,* 12**,** 89-102.

WANG, W. & STRUHL, G. (2004) Drosophila Epsin mediates a select endocytic pathway that DSL ligands must enter to activate Notch. *Development,* 131**,** 5367-80.

WANG, W. & STRUHL, G. (2005) Distinct roles for Mind bomb, Neuralized and Epsin in mediating DSL endocytosis and signaling in Drosophila. *Development,* 132**,** 2883-94.

WANG, X., NADARAJAH, B., ROBINSON, A. C., MCCOLL, B. W., JIN, J. W., DAJAS-BAILADOR, F., BOOT-HANDFORD, R. P. & TOURNIER, C. (2007) Targeted deletion of the mitogen-activated protein kinase kinase 4 gene in the nervous system causes severe brain developmental defects and premature death. *Mol Cell Biol,* 27**,** 7935-46.

WANG, X. S., DIENER, K., TAN, T. H. & YAO, Z. (1998) MAPKKK6, a novel mitogen-activated protein kinase kinase kinase, that associates with MAPKKK5. *Biochem Biophys Res Commun,* 253**,** 33-7.

WANG, Y. N., CHEN, Y. J. & CHANG, W. C. (2006) Activation of extracellular signal-regulated kinase signaling by epidermal growth factor mediates c-Jun activation and p300 recruitment in keratin 16 gene expression. *Mol Pharmacol,* 69**,** 85-98.

WATARAI, H., RYBOUCHKIN, A., HONGO, N., NAGATA, Y., SAKATA, S., SEKINE, E., DASHTSOODOL, N., TASHIRO, T., FUJII, S., SHIMIZU, K., MORI, K., MASUDA, K., KAWAMOTO, H., KOSEKI, H. & TANIGUCHI, M. (2010) Generation of functional NKT cells in vitro from embryonic stem cells bearing rearranged invariant Valpha14-Jalpha18 TCRalpha gene. *Blood,* 115**,** 230-7.

WEI, W., JIN, J., SCHLISIO, S., HARPER, J. W. & KAELIN, W. G., JR. (2005) The v-Jun point mutation allows c-Jun to escape GSK3-dependent recognition and destruction by the Fbw7 ubiquitin ligase. *Cancer Cell,* 8**,** 25-33.

WEISSMAN, A. M. (2001) Themes and variations on ubiquitylation. *Nat Rev Mol Cell Biol,* 2**,** 169-78.

WELCKER, M. & CLURMAN, B. E. (2007) Fbw7/hCDC4 dimerization regulates its substrate interactions. *Cell Div,* 2**,** 7.

WELCKER, M. & CLURMAN, B. E. (2008) FBW7 ubiquitin ligase: a tumour suppressor at the crossroads of cell division, growth and differentiation. *Nat Rev Cancer,* 8**,** 83-93.

WELCKER, M., ORIAN, A., GRIM, J. E., EISENMAN, R. N. & CLURMAN, B. E. (2004a) A nucleolar isoform of the Fbw7 ubiquitin ligase regulates c-Myc and cell size. *Curr Biol,* 14**,** 1852-7.

WELCKER, M., ORIAN, A., JIN, J., GRIM, J. E., HARPER, J. W., EISENMAN, R. N. & CLURMAN, B. E. (2004b) The Fbw7 tumor suppressor regulates glycogen synthase kinase 3 phosphorylation-dependent c-Myc protein degradation. *Proc Natl Acad Sci U S A,* 101**,** 9085-90.

WENG, A. P., FERRANDO, A. A., LEE, W., MORRIS, J. P. T., SILVERMAN, L. B., SANCHEZ-IRIZARRY, C., BLACKLOW, S. C., LOOK, A. T. & ASTER, J. C. (2004) Activating mutations of NOTCH1 in human T cell acute lymphoblastic leukemia. *Science,* 306**,** 269-71.

WENG, A. P., MILLHOLLAND, J. M., YASHIRO-OHTANI, Y., ARCANGELI, M. L., LAU, A., WAI, C., DEL BIANCO, C., RODRIGUEZ, C. G., SAI, H., TOBIAS, J., LI, Y., WOLFE, M. S., SHACHAF, C., FELSHER, D.,

BLACKLOW, S. C., PEAR, W. S. & ASTER, J. C. (2006) c-Myc is an important direct target of Notch1 in T-cell acute lymphoblastic leukemia/lymphoma. *Genes Dev,* 20**,** 2096-109.

WERNIG, M., ZHAO, J. P., PRUSZAK, J., HEDLUND, E., FU, D., SOLDNER, F., BROCCOLI, V., CONSTANTINE-PATON, M., ISACSON, O. & JAENISCH, R. (2008) Neurons derived from reprogrammed fibroblasts functionally integrate into the fetal brain and improve symptoms of rats with Parkinson's disease. *Proc Natl Acad Sci U S A,* 105**,** 5856-61.

WESSEL, T. C., JOH, T. H. & VOLPE, B. T. (1991) In situ hybridization analysis of c-fos and c-jun expression in the rat brain following transient forebrain ischemia. *Brain Res,* 567**,** 231-40.

WHITFIELD, J., NEAME, S. J., PAQUET, L., BERNARD, O. & HAM, J. (2001) Dominant-negative c-Jun promotes neuronal survival by reducing BIM expression and inhibiting mitochondrial cytochrome c release. *Neuron,* 29**,** 629-43.

WILKIN, M., TONGNGOK, P., GENSCH, N., CLEMENCE, S., MOTOKI, M., YAMADA, K., HORI, K., TANIGUCHI-KANAI, M., FRANKLIN, E., MATSUNO, K. & BARON, M. (2008) Drosophila HOPS and AP-3 complex genes are required for a Deltex-regulated activation of notch in the endosomal trafficking pathway. *Dev Cell,* 15**,** 762-72.

WILSON, J. J. & KOVALL, R. A. (2006) Crystal structure of the CSL-Notch-Mastermind ternary complex bound to DNA. *Cell,* 124**,** 985-96.

WINSTON, J. T., KOEPP, D. M., ZHU, C., ELLEDGE, S. J. & HARPER, J. W. (1999) A family of mammalian F-box proteins. *Curr Biol,* 9**,** 1180-2.

WON, K. A. & REED, S. I. (1996) Activation of cyclin E/CDK2 is coupled to site-specific autophosphorylation and ubiquitin-dependent degradation of cyclin E. *EMBO J,* 15**,** 4182-93.

WOO LEE, J., HWA SOUNG, Y., YOUNG KIM, S., WOO NAM, S., SANG PARK, W., YOUNG LEE, J., JIN YOO, N. & HYUNG LEE, S. (2006) Somatic mutation of hCDC4 gene is rare in lung adenocarcinomas. *Acta Oncol,* 45**,** 487-8.

WRIGHT, G. J., LESLIE, J. D., ARIZA-MCNAUGHTON, L. & LEWIS, J. (2004) Delta proteins and MAGI proteins: an interaction of Notch ligands with intracellular scaffolding molecules and its significance for zebrafish development. *Development,* 131**,** 5659-69.

WU, G., HUBBARD, E. J., KITAJEWSKI, J. K. & GREENWALD, I. (1998) Evidence for functional and physical association between Caenorhabditis elegans SEL-10, a Cdc4p-related protein, and SEL-12 presenilin. *Proc Natl Acad Sci U S A,* 95**,** 15787-91.

WU, G., LYAPINA, S., DAS, I., LI, J., GURNEY, M., PAULEY, A., CHUI, I., DESHAIES, R. J. & KITAJEWSKI, J. (2001) SEL-10 is an inhibitor of notch signaling that targets notch for ubiquitin-mediated protein degradation. *Mol Cell Biol,* 21**,** 7403-15.

WU, H., XU, J., PANG, Z. P., GE, W., KIM, K. J., BLANCHI, B., CHEN, C., SUDHOF, T. C. & SUN, Y. E. (2007) Integrative genomic and functional analyses reveal neuronal subtype differentiation bias in human embryonic stem cell lines. *Proc Natl Acad Sci U S A,* 104**,** 13821-6.

WU, L., ASTER, J. C., BLACKLOW, S. C., LAKE, R., ARTAVANIS-TSAKONAS, S. & GRIFFIN, J. D. (2000) MAML1, a human homologue of Drosophila mastermind, is a transcriptional co-activator for NOTCH receptors. *Nat Genet,* 26**,** 484-9.

XIA, Y. & KARIN, M. (2004) The control of cell motility and epithelial morphogenesis by Jun kinases. *Trends Cell Biol,* 14**,** 94-101.

XIA, Y., WU, Z., SU, B., MURRAY, B. & KARIN, M. (1998) JNKK1 organizes a MAP kinase module through specific and sequential interactions with upstream and downstream components mediated by its amino-terminal extension. *Genes Dev,* 12**,** 3369-81.

XU, P., DUONG, D. M., SEYFRIED, N. T., CHENG, D., XIE, Y., ROBERT, J., RUSH, J., HOCHSTRASSER, M., FINLEY, D. & PENG, J. (2009) Quantitative proteomics reveals the function of unconventional ubiquitin chains in proteasomal degradation. *Cell,* 137**,** 133-45.

XUE, Y., GAO, X., LINDSELL, C. E., NORTON, C. R., CHANG, B., HICKS, C., GENDRON-MAGUIRE, M., RAND, E. B., WEINMASTER, G. & GRIDLEY, T. (1999) Embryonic lethality and vascular defects in mice lacking the Notch ligand Jagged1. *Hum Mol Genet,* 8**,** 723-30.

YADA, M., HATAKEYAMA, S., KAMURA, T., NISHIYAMA, M., TSUNEMATSU, R., IMAKI, H., ISHIDA, N., OKUMURA, F., NAKAYAMA, K. & NAKAYAMA, K. I. (2004) Phosphorylation-dependent degradation of c-Myc is mediated by the F-box protein Fbw7. *EMBO J,* 23**,** 2116-25.

YAMANAKA, Y., RALSTON, A., STEPHENSON, R. O. & ROSSANT, J. (2006) Cell and molecular regulation of the mouse blastocyst. *Dev Dyn,* 235**,** 2301-14.

YAN, T., WUNDER, J. S., GOKGOZ, N., SETO, K. K., BELL, R. S. & ANDRULIS, I. L. (2006) hCDC4 variation in osteosarcoma. *Cancer Genet Cytogenet,* 169**,** 138-42.

YAN, Y., YANG, D., ZARNOWSKA, E. D., DU, Z., WERBEL, B., VALLIERE, C., PEARCE, R. A., THOMSON, J. A. & ZHANG, S. C. (2005) Directed differentiation of dopaminergic neuronal subtypes from human embryonic stem cells. *Stem Cells,* 23**,** 781-90.

YANG, D. D., CONZE, D., WHITMARSH, A. J., BARRETT, T., DAVIS, R. J., RINCON, M. & FLAVELL, R. A. (1998) Differentiation of CD4+ T cells to Th1 cells requires MAP kinase JNK2. *Immunity,* 9**,** 575-85.

YANG, D. D., KUAN, C. Y., WHITMARSH, A. J., RINCON, M., ZHENG, T. S., DAVIS, R. J., RAKIC, P. & FLAVELL, R. A. (1997) Absence of excitotoxicity-induced apoptosis in the hippocampus of mice lacking the Jnk3 gene. *Nature,* 389**,** 865-70.

YASUDA, J., WHITMARSH, A. J., CAVANAGH, J., SHARMA, M. & DAVIS, R. J. (1999) The JIP group of mitogen-activated protein kinase scaffold proteins. *Mol Cell Biol,* 19**,** 7245-54.

YE, Y. & RAPE, M. (2009) Building ubiquitin chains: E2 enzymes at work. *Nat Rev Mol Cell Biol,* 10**,** 755-64.

YEO, W. & GAUTIER, J. (2004) Early neural cell death: dying to become neurons. *Dev Biol,* 274**,** 233-44.

YING, Q. L., STAVRIDIS, M., GRIFFITHS, D., LI, M. & SMITH, A. (2003) Conversion of embryonic stem cells into neuroectodermal precursors in adherent monoculture. *Nat Biotechnol,* 21**,** 183-6.

YOON, K. & GAIANO, N. (2005) Notch signaling in the mammalian central nervous system: insights from mouse mutants. *Nat Neurosci,* 8**,** 709-15.

YOON, K., NERY, S., RUTLIN, M. L., RADTKE, F., FISHELL, G. & GAIANO, N. (2004) Fibroblast growth factor receptor signaling promotes radial glial identity and interacts with Notch1 signaling in telencephalic progenitors. *J Neurosci,* 24**,** 9497-506.

YOON, K. J., KOO, B. K., IM, S. K., JEONG, H. W., GHIM, J., KWON, M. C., MOON, J. S., MIYATA, T. & KONG, Y. Y. (2008) Mind bomb 1-expressing intermediate progenitors generate notch signaling to maintain radial glial cells. *Neuron,* 58**,** 519-31.

YOU, L. R., LIN, F. J., LEE, C. T., DEMAYO, F. J., TSAI, M. J. & TSAI, S. Y. (2005) Suppression of Notch signalling by the COUP-TFII transcription factor regulates vein identity. *Nature,* 435**,** 98-104.

ZERIAL, M., TOSCHI, L., RYSECK, R. P., SCHUERMANN, M., MULLER, R. & BRAVO, R. (1989) The product of a novel growth factor activated gene, fos B, interacts with JUN proteins enhancing their DNA binding activity. *EMBO J,* 8**,** 805-13.

ZHANG, P., BEHRE, G., PAN, J., IWAMA, A., WARA-ASWAPATI, N., RADOMSKA, H. S., AURON, P. E., TENEN, D. G. & SUN, Z. (1999) Negative cross-talk between hematopoietic regulators: GATA proteins repress PU.1. *Proc Natl Acad Sci U S A,* 96**,** 8705-10.

ZHANG, P., ZHANG, X., IWAMA, A., YU, C., SMITH, K. A., MUELLER, B. U., NARRAVULA, S., TORBETT, B. E., ORKIN, S. H. & TENEN, D. G. (2000) PU.1 inhibits GATA-1 function and erythroid differentiation by blocking GATA-1 DNA binding. *Blood,* 96**,** 2641-8.

ZHANG, Q., TIAN, H., FU, X. & ZHANG, G. (2003a) Delayed activation and regulation of MKK7 in hippocampal CA1 region following global cerebral ischemia in rats. *Life Sci,* 74**,** 37-45.

ZHANG, Q., ZHANG, G., MENG, F. & TIAN, H. (2003b) Biphasic activation of apoptosis signal-regulating kinase 1-stress-activated protein kinase 1-c-Jun N-terminal protein kinase pathway is selectively mediated by Ca2+-permeable alpha-amino-3-hydroxy-5-methyl-4-isoxazolepropionate receptors involving oxidative stress following brain ischemia in rat hippocampus. *Neurosci Lett,* 337**,** 51-5.

ZHANG, W. & KOEPP, D. M. (2006) Fbw7 isoform interaction contributes to cyclin E proteolysis. *Mol Cancer Res,* 4**,** 935-43.

ZHENG, H., YING, H., YAN, H., KIMMELMAN, A. C., HILLER, D. J., CHEN, A. J., PERRY, S. R., TONON, G., CHU, G. C., DING, Z., STOMMEL, J. M., DUNN, K. L., WIEDEMEYER, R., YOU, M. J., BRENNAN, C., WANG, Y. A., LIGON, K. L., WONG, W. H., CHIN, L. & DEPINHO, R. A. (2008) p53 and Pten control neural and glioma stem/progenitor cell renewal and differentiation. *Nature,* 455**,** 1129-33.

ZHENG, N., SCHULMAN, B. A., SONG, L., MILLER, J. J., JEFFREY, P. D., WANG, P., CHU, C., KOEPP, D. M., ELLEDGE, S. J., PAGANO, M., CONAWAY, R. C., CONAWAY, J. W., HARPER, J. W. & PAVLETICH, N. P. (2002) Structure of the Cul1-Rbx1-Skp1-F boxSkp2 SCF ubiquitin ligase complex. *Nature,* 416**,** 703-9.

ZHOU, S., FUJIMURO, M., HSIEH, J. J., CHEN, L., MIYAMOTO, A., WEINMASTER, G. & HAYWARD, S. D. (2000) SKIP, a CBF1-associated protein, interacts with the ankyrin repeat domain of NotchIC To facilitate NotchIC function. *Mol Cell Biol,* 20**,** 2400-10.